University of Southampton

University of Southampton Research Repository

Copyright © and Moral Rights for this thesis and, where applicable, any accompanying data are retained by the author and/or other copyright owners. A copy can be downloaded for personal non-commercial research or study, without prior permission or charge. This thesis and the accompanying data cannot be reproduced or quoted extensively from without first obtaining permission in writing from the copyright holder/s. The content of the thesis and accompanying research data (where applicable) must not be changed in any way or sold commercially in any format or medium without the formal permission of the copyright holder/s.

When referring to this thesis and any accompanying data, full bibliographic details must be given, e.g.

Thesis: Author (Year of Submission) "Full thesis title", University of Southampton, name of the University Faculty or School or Department, PhD Thesis, pagination.

Data: Author (Year) Title. URI [dataset]

University of Southampton

Faculty of Environmental and Life Sciences

School of Geography and Environmental Science

Towards High Temporal and In Situ Estimations of Suspended Sediment Sources

by

Niels Fedde Lake

ORCID ID 0000-0002-5909-2005

https://orcid.org/0000-0002-5909-2005

Thesis for the degree of Doctor of Philosophy

March 2023

University of Southampton

Abstract

Faculty of Environmental and Life Sciences

School of Geography and Environmental Science

Doctor of Philosophy

Towards High Temporal and In Situ Estimations of Suspended Sediment Sources

by

Niels Fedde Lake

Natural soil erosion and sediment transport processes are important in shaping the Earth's critical zone. However, excess soil erosion and sediment delivery may pose different problems related to soil health, surface water quality and the safety of human living environments. To obtain robust information on the location of sediment source areas and to quantify their contributions to the sampled in-stream suspended sediment (SS) is important to guide the implementation of targeted management measures. Sediment fingerprinting is a widely applied approach to obtain such information, relying on the comparison of chemical and/or physical properties (i.e., fingerprints) between potential soil sources and target SS. However, there are several limitations and challenges associated with this approach. One of the major limitations relates to the available resources, which are often prohibitive in the context of research budgets. Given the relatively high costs and workloads involved in conventional source and SS sampling, and the subsequent laboratory fingerprint analysis procedures, repeat source and target SS sampling campaigns, or long durational studies, are limited. This situation remains despite the fact that it is widely known that catchments are rather dynamic, causing different source areas to be activated and deactivated over time. To this end, the work described in this thesis aims to develop new fingerprints (i.e., absorbance measurements at the UV-VIS wavelength range, and SS particle size distribution) that allow for increased temporal observations (i.e., up to minutes), by testing instruments that could directly obtain these fingerprints from water samples, and eventually measure *in situ* at high temporal resolution. Both fingerprints were tested at two scales in proof-of-concept studies: (i) in a laboratory scale setting, using artificial mixtures with known soil sample contributions to evaluate un-mixing model soil sample apportionment outcomes, and (ii) in a catchment scale setting, comparing un-mixing model source apportionment results with source apportionment results through sediment source budget estimations. The laboratory scale experiments showed rather small mean deviations to the known soil sample contributions (i.e., 15% and 7%, using absorbance and particle size distribution, respectively), comparable to other SS fingerprinting studies using artificial mixtures to evaluate un-mixing model results. Catchment scale experiments showed more variable outcomes, indicating the need for careful evaluation of the un-mixing model source apportionment results. Using absorbance; mean deviation between model results and sediment budget was 18%, though deviations were shown to reach up to 52%. Using particle size distribution; relatively low mean deviations (19%) were observed between model outcomes and sediment budget at relatively high discharge values (which were exceeded 12% of the time during the 5 month study period, during which 82% of the total SS load was transported). Overall, results presented the potential usability of both fingerprints, allowing for increasing high temporal resolution source ascription due to easy and rapid measurements that could be obtained directly from water samples.

Table of Contents

Table of Tables

Table of Figures

Table of Figures

Table of Figures

Research Thesis: Declaration of Authorship

Print name: Niels Fedde Lake

Title of thesis: Towards High Temporal and In Situ Estimations of Suspended Sediment Sources

I declare that this thesis and the work presented in it are my own and has been generated by me as the result of my own original research.

I confirm that:

1. This work was done wholly or mainly while in candidature for a research degree at this University;
2. Where any part of this thesis has previously been submitted for a degree or any other qualification at this University or any other institution, this has been clearly stated;
3. Where I have consulted the published work of others, this is always clearly attributed;
4. Where I have quoted from the work of others, the source is always given. With the exception of such quotations, this thesis is entirely my own work;
5. I have acknowledged all main sources of help;
6. Where the thesis is based on work done by myself jointly with others, I have made clear exactly what was done by others and what I have contributed myself;
7. Parts of this work have been published as:
    - Lake, N.F., Martínez-Carreras, N., Shaw, P.J., Collins, A.L., 2022a. High frequency un-mixing of soil samples using a submerged spectrophotometer in a laboratory setting—implications for sediment fingerprinting. Journal of Soils and Sediments 22 (1), 348–364. https://doi.org/10.1007/s11368-021-03107-6
    - Lake, N.F., Martínez-Carreras, N., Shaw, P.J., Collins, A.L., 2022b. Using particle size distributions to fingerprint suspended sediment sources — Evaluation at laboratory and catchment scales. Hydrological Processes 36 (10), e14726. https://doi.org/10.1002/hyp.14726
    - Lake, N.F., Martínez-Carreras, N., Iffly, J.F., Shaw, P.J. and Collins, A.L., 2023. Use of a submersible spectrophotometer probe to fingerprint spatial suspended sediment sources at catchment scale. Science of the Total Environment, p.162332. https://doi.org/10.1016/j.scitotenv.2023.162332

Conceptualisation was undertaken by NFL, NMC, PJS and ALC. Laboratory and field setups were designed by NFL and NMC, with the help of PJS, ALC and JFI. NFL and NMC collected the soil samples, NFL collected water samples. NFL executed all laboratory preparations and measurements. NFL analysed the data under the supervision of NMC, PJS and ALC. Original drafts were prepared by NFL, subsequent reviews and edits by NMC, PJS and ALC.

Signature: ..... Date: March 2023

Acknowledgements

The completion of this thesis would not have been possible without the support I have received over these last four years, for which I am very thankful.

Firstly, I would like to thank my supervisors, Núria, Pete and Adie, for their support, advice and discussions. I am especially thankful to Núria for her support and advice during this PhD project. And I am very thankful to Pete and Adie for making my stays in England very enjoyable and for their very valuable contributions throughout these past four years.

I would also like to acknowledge everyone at LIST who have contributed to a nice and friendly atmosphere. Especially the other PhD`s from my office (Gitanjali, Emmanuella, Louis, Adnan, Carol, Judith, Dhruv), and PostDoc (Remko). I have been very lucky to meet all of these great people, starting our PhD journey around the same time. Their support, positivity and random talks have made my stay at LIST and in Luxembourg very special. With Dhruv, I have found a great colleague, who started his PhD at the same day and worked at a related topic. We have had many discussions and he has been of great support over these past four years.

My stay at Rothamsted Research was very special, and would not have been the same without the people I have met there. I will especially remember the nice moments spent with the other people staying in the cottages: playing table tennis, going out for dinner, and going for trips to Exeter and the Christmas market.

I am very thankful to friends I have met in Luxembourg. Dhruv, we have explored many places together in Luxembourg, and you introduced me to a great variety of Indian restaurants! My tennis friends (especially Francesco, Mathieu and Youri), with whom I have spent many happy hours on the court. My special thanks go to Youri, as next to playing tennis at least once a week over these past four years, we have had a lot of fun moments outside the tennis court as well!

Finally, I am very thankful to my family. They have always been of great support. I am lucky that they were always there to listen to me, whether I was in a good or bad mood! It was also very nice to be sharing part of this PhD journey together with my brother, who more than once has helped me to see things from a different perspective!

Definitions and Abbreviations

Abs. ..... Absorbance

ACT ..... Administration du Cadastre et de la Topographie

AE ..... Absolute Error

ASTA ..... Administration des Services Techniques de l'Agriculture

Conc. ..... Concentration

D_{50} ..... 50% of total particles are smaller than this size; Median particle size

D_{60} ..... 60% of total particles are smaller than this size

D_{70} ..... 70% of total particles are smaller than this size

DOC ..... Dissolved Organic Carbon

EM ..... End-member

EU ..... European Union

GIS ..... Geographic Information Systems

H_2O_2 ..... Hydrogen peroxide

LIST ..... Luxembourg Institute of Science and Technology

OM ..... Organic Matter

PSD ..... Particle Size Distribution

RBG ..... Red, Green, Blue

SS ..... Suspended Sediment

SSC ..... Suspended Sediment Concentration

US ..... Ultrasound

UV-VIS ..... Ultraviolet-Visible

WFD ..... Water Framework Directive

XRD ..... X-ray diffraction analysis

XRF ..... X-ray fluorescence spectroscopy

Chapter 1 Introduction

1.1 Motivation – the Global Sediment Problem

Despite erosion and sediment transport being natural processes, the rates and extent of erosion and sediment delivery across the globe have significantly increased due to land use changes and human-induced climate change (Poesen, 2018). With soil formation processes being very slow, any soil loss rate exceeding 1 t ha^{-1} yr^{-1} can be considered as irreversible within a 50-100 year time span (Jones et al., 2003), with about 7.5 million km^2 (6.1% of land) exceeding this this threshold value (Borrelli et al., 2017; Figure 1.1). In perspective, losses of 20 to 40 t ha^{-1} are being observed in individual storm events that may occur in Europe once every two to three years, with losses exceeding 100 t ha^{-1} being observed in very extreme events (Morgan, 1995). In the US, average soil erosion rates on croplands in 2007 were estimated to be 10.8 t ha^{-1} yr^{-1} (USDA/NRCS, 2010). Overall, soil loss rates from agricultural areas are thus 10 to 40 times larger compared to the rate of natural soil formation processes (Pimentel and Burgess, 2013).

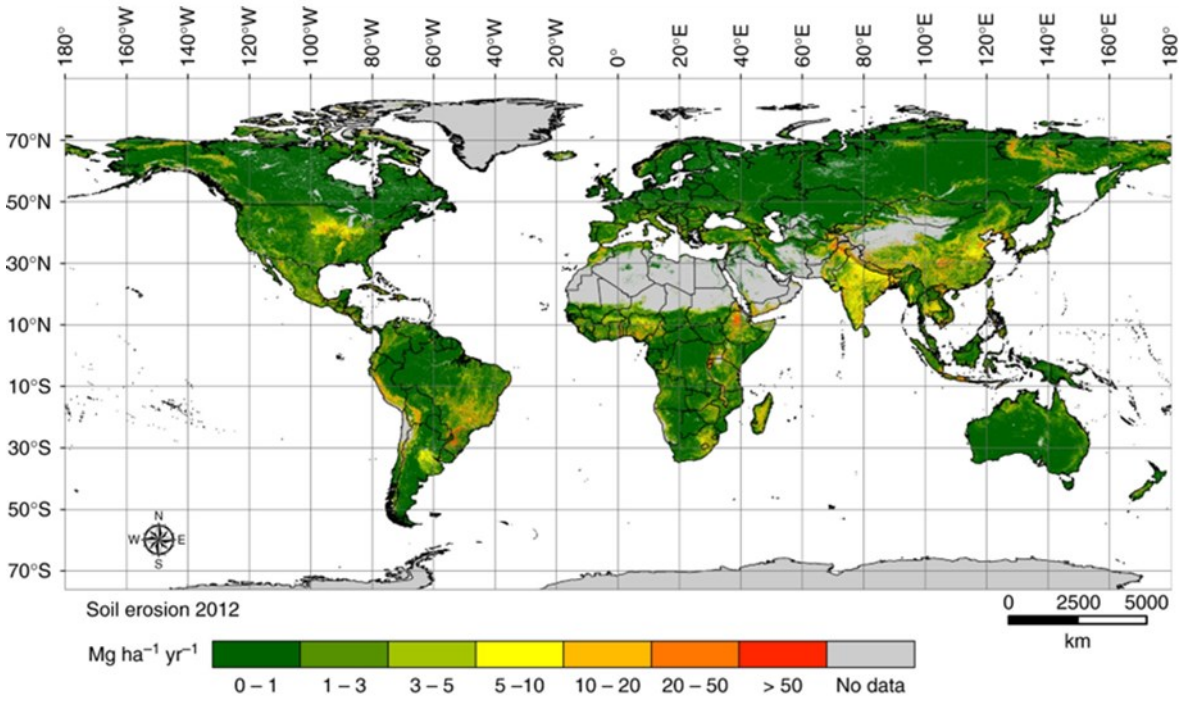

Figure 1.1 Modelled global soil water erosion rates for the year 2012. From Borrelli et al. (2017).

Water and wind are the major drivers of soil erosion (Borrelli et al., 2020), with Lal (2003) indicating globally affected land areas to be 1094 million hectares and 594 million hectares, respectively. Soil erosion directly affects the fertile (top)soil and its associated nutrients, with the majority of erosion thus induced by water (Lal, 2003). Losing these fertile soils decrease the agricultural potential

(Amundson et al., 2015; Borrelli et al., 2022; Panagos et al., 2015; Pimentel et al., 1995). On a yearly basis, an estimated 75 billion tonnes (Pg) of agricultural soil is eroded globally (e.g., FAO, 2016; Montanarella, 2015; Pimentel et al., 1995). This equates to an annual loss of 10 million ha of croplands (Pimentel and Burgess, 2013), causing an estimated loss in agricultural production of $400 billion per year (FAO, 2016; Noel et al., 2015). At the same time, rising populations and higher incomes demand a global increase in agricultural production (Foley et al., 2011; Mueller et al., 2012). Soil erosion is therefore of particular importance, with e.g., the European Union (EU) making soil erosion part of its environmental agenda (Boardman and Poesen, 2006; Borrelli et al., 2022; Panagos et al., 2022).

Suspended sediment (SS) originating from eroded soil particles, or from other sources such as eroded channel banks, play an essential role in the hydrological, geomorphological and ecological functioning of aquatic ecosystems (Owens et al., 2005; Vercruysse et al., 2017; Wohl et al., 2015). Sediments structure landscapes, create ecological habitats and transport nutrients and contaminants (i.e., organic contaminants, pesticides, trace and heavy metals) (Affandi and Ishak, 2019; Dean et al., 2016; Koiter et al., 2013). However, increasing SS loads can impact water quality negatively. Sediment-associated nutrients and contaminants are a common reason why good ecological status of surface waters is often not achieved (Tye et al., 2016). In Europe, deterioration in water quality is a major policy challenge, as evidenced by the introduction and implementation of the European Water Framework Directive (WFD; 2000/60/EC, 2000) which aims for a `good` ecological status in surface (and ground) waters. Besides, increasing SS loads can also cause economic damages and direct risk for humans, due to e.g., reservoir sedimentation (Syvitski et al., 2005; Walling, 2006), channel and harbour siltation (Netzband et al., 2002), elevated flood risks (Owens et al., 2005), and increasing water treatment costs (Hilton et al., 2006; Owens et al., 2005).

In the view of the aforementioned issues, it is essential to mitigate excess erosion and sediment delivery rates for more sustainable catchment and river management. To this end, information on catchment sediment dynamics is necessary. This includes a thorough understanding of which sediment sources are mainly responsible for the excessive erosion and sediment delivery rates, and how this sediment is routed through the catchment system. Thereby, robust quantifications of SS source contributions to rivers and streams is an absolute must if effective sediment management and control strategies are to be implemented (Vercruysse et al., 2017; Walling, 2005), as these measures can then specifically target those areas contributing most to the in-stream SS load.

1.2 Soil Erosion and Sediment Transport

1.2.1 Erosion Processes

Zorn and Komac (2013) defined erosion as "a geomorphic process that detaches and removes material (soil, rock debris, and associated organic matter) from its primary location by some natural erosive agents or through human or animal activity". The main natural agents causing soil erosion are water and wind (Pimentel and Burgess, 2013), though erosion can also be initiated by glaciers, snow, sea/lake waves and gravity (Osman, 2014). Whilst wind erosion is a major concern in Arid and Semi-Arid regions, erosion by water is of major concern in the more Temperate, Mediterranean and Tropical climatic regions (Amundson et al., 2015; Osman, 2014).

Erosion by water comprises a complex interplay of processes, starting with the detachment of soil particles through rain splash (Bryan, 2000). When the force of the raindrop, influenced by its mass and impact velocity (Bryan, 2000), contacts the soil surface, the soil structure can be destroyed with soil particles being loosened and potentially displaced (Pimentel and Burgess, 2013). Furthermore, soil particles and small aggregates can be detached from the *in situ* soil by running water, biological activity, geochemical and physical weathering, freeze-thaw cycles and wind (Vercruysse et al., 2017). The subsequent mobilisation of these detached particles is dependent on processes related to water infiltration, storage and overland flow, with the relative magnitude of these processes depending on factors including soil type, topography, climate, land management practises and antecedent hydrological conditions (Römkens et al., 2002). The antecedent soil water conditions herein play an important role in the transport of the detached particles (Bryan, 2000). For dry soils, the majority of the kinetic energy of the rainfall causes the disruption and detachment of soil particles. When soil moisture levels increase, the shear strength between the soil particles decreases due to a more plastic behaviour, thereby causing increased sediment entrainment in overland flow.

With splash erosion being the main initial step in soil erosion by water, other erosion processes are then responsible for the downslope movement of particles (Figure 1.2). Sheet erosion represents the removal of a thin, rather uniform layer of the soil surface by means of splash erosion and subsequent shallow surface flow over large parts of the hillslope, which may lead to the loss of the fertile topsoil that is rich in nutrients and organic matter (Osman, 2014). Both splash erosion and sheet erosion are diffuse, non-concentrated, forms of soil erosion (Oakes et al., 2012). However, with most slopes not being uniform, water moving downslope often concentrates into small channels, referred to as rills (Osman, 2014). Detached soil particles may then be transported towards these rills by means of overland flow, which is referred to as interrill erosion (Osman,

2014). Rill erosion occurs when water concentrated in the rills can further entrain particles, due to the kinetic energy of the flowing water. Rill channels are generally less than 0.3 m deep (e.g., Valentin et al., 2005), which can, in the main, still be removed by e.g., tillage. When in-field eroded channels become deeper, they become more difficult to remove, ending up as permanent features. This type of erosion is referred to as gully erosion, where large water quantities in combination with high kinetic energy results in increasing levels of entrainment and thus rather high sediment loads (Osman, 2014). In extreme situations, gullies can ultimately form Badlands, which are areas that cannot be used for cultivation anymore. Being characterised by highly eroded areas comprising of steep slopes and low soil cover, these Badlands act as an important source of sediments (Valentin et al., 2005). Other processes that can serve as important sources of sediment are mass movements such as landslides, caused by e.g., unstable geological conditions, saturated soils due to intense rainfall or earthquakes (Osman, 2014). Additionally, erosion by water can also occur within rivers and streams, where the water velocity erodes channel banks and channel beds (Osman, 2014).

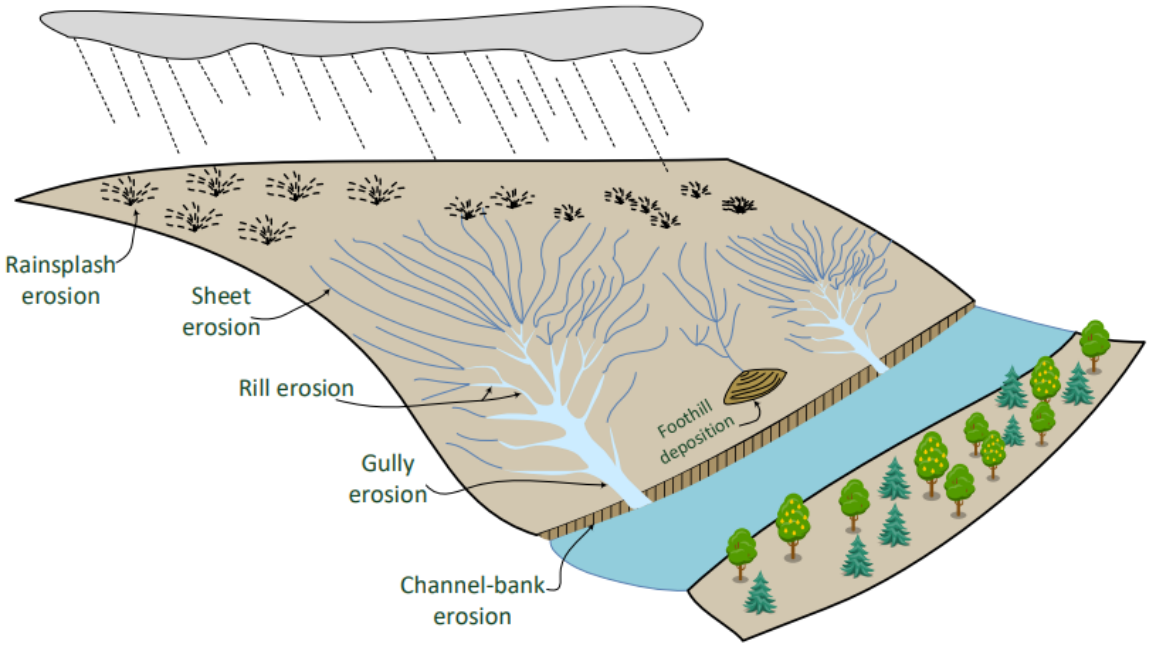

Figure 1.2 Graphical representation of water erosion processes. From Sotiri (2020).

Human activities have had an increasingly important role over time in observed erosion rates, related to agriculture, resource extraction, construction (Owens, 2020), and continuing land use changes (Borrelli et al., 2017). With 75% of the Earth's surface experiencing some sort of human pressure (Venter et al., 2016), agricultural activities account for 38% of the total Earth surface cover (Viana et al., 2022; Zabel et al., 2019). With human livelihoods strongly dependent on agricultural production and livestock, maintaining soils of good quality is of great importance (Pimentel and Burgess, 2013). However, overgrazing, unsuitable agricultural practises, and deforestation are amongst the main causes of elevated soil erosion, being induced by human activities (Montgomery,

2007; Pimentel and Burgess, 2013). Consequent sediment-associated nutrient losses, reduction of carbon storage and a lowering of both soil and ecosystem health cause the majority of the world`s soil resources to be only in a fair, poor or very poor condition (FAO, 2015).

Furthermore, human induced climate change increasingly affects soil erosion by causing more extreme and intense rainfall amounts (e.g., Mullan et al., 2012; O'Neal et al., 2005). Here, water erosion is predicted to increase globally by 30-66% in the near future (Borrelli et al., 2020). More intense and higher quantities of rainfall have the potential to increase splash erosion, and induce higher amounts of overland flow that increase entrainment of soil particles. Conversely, soil erosion itself has potential impacts on global climate change, as it influences the movement and sequestration of carbon (Owens, 2020). Several studies (e.g., Lal, 2003; Stallard, 1998; Van Oost et al., 2007) have focused on the role erosion has on the terrestrial carbon cycle, as erosion can both increase and decrease CO_2 emissions by mineralization and sediment burial, respectively.

1.2.2 Sediment Connectivity

Following erosion processes, subsequent sediment delivery within the catchment is dependent on the catchment connectivity, which is defined as the degree of coupling between sediment sources and sinks (e.g., Cavalli et al., 2013; Heckmann and Schwanghart, 2013). Spatial changes in these connectivity pathways (i.e., the coupling or decoupling of certain sources to the sink) are essentially responsible for the inconsistency between erosion occurring within the catchment and observed SS yields at the catchment outlet (i.e., the 'sediment delivery problem'; Walling (1983). Understanding connectivity patterns and temporal changes therein inform about landscape processes, allowing for the implementation of measures combatting soil erosion and sediment delivery, and contribute to improving soil erosion and sediment transport modelling (Keesstra et al., 2018).

The degree of connectivity is, under natural conditions, influenced by geological and geomorphological factors (e.g., parent material, tectonics, relief, landforms), climatic conditions (e.g., rainfall amount and intensity, temperature) and biota (vegetation and fauna) (Keesstra et al., 2018). Furthermore, human activities including agricultural practises, grazing, mining, burning and roads, have distinct impacts on structure and functioning, and thus on the existing connectivity of geomorphic systems (Marsh, 1864). An important factor in connectivity research is the dis-connectivity that is often prevalent, due to interferences in relief patterns, fauna, flora or reservoirs in rivers and streams (Fryirs et al., 2007) that are present at the aggregate, pedon, slope and catchment scale (Keesstra et al., 2018). Fryirs (2012) identified buffers, barriers and blankets as the three different types of intermediate sediment stores that could interrupt catchment connectivity

patterns. Buffers are identified as landforms that prevent sediment from entering the channel network. These often include large sediment sinks such as alluvial fans and swamps. Barriers interrupt sediment movement along the channel network, and include dams and woody debris. Blankets are features disrupting the surface-subsurface interaction and are controlled by the bed material and characteristics of the soil, such as sand sheets and fine material in the interstices of gravel bars. These blockages prevent most of the eroded sediment from being directly transported towards the streams or catchment outlet, explaining why observed runoff and sediment yields are not just the simple sum of the erosion of the key sources (e.g., Keesstra et al., 2018; Walling, 1983).

Spatial connectivity pathways are not fixed features, but change over time due to differences in prevailing conditions (e.g., Baartman et al., 2013a, 2013b; Parsons and Stone, 2006; Römkens et al., 2002). Laboratory experiments and modelling have shown that the same rainfall events, run in different sequences, did not result in the same SS yields (Baartman et al., 2013a, 2013b; Parsons and Stone, 2006; Römkens et al., 2002). Differences in connectivity patterns explained these variations (Fryirs et al., 2007): large, high intensity, rainfall events, are generally able to create better connectivity between sources and streams, while smaller rainfall events result in less well-developed connectivity patterns, resulting in higher levels of intermediate sediment storage and higher numbers of blockages.

1.2.3 In-Stream Sediment Transport Processes

The eroded particles are subsequently deposited at other locations within the catchment or reach surface water bodies, mostly rivers and streams (e.g., Walling, 1983). There, sediments are further transported when the bed-shear velocity surpasses the critical point for the initiation of motion. Whether sediment is transported or not depends on the ratio of this bed-shear velocity to the settling velocity (van Rijn, 1984). The settling velocity, in turn, depends on the particle shape, size and density. Depending on this ratio, transport can then take place through a range of different processes (Grotzinger et al., 2007; van Rijn, 1984). Coarser particles (i.e., boulder to sand size classes) are usually transported as bedload, while finer particles (i.e., fine sand to clay classes) are transported within the water column as suspended sediment (SS) load or (dissolved) wash load (Figure 1.3).

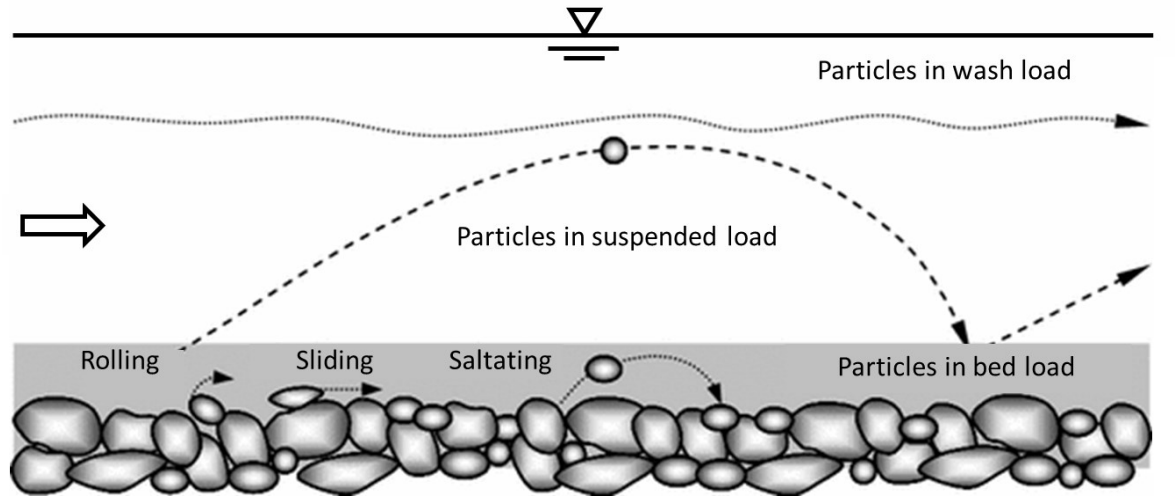

Figure 1.3 Sediment transport in rivers, as bed load, suspended load and wash load. From Dey (2014).

For the coarser particles, the bed-shear velocity might just be strong enough to initiate their movement. This results in transport processes such as rolling or sliding, where particles remain in constant contact with the riverbed (van Rijn, 1984). With increasing values of the bed-shear velocity, or with decreasing particle sizes, particles can be moved along the riverbed by the process of saltation (van Rijn, 1984). Large proportions of the sediment load observed within rivers comprise SS (e.g., Misset et al., 2019; Turowski et al., 2010), which is kept in suspension by the prevailing hydraulic conditions, and generally accounts for 80-90% of the total sediment load (Turowski et al., 2010). Several authors have divided the SS load into two categories. The first category concerns the fraction of the SS that does interact with the riverbed (van Rijn, 1984). Upon a lowering of the bed-shear velocity, the transport of SS might be reduced. This can cause the SS to be temporarily stored in the riverbed, from where it can be remobilised upon an renewed increase in bed-shear velocity (e.g., Lawler et al., 2006; Walling et al., 2000). Therefore, the riverbed can act as a source or sink of fine sediment, depending on the prevailing hydraulic conditions. The second category concerns the particles that do not interact with the riverbed or bank, the so-called (dissolved) wash load fraction (e.g., Navratil et al., 2012). These particles are expected to be transported through the river system without any notable deposition and resuspension from the riverbed.

Suspended sediment is mainly transported as flocculated material (Droppo and Ongley, 1994), with flocs representing a complex matrix composed of microbial communities, organic particles (e.g., detritus), inorganic particles (e.g., clays and silts) and interfloc spaces (pores) that allow for the retention or through-flow of water (Droppo, 2001). In-stream hydrodynamic processes affect the formation and aggradation of flocs, having the capacity to potentially alter the flocs in terms of their size, shape, density and porosity. Flocculated and aggregated particles continuously interact with

other entities within the aquatic environment, which influences their composition (e.g., Grangeon et al., 2012; Spencer et al., 2022): the aquatic environment provides new building materials that can be incorporated in these particles, as well as energy, nutrients and chemicals for biological growth (Droppo, 2001). These processes can change the way flocs behave; for example, in terms of physical behaviour (e.g., settling faster with increasing weight) and chemical behaviour (e.g., how contaminants and nutrients are adsorbed and transformed) (e.g., Leppard, 1985; Liss et al., 1996). Therefore, changes to the composition of the flocs have important implications for the fate of SS and its associated contaminants.

Elevated concentrations of SS (Figure 1.4) can be a direct cause of freshwater pollution (Vörösmarty et al., 2010). Sediment-associated contaminants and nutrients can negatively affect aquatic ecosystems by means of e.g., eutrophication, together with losses in ecosystem services and biodiversity (e.g., Koiter et al., 2013). Furthermore, aquatic biota can be negatively affected, since elevated SS loads could cause, e.g., the clogging of fish gills and smothering of salmonid spawning grounds (e.g., Acornley and Sear, 1999; Bilotta and Brazier, 2008; Hilton et al., 2006). Other negative effects can be related to elevated levels of turbidity, resulting in lower clarity of the water leading to e.g., reduced dissolved oxygen concentrations due to a decrease in light transmittance through the water column (Ozturk and Work, 2016). Increasing SS loads could thus potentially cause an imbalance in the healthy, natural functioning of aquatic ecosystems (e.g., Farnsworth and Milliman, 2003).

Other SS related issues can be associated with dams and reservoirs. These structures largely impact the functioning of river systems by interrupting water flows, thereby hindering the transport of SS downstream (Kondolf et al., 2018). This impacts the delivery of sediment to downstream areas, affecting the livelihoods of people living in deltas and coastal zones due to the combination of reducing sediment supplies (and sediment-bound nutrients) and rising sea water levels (Kondolf et al., 2018). As many of the reservoirs are constructed as a source of drinking water or irrigation, sedimentation reduces storage capacity and thereby affects supplies (Morris, 2020). Other disadvantages of high SS transport rates can be related to increasing water treatment costs (Hilton et al., 2006; Owens et al., 2005; Vörösmarty et al., 2010). Furthermore, sediment transport and subsequent morphological changes to rivers and streams can impact flood risk, mainly induced by a reduction of the channel capacity (e.g., Nones, 2019; Wheater and Evans, 2009).

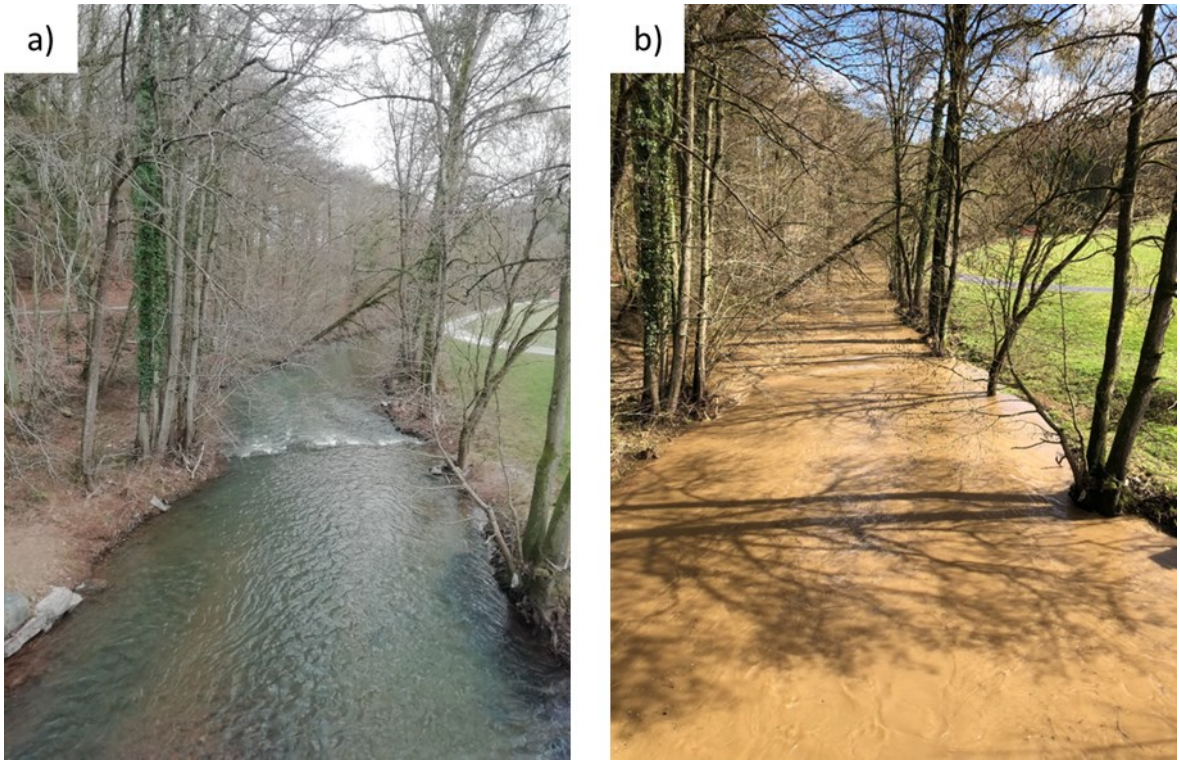

Figure 1.4 Attert River at Everlange (Luxembourg) during low flow conditions on the 22nd of February 2021 (a), and after a storm runoff event on the 13th of March 2021, showing high concentrations of suspended sediments (b).

1.2.4 Sediment Management

The off-site impacts of elevated SS delivery can be detrimental (e.g., Mekonnen et al., 2015), leading to potential problems (see section 1.2.3). Many studies have therefore focused on attempting to tackle the problem at its roots, by trying to reduce erosion rates. Mekonnen et al. (2015), however, highlights that in many situations, especially in developing countries, it is hard to control soil erosion. Therefore, it can instead be more useful to better understand sediment flow paths and dynamics to thereby delay or hamper sediment delivery (Abedini et al., 2012; Baartman et al., 2012, 2013a; Keesstra, 2007; Keesstra et al., 2009). To this end, the challenge is to create sediment sinks inside the catchment. These measures do not prevent erosion, but can help reduce water flow velocities, enhancing water infiltration, and trapping of sediment.

There is a range of different vegetation types that can be used to achieve such sediment trapping effects, e.g., grass strips planted along the contours of agricultural fields (Kagabo et al., 2013; Wanyama et al., 2012). These grass strips allow for better infiltration of water, reducing the runoff and runoff velocity, thereby reducing the sediment transport capacity (Kagabo et al., 2013; Wanyama et al., 2012). The sediment trapping efficiency has been found to be dependent on the grass species used (Wanyama et al., 2012). Furthermore, grassed waterways can prevent erosion

and gully formations by planting grasses along man-made or natural drainage lines. Other types of vegetation, such as shrubs, trees and riparian vegetation can also be used to trap mobilised sediment (e.g., Richet et al., 2017).

Besides vegetation, barriers can comprise structural measures. Such measures are designed to intercept runoff, thereby reducing sediment transport through the trapping of sediments transported by surface runoff or by river flows (Mekonnen et al., 2015). Based on the same principle as the vegetative sediment trapping measures, Frankl et al. (2018) reported on the successful reduction of sediment transport upon the implementation of woody barriers. These barriers were placed inside an open-field agricultural catchment, where gullies had formed. Results showed that large amounts of sediments were stored by the barriers and that gully erosion rates were reduced. Other examples of structural sediment trapping measures include, amongst others, terraces, check dams, dams, basins and ponds. Terraces are built on sloping lands to decrease the slope of fields, thereby increasing on-site infiltration, reducing erosion and decreasing sediment transport (see review by Chen et al., 2017). Features such as grass strips could as well develop over time into terraces, reducing in the longer term the slope of the land due to the accumulated in-field sediment (Kagabo et al., 2013). Basins and ponds are implemented within channels or at edge-of-field to trap sediment from concentrated runoff, preventing off-site sedimentation (e.g., Fiener et al., 2005; Verstraeten and Poesen, 2001). Ponds constructed within channels can also capture sediment originating from stream bank erosion, which can be a major contributing source (Ramos-Scharrón and MacDonald, 2007). Check dams are mostly constructed within gullies and channels, where these fixed structures aim to control concentrated flows of water to be able to trap sediment in the eroding channels and further reduce gully erosion (Abedini et al., 2012; Sougnez et al., 2011).

All these vegetational and structural sediment trapping measures aim to reduce the amounts of sediment transport downslope. To be able to apply these measures to specific sediment source areas within a catchment, especially to those areas significantly contributing to SS load, there is a need to identify where these sources are located. This is essential for developing appropriate and targeted management solutions (Vercruysse et al., 2020). To this end, the sediment fingerprinting approach is widely used to study sediment sources within catchments (Collins et al., 2017, 2020; Collins and Walling, 2004; Krishnappan et al., 2009; Owens et al., 2016; Walling, 2005, 2013).

1.3 Sediment Fingerprinting

1.3.1 Sediment Fingerprinting - History

The sediment fingerprinting approach was developed in the 1970s to provide information on the sources of SS transported by rivers and streams (e.g., Klages and Hsieh, 1975; Oldfield et al., 1979; Wall and Wilding, 1976; Walling et al., 1979). The approach relies on comparing physical and/or chemical properties measured on potential source samples to those measured on target SS samples. For example, the initial studies used minerology, geochemical properties and mineral magnetic properties as sediment fingerprints to discriminate between the potential SS sources, and thereby identify the origin of the SS sampled in the studied catchments.

Even at the initial stages, different ways to classify potential sources were used. Studies by Oldfield et al. (1979), Walling et al. (1979) and Wall and Wilding (1976) presented a discrimination based on source types, with a differentiation made between surface, subsurface and channel banks. The assessment was limited to identifying which source was most likely to be the dominant contributor. Klages and Hsieh (1975), on the other hand, applied a more spatially distributed approach by considering different tributaries within a catchment as SS sources. At a later stage, sediment fingerprinting approaches became more quantitative by using increasingly advanced statistical methods and modelling approaches, allowing quantification of the relative SS source contributions to the observed in-stream target SS samples (e.g., Collins et al., 1997a). Since the early studies, an array of new fingerprint properties has been tested and applied over time, creating increasing opportunities to achieve more rigorous and robust source apportionment results (Owens, 2022). As highlighted in reviews (e.g., Collins et al., 2020; Walling, 2013), the number of sediment fingerprinting studies rapidly increased after the initial studies and continues to rise. Another key advancement in sediment fingerprinting studies considers the use of composite fingerprints (Walling, 2005); using more than one sediment fingerprint property to distinguish between sediment sources. Walling et al. (1993) showed that single diagnostic sediment properties were not reliable for discriminating between sources, stating that physical and chemical properties might be subject to changes. Moreover, values of specific properties as measured in the SS transported through the river system might be representative of more than one potential source (Collins and Walling, 2002). In response to this potential challenge, composite fingerprints were used (Collins, 1995; Collins et al., 1996; He and Owens, 1995; Oldfield and Clark, 1990; Walling et al., 1993; Walling and Woodward, 1995). The use of several properties within the composite fingerprint improves the likelihood that source-sediment relations can be more discriminating, using a set of properties that is more likely to be unique for one or a limited number of sources. Furthermore, developments in quantitative, as opposed to qualitative procedures, were introduced, using statistical verification of

a range of properties to discriminate sources, as well as multivariate un-mixing models to determine sources in a more reliable and consistent manner (Collins, 1995; Collins et al., 1996, 1997a; He and Owens, 1995; Walling et al., 1993; Walling and Woodward, 1995; Yu and Oldfield, 1989, 1993). Combined with techniques assessing the uncertainty in source properties through the use of Monte Carlo techniques (Franks and Rowan, 2000; Rowan et al., 2000), where the outcomes were then used to give an uncertainty range (e.g., mean and standard deviation) on the modelled source apportionment. Including an uncertainty assessment in sediment fingerprinting modelling has now become a standard procedure.

Initially, the sediment fingerprinting approach was mainly applied for scientific interests. It was advocated (e.g., Gregory and Walling, 1973; Schumm, 1977) that information on sediment sources is an important requirement to create an improved understanding of erosion and hydro-sedimentary processes, as well as integrating studies regarding sediment mobilisation and sediment transportation within a catchment framework. Other early applied studies focused on environmental issues associated with the importance of sediment as a carrier of nutrients and contaminants. This because during the same time in which the first sediment fingerprinting approaches were developed and reported on, the transfer of nutrients and contaminants by fine sediment was increasingly recognised as a threat to aquatic ecosystems (e.g., Allan, 1986; Förstner and Muller, 1974; Golterman, 1977; Golterman et al., 1983; Horowitz, 1985; Shear and Watson, 1977).

In later years, the focus of the sediment fingerprinting approach has shifted to address issues related to catchment management (e.g., Bilotta and Brazier, 2008; Owens et al., 2005; Poesen, 2018). Many studies have investigated dominant SS sources inside certain catchments, allowing a targeted approach to those sources that are mainly responsible for the in-stream observed SS. The sediment fingerprinting approach has thus provided the means to assist in making management decisions and policy developments (Owens, 2022).

1.3.2 Current Status of Sediment Fingerprinting Research

The sediment fingerprinting approach generally consists of three steps (Figure 1.5). The first step concerns the identification and subsequent sampling of potential sediment sources. Sources are identified e.g., during field visits, in which areas showing erosion (e.g., rills and gullies) and potential sediment connectivity pathways are used as evidence (e.g., Walling, 2013). Sources can also be identified using satellite images or Geographic Information Systems (GIS) tools to detect potential source areas or connectivity patterns (e.g., Borselli et al., 2008; Cavalli et al., 2013). Once potential sources are identified, samples are collected. Target sediment samples are also collected, using e.g.,

time-integrated SS sampling (e.g., Philips sediment trap; Phillips et al., 2000) or manual sampling by collecting deposited bed sediment (e.g., Nosrati et al., 2018; Vale et al., 2016). Soil source and target sediment samples are then brought to the laboratory for preparation (e.g., drying and sieving).

In a second step, source and sediment samples are analysed, generally for physical or geochemical properties, which are used as sediment fingerprints (Walling, 2013). A wide range of fingerprints has been applied and reported on, including: geochemistry (Foster and Walling, 1994), sediment colour (Grimshaw and Lewin, 1980), colour properties (Martínez-Carreras et al., 2010a), plant pollen content (Brown, 1985), mineral magnetic properties (Oldfield et al., 1985), fallout radionuclides (Wallbrink et al., 1998), stable isotopes (Revel-Rolland et al., 2005), Compound Specific Stable Isotope (CSSI) (Blake et al., 2012; Upadhayay et al., 2022), eDNA (Frankl et al., 2022), spectral reflectance in the visible and near infrared range (Martínez-Carreras et al., 2010a) and infrared spectroscopy (Poulenard et al., 2009). An informed decision is needed to select those fingerprint properties that could be best used under given circumstances (i.e., to allow for proper discrimination between potential sediment sources). An important requirement regarding the use of measured fingerprints is that they need to behave in a conservative manner, meaning that the properties must not undergo physical or chemical transformations during the processes of erosion, transportation and possible deposition and resuspension (e.g., Collins et al., 2020; Koiter et al., 2013; Walling, 2013). Applied fingerprint selection methods therefore often involve the elimination of those sediment-associated properties that are non-conservative, followed by statistical tests to (i) identify the discriminatory power of potential fingerprints between at least on the sources (i.e., Kruskal-Wallis H test), and (ii) define a minimum set of fingerprints that maximizes discrimination between the potential sources (e.g., linear discriminant analysis).

Then, in a third step, un-mixing models are often applied (see also section 1.4.4), using the selected set of fingerprints to quantify contributions of the potential sources to the target sediment. So-called frequentist models have been used, commonly minimizing the sum of squared residuals (Collins et al., 1997a), or e.g., using parameter optimization couples with Monte Carlo uncertainty analysis (Collins et al., 2013). However, these models were often shown to be inconsistent in their uncertainty representations, and also to lack structural flexibility to coherently translate all sources of error into modelling results. Bayesian un-mixing models have become widely adopted as a more robust alternative (Cooper et al., 2014a).

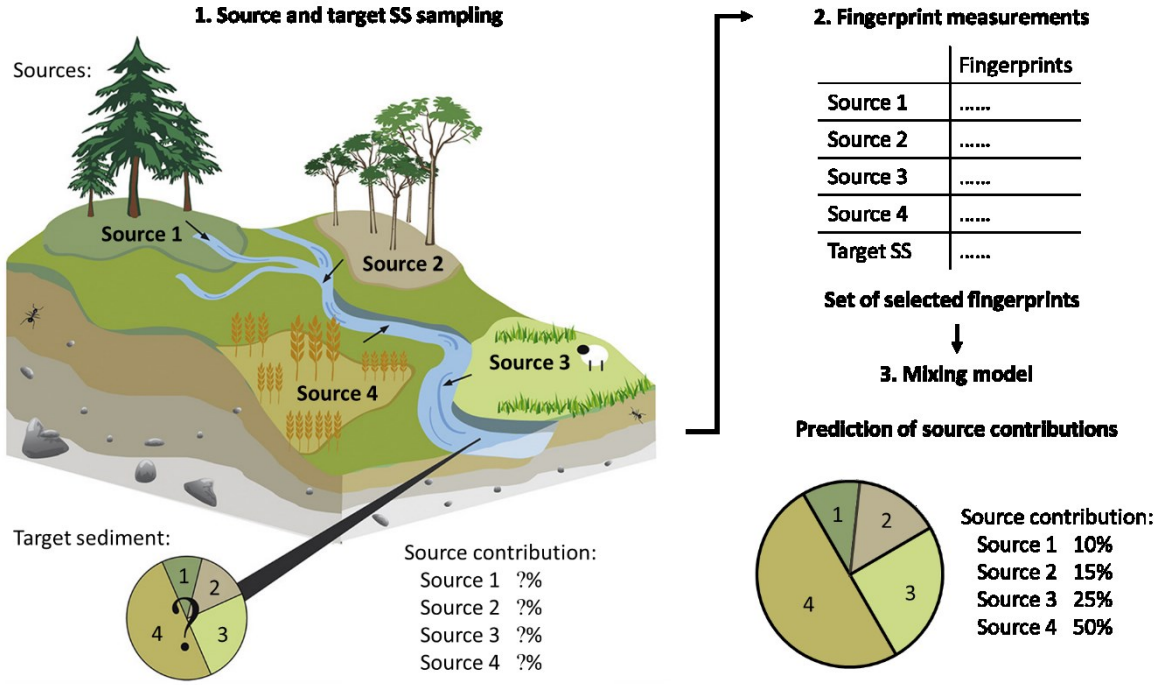

Figure 1.5 Schematic representation of the typical sediment fingerprinting methodology. Panel (1) is adapted from Gaspar et al. (2019).

1.4 Sediment Fingerprinting: Limitations and Research Gaps

1.4.1 Particle Size

One of the most important issues in sediment fingerprinting is that of particle size (see review by Laceby et al., 2017). Erosion and sediment transport processes are selective with respect to particle size. This process starts with the initial detachment of particles from the soil surface, with clay particles being more resistant to detachment due to their bonding with the substrate, while coarse sand may be resistant to detachment due to size and weight (Bradford et al., 1992; Poesen, 1992). In contrast, silts and finer sands can be more subject to detachment due to the absence of bonding with the substrate and their lighter weights (Poesen, 1992). Once particles are detached and transported to the stream network, particle size directly influences settling velocities and thus the transport and deposition of sediment (Walling et al., 2000).

Fluvial SS transport processes change the properties of the material transported, when compared with the properties observed in the original source material (Laceby et al., 2017). Generally, average particle size decreases, while the roundness of particles and the sorting of the SS increases with distances travelled. These changes to the particle sizes and shaping of the particles subsequently affect the associated properties that are used to fingerprint SS sources. There are many fingerprints used within the sediment fingerprinting community that are recognized for their different affinities

to different particle sizes, with fingerprint property values often varying with particle size in a manner that is non-linear and difficult to generalize (Horowitz and Elrick, 1987; Russell et al., 2001). These include fallout radionuclides (Horowitz and Elrick, 1987) and geochemical properties such as total organic carbon (Wynn et al., 2005), that are generally enriched in the finer particle size fractions. Furthermore, mineral magnetic properties (e.g., Hatfield and Maher, 2009) and colour parameters (e.g., Pulley and Rowntree, 2016) are linked to different size fractions.

Changes observed to the particle sizes between potential sediment sources and target sediment might therefore complicate sediment fingerprinting procedures, as potential source materials cannot simply be compared with the target SS. To this end, several methods have been introduced to ensure that the same size fractions are compared, and thus comparable fingerprint properties between the source and target sediment material are considered. Fractionation is commonly used (Laceby et al., 2017), which addresses the potential impacts of different particle size related fingerprints by sieving both the collected potential source and target sediment samples to defined, comparable particle size fractions. Thereby, the isolated fraction should include the range of fingerprint property values in the potential sources (Laceby et al., 2017). The size fraction <63 µm is often used (Walling et al., 1993), as this fraction is considered to account for the majority of the SS load transported in rivers (e.g., Legout et al., 2013; Walling et al., 2000).

However, different size fractions are also used since it is recognised that the <63 µm fraction should not be adopted without scrutiny. For example, the <10 µm fraction is often used in Australian rivers (Douglas et al., 2003; e.g., Olley and Caitcheon, 2000). The fine silts and clay material in Australian river systems is considered as the dominant size fraction, being of particular interest due to the fact that this fraction has the largest impact on the water quality. Fractionation can thus also be applied to a fraction that is of particular interest (Laceby et al., 2017). Therefore, simply selecting a commonly used fraction of <63 µm may not be sufficient to give robust un-mixing outputs that are not affected by further differences in particle size between sources and target SS (Collins et al., 2017, 2020). The choice of the fraction used for investigation requires robust justification, as the chosen fraction for analysis influences the source apportionment results (Haddadchi et al., 2015). Ways to investigate different fractions, and their effects on the sediment fingerprinting results are presented by, for example Gaspar et al. (2019, 2022) and Motha et al. (2002).

Furthermore, though controversial in sediment fingerprinting (Owens et al., 2016), another approach to deal with differences in particle size is through the application of correction factors. Simple correction factors are based on the ratio of particle size distribution (PSD) measures such as median particle size or specific surface area (Collins et al., 1997a; Koiter et al., 2018). It is thereby mostly assumed that there is a linear relation between the fingerprint property concentration and

particle size. Several studies (Foster et al., 1998; Russell et al., 2001; Smith and Blake, 2014; Taylor et al., 2014) have shown, however, that such relationships can be much more complex, being fingerprint-specific and site-dependent. Other studies have shown that relationships can be variable during different times of sediment transport (Stone and Walling, 1997); particle size composition and organic matter content change when being transported from source to sink. Due to the reported uncertainties involved with these correction factors (Smith and Owens, 2014), care must be taken as source apportionment results might be significantly impacted by their adaption and it has become more commonplace not to apply them when using un-mixing models (Collins et al., 2017).

1.4.2 Fingerprint Conservatism

An important aspect within sediment fingerprinting is the selection of those fingerprints that allow for source discrimination and ultimately for the apportionment of the source contributions to the target sediment (e.g., Collins et al., 2017; Walling et al., 1993). To select a useful sediment fingerprint, there are two important aspects that need to be considered. First, it must be able to differentiate between the identified potential sources. Second, fingerprints must behave in a conservative manner. In the context of the sediment fingerprinting approach, conservatism refers to the concentration of the sediment fingerprint property that has to remain unchanged when being transported from the sources to the sink (i.e., the location from where the target sediment sample is collected). However, evidence has shown that fingerprint properties might change at different moments during transportation (see reviews by e.g., Collins et al., 2020; Koiter et al., 2013; Walling, 2013). Changes in fingerprint properties depend on the level of chemical, geochemical and/or mineralogical stability related to specific fingerprints (e.g., Davis and Fox, 2009; Koiter et al., 2013; Motha et al., 2002). That stability depends on the chemical reactivity of the fingerprint in response to the prevailing physical-chemical and biological conditions.

However, while the assessment of fingerprint conservatism is of important consideration, current tests assessing fingerprint conservatism remain a black-box approach (Koiter et al., 2013). There is only limited work exploring fingerprint conservatism during the sediment transport process (e.g., Motha et al., 2002). Standard procedures consider whether or not fingerprint values from target SS are within the limits of the fingerprint values measured from the different identified source samples. To this end, fingerprint values falling within the limits are thus potentially used even when transformations during transport cannot be discounted, eventually adding uncertainties to the estimation of source contributions. Despite the sediment fingerprinting community being aware of this problem (Cooper and Krueger, 2017; Sherriff et al., 2015), there are no formally agreed tests to investigate potential fingerprint transformations during sediment transport (Collins et al., 2017).

Changes to sediment fingerprint properties can also occur after sediment is deposited (Koiter et al., 2013). This could thus as well challenge fingerprint conservatism, with sediment fingerprinting properties no longer representing the properties of its original sources (Koiter et al., 2013). This has for instance been observed by Foster et al. (2006), who reported that the radionuclide ^{137}Cs was mobilised from deposited sediments. Furthermore, Hudson-Edwards et al. (1998) reported on the chemical remobilisation and the downward translocation of different chemical elements in floodplain deposits. In Smith and Owens (2014), bed samples were compared with the samples collected by a Phillips sediment trap (Phillips et al., 2000). It was observed that although there was no significant difference in particle size composition, properties such as geochemical and biological characteristics might vary between the two. It is therefore important to carefully consider sediment conservatism. Especially with fingerprint properties (e.g., particle size and geochemical properties) that can change when samples are left inside sampling equipment such as the Phillips sediment trap for long times, or when samples are stored before starting laboratory analyses (e.g. due to adsorption/desorption; Smith and Owens, 2014).

1.4.3 Fingerprint Selection and Source Discrimination

Sediment fingerprinting studies use a wide range of soil and sediment properties for source fingerprinting (see section 1.3.2). This array of available fingerprints has increased over time due to improved analytical capabilities, whereby samples can be analysed faster for a greater number of fingerprints (Sherriff et al., 2015). Walling (2013) describes the need that for most early sediment fingerprinting studies, sampling techniques were heavily depending on the amount of soil sample and sediment that had to be collected in order to proceed with the analysis of fingerprint properties. For instance, for the analysis of radionuclides or geochemical sediment properties, relatively large amounts of sediment were needed (e.g., ≥20 g). Developments have helped to progressively reduce the required masses needed (Walling, 2013).

Another major development concerns the transition from using a single fingerprinting property towards the use of composite (i.e., multiple property) fingerprints for source discrimination (Collins et al., 2020). A single sediment property was used in source fingerprinting in the early stages of the approach. However, later work acknowledged that the use of several fingerprints was needed to be able to discriminate between several potential SS sources and to provide more robust source apportionment outcomes (Collins and Walling, 2002; Walling et al., 1993; Wasson et al., 2002). This is related to the potential uncertainties of using fingerprinting properties, such as non-conservatism, which can influence the fingerprinting results. Therefore, by including several properties, some uncertainties are mitigated (Collins et al., 2020), with a further strengthening of the reliability of the un-mixing results upon the inclusion of additional properties (Walling, 2013).

As a minimum, n-1 fingerprint properties must be included in the linear un-mixing models to discriminate between n sources (Phillips and Gregg, 2003), where the structure of a standard linear un-mixing model should fulfil the following requirements:

$$\sum_{j=1}^{m} a_{i,j} \times w_j = b_i$$

which satisfies the following constraints:

$$\sum_{j=1}^{m} w_j = 1$$

and

$$0 \leq w_j \leq 1$$

where bi is the fingerprint property i (i = 1 to n) of the sediment mixture, $a_{i,j}$ represents the fingerprint property in the source j (j = 1 to m), w_j is the unknown relative source contributions of the source j. Herein, m represents the number of potential sources and n represents the number of fingerprint properties selected.

Furthermore, the use of composite fingerprints that include properties from different groups of fingerprinting properties (e.g., combining geochemistry and colour properties) can further improve source discrimination (Collins et al., 2020; Collins and Walling, 2002; Walling, 2013). These composite fingerprints can thereby improve the robustness of the un-mixing results, providing a greater assurance that the influence of non-conservative fingerprints or certain fingerprints with poor discrimination potential is further limited (Collins et al., 2020). Collins et al. (2020) highlighted that the selection of fingerprint properties needs to be carefully assessed and analysed to create robust composite fingerprint signatures. Therein, the physical basis for discrimination of the potential SS sources is an important consideration, though explicit assessment of this physical basis is often lacking in sediment fingerprinting studies. This while the selection of fingerprints is shown to potentially impact SS source apportionment results (e.g., Gaspar et al., 2019; Laceby et al., 2015; Lizaga et al., 2020b).

Current approaches to selecting suitable fingerprints often rely on a three step procedure, using (i) a range test to exclude properties outside the source property values, (ii) a Kruskal-Wallis test to identify those fingerprints that discriminate between at least one of the sources, and (iii) a discrimination (e.g., linear discriminant function analysis) to define the minimum set of fingerprints that allow for the best discrimination between the sources (e.g., Collins and Walling, 2002; Palazón et al., 2015; Smith and Blake, 2014). However, other fingerprint selection methods are applied (as highlighted in Evrard et al., 2022) including: (i) maximising the number of fingerprints by only

disregarding those failing the range test; (ii) process- or knowledge-based frameworks that consider the interpretation of the source fingerprinting properties, and (iii) methods that identify consistent fingerprints, which do not create mathematical inconsistencies in the potential modelling results. The reliability of these often used methods is however debated by (Latorre et al., 2021; Lizaga et al., 2020b), who proposed new methods for robust fingerprint selection, allowing non-erroneous, consistent and conservative input fingerprints for models.

There are limitations on the total number of sources that can be accurately discriminated. There are specific suggestions to limit the number of sources, where e.g., Lees (1997) and Vale et al. (2022) suggested to include a maximum of four sources. Limiting the number of sources is related to the observed decrease in discrimination as sources are likely to become more similar when including an increasing number of sources (Vale et al., 2022). This means that finding a fingerprint property that strongly discriminates one source from all other sources is becoming increasingly difficult, resulting in less robust source apportionments results.

The development of new fingerprint properties and the use of approaches such as composite fingerprints has contributed to an increasing range of potential SS sources being successfully discriminated (Walling, 2013). This development has thereby enhanced the sediment fingerprinting technique, providing more rigorous and robust source apportionment results (Owens, 2022). Therefore, the development of new fingerprints is likely to remain an important direction of research to progress developments for the sediment fingerprinting approach.

1.4.4 Model Evaluation

Sediment fingerprinting un-mixing models are used to quantitatively estimate the relative contributions of the potential sources to the target sediment. Modelling exercises were initially undertaken by applying frequentist-based approaches (e.g., Collins et al., 1997a; Walling et al., 1999), using optimization techniques to minimize residuals between source and target SS properties to estimate relative source contributions. More recently, Bayesian modelling approaches have gained a more widespread attention in sediment fingerprinting (Cooper et al., 2014a). The advantages of Bayesian un-mixing models include a better incorporation of prior information on source contributions (Cooper and Krueger, 2017), and a more robust incorporation of uncertainty (Nosrati et al., 2014; Rowan et al., 2012). Bayesian un-mixing models can thereby capture source uncertainties including spatial variability in sediment fingerprint properties across the study area, uncertainties associated with instrumental precision, covariances between properties of fingerprints, and residual model errors (Cooper et al., 2015). With several of these Bayesian un-mixing model frameworks (as well as several frequentist models) being open-source,

including standard operating procedures and graphical user interfaces, they provide the tools to achieve some sort of standardisation which should enable the reproduction and comparison of results (Owens et al., 2016).

Uncertainties related to the use of un-mixing models and especially the estimation of un-mixing uncertainties, are not well quantified and remain difficult to assess. Peart and Walling (1988) already identified the need to use independent evidence to evaluate sediment fingerprinting results. With datasets becoming increasingly complex, the evaluation of the un-mixing model outcomes is becoming even more important (Gaspar et al., 2019). This is especially pertinent when trying to understand the sediment dynamics within complex landscapes, where soil erosion, storage and export of sediments are influenced by complicated topography and land use patterns (Gaspar and Navas, 2013; Navas et al., 2013). Subsequent evaluation can then support the managers and stakeholders who require both accurate (low error) and precise (low uncertainty) sediment source information. While model precision can often be evaluated from modelling frameworks based on Bayesian and/or Monte Carlo based methods (Batista et al., 2022), evaluating the subsequent accuracy is more challenging. To help evaluate this accuracy of sediment fingerprinting model outcomes, artificial mixtures consisting of known proportions of sediment sources can be used (e.g., Franks and Rowan, 2000; Gaspar et al., 2019; Haddadchi et al., 2014b; Martínez-Carreras et al., 2010c). These artificial mixtures can be created in the laboratory by combining known contributions of source material, with subsequent source proportions estimated by the un-mixing model then being compared to the known source input contributions to the artificial mixtures.

To reduce the laboratory workloads involved in the preparation and analysis of fingerprints from artificial source mixtures, virtual mixtures have gained increasing attention in recent years (e.g., Batista et al., 2022; Palazón et al., 2015; Sherriff et al., 2015). In these virtual mixtures, fingerprint values are generated mathematically. Virtual mixtures can be easily created without additional costs, being of particular advantage when costs involving the analyses of fingerprint properties are rather high. Furthermore, virtual mixtures allow for the introduction of different uncertainties, and different levels of uncertainty effects on un-mixing model outcomes that can therefore be relatively easily evaluated. Batista et al. (2022) showed that the use of virtual mixtures was as robust as using laboratory artificial mixtures.

With the application of artificial or virtual mixtures, both the accuracy of the un-mixing model procedures (Gaspar et al., 2019), or proof-of-concept experiments that propose novel sediment fingerprint approaches (Batista et al., 2022) can be assessed. Evaluation can thus help to provide a further strengthening of the un-mixing model used by assigning a measure of robustness to their predicted source apportionments. This is now increasingly seen as being crucial for the support of

decision making and advancing modelling approaches (Batista et al., 2022). However, only few studies have evaluated un-mixing model outputs by using real soil sources and artificial mixtures (e.g., Batista et al., 2022; Gaspar et al., 2019; Haddadchi et al., 2014b).

Though artificial and virtual mixtures can be used to evaluate the ability of models to un-mix source apportionments in controlled settings, they cannot provide definite information with regard to the source apportion accuracy in real world situations. It could therefore be useful to pursue other means of evaluating the un-mixing modelling results. Other potential evaluation methods could be based on the use of alternative datasets such as sediment transport rates (Batista et al., 2021), sediment budgets (Tiecher et al., 2022), outputs of hydro-sedimentary models, modelled catchment erosion (Wynants et al., 2020), remote sensing data (Lizaga et al., 2020a), or simple knowledge based approaches depending on local knowledge and self-made observations (Evrard et al., 2022).

1.4.5 Source Variability

The number of sources used to discriminate amongst should be limited, though the number of sources need to provide meaningful insights into the erosion and sediment delivery processes that occur within a catchment (Evrard et al., 2022). To allow for a proper discrimination, Evrard et al. (2022) suggest that researchers make sure that the sources considered are sufficiently different to allow proper discrimination. To correctly characterize each source (i.e., land use), a sufficient number of samples should be collected, where samples should well represent the spatial variability of that particular source inside the catchment.

To this end, various sampling methods are commonly used to ensure all major sources within a field are being sampled (see review by Collins et al., 2020). Collins et al. (2020) thereby suggest that the common practise of bulking replicate samples from the same field into a single composite sample should be avoided; there is no guarantee that a bulked sample value is similar to the average value of separately analysed samples. However, to investigate each collected sample separately requires more resources (i.e., related to sampling and analysis), which is often not feasible. Thus, limitations in the number of samples that can be collected and analysed can be a major restriction in gaining insights into the spatial variations of fingerprint properties.

The same limitations apply to the characterisation of temporal changes in potential source properties. Source material sampling is mostly conducted during a single sampling campaign (Collins and Walling, 2004). For many fingerprints this sampling strategy might be sufficient, though, there are certain fingerprint properties (e.g., organic fingerprints) that are influenced by seasonal variations (Ben-David et al., 1998; Bilby et al., 1996), as well as by biotic and abiotic factors (Collins

et al., 2019; Lauber et al., 2013). Investigations into changes of source properties are often limited and there is a lack of understanding of their magnitude and predictability over space and time. Therefore, if repeat source sampling campaigns are absent, careful consideration might be needed regarding when certain fingerprints can be used.

1.4.6 Non-Standardized Methods

With an increasing number of publications over recent years, an expansion in methodologies has been reported in source fingerprinting studies (Collins et al., 2020; Owens, 2022). Diversity in method developments has originated from a growing number of groups working on the sediment fingerprinting approach (Collins et al., 2020). The method developments as outlined by Owens (2022) comprise several elements, involving: (i) the examination of potential new fingerprints, (ii) assessing ways to better sample and characterize sediment and source material, (iii) developing protocols, statistical approaches and models that provide more accurate source contribution estimates and information on their uncertainties, and (iv) evaluating the accuracy and precision of the results derived from models by using either artificial and virtual mixtures. These developments helped the sediment fingerprinting technique to evolve, allowing for a more robust and rigorous sediment source apportionment. However, too much method development can lead to a divergence of approaches and thereby a lack of method standardization. This has occurred despite calls for, and development of, more generic methodological steps (e.g., generic decision trees: Collins et al., 2017; Collins and Walling, 2004).

For example, there is a lack of general agreement within the sediment fingerprinting community regarding the different fingerprint selection methods. The large ranges of applied methods and the lack in general of agreed methodological procedures challenges a more widespread uptake of the approach as a standard tool for scientific and management goals (Collins et al., 2017; Mukundan et al., 2012). Furthermore, as highlighted by Collins et al. (2017), many papers do not include the description of key methodological steps, increasing the possibility of major uncertainties related to the study outputs. This lack of standardisation is therefore undermining the credibility of the sediment fingerprinting approach (Collins et al., 2020).

1.4.7 Disconnection between Science and Catchment Management

Sediment source fingerprinting has gained widespread popularity in scientific research due to its potential to reduce problems of cost and representativeness of traditional sediment monitoring methods (Collins and Walling, 2004). Initially, the sediment fingerprinting approach was conceptually simple and cost-effective against other alternatives (Owens, 2022). With the current

developments creating increasingly complex methodologies, it is likely to be less appealing as a management or operational tool (Mukundan et al., 2012). This inhibits a more widespread application of the approach.

One of the other major limitations preventing the widespread uptake by managers relates to the fact that the majority of fingerprint properties require labour intensive analysis using expensive equipment (Collins and Walling, 2004). This, together with the complex measurement methods and specific equipment needed, requiring expert knowledge (Pulley and Collins, 2021). Another reason that might explain the limited uptake beyond the academic field lies in the advanced statistical analyses and complicated modelling techniques used (Owens, 2022). To this end, the sediment fingerprinting approach is not used by managers and regulators as much as expected or desirable, causing a disconnection between science and practise (Owens, 2022).

1.5 High Temporal Frequency Sediment Fingerprinting

1.5.1 Limitations in Sampling and Analysis Procedures

Resources needed for target sediment sampling and subsequent analyses limit the number of samples that are generally analysed. Consequently, single sampling campaigns or a restricted number of sampling campaigns are performed, giving rather limited insights in the temporal variability of source contributions to the target SS (Collins et al., 2020). These limitations are inherent to the applied sampling procedures for collecting target sediment samples, with sampling strategies including: (i) point sampling, (ii) time-integrated sampling, and (iii) the automated collection of water samples. Point sampling can be done by e.g., taking large stream water samples and extracting the SS by means of flow centrifuges (Devereux et al., 2010; Motha et al., 2003), or in-stream dewatering techniques using portable centrifuge or filtration systems (Horowitz et al., 1989). Time-integrated sediment traps, e.g., as presented by Phillips et al. (2000) (Figure 1.6), rely on the large difference in diameter between the inlet of the samplers (4 mm) and the diameter of the sampler chamber (98 mm). This increase in diameter reduces the flow velocity and thereby leads to the settling of the SS. These samplers are often used for sampling during storm runoff events. The Phillips sediment trap has been shown to trap a representative SS sample with an effective particle size of <63 µm (Phillips et al., 2000; Russell et al., 2001). Automated water samplers (e.g., Oeurng et al., 2010) (Figure 1.6) collect stream water samples at fixed time intervals after starting a manual sampling programme, or can be triggered by a sensor signal (e.g., when a specified stream water level is surpassed). These samplers allow for discrete sampling, offering the potential of a finer temporal resolution (i.e., compared with a single composite sample over the whole hydrograph obtained by the sediment trap) when sampling at different times over the

hydrograph. However, automated samplers result in higher numbers of samples that need to be processed and analysed, adding to workloads and costs. Furthermore, the rather small mass of SS collected (i.e., stream water samples of only 0.5 or 1 L per sample bottle) might not be sufficient for specific fingerprint analysis.

Besides the costs and workloads associated with the deployment and maintenance of the sampling equipment, subsequent costs involved in laboratory analysis can contribute significantly. For instance, geochemistry analyses are estimated at a cost of ca. US$10-$50 per sample (Owens, 2022). The high costs involved in analysing each collected target SS sample is an important limitation in any research or monitoring budget, meaning that a limited number of samples can be analysed (e.g., Walling, 2013). As a consequence, information regarding high temporal resolution changes in source contributions to the target SS are sparse (e.g., Collins et al., 2020).

1.5.2 Problems Associated with the Current Lack of High Temporal Resolution Observations

Due to the aforementioned resource limitations, target SS samples are often collected during single measurement campaigns (Collins et al., 2020). This is despite many studies having shown that there is a potential large inter and/or intra event variability in source contributions (e.g., Cooper et al., 2015; Legout et al., 2013; Navratil et al., 2012; Vale et al., 2020; Vercruysse and Grabowski, 2019). Single campaigns might thus miss information on how SS source contributions change over time.

These temporal changes in SS source contributions can be related to the aforementioned changes in erosion and sediment transport due to e.g., variations in climatic conditions and prevailing sediment connectivity pathways (section 1.2.1 and 1.2.3). For example, when most sediment is transported during specific periods throughout the year (e.g., during extreme rainfall-runoff events or during certain seasons) (Gonzalez-Hidalgo et al., 2010), missing out on sampling these specific periods will therefore not provide the information needed to develop robust targeted management strategies. Successfully capturing the variability in source contributions thus requires methodological improvements concerning the application of high temporal frequency and/or long durational observations (Poulenard et al., 2012).

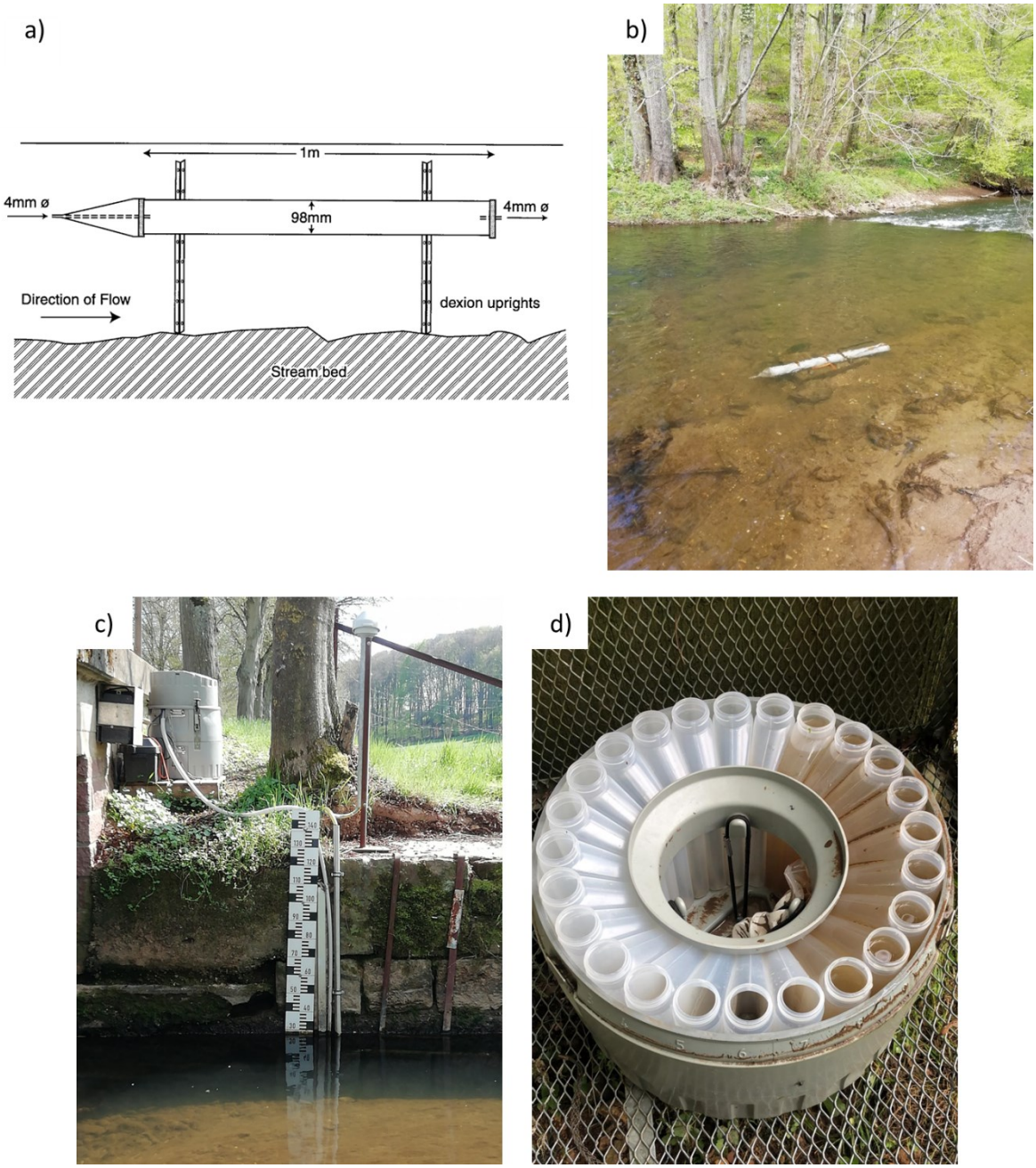

Figure 1.6 Commonly used SS sampling methods for sediment fingerprinting purposes. (a) and (b) show the schematic design of a time-integrated SS trap sampler (figure from Phillips et al., 2000) (a), and a time-integrated trap sampler installed in the Attert River at Everlange (Luxembourg) (b). (c) and (d) show an automated water sampler installed in the Roudbach River at Platen (Luxembourg) (c), and an example with filled bottles (d).

1.5.3 Low Cost Fingerprints and Resource Implications

The analyses of conventionally used sediment fingerprints is often expensive due to the required expertise, workloads involved in the sampling and analysis, and the required analytical equipment (Collins et al., 2020; e.g., Walling, 2013). To partly solve this problem, several sediment fingerprints that are easy to use and require lower associated costs and workloads have been developed. These fingerprints, which are referred to as low-cost fingerprints, are mainly developed with the goal to reduce the costs and complexities involved in the analysis of the fingerprints, by allowing fingerprints to be measured in an easier and faster manner (Pulley and Collins, 2021).

One such low-cost fingerprint is based on sediment colour, derived from scanned images obtained from an ordinary office scanner as presented in Pulley and Rowntree (2016) and further applied elsewhere (e.g., García-Comendador et al., 2021; Pulley and Collins, 2021, 2022). This method relies on commonly used approaches for sample preparation, including sieving and drying of the collected source and sediment samples. Samples are then simply placed into clear bags and scanned using an office scanner. From the scanned images, colour parameters are derived using an RGB colour model, where differences in colour parameters between the sources are then used for discrimination. Colour parameters have also been derived using different colour models from the VIS part of the reflectance spectra measured with a reflectance spectrophotometer (Legout et al., 2013; Martínez-Carreras et al., 2010a, 2010b). Here, spectra were obtained from dried and sieved samples, which were placed on a reference white panel. From the raw reflectance data, colour coefficients were computed. Besides colour derived parameters, geochemical fingerprints were also derived from the reflectance measurement in the visible and near-infrared (Cooper et al., 2014b, 2015; Martínez-Carreras et al., 2010b). Chemometrics (i.e., partial least-square regression models) were used to calibrate the spectral data with the source and SS chemistry data measured in the laboratory and later used in a predictive mode.

These low-cost fingerprinting methods still require resource-intensive sampling workloads and initial preparation of the samples that are similar to conventionally applied fingerprinting methods. These remaining resource needs can thereby still pose limitations to a wider uptake of the sediment fingerprinting approach. Furthermore, they still pose limitations to feasible repeat sampling campaigns and subsequent analyses, hampering further insights into how source contributions to the target SS change at different temporal scales. To this end, there is further need to develop strategies and methods that, besides challenging resource needs related to the analysis of conventional fingerprints, overcome the resource needs related to the initial sampling and preparation of samples.

1.5.4 The Potential for High Temporal Resolution Sediment Fingerprinting

Devices measuring e.g., discharge, SSC, turbidity and hydro-chemical data *in situ* and at high temporal resolution have supported significant improvements in the mechanistic understanding of catchment and stream functioning (Kirchner et al., 2004). Such approaches remove the needs for sampling and/or subsequent laboratory preparation of samples. However, instruments for measuring sediment-associated properties *in situ* and at high temporal frequency are limited and remain largely unexplored for sediment fingerprinting purposes (Martínez-Carreras et al., 2016).

Submersible spectrophotometers could potentially fill this gap. Spectrophotometer probes are widely used for drinking water quality monitoring (e.g., D'Acunha and Johnson, 2019; González-Morales et al., 2020; Prairie et al., 2020). They are used to detect and measure harmful metals, as well as for measuring a wide range of different inorganic, organic and biological chemicals, and colour (e.g., Prairie et al., 2020; Shi et al., 2022). Attempts to use the absorbance readings to estimate SS properties have been reported by (Bass et al., 2011; Martínez-Carreras et al., 2016; Sehgal et al., 2022). These studies used *in situ* measurements to predict concentrations of particulate organic carbon, SS loss-on-ignition, and SS carbon content and particle size, respectively.

The working principle of spectrophotometer sensors is based on the emittance of a light beam (e.g., using a Xenon-flash light; Figure 1.7). In the optical measuring path, the emitted light passes through the medium that is to be analysed (e.g., water and SS). The detector, which is located at the other side of the optical measuring path measures the transmittance, calculating the absorption over the full wavelength range. In Figure 1.7, there is a second light beam that is guided through an internal comparison section within the spectrophotometer probe. The measurement through this internal section is used for the compensation of any disturbances (e.g., ageing of the lamp).

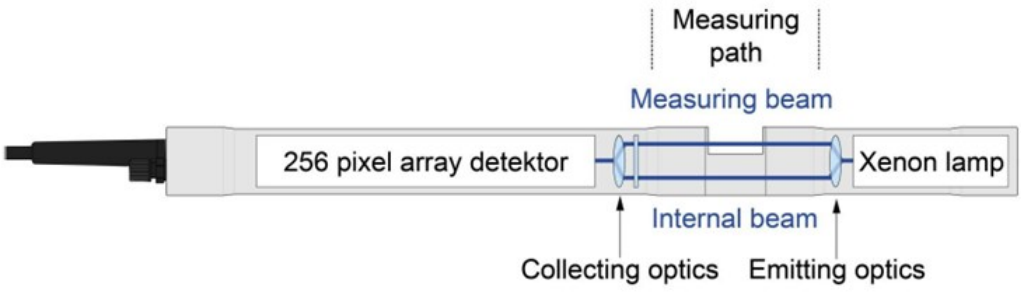

Figure 1.7 Schematic representation of the working principle of an example submersible spectrophotometer (S::can spectro::lyser™ probe ; Scan Messtechnik GmbH, Vienna, Austria). From: Scan Messtechnik GmbH (2018).

Concentrations of substances are subsequently determined by the amount of light that is partially absorbed, in specific spectral regions (e.g., as shown in Figure 1.8), using the Beer-Lambert law (Equation 1.1; as described in e.g., Fuwa and Valle, 1963).

$$A = \varepsilon \times l \times c \qquad \text{[Equation 1.1]}$$

where A is the total absorption of light, ε the absorptivity (i.e., measure on how strongly a chemical species absorbs), l the path length and c the concentration of the attenuating species.

In this thesis, it is hypothesized that different SS properties (e.g., colour, geochemistry) influence the absorbance spectra at different ranges of wavelengths (i.e., fingerprints) in which the spectrophotometer measures (e.g., UV-VIS wavelength range; Figure 1.8). Differences in observed absorbance spectra, induced by differences in properties between SS sources, can then be used for discrimination, providing a basis for source apportionment of target SS. By directly measuring absorbance *in situ*, submersible spectrophotometers could potentially eliminate sampling and subsequent laboratory analysis needs. This approach may therefore offer the means to drastically increase insights in potentially changing SS source contributions through time.

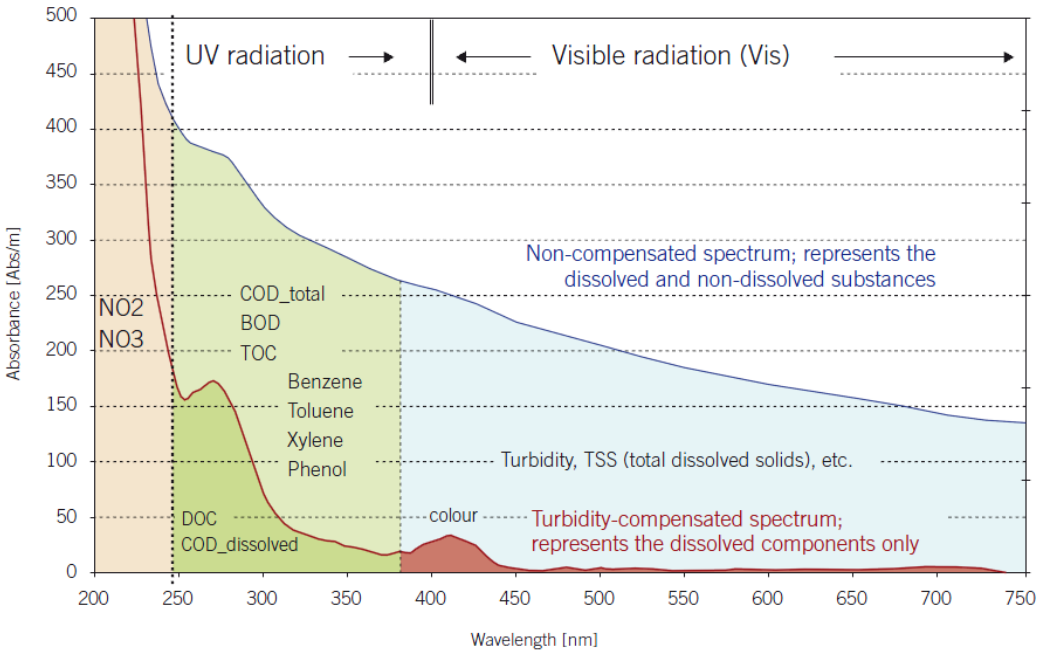

Figure 1.8 Example of an UV-VIS absorption spectrum, with examples of water quality parameters derived from the spectrum at specific wavelength ranges. From: Scan Messtechnik GmbH (2018).

Particle size analysers are instruments that could also be used to obtain *in situ* and high temporal frequency observations on SS-associated properties (i.e., SS PSD). Differences in parent material, weathering and erosion processes can influence transported PSDs, and it is hypothesized in this

thesis that this information can be used to discriminate between potential SS sources (as suggested by Laceby et al., 2017). Particle size distributions of stream water samples can be measured using laboratory-based particle size analysers. These instruments require no initial sample preparation and analysis times are short. Additionally, submersible PSD analyser probes could help in even further reducing resource needs, eliminating sampling workloads and laboratory analysis needs.

Particle size distribution analysers work on the principles of laser diffraction (Figure 1.9). The process relies on the emittance of a laser beam by a laser diode. The diffraction of the laser beam is subsequently influenced by the particles in suspension, where different sizes of particles diffract the light at different angles (i.e., with larger particles scattering the light at small angles relative to the laser beam and small particles scattering the light at large angles relative to the laser beam). The measured angular scattering intensity distribution data are then used to calculate the PSDs. The mathematical conversion of the scattering data into the PSDs is achieved by employing the Mie scattering model (Malvern Instruments, 2013; Sequoia Scientific, 2018). The Mie theory assumes scattering to be dependent on the size of the particle and its reflective index relative to the water. However, the Mie theory assumes particles to be spherical, whereas non-spherical particles are dominant in nature (Fettweis and Lee, 2017). Therefore, certain particle size analysers provide an alternative model, to convert the scattering under the assumption that the particles are randomly/irregularly shaped (e.g., Agrawal et al., 2008). This model can either be an empirically determined (e.g., Sequoia Scientific, 2018), or based on reference optical properties of the sample to be tested (e.g., Malvern Instruments, 2013).

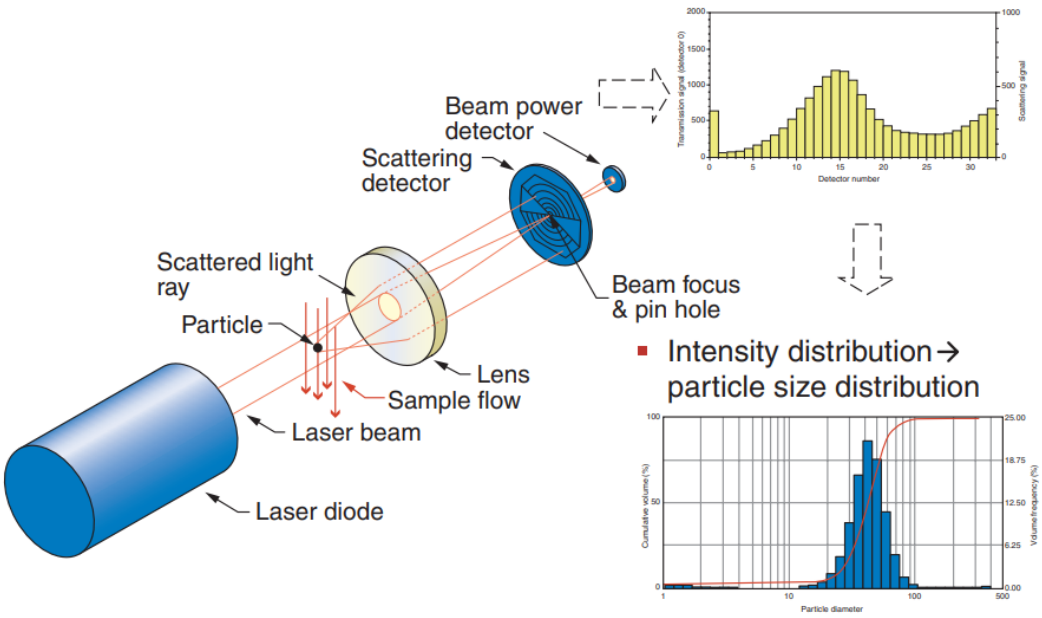

Figure 1.9 Principles of laser diffraction analysis for obtaining the particle size distribution. From Kongas (2003).

1.6 Aims and Objectives

1.6.1 Main Aim

Though the sediment fingerprinting approach is well-adopted globally, key challenges and uncertainties remain. One of the main challenges is the requirement for resources in the sampling and analysis procedures, which hampers the opportunities to gain high temporal insights into changing SS source contributions. Hence, the sediment fingerprinting technique is constantly testing new fingerprints, in combination with improved analysis techniques, to allow for an increasing number of samples to be analysed against limited budgets and with the need to manage workloads. The recent development of new, so-called low-cost fingerprints could potentially overcome some of these resource limitations. However, even with these low-cost methods, resource needs associated with source and target SS sampling, and subsequent laboratory sample preparation remain.

While instruments that allow for *in situ* and high temporal frequency measurements have been shown to improve the mechanistic understanding of catchment-related processes, such instruments have, in the main, not been deployed for measuring sediment-associated properties, and are therefore absent from sediment fingerprinting studies. To this end, the main aim of this thesis is to investigate whether *in situ* instruments (i.e., UV-VIS spectrophotometer and particle size analyser probes) allow for long-term and high temporal resolution SS source apportionment, to ultimately provide a better understanding of catchment hydro-sedimentary dynamics and to facilitate the implementation of targeted management solutions.

1.6.2 Research Questions

The main aim of this thesis will be addressed by answering the following research questions (RQ), constituting the core chapters of this thesis:

- RQ 1 (Chapter 2): *How can absorbance readings of a submerged spectrophotometer be used as sediment fingerprints to estimate source contributions from artificially created sediment mixtures in a proof-of-concept laboratory experiment?*
- RQ 2 (Chapter 3): *Can absorbance differences from source streams in confluences be used to apportion spatial SS sources at the catchment scale?*
- RQ 3 (Chapter 4): *Can SS source particle size distributions be used as a sediment fingerprint, in combination with an end-member grain size un-mixing model?*

1.7 Thesis Structure

The overall structure (see also Figure 1.10) of the remainder of this thesis is as follows:

Chapters 2 and 3 describe the use of absorbance measured over the 200-730 nm wavelength range as sediment fingerprints. Chapter 2 describes a proof-of-concept laboratory experiment, in which absorbance measurements were made on prepared laboratory soil samples and artificial mixtures consisting of known soil samples contributions. Artificial mixtures were un-mixed, using the MixSIAR Bayesian un-mixing model (Stock et al., 2018; Stock and Semmens, 2016), to evaluate the usability of absorbance data as a sediment fingerprint under controlled conditions. Chapter 3 then elaborates on the proof-of-concept laboratory study by using absorbance as a sediment fingerprint in a catchment scale study. Here, a confluence-based sampling strategy was applied to a series of confluences within a small catchment (44 km^2), comprising of diverse lithologies and land uses. Absorbance measurements on grab water samples were used for un-mixing (using the MixSIAR model), with the tributary source contributions being evaluated against calculated sediment budgets.

Chapter 4 describes an experiment study into the use of PSD as a sediment fingerprint. This study is composed of two parts. First, a proof-of-concept investigation was performed. Particle size distributions were measured on artificially created soil samples, sieved to three different fractions. Artificial mixtures, composed of soil samples sieved to different fractions, were then un-mixed using the AnalySize grain-size un-mixing model (version 1.2.1; Paterson and Heslop, 2015). Modelled source estimates were then evaluated against the known soil sample contributions in each mixture. Subsequently, the approach was applied in a catchment scale study, using a confluence-based sampling strategy. Herein, contributions to the confluence downstream SS were un-mixed (using the AnalySize model) based on the PSD differences in the upstream tributary sources. Un-mixing results were subsequently evaluated against calculated sediment budgets.

Chapter 5 synthesises the overall findings of the study, reflecting on the research questions and the main aim of this thesis, and followed by conclusions. Finally, an outlook is provided on how the presented methodological approaches and findings could be used in future applications.

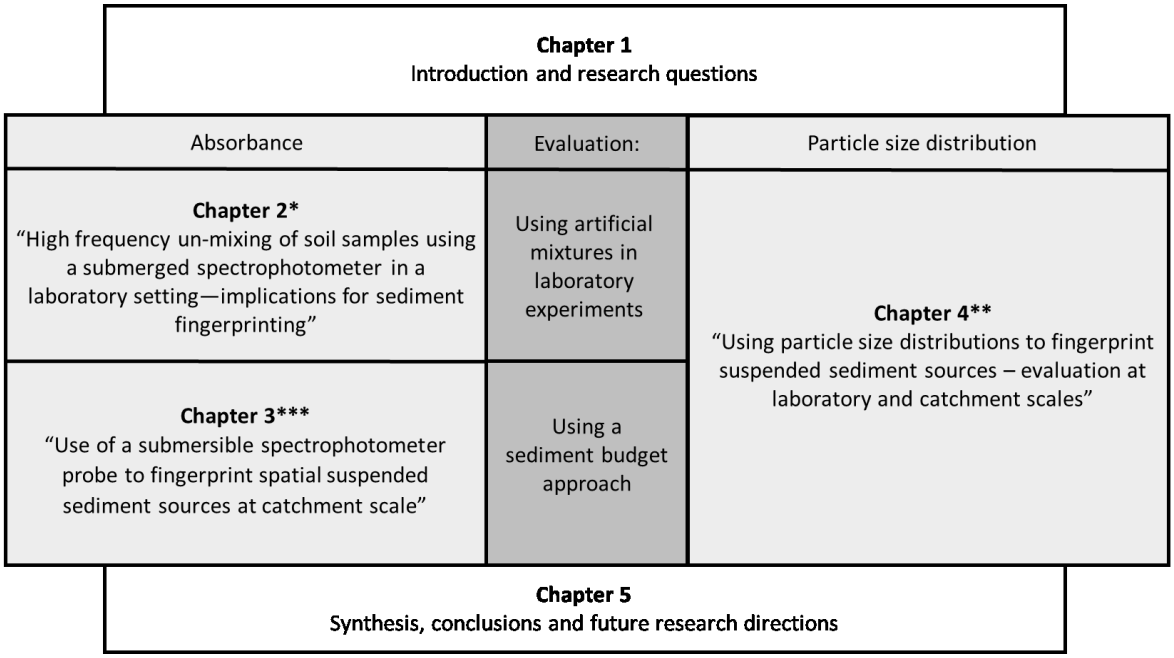

Figure 1.10 The organisational framework of the thesis.

* This chapter is published as: Lake, N.F., Martínez-Carreras, N., Shaw, P.J., Collins, A.L., 2022a. High frequency un-mixing of soil samples using a submerged spectrophotometer in a laboratory setting—implications for sediment fingerprinting. Journal of Soils and Sediments 22 (1), 348–364. https://doi.org/10.1007/s11368-021-03107-6

** This chapter is published as: Lake, N.F., Martínez-Carreras, N., Shaw, P.J., Collins, A.L., 2022b. Using particle size distributions to fingerprint suspended sediment sources — Evaluation at laboratory and catchment scales. Hydrological Processes 36 (10), e14726. https://doi.org/10.1002/hyp.14726

*** This chapter is published as: Lake, N.F., Martínez-Carreras, N., Iffly, J.F., Shaw, P.J. and Collins, A.L., 2023. Use of a submersible spectrophotometer probe to fingerprint spatial suspended sediment sources at catchment scale. Science of the Total Environment, p.162332. https://doi.org/10.1016/j.scitotenv.2023.162332

Chapter 2 High Frequency Un-Mixing of Soil Samples using a Submerged Spectrophotometer in a Laboratory Setting—Implications for Sediment Fingerprinting

Abstract

This study tests the feasibility of using a submersible spectrophotometer as a novel method to trace and apportion suspended sediment sources *in situ* and at high temporal frequency. Laboratory experiments were designed to identify how absorbance at different wavelengths can be used to un-mix artificial mixtures of soil samples (i.e., sediment sources). The experiment consists of a tank containing 40 L of water, to which the soil samples and soil mixtures of known proportions were added in suspension. Absorbance measurements made using the submersible spectrophotometer were used to elucidate: (i) the effects of concentrations on absorbance, (ii) the relationship between absorbance and particle size, and (iii) the linear additivity of absorbance as a prerequisite for un-mixing. The observed relationships between soil sample concentrations and absorbance in the ultraviolet visible (UV-VIS) wavelength range (200-730 nm) indicated that differences in absorbance patterns are caused by soil-specific properties and particle size. Absorbance was found to be linearly additive and could be used to predict the known soil sample proportions in mixtures using the MixSIAR Bayesian tracer mixing model. Model results indicate that dominant contributions to mixtures containing two and three soil samples could be predicted well, while accuracy for four soil sample mixtures was lower (with respective mean absolute errors of 15.4%, 12.9% and 17.0%). The results demonstrate the potential for using *in situ* submersible spectrophotometer sensors to trace suspended sediment sources at high temporal frequency.

2.1 Introduction

Suspended sediment (SS) plays an essential role in the hydrological, geomorphological and ecological functioning of aquatic ecosystems (Bilotta and Brazier, 2008; Owens et al., 2005; Vercruysse et al., 2017; Wohl et al., 2015). Suspended sediment export is mainly driven by hydro-meteorological variables (Vercruysse and Grabowski, 2019) and factors such as hillslope erosion, sediment delivery to stream channels and stream channel bank or bed erosion (Fryirs, 2012; Mukundan et al., 2012). However, excessive amounts of SS can degrade aquatic ecosystems by

causing siltation, habitat deterioration or pollution, linked to the key role of SS in the transportation of contaminants and nutrients (e.g., Affandi and Ishak, 2019; Carter et al., 2006; House, 2003; Kronvang et al., 2003). Hence, the need to identify the sources of SS is increasingly recognised as a priority to support management strategies for stream ecology, geomorphology and water quality issues (Collins et al., 2017; Mukundan et al., 2012; Walling and Collins, 2008) in alignment with environmental policies (e.g., WFD; 2000/60/EC, 2000).

Sediment fingerprinting is one direct approach to estimating SS contributions from catchment sources. This approach compares properties of potential source materials with properties of SS, using distinct diagnostic signatures or so-called 'composite fingerprints' comprising several constituent properties (e.g., Oldfield et al., 1979; Peart and Walling, 1986, 1988; Walling and Woodward, 1992). These properties are selected on the basis that they are clearly distinctive between individual sources, allowing for the un-mixing of SS to estimate source proportions.

Despite the fingerprinting approach being increasingly adopted globally (see reviews by Collins et al., 2017, 2020; Guan et al., 2017; Haddadchi et al., 2013; Owens et al., 2016; Tang et al., 2019), there remain some major limitations that continue to hamper its use as either a scientific or management tool. These limitations include the pre-selection of the most robust fingerprints for different environmental settings (Collins et al., 2020; Koiter et al., 2013) and methods for SS sampling (Haddadchi et al., 2013). Robust fingerprint properties must both differentiate between potential SS sources and behave conservatively during mobilisation and delivery to the river, stream or lake (Walling et al., 1993). Conservative behaviour is important because erosion and SS transport processes are particle size selective which, in turn, influences sediment properties and the reliability of the direct comparisons between source materials and target SS samples (e.g., Collins et al., 2017; Laceby et al., 2017). A major limitation associated with common SS sampling methods concerns the limited insights they provide on how sediment sources change over short (i.e., minutes) time intervals and during longer (e.g., seasons or years) periods (e.g., Collins et al., 2020; Navratil et al., 2012; Vercruysse et al., 2017). The commonplace deployment of time-integrating samplers (Phillips et al., 2000), for example, is limited with regard to the temporal resolution of the SS source estimates generated (often limited to one or a small number of samples per event; Collins and Walling, 2004). Furthermore, sediment particle size and geochemical properties might be altered during sampling deployment and sample storage prior to analysis (e.g., due to adsorption/desorption; Smith and Owens, 2014). The collection and use of high frequency instantaneous SS samples is constrained by the associated analytical costs for many fingerprint properties/tracers commonly used in source fingerprinting investigations (Collins and Walling, 2004; Haddadchi et al., 2013). High frequency observations (minutes) for prolonged periods could contribute to the understanding of catchment sediment dynamics (e.g., which SS sources are active

under what conditions), which is key to eventually taking suitable countermeasures against excessive sediment input to rivers and streams (Navratil et al., 2012; Vercruysse et al., 2017).

The current absence of well-established methods to measure SS properties *in situ* at high frequency compounds the current limited capacity to document SS source contributions over short time intervals for longer durations of measurement. Thus far, attempts to overcome this limitation still rely on the collection of physical samples in the field at high frequency, in conjunction with subsequent laboratory analyses of tracer properties. Such work has included the use of diffuse reflectance infrared Fourier transform spectrometry (e.g., Cooper et al., 2014b, 2015; Poulenard et al., 2012), spectral reflectance analysis of sediment chemical properties on samples placed on glass fibre filters (Cooper et al., 2014b; Martínez-Carreras et al., 2010b), colour parameters obtained from spectro-colorimetry (Martínez-Carreras et al., 2010c), colour parameters derived from office scanners (Pulley and Rowntree, 2016) and deployment of handheld XRF instruments (Smith and Blake, 2014). Whilst these procedures reduce resource needs for the analysis of tracer properties in numerous target sediment samples, they do not overcome the resource needs pertaining to high frequency collection of such samples.

Submersible spectrophotometer sensors, widely used for drinking water quality monitoring (e.g., D'Acunha and Johnson, 2019; González-Morales et al., 2020; Prairie et al., 2020), may, however, offer a reliable means to provide data on SS fingerprint properties at high frequency. Bass et al. (2011) and Martínez-Carreras et al. (2016) used submersible spectrophotometer sensors, measuring absorbance in the ultraviolet visible (UV-VIS) range, to estimate SS properties *in situ*. The former used such a sensor to estimate particulate organic carbon content, whilst the latter estimated sediment loss-on-ignition, with both studies calibrating the sensor readings using physical samples. This work demonstrated the potential value of such sensors to discriminate between sediment sources with contrasting tracer properties and for un-mixing source proportions. The ability of these sensors to measure *in situ* suggests limited physical SS sampling is only required for sensor validation. Furthermore, given the facility to measure at high frequency (e.g., minutes) for long duration, since maintenance needs of the sensor are low, a spectrophotometer sensor has the potential to resolve current constraints pertaining to both sediment sampling and ensuing tracer analysis.

When the influence of dissolved species in water is negligible, absorbance measurements are mainly affected by SS concentration (Thomas et al., 2017) and the size of the SS particles (Berho et al., 2004). Thomas et al. (2017) reported that absorbance increases with SS concentrations. Berho et al. (2004) showed that smaller particles resulted in higher absorbance values than coarser particles with the same minerology. These studies clearly demonstrated that the exact relationships

between absorbance and both concentration and particle size warrant detailed investigation to determine if, and to what extent, absorbance values need to be compensated to facilitate high frequency sediment source fingerprinting.

Given the above context and the ongoing need to continue testing devices for assembling high temporal resolution data on SS properties *in situ*, we conjecture that the absorbance readings of a submerged spectrophotometer can be used as sediment fingerprints to estimate SS sources. Herein, we present a proof-of-concept laboratory experiment where we use absorbance data to un-mix artificial mixtures of soil samples sieved to three different particle size fractions. To this end, we tested how the absorbance data is influenced by SS concentration and particle size distribution (PSD), as well as the suitability of the absorbance data for estimating sediment source proportions.

2.2 Materials and Methods

Experimental assessment of the submersible spectrophotometer was undertaken in a series of laboratory tests. Soil samples of known origin and composition were used to create a series of water samples containing SS of differing composition and concentration; measurements of absorbance spectra *in situ* could then be interpreted in relation to the composition and concentration, and to the expected outcomes in terms of the spectra.

2.2.1 Soil Samples and Artificial Mixtures

Six soils samples were collected in Luxembourg based on differences in colour (visual inspection) and differences in underlying geology (Figure 2.1). Soils were air-dried at room temperature before being disaggregated manually using a pestle and mortar. Samples were then dry sieved to three different size fractions: <32 µm, 32-63 µm and 63-125 µm. Due to its PSD, retrieving the 63–125 µm fraction of soil 6 was not possible and this soil sample was therefore omitted, resulting in 17 size-fractionated soil samples. The fractions were selected based on commonly used upper particle size boundaries in sediment fingerprinting studies (see Laceby et al., 2017). Minerology of the soil samples is shown in Table A.1 (Appendix A).

From the resulting 17 size-fractionated soil samples, we created artificial mixtures of two, three and four different samples. Mixtures were classified into two groups: (i) mixtures of soil samples sieved to the same particle size fraction, and; (ii) mixtures of soil samples sieved to different size fractions. The soil sample contributions to the artificial mixtures were based on having either a clearly dominant sample or more equal contributions (see Table A.2).

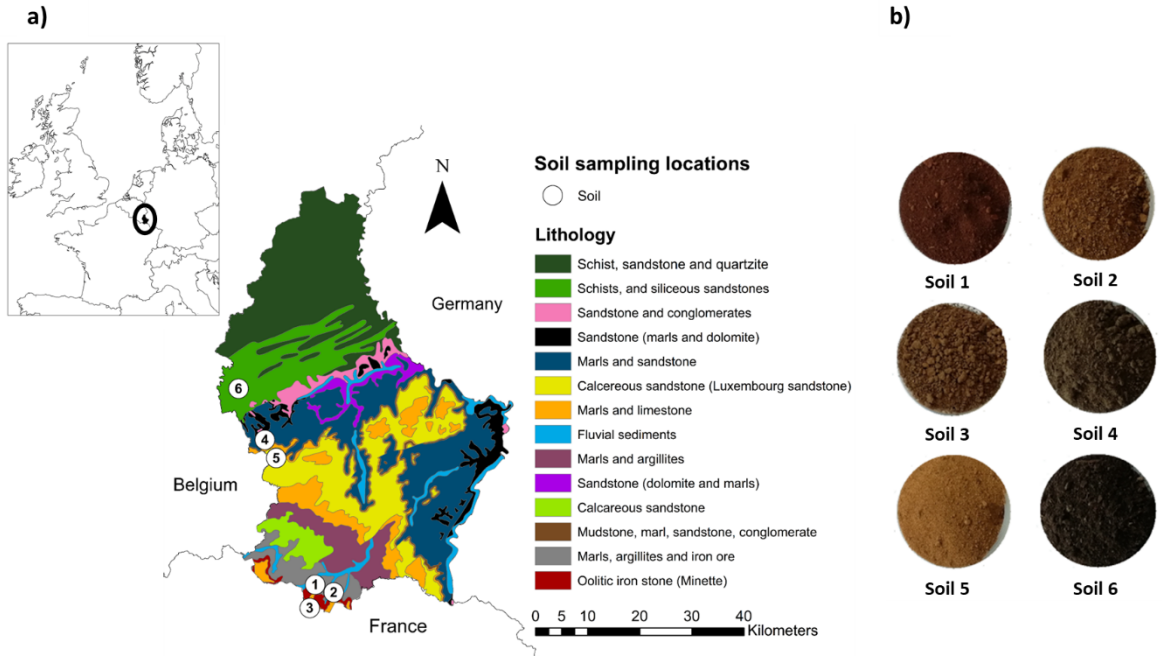

Figure 2.1 Soil sampling locations within Luxembourg (a) and images of the six collected soils (b). Source N.W. Europe map (a) adapted from: ArcGIS online (Europe_data_WG_NPS); source geological map of Luxembourg (a): Service Géologique du Luxembourg.

2.2.2 Sensors

Laboratory experiments used the S::can spectro::lyser™ probe (Scan Messtechnik GmbH, Vienna, Austria) submersible spectrophotometer. This sensor measures transmittance of a light beam (i.e., xenon-flash light) after contact with water in the optical measurement window, which is then converted to absorption over the UV-VIS wavelength range (200-730 nm, at 2.5 nm intervals). The detector is located at the opposite side of the optical window. Measurement frequency was set at 2 minute intervals, which is the smallest interval possible. Measured absorbance data were saved onto the corresponding Con::cube logger (Scan Messtechnik GmbH, Vienna, Austria).

In tandem with the spectrophotometer, a LISST-200X laser diffraction (Agrawal and Pottsmith, 2000) sensor (Sequoia Scientific, Bellevue, WA, United States) was used to measure PSD. This instrument works on the principle of laser diffraction with a laser beam emitted by a laser diode (Agrawal and Pottsmith, 2000). The LISST sensor assigns the diffracted laser beams into one of 36 sediment sizes classes, providing estimates of PSD and average particle size. Measurements were taken at 1.5 second intervals using the random shape model algorithm (Sequoia Scientific, 2018).

2.2.3 Laboratory Set-Up

The laboratory set-up consisted of a 75.4 L capacity, round tank. The spectrophotometer and LISST sensor were installed in a horizontal orientation to prevent sedimentation of particles on the measuring windows (Figure 2.2a, c). Using 40 L of demineralised water, both sensors were located more than 10 cm below the water surface as advised by the manufacturers.

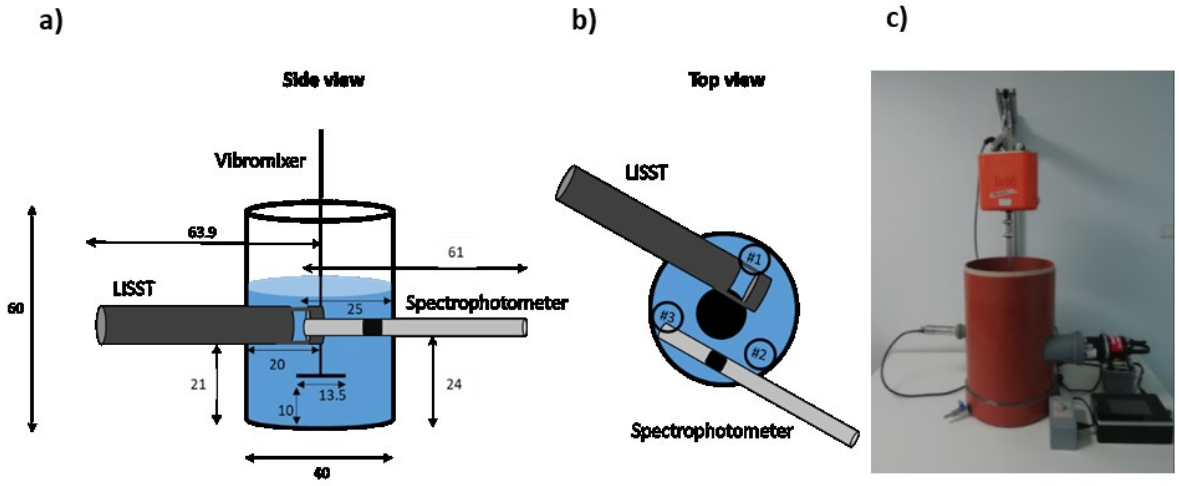

Figure 2.2 Laboratory setup: side view schematic representation with dimensions in cm (a); top view schematic representation with water sampling locations #1, #2 and #3 (b), and photograph (c).

Homogeneous concentrations inside the tank were established using a Fundamix vibromixer (DrM, Dr. Mueller AG, Switzerland), a vibrating device. This method avoids cone and vortex formation which are possible with rotational stirring techniques (Orlewski et al., 2018). To test homogeneity of concentrations during the experiments, water samples were collected at three locations within the tank set-up (Figure 2.2c) using a pipette (see Figure A.1, A.2 and A.3 for initial testing on vibromixer speed and position, and homogeneity of concentrations at different depth and locations; supplementary material). These samples were subsequently transferred into pre-weighted aluminium buckets, dried, and weighed again to determine concentrations. These concentrations (hereafter referred to as 'measured concentrations') were determined for all theoretical concentrations (10 concentrations in total; 100 mg L^{-1} – 1000 mg L^{-1} at 100 mg L^{-1} increments) for all experiments (20 values associated with erroneous measurements were omitted). Selected theoretical concentrations are representative of SS concentrations values measured across Luxembourgish rivers (Martínez-Carreras, 2010). The experiments consisted of testing the 17 soil samples individually, followed by testing the 25 artificial soil sample mixtures (see Table A.2 for a detailed overview of the experiments and known soil sample contributions in

the artificial mixtures and Protocol A.1 for more detail of the steps adopted during the experiments and specific equipment settings).

2.2.4 Data Pre-Treatment

LISST background measurements, taken before each experiment, were saved onto the instrument and automatically compensated for by the LISST software during subsequent measurements. Accordingly, the spectrophotometer absorbance data were compensated by using the data collected before the start of the actual experiment (i.e., subtracting the background readings from all consecutive absorbance data readings acquired during each experiment). Data obtained from the spectrophotometer and LISST sensors were thus only affected by the soil sample materials added to the experimental tank, and not influenced by the properties of the demineralised water. Absorbance data were measured over a 10 minute period at 2 minute intervals; only the last four measurements were used for analysis (allowing time for the soil sample material to become fully mixed). LISST data were measured over the same 10 minute period, with only the last 6 minutes of measurements used in subsequent analyses.

2.2.5 Concentrations and Relationship with Absorbance

Both theoretical and measured concentrations do not fully represent the actual concentrations inside the experimental tank. The former is subject to the settling of particles during mixing, whereas the latter is subject to uncertainties associated with pipette sampling and the weighing of aluminium cups. Three steps were used to quantify to what extent measured concentrations (see section 2.2.3) deviated from theoretical concentrations, and if deviations differed for the three particle size fractions investigated (i.e., <32 µm, 32-63 µm and 63-125 µm). Firstly, differences between measured and theoretical concentrations were calculated for the experiments using only soil samples. Measured concentrations were expressed as a percentage of theoretical concentrations, to assess whether there is a consistency in soil sample material losses. Secondly, 'expected' mixture concentrations were then calculated using a mass-balance (Equation 2.1), using the measured concentrations of the soil samples and their known contributions to the artificial mixture. This value was then compared with the directly measured concentration of the mixture itself.

$$\text{Expected mixture concentration} = \sum_{j=1}^{n} \mathrm{w}_j \times \mathrm{conc}_j \qquad \text{[Equation 2.1]}$$

where w_j is the relative contribution of each soil sample to the artificial mixture (j = 1 to n, with n being the number of soil samples mixed), and $conc_j$ is the measured concentration for soil sample j (resulting from the individual soil sample experiments).

As a final step, we investigated the relationship of absorbance with both concentration and sieved particle size. To analyse patterns in the absorbance spectra for the 17 soil samples, the responses to increasing concentrations and particle size were examined. Randomly-selected absorbance values were used at low, medium and high range spectra (210 nm, 400 nm and 700 nm, respectively, example shown in Figure A.4; supplementary material). Besides these three randomly-selected absorbance values, the average absorbance value over the whole range of measured wavelengths (200-730 nm) was used. These values were scaled, dividing the absorbance values by their respective theoretical concentrations, to obtain average increases in absorbance per mg L^{-1} (n = 10, for the 10 concentrations) for each soil sample, with accompanying standard deviations. This process was designed to obtain more insight into how absorbance changes with concentration at the different selected wavelengths for all soil samples. These scaled absorbance values were then related to the particle size measured at every concentration in every experiment. Using a Mann-Whitney test, we tested if the absorbance values (n = 10, for the 10 concentrations) from the 17 soil samples were significantly different ($p < 0.05$). This test was carried out for the average absorbance values, as well as for the absorbance values resulting from the three selected wavelengths (210 nm, 400 nm and 700 nm). Absorbance data in this analysis were compensated for theoretical concentrations (see section 2.3.1).

2.2.6 Linear Additivity

The directly measured absorbance values from the artificial mixtures were compared with the absorbance values resulting from the individual soil sample experiments to test if: (i) absorbance behaves as a linearly additivity property, and; (ii) the combination of relative absorbance values of the individual soil samples, as used in the artificial mixtures, results in similar absorbance values when directly measured on the mixture (Equation 2.2).

$$\text{Expected mixture absorbance} = \sum_{j=1}^{n} w_j \times \text{Abs}_j \qquad \text{[Equation 2.2]}$$

where w_j is the relative contribution of each soil sample to the artificial mixture (j = 1 to n), and Abs_j represents the absorbance value of that particular soil sample j when measured individually. The absorbance data over the whole wavelength range (200-730 nm) was used (example shown in Figure A.4). This comparison was undertaken for all 10 different concentrations, for each mixture

experiment, and compared with the measured mixture absorbance data corresponding to the same theoretical concentrations.

2.2.7 Un-mixing Artificial Mixtures using the MixSIAR Model

The MixSIAR Bayesian un-mixing model (Stock et al., 2018; Stock and Semmens, 2016) open source R-package was used to un-mix the artificial mixtures, and investigate how a well-established model for sediment fingerprinting (e.g., Upadhayay et al., 2020; Wynants et al., 2020) deals with the highly collinear absorbance data. As model input, data obtained from the mixture experiments (mixture data) were used, together with the absorbance data from the single soil samples (i.e., soil source data). To investigate performances between concentrations, only sources and mixture absorbance data from the same theoretical concentrations were used. Source data were represented by the mean, variance and sample size (Blake et al., 2018). The MixSIAR model calculates the relative average contributions of each sample mixed and the corresponding standard deviations. For all model runs, the Markov Chain Monte Carlo parameters were used according to the predefined 'short' settings (chain length = 50000, burn = 25000, thin = 25, chains = 3). Model convergence was evaluated using the Gelman-Rubin diagnostics (variables <1.1). All models were run using the High Performance Computing facility at the Luxembourg Institute of Science and Technology. For the MixSIAR runs, the whole range of absorbance values was used, with each wavelength being regarded as a tracer. This resulted in 213 tracer values (wavelength range 200-730 nm, with 2.5 nm intervals). The known source contributions to each artificial mixture were compared with the source contributions estimated by the model. This comparison was made by calculating the absolute error (AE); the absolute difference between the known soil source contributions and the predicted source contributions generated by MixSIAR.

2.3 Results

2.3.1 Concentrations and Relationship with Absorbance

The measured concentrations inside the tank were generally lower than the theoretical concentrations intended (Figure 2.3); measured concentration decreased with increasing particle size. The relationship between measured and theoretical concentrations varied little at increasing concentrations for all soil samples in the <32 µm fraction (Figure 2.3). Measured concentrations represented ca. 90% of the theoretical concentrations. Corresponding standard deviations ranged up to 4% (for 95% of all measured concentration values), with the remaining 5% of the values having higher deviations (observed at lower theoretical concentrations; i.e., 100-300 mg L^{-1}).

For the two coarser fractions, measured concentrations showed larger deviations from the theoretical concentrations (Figure 2.3). For the 32-63 µm fraction, average measured concentrations mostly ranged between 60 to 90% of the theoretical concentrations. The average measured concentrations for the 63-125 µm fraction mostly ranged from 30% to 75%, with soil 5 giving very low measured concentrations compared with the other soil samples. Despite the larger differences, the relationship between measured and theoretical concentrations remained constant with increasing concentrations for the separate soil samples (Figure 2.3). These average values had low standard deviations (i.e., <10% for 97.5% of the values and <5% for 81% of the values for the 32-63 µm fraction; <10% for 95% of the values and <5% for 56% of the values for the 63-125 µm fraction).

Deviations between expected and measured mixture concentrations (Equation 2.1) are shown in Table 2.1. Around 50% of the expected mixture concentrations showed a deviation of <5% compared with the measured mixtures concentrations. Around two thirds of mixtures showed a deviation <10%, and around 90% a deviation <20%. Furthermore, deviations between expected and measured mixture concentrations decreased slightly when the number of soil samples in the artificial mixtures was increased.

Table 2.1 Deviations between expected and measured artificial mixture concentrations.

	Total n values	n values <5% deviation (in %)	n values <10% deviation (in %)	n values <20% deviation (in %)
2 sample mixture	115	50 (43.5%)	71 (61.7%)	100 (87.0%)
3 sample mixture	65	30 (46.2%)	43 (66.1%)	60 (92.3%)
4 sample mixture	50	29 (58.0%)	35 (70.0%)	45 (90.0%)
All mixtures	230	108 (47.0%)	147 (63.9%)	201 (87.4%)

Both when using theoretical (Figure A.5) and measured (Figure A.6) concentrations, strong correlations with absorbance measured at the three selected wavelengths (i.e., 210, 400, 700 nm) were observed, as well as for the average absorbance over all wavelengths. Using theoretical concentrations (Figure A.5), r^2 values were >0.99, with the exception of soil sample #5.3 (soil 5, 63-125 µm fraction), where the r^2 values decreased to ca. 0.96-0.97.

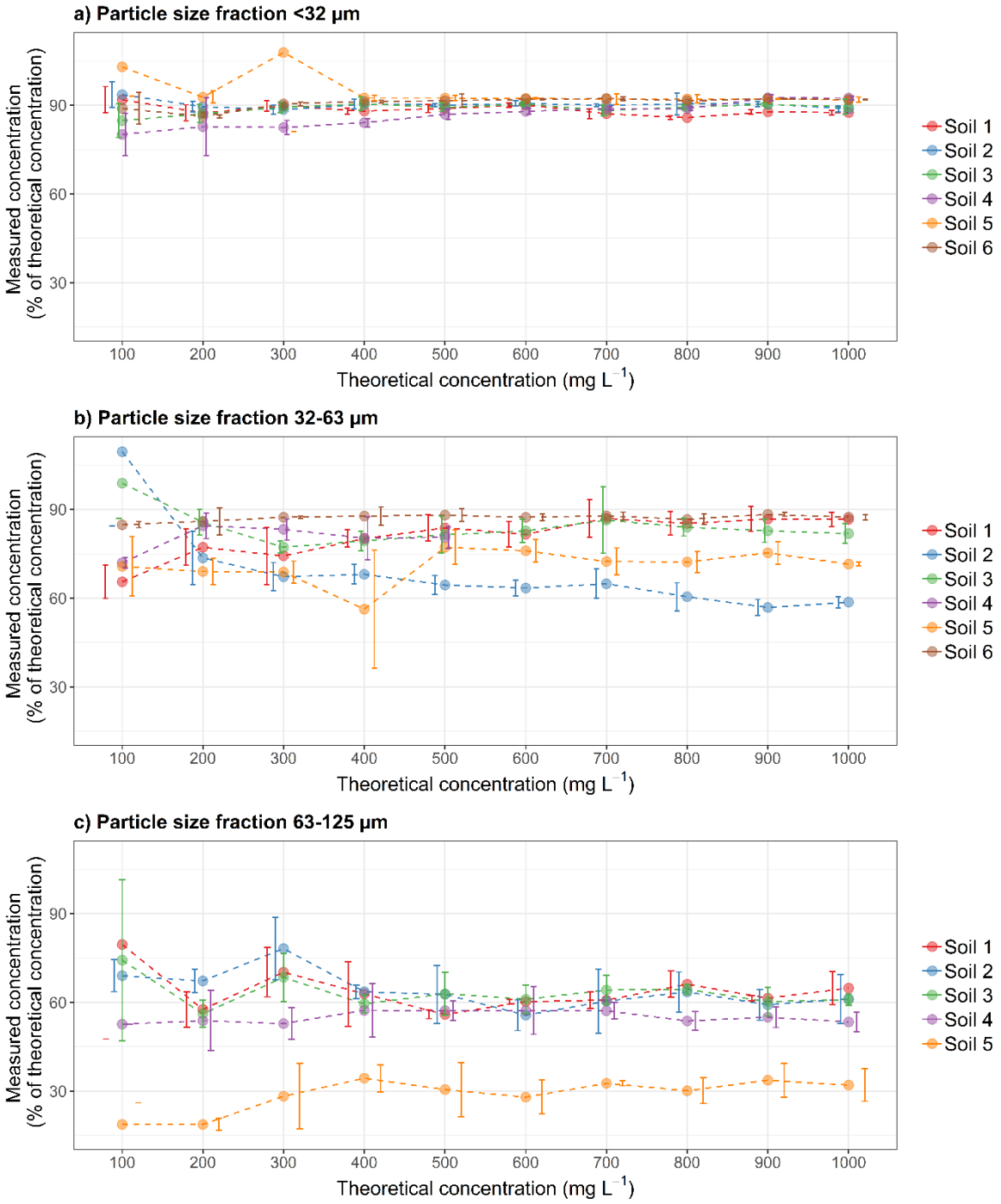

Figure 2.3 Average and standard deviation (n = 3) of measured concentrations inside the experimental tank expressed as a percentage of the theoretical concentrations for the six test soils (Figure 2.1), sieved to < 32 µm (a), 32–63 µm (b) and 63–125 µm (c). Error bars are plotted adjacent to the dots which represent the mean values.

Taking into consideration the finding that absorbance showed a slightly stronger correlation with theoretical concentration, together with the data presented above, it was decided to compensate absorbance data using the theoretical concentrations in the following final results of this laboratory experiment. For reference, figures using similar analysis as shown in section 2.3.2 and section 2.3.3 using measured rather than theoretical concentration, are available for consultation in the supplementary material. Since deviations between measured and theoretical concentrations are essentially constant for each tested soil sample (i.e., deviation percentages are independent of theoretical concentrations; see Figure 2.3), the calculated 'expected' mixture concentrations and the measured mixture concentrations should correspond (Table 2.1). These results confirm that there is no need to compensate absorbance readings for concentration effects when comparing soil samples and mixtures that are using the same theoretical concentrations.

2.3.2 Patterns in Absorbance Spectra

Average increases in absorbance were found to be greater for smaller than larger particle sizes (Figure 2.4). Standard deviations for all soil samples were relatively small, with values mostly <10% compared with their average values. The exceptions here were standard deviations of 11.8%, 12.7% and 14.3% for soil samples #1.3, #6.2 and #5.3, respectively (Figure 2.4a). Furthermore, soil sample #1.3 showed a deviation exceeding 10% for the 210 nm (14.3%) and 400 nm (12.4%) wavelengths (Figure 2.4b, c). For the 700 nm wavelength (Figure 2.4d), only soil sample #5.3 showed a deviation exceeding 10% (10.3%).

The Mann-Whitney test results (Table 2.2) showed that three pairs of soil samples were not significantly different (average of all wavelengths). Six pairs of samples were not significantly different for the 210 nm wavelength, and two pairs of samples were not significantly different for the 400 nm and 700 nm wavelengths, respectively. These pairs of soil samples (Table 2.2) were also not significantly different when analysing the average of all wavelengths. From the pairs shown in Table 2.2, only 1 combination (#3.1 - #5.1) was used together in an artificial mixture (Table A.2).

Finer particle sizes (i.e., a smaller mean effective particle size measured with the LISST 200X sensor) resulted in larger average increases in absorbance per mg L^{-1}, while coarser particle sizes showed smaller average increases per mg L^{-1}. This relationship appears to be logarithmic, with an r^2 value of 0.78 (Figure 2.5). Analyses performed when using measured concentrations, instead of theoretical concentrations, showed rather similar outcomes (Figure A.7 and Figure A.8).

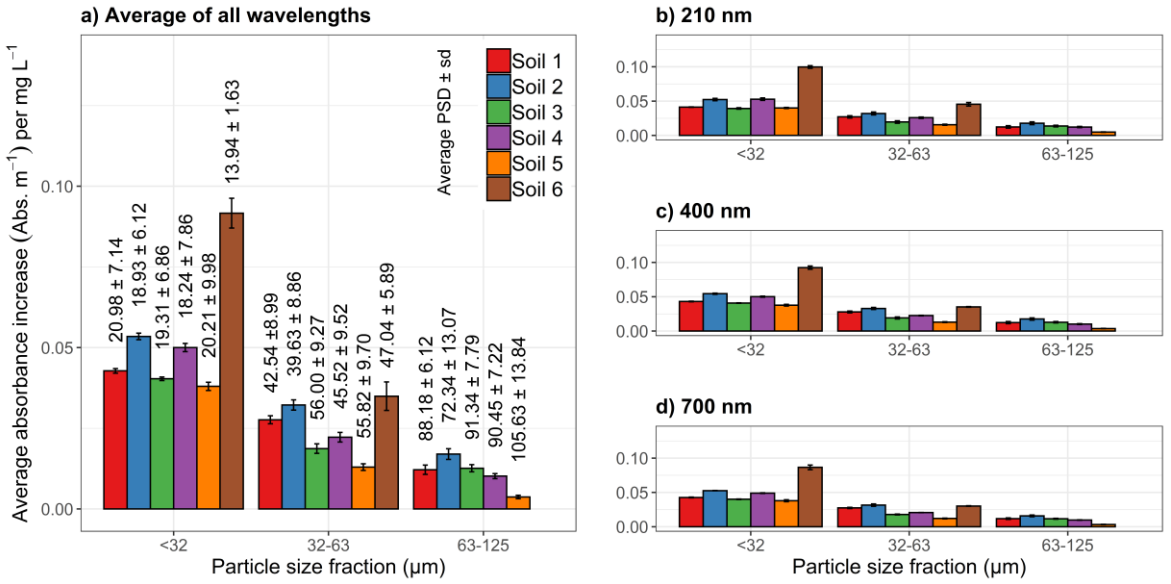

Figure 2.4 Average increases in absorbance per mg L^{-1} (absorbance values divided by theoretical concentrations) for average absorbance over all wavelengths (a), 210 nm (b), 400 nm (c) and 700 nm (d), for all 17 soil samples (indicated by #soil.fraction, with 'soil' representing the test soils (n = 6), and 'fraction' the sieved fraction size (.1 for < 32 µm; .2 for 32–63 µm; .3 for 63–125 µm). Values inside the plot (a) refer to the average and standard deviation of the measured particle size distribution (PSD) per sample and dry sieved fraction measured with the LISST sensor inside the experimental tank.

Table 2.2 Mann–Whitney test results for soil samples that were not significantly different (p > 0.05) for the average of all wavelengths, 210 nm, 400 nm and 700 nm. Soil samples are indicated by #soil.fraction, with 'soil' representing the test soils (n = 6, Figure 2.1), and 'fraction' the sieved fraction size (.1 for < 32 µm; .2 for 32–63 µm; .3 for 63–125 µm).

Average of all wavelengths	p-value	210 nm	p-value	400 nm	p-value	700 nm	p-value
#1.3 & #3.3	0.58	#2.1 & #4.1	0.97	#1.3 & #3.3	0.48	#1.3 & #3.3	0.97
#1.3 & #5.2	0.19	#3.1 & #5.1	0.44	#3.3 & #5.2	0.85	#3.3 & #5.2	0.25
#3.3 & #5.2	0.44	#1.2 & #4.2	0.052				
		#1.3 & #3.3	0.12				
		#1.3 & #4.3	0.74				
		#2.3 & #3.2	0.089				

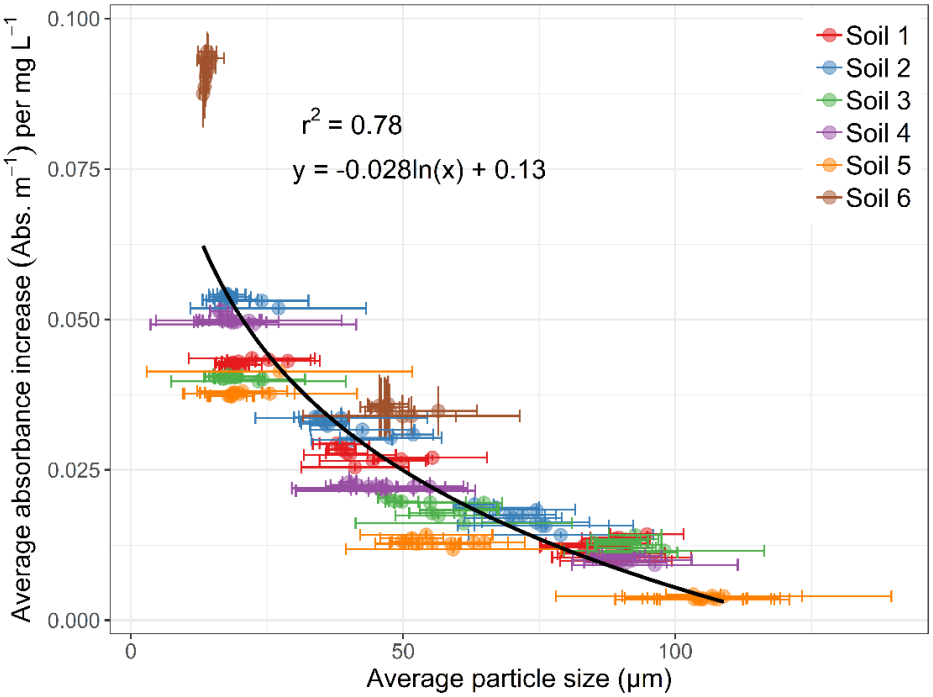

Figure 2.5 Relationship between average increases in absorbance per mg L^{-1} (absorbance values divided by theoretical concentrations) as a function of average particle size measured with the LISST sensor inside the experimental tank. Particle size values and corresponding standard deviations were calculated for every sample and for every concentration separately.

2.3.3 Linear Additivity

Comparison of expected and measured mixture absorbance (Equation 2.2) generated deviations of generally <20% (Figure 2.6). This was true for all mixtures except for three values where the deviations were slightly higher. Furthermore, a high percentage of the values (57%, 63% and 82% for the two, three and four soil sample mixtures, respectively) showed deviations of <10%. Deviations of <5% were noted for 35% (two sample mixture), 25% (three sample mixture), and 6% (four sample mixture) of the artificial mixture values. Values can be positive or negative, indicating whether the expected absorbance (Equation 2.2) is higher or lower than the absorbance measured directly for the artificial mixture. In Figure A.9 the deviations between the expected and measured absorbance are shown, with absorbance being compensated for measured concentrations.

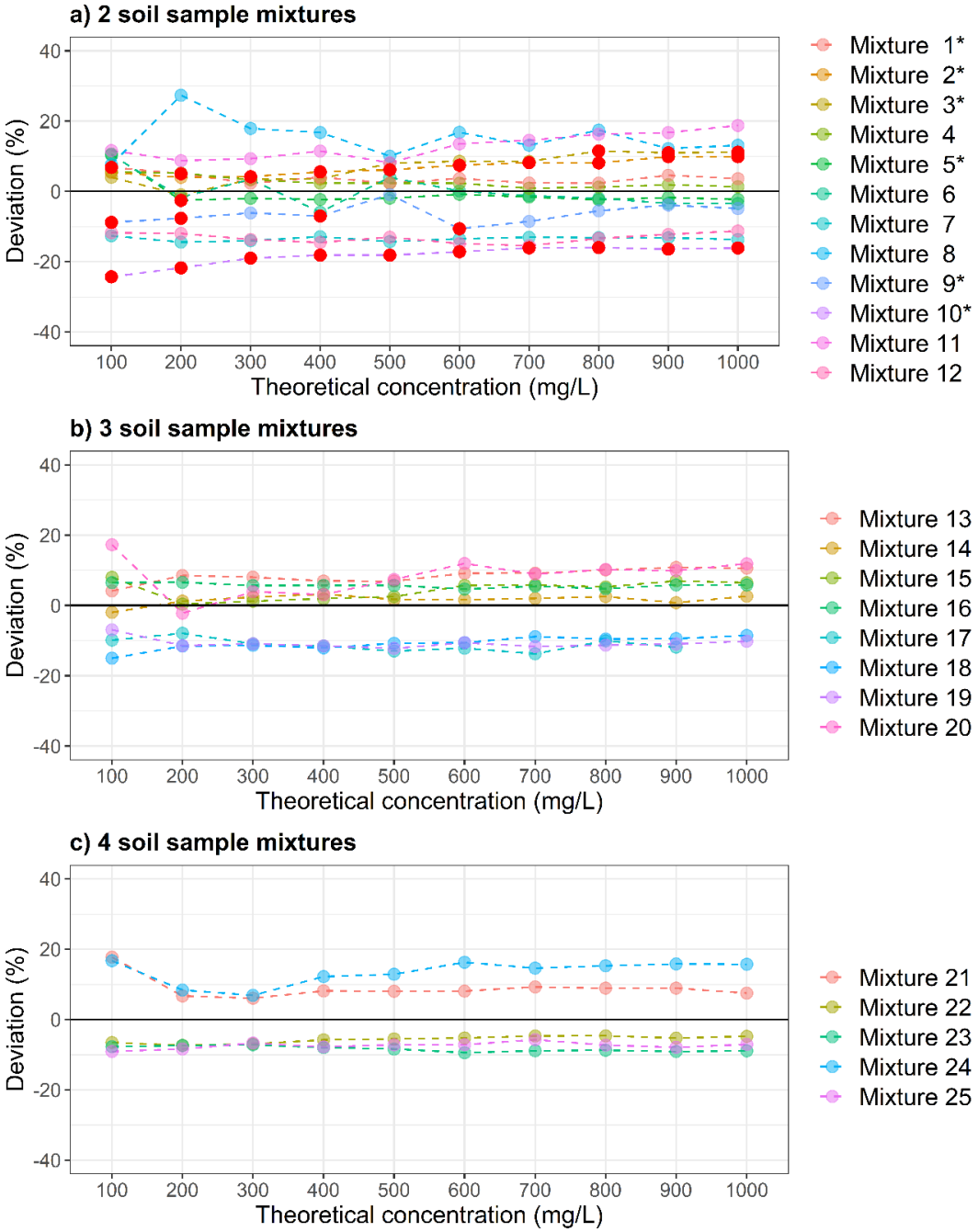

Figure 2.6 Deviations between measured absorbance and 'expected' absorbance based on a single soil sample absorbance signal (mass-balance), shown for two- (a), three- (b) and four- (c) soil sample mixtures. Red dots (a) indicate those situations in which absorbance values from the artificial mixtures are larger or smaller than the absorbance values measured for both individual soil samples comprising that mixture (concerned mixtures are indicated by * in the legend).

2.3.4 Un-Mixing Artificial Mixtures (MixSIAR)

The MixSIAR calculations using the two soil sample mixtures showed that dominant soil sample contributions were reliably predicted (Figure 2.7). MixSIAR predicted the correct dominant soil samples for ten out of eleven such mixtures. From these mixtures, eight showed an overestimation of the dominant soil sample. For mixture 11, the dominant sample was not well predicted, with MixSIAR outputting equal contributions of the soil samples mixed. For the one mixture using equal (50%) contributions (mixture 8), MixSIAR over (70%) and underpredicted (30%) the known relative contributions. The results of the tests using artificial mixtures with different particle size fractions (mixtures 10, 11 and 12) indicated there were no clear differences in MixSIAR predictions compared with those from the artificial mixtures using samples sieved to the same particle size fraction.

For the eight artificial mixtures using three soil samples, MixSIAR predicted the dominant soil sample contribution well in six cases. From these six cases, MixSIAR over-predicted the contribution of the dominant soil for mixtures 18 and 20, whereas it under-predicted the contribution of the dominant contributing soil sample for mixtures 14, 15, 16, 17. Mixtures 18 and 20 were, together with mixture 17, the mixtures using samples sieved to different particle size fractions. In the case of mixture 19, MixSIAR predictions deviated from the known inputs, with the more dominant soil sample (50%) constantly being predicted by the model as the soil sample with least contribution.

For the four soil sample mixtures, four out of five were mixed to have a clearly dominant contributing (70%) soil sample. Dominant contributions in mixtures 21 (under-estimated compared to known input) and 25 (over-estimated compared to known input) were predicted by MixSIAR. For mixture 22, the model failed to predict a dominant soil sample and for mixture 24, an erroneous soil sample was predicted as the dominant source. In the case of mixture 23, with known equal (25%) proportions for all four soil samples, the predictions from MixSIAR showed variable levels of agreement.

Table A.3 presents an overview of the accuracy of the MixSIAR predictions relative to the known soil sample proportions comprising the different artificial mixtures. Absolute errors varied between 6% and 26.7% for the two sample mixtures, 1.8% and 41.0% for the three sample mixtures, and between 2.8% and 48.8% for the four sample mixtures. Standard errors for the MixSIAR predictions were also calculated, returning values ranging up to 6.2%, 10.7% and 3.2% for the two, three and four soil sample mixtures, respectively. Not all models passed the Gelman-Rubin diagnostics, where variables exceeding the value of 1.1 were observed in one or several concentrations within five out of eight three-sample mixtures and in all five four-sample mixtures. Details on the Gelman-Rubin diagnostics are shown in Table A.4.

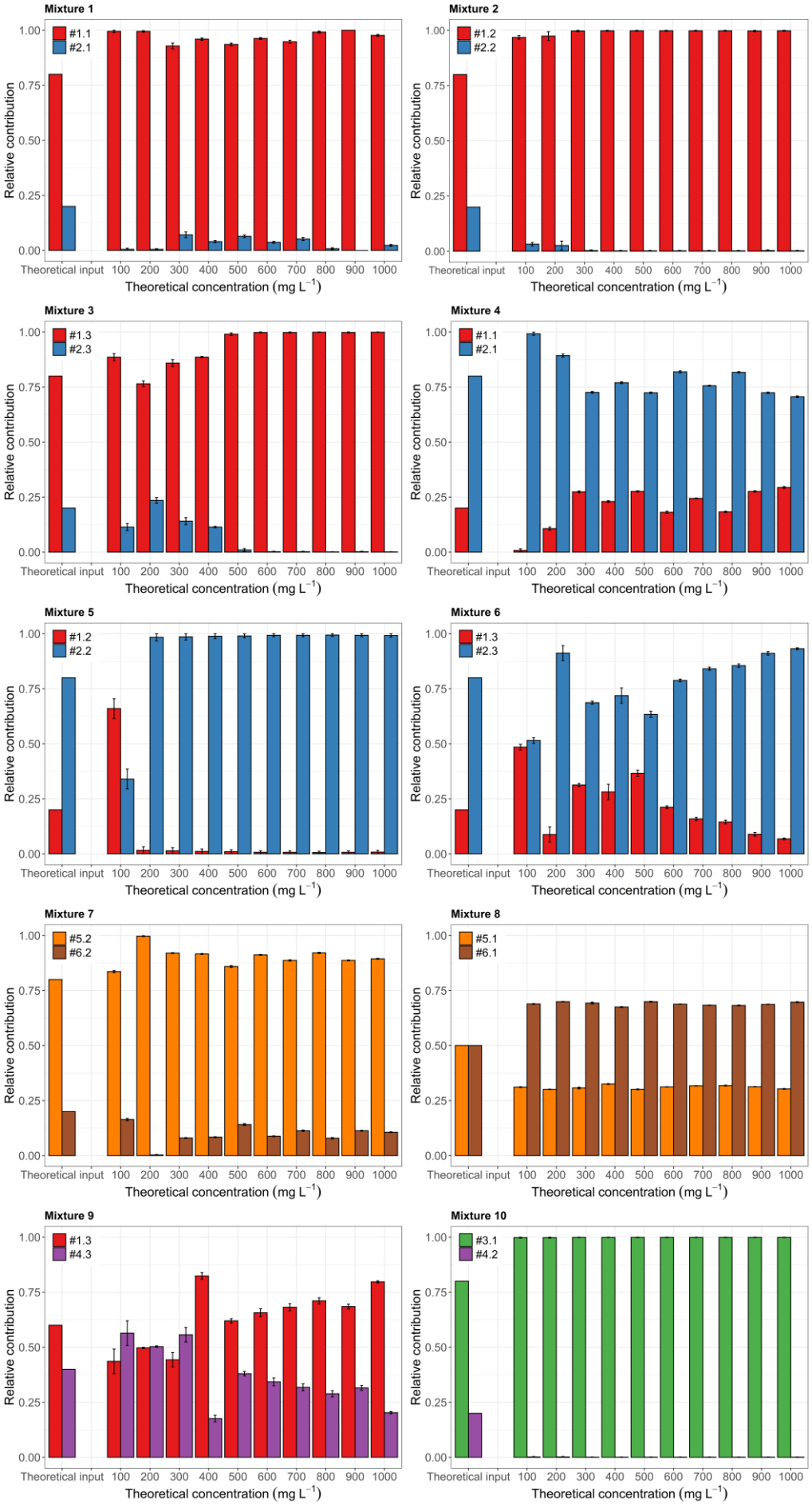
Mixture 1
#1.1
#2.1
Mixture 2
#1.2
#2.2
Mixture 3
#1.3
#2.3
Mixture 4
#1.1
#2.1
Mixture 5
#1.2
#2.2
Mixture 6
#1.3
#2.3
Mixture 7
#5.2
#6.2
Mixture 8
#5.1
#6.1
Mixture 9
#1.3
#4.3
Mixture 10
#3.1
#4.2
Relative contribution
0.00
0.25
0.50
0.75
1.00
Theoretical input 100 200 300 400 500 600 700 800 900 1000
Theoretical concentration (mg L^{-1})

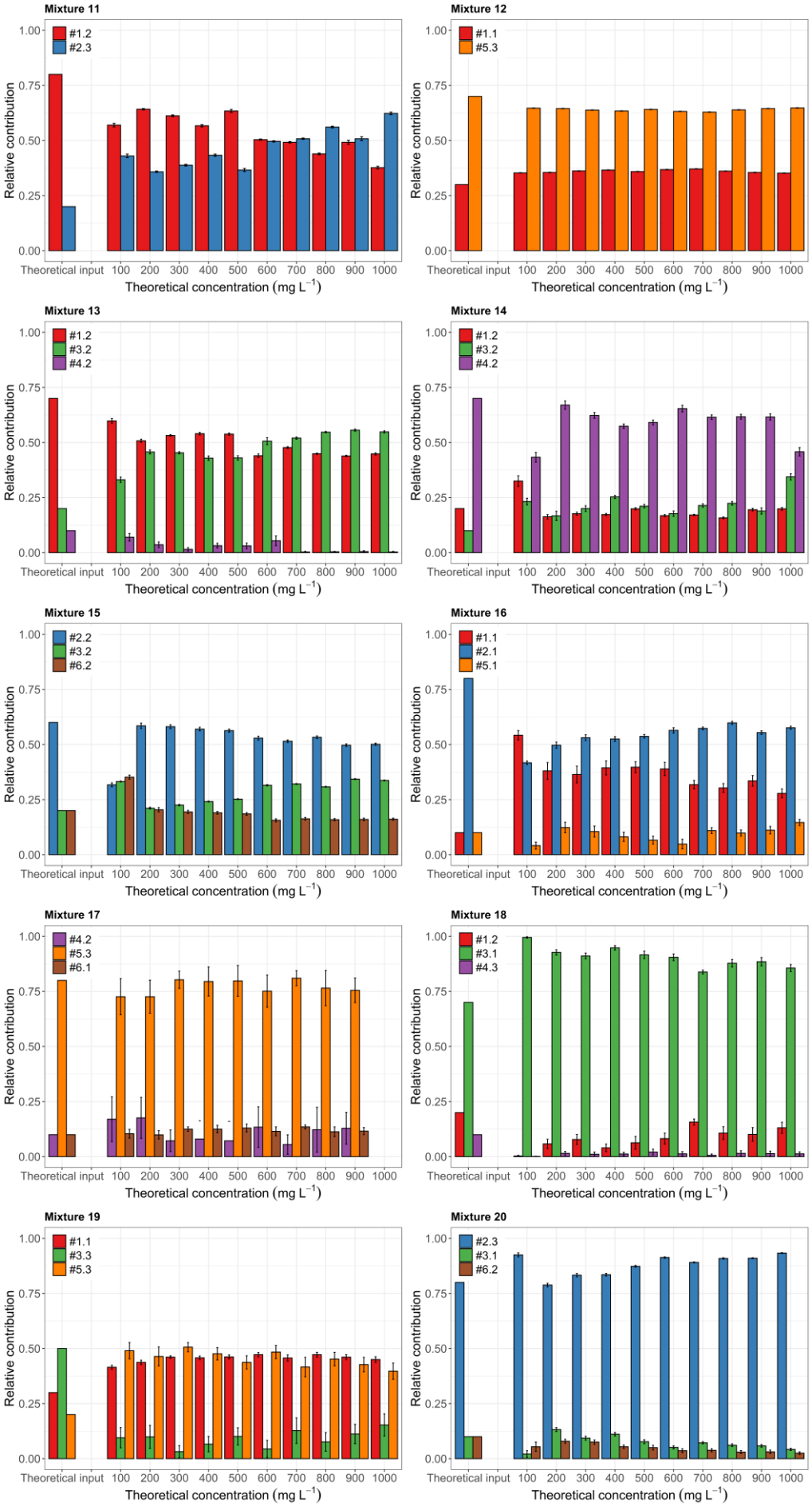
Mixture 11
#1.2
#2.3
Mixture 12
#1.1
#5.3
Mixture 13
#1.2
#3.2
#4.2
Mixture 14
#1.2
#3.2
#4.2
Mixture 15
#2.2
#3.2
#6.2
Mixture 16
#1.1
#2.1
#5.1
Mixture 17
#4.2
#5.3
#6.1
Mixture 18
#1.2
#3.1
#4.3
Mixture 19
#1.1
#3.3
#5.3
Mixture 20
#2.3
#3.1
#6.2
Relative contribution
0.00
0.25
0.50
0.75
1.00
Theoretical input 100 200 300 400 500 600 700 800 900 1000
Theoretical concentration (mg L^{-1})

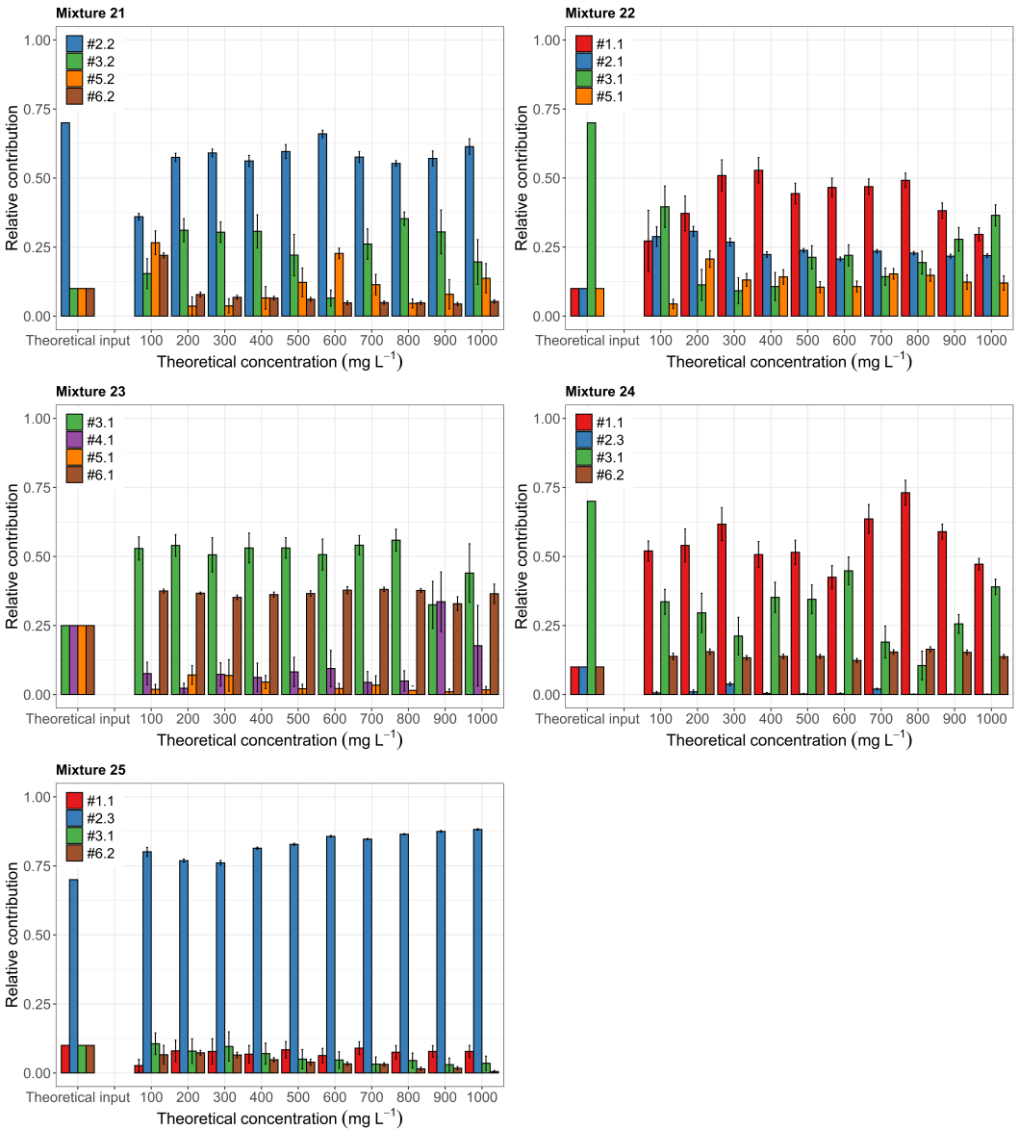

Figure 2.7 Un-mixing results for artificial mixtures of two soil samples (mixtures 1 and 12), three soil samples (mixtures 14 and 20) and four soil samples (mixtures 22 and 25) using MixSIAR at increasing theoretical concentrations. Model predictions are compared with the known proportions (theoretical input) of soil samples mixed (indicated by #soil.fraction, with 'soil' representing the test soils (n = 6), and 'fraction' the sieved fraction size (.1 for < 32 µm; .2 for 32–63 µm; .3 for 63–125 µm).

2.4 Discussion

2.4.1 Specific Consideration for Using the High Frequency Spectrophotometer Approach

Absorbance data are known to be influenced by concentration (Thomas et al., 2017). Our results show that concentrations are strongly linearly correlated with absorbance (Figure A.4 and A.5). However, the correlations are soil sample-dependent, which renders it necessary to correct the

absorbance data from each soil sample with its specific concentration when comparing different soil samples. As the aim here was to un-mix artificial mixtures into the known individual contributions of the constituent samples, it is essential to make sure that compensation is made for the correct concentrations in order to avoid over- or under-estimations of contributions. To this end, theoretical input concentrations were compared with measured concentrations. Theoretical concentrations are subject to the mixing processes inside the tank and the possible incomplete suspension of particles. This latter process seems to be important in the measured concentration results, showing that samples sieved at a larger mesh size deviate more from theoretical concentrations (Figure 2.3). Despite this observation, and based on the data shown in Figure 2.3 and Table 2.1, losses observed in measured concentrations were consistent. These concentrations were, however, subject to representative sampling and weighing errors, and show slightly weaker correlations with absorbance; hence, the use of theoretical concentrations in this study.

In addition to the influence of concentration, particle size affects absorbance readings (Berho et al., 2004). Finer particles, at the same concentrations, resulted in higher absorbance values over the whole range of wavelengths compared with particles with coarser sizes. Together with the influence that particle size can have on sediment properties (Collins et al., 2017; Laceby et al., 2017), different particle sizes can also induce different absorbance patterns over specific wavelength ranges, as certain wavelengths might be subject to specific SS properties (Byrne et al., 2011). These differences were, however, found to be rather small in the present study (Figure 2.4 and A.7) when compared with the effects of concentration and particle size. Since the LISST sensor measurements showed that particle size is an intrinsic SS property remaining unchanged (assuming minimal dissolution of particles and minimal breakdown of particles in suspension) during the experiments presented here, the analysis focused more on the compensation of absorbance in relation to concentration so as to allow proper comparisons between the absorbance values of the soil sources and between the absorbance values of the soil sources and target SS.

Effective tracers or fingerprints should behave in a linearly additive manner (Lees, 1997; Walling et al., 1993). Our results show that the absorbance readings of particles suspended in distilled water are linearly additive (Figure 2.6) and consistently so over the range of concentrations tested. Some deviations were found, however, at the lower concentrations, which are likely to be due to the smaller amounts of particles and thus larger relative errors where mixing is inconsistent or incomplete. In testing the linear additivity, artificial mixtures containing samples sieved to the same or different particle size fractions were used. The two groups of samples did not show significantly different results for linear additivity (Figure 2.6). Tests in which only finer or only coarser size fractions were used did not result in clear differences in the linear additivity.

The un-mixing results using the MixSIAR model followed a similar pattern to the results for the linear additivity tests. Higher deviations between modelled and known soil sample proportions occurred at the lowest concentrations but were found to deviate less at higher concentrations. No significant difference in performance was found when un-mixing soil samples sieved to the same or different particle size fractions (Table A.3). These results contrast with observations reported by Gaspar et al. (2019), who found estimations were less reliable at finer particle sizes. Gaspar et al. (2019) tested the un-mixing performance of artificial soil mixtures (dry material), looking at geochemical composition, using estimations from the FingerPro model. However, these authors only sieved one mixture to three different size fractions (with 10 replicates for each fraction) whereas the source samples were sieved to just one fraction (<63 µm). On the contrary, in the present study the soil sources were sieved to different size fractions (no replicates, with different concentrations tested). Our approach thus results in a comparison between mixtures and sources with a common particle size range and helps to eliminate uncertainties in the un-mixing induced by particle size.

It is informative to compare results of the present study to others with respect to the accuracy of un-mixing, although it is important to acknowledge that un-mixing model structures vary and this can influence performance. Haddadchi et al. (2014b) tested four different mixing models (Modified Hughes, Modified Collins, Landwehr and Distribution models) using the geochemical properties of sources and mixtures, with mixtures being artificially created. Maximum model deviations ranged from 10.8% to 29% depending on the model used, indicating that therefore the choice of the un-mixing model is an important consideration, with the choice partially depending on the type of tracer used (Haddadchi et al., 2014b). Gaspar et al. (2019) reported a maximum AE of 10% for un-mixing using both dominant and non-dominant mixtures (using elemental geochemistry). The present study, in comparison, found AE >10% in most of the 25 different mixtures (except 2 out of the 12 two-sample mixtures and 3 out of the 8 three-sample mixtures), with maximum AE up to 26.7% for two-sample mixtures, 41.0% for three-sample mixtures and 48.8% for four-sample mixtures. The observed high AE for the three-sample mixtures is an extreme value however, since the second highest AE shows a value of 27.7%. Furthermore, the extreme outlier in the three-sample mixtures was found in mixture 19 where soil sample contributions added were rather equal (20%, 30%, 50%), while the extremes in the four-sample mixtures were found in mixtures 22 and 24 where there was a clear dominant soil sample present (70%, with other soil sample contributions of 10%). These results suggest that the absorbance readings from a submerged spectrophotometer can be used as fingerprints and thus to estimate the soil sample contributions of two and three-sample artificial mixtures with similar accuracy than the existent methods. However, some of the

four-sample artificial mixtures showed unacceptably high AE, showing the limitation of the method to distinguish four soil samples when these present similar absorbance signals.

Models for the three and four-sample mixtures did not always converge, exceeding the Gelman-Rubin diagnostics threshold value. Tests showed that increasing the number of iterations (chain length) improved the diagnostics for certain mixtures. However, we decided not to extend beyond the selected 'short' settings due to long computation times (>5 days for each model run). Furthermore, we observed that, for all but one mixture, certain concentrations satisfied the diagnostics. Combined with the consistency in modelling results over the different concentrations within each mixture, this indicated the reliability of the modelling outcomes for those situations in which the diagnostics were not satisfied.

These highest AE values found herein can be partly explained by examining the spectra in more detail. For the two source artificial mixtures, the high AE (20%) values were seen in situations where the mixture absorbance values did not fall in between the range of absorbance values of the individual soil samples mixed (i.e., the artificial mixture has lower or higher absorbance values compared to the values of the individual soil samples; see also red dots indicated in Figure 2.6). Failures can be due to small deviations in concentrations (e.g., settling), as expected and aimed concentration slightly differ (Figure 2.3). Such situations violate the so-called bracket or range test used as a conventional screening step in sediment source fingerprinting decision-trees (Collins et al., 2017). Failure of the bracket test was only observed in the case of mixtures using two soil samples (Figure 2.6a; for 23% of the total values here). Using measured instead of theoretical concentrations, did not improve this result, resulting in a larger number of violations (Figure A.9). In the three soil source mixtures, predicted soil source contributions seemed to vary between soil samples that show a similar course of absorbance values over the whole range of measured wavelengths. This was, for example, observed for mixtures 13 and 16. MixSIAR failed to predict one clear dominant soil sample in these mixtures (i.e., 70% and 80% dominant soil samples used as input), but rather predicted two soil samples each with relatively high contributions around 40-50%. These two soil samples exhibit the same absorbance patterns (i.e., the absolute differences between the absorbance values of the soil samples are highly similar at all wavelengths tested); using the model to predict the dominant soil sample under such circumstances is problematic. The same pattern holds for the four-soil sample mixtures; in both mixtures 22 and 24 (with the highest reported AE values) the model failed to predict the dominant soil source. Both these mixtures used soil samples 1.1 and 3.1, which had absorbance values that showed minimal deviations between them (absolute values) and followed the same patterns (i.e., small absolute differences between all wavelengths tested), making it difficult for the model to differentiate between these two soil source samples. Furthermore, the mixture absorbance data in both these mixtures plotted exactly in

between the absorbance values of the two soil samples; this most likely caused the model to fail to predict the correct dominant soil source. This outcome can be observed in Figure 2.7, where model predictions show more equal contributions for the artificially mixed soil samples (mixture 22) and a more dominant soil sample 1.1 (mixture 24) despite soil sample 3.3 being the dominant soil source in both mixtures.

Scaling up beyond the laboratory scale, it would be informative to use independent evidence to validate any source apportionment estimates using absorbance spectra (which need to be statistically significantly different for the individual sources in question). However, this requirement for independent evidence is difficult to fulfil meaning that many source fingerprinting studies continue to rely on the use of mixture tests as verification of predicted source proportions (Collins and Walling, 2004).

2.4.2 Wider Implications for Suspended Sediment Fingerprinting

The use of sensors that measure spectrophotometrically at high frequency in situ substantially reduces the need for extensive analyses in the laboratory in conjunction with the collection of conventional physical water samples; such sensors thereby allow much faster acquisition of tracer data (Martínez-Carreras et al., 2016), due to the in situ measurements. Therefore, despite the initial purchasing costs of the spectrophotometer (ca. US$20.000), and the need to control for sensor drifts to validate the absorbance data results (Gamerith et al., 2011), total costs decrease over time. This is in contrast to classical sediment fingerprinting approaches, wherein laboratory analyses of all samples is required (e.g., different geochemistry analyses estimated at as much as ca. US$1.500-2.000 per sample; Horowitz, 2013), increasing both labour and analysis costs substantially when increasing measurement intervals and sampling campaign duration. The collection of absorbance data in situ could therefore improve the temporal resolution of sediment source fingerprinting and eventually give better insights into how sources of SS change over short time scales. This evidence gap has been highlighted by Navratil et al. (2012) and Vercruysse et al. (2017), who argued that a better understanding of sediment dynamics over short time scales is key to improving sediment transport modelling and for devising more robust solutions to catchment sediment management problems. With regard to the present study, it clearly remains important to test the use of the spectrophotometer for un-mixing source contributions in real world settings, including at catchment scales. In the experiments here, using Luxembourgish soil samples with differences in both colour and expected geochemistry, absorbance data of the soil samples were in most situations sufficiently different for un-mixing. It is therefore a prerequisite to investigate if absorbance spectra responses of potential SS sources in a real world setting are sufficiently different enough to allow source discrimination.

Initial steps to identify areas or sources that could permit robust discrimination could be based on, for instance, differences in underlying geology as was done in this study. Looking at the results presented herein, seeing the uncertainties associated with four samples mixtures, applying this approach in a field setting might require the selection of a limited number of potential sources to avoid poor discrimination and thus poor source apportionment results. Another approach that could potentially increase the ability to differentiate between sediment sources could be achieved by selecting only a number of wavelengths (i.e., selecting those tracers that best discriminate between sources). Reducing the number of tracers could also overcome issues with the long model calculation times faced when using all wavelengths as tracers.

Dissolved compounds in natural waters (e.g., nitrates and DOC) will influence the absorbance readings of the spectrophotometer (D'Acunha and Johnson, 2019). Furthermore, the composition of the water (which was compensated for in the present study by subtracting the blank water background signal from the absorbance data) may well fluctuate in field settings (Wilson et al., 2013). To establish this background signal in field conditions might be challenging and ways to overcome this remain to be investigated. One possible solution to this challenge might be to use only absorbance values from those wavelengths that are less responsive to dissolved compounds. This consideration warrants further research.

In our proof-of-concept laboratory experiments, the individual soil sample ('source') absorbance spectra were sufficiently able to un-mix the majority of the absorbance spectra of the artificial soil mixtures. However, the absorbance signatures of potential SS sources (e.g., surface soils and channel banks) would be difficult to obtain because the spectrophotometer employed in this study is only able to measure while submerged. One approach here could be to sample material being mobilised and routed from potential sources towards the river channel (e.g., from rill erosion, or during/immediately after rainfall events when clear patterns of erosion or mobilisation of source materials have emerged). Such intermediate sampling would help address uncertainties associated with particle size selectivity (Laceby et al., 2017) and ensure, when measuring in a laboratory experiment as presented in this study, direct comparison of absorbance spectra representative of eroded material from individual sources with the spectra for SS. Clearly, however, the use of the approach reported herein would face challenges for some source types on this basis, with the obvious problematic source being eroding channel banks. Given the juxtaposition of banks to the river water, all particle size fractions are delivered to the water column, since there is no runoff pathway to result in selective delivery. Given this issue, it is more likely that the use of spectrophotometers *in situ* will be more relevant to un-mixing spatial SS sources using a confluence-based approach (e.g., Wynants et al., 2020). Here, sensors could be placed near the outlets of tributaries to create an archive of absorbance spectra of tributary-based spatial sources and on the

main stem further downstream to represent the spectra of target SS. Concentration issues could be handled similarly to the laboratory experiment reported herein since by dividing the absorbance of both sources (i.e., tributaries) and the main stem measurements by the measured concentrations (which could be estimated using sediment rating curves, showing the relationships between SSC and turbidity using either turbidity meters or using the turbidity measured by the spectrophotometer itself), they can be scaled to the same SS concentrations (Figure 2.4). Spectrophotometers can be equipped with an automatic brush (ruck::sack; Scan Messtechnik GmbH, Vienna, Austria) that cleans the sensor lens before every measurement. Next to that, optical sensors require regular maintenance to avoid instrument drifts caused by biofouling (e.g., bi-weekly cleaning as proposed by Martínez-Carreras et al., 2016).

2.5 Conclusions

The following conclusions can be drawn from the laboratory experiments conducted herein:

(1) Absorbance data and concentration show a strong linear relationship. It is thus essential to compensate absorbance data with concentration to un-mix different sources in artificial mixtures.

(2) There is a logarithmic relationship between absorbance and particle size, with a strong influence of particle size on the absorbance data with increasing concentrations (e.g., finer particle sizes result in higher absorbance values per mg L^{-1}).

(3) Absorbance data behave in a linearly additive manner, with deviations between expected and measured absorbance for artificial mixtures being <20% for all comparisons and <10% for more than half of the cases.

(4) The MixSIAR model mostly successfully un-mixed the artificial soil sources (with an average AE of 14.9% for all soil samples in all mixtures), correctly predicting dominant soil samples in the mixtures. The MixSIAR model worked better for the two and three soil sample mixtures in the present study. Results for the four sample mixtures were less promising, but most likely inherent to the choice of soil samples used in those mixtures.

To be able to use the approach described in field settings, the following issues must be addressed:

(1) There is a need to create robust methods to define sediment source absorbance signals. A key challenge here is the selection of the most appropriate sediment particle size to define source material absorbance. A prerequisite is that the sediment sources result in absorbance signals that are sufficiently different to provide a basis for robust source discrimination and apportionment.

(2) Concentrations of SS need to be measured accurately. This information is needed to compensate the absorbance data for concentration in order to compare source absorbance data with the corresponding target SS data.

Chapter 3 Use of a Submersible Spectrophotometer Probe to Fingerprint Spatial Suspended Sediment Sources at Catchment Scale

Abstract

Sediment fingerprinting is used to identify catchment sediment sources. Traditionally, it has been based on the collection and analysis of potential soil sources and target sediment. Differences between soil source properties (i.e., fingerprints) are then used to discriminate between sources, allowing the quantification of the relative source contributions to the target sediment. The traditional approach generally requires substantial resources for sampling and fingerprint analysis, when using conventional laboratory procedures. In pursuit of reducing the resources required, several new fingerprints have been tested and applied. However, despite the lower resource demands for analysis, most recently proposed fingerprints still require resource intensive sampling and laboratory analysis. Against this background, this study describes the use of UV-VIS absorbance spectra for sediment fingerprinting, which can be directly measured by submersible spectrophotometers on water samples in a rapid and non-destructive manner. To test the use of absorbance to estimate spatial source contributions to the target suspended sediment (SS), water samples were collected from a series of confluences during three sampling campaigns in which a confluence-based approach to source fingerprinting was undertaken. Water samples were measured in the laboratory and, after compensation for absorbance influenced by dissolved components and SS concentration, absorbance readings were used in combination with the MixSIAR Bayesian mixing model to quantify spatial source contributions. The contributions were compared with the sediment budget, to evaluate the potential use of absorbance for sediment fingerprinting at catchment scale. Overall deviations between the spatial source contributions using source fingerprinting and sediment budgeting were 18% for all confluences (n=11). However, some confluences showed much higher deviations (up to 52%), indicating the need for careful evaluation of the results using the spectrophotometer probe. Overall, this study shows the potential of using absorbance, directly obtained from grab water samples, for sediment fingerprinting in natural environments.

3.1 Introduction

Sediment fingerprinting is commonly used to estimate suspended sediment (SS) sources (see e.g., reviews by Collins et al., 2017, 2020). It is increasingly used to assemble much needed information for targeting best management interventions for addressing issues resulting from excessive SS inputs, such as reduced light penetration in the water column (Owens et al., 2005) and increased siltation (Nones, 2019; Owens et al., 2010). Identifying SS sources is especially important in the pursuit of improving the ecological status of surface waters, as dictated by legislation such as the European Water Framework Directive (WFD; 2000/60/EC, 2000). The need to take action is becoming even more crucial in the context of global change, as human activities and related changes to land use are accelerating soil erosion and concomitant sediment delivery at global scale (Borrelli et al., 2017).

The sediment fingerprinting approach is based on the identification and collection of samples of potential sediment sources, which, together with target SS samples, are analysed in the laboratory. Differences between the properties of the sampled sources, i.e., their fingerprints, are then used to estimate the relative contribution of each source to the target SS (e.g., Collins et al., 2020). However, collection of representative source material and SS sampling, and conventional laboratory analyses of commonly-used fingerprints generally require high workloads and generate substantive analytical costs (Collins et al., 2020; Evrard et al., 2022), therefore limiting their application beyond academic research (Pulley and Collins, 2021). There is thus a need for easier-to-measure fingerprints in combination with simplified sampling procedures to allow for a wider uptake of the approach (Pulley and Collins, 2021).

To this end, fingerprinting procedures based on cheaper and easier measurements have been developed and tested. These include, for instance, the use of conventional document scanners (e.g., Pulley and Collins, 2022; Pulley and Rowntree, 2016) to measure colour fingerprints, and spectrometers from which both colour (e.g., Legout et al., 2013; Martínez-Carreras et al., 2010c) and geochemical fingerprints (e.g., Cooper et al., 2014b, 2015; Martínez-Carreras et al., 2010b) have been derived. These less onerous techniques offer the potential to increase the number of observations to subsequently inform how SS sources change at finer temporal and spatial scales (e.g., Cooper et al., 2014b, 2015). High frequency temporal data might facilitate a better and fuller understanding of which SS sources contribute at which time and in what proportions to the target SS, as sediment delivery from sources to streams is complex, involving different processes at multiple spatial and temporal scales (Fryirs, 2012).

While some techniques allow for fingerprints to be measured with relative ease, the need for SS sampling, preparation and laboratory analysis remains. In an attempt to overcome such resource

demands, Lake et al. (2022a) tested the novel use of a UV-VIS spectrophotometer sensor for sediment fingerprinting purposes. Artificially created mixtures were used, consisting of soil source samples with clear contrasts in colour and geochemistry, i.e., differences that were expected to influence the absorbance spectra at different wavelengths (i.e., fingerprints) (Lake et al., 2022a). Known soil source contributions for each mixture were used to evaluate the mixing model results (when using the MixSIAR Bayesian mixing model) (Stock et al., 2018; Stock and Semmens, 2016). Evaluation indicated satisfactory results for the un-mixing of mixtures consisting of two and three different soil samples (with respective mean absolute errors be- tween known inputs and model results of 15 % and 13 % respectively); but the un-mixing results for mixtures consisting of four soil samples were slightly less robust (with respective mean absolute errors of17%). Analysis showed that SS concentration, particle size and the water environment influenced the absorbance data. During these initial tests, only controlled experiments in a laboratory tank (with 40 L of water) were conducted. As the submersible spectrophotometer used was designed to conduct in-stream measurements, it was proposed that the spectrophotometer probe could be used in field studies to fingerprint SS source contributions at high temporal resolution. Contrary to other fingerprinting methods that require laboratory analysis, this approach could decrease the interval between measurements (e.g., measurement interval of minutes) without adding to resource needs for sampling and analysis (i.e., direct in-stream fingerprint measurements). Insights into temporal changes in SS source contributions changes and, specifically, a more detailed investigation into the activation of specific sources at different times might thus be improved (e.g., Cooper et al., 2015; Navratil et al., 2012; Vercruysse et al., 2017). This information is essential to understand the hydro-sedimentary dynamics of a catchment (i.e., changes over short temporal scales), and important if targeted sediment control strategies are to be implemented (e.g., Vercruysse et al., 2017).

Despite the reliable laboratory performance, it remains to be assessed how well the approach presented by Lake et al. (2022a) performs with 'real world' samples. Fingerprints do not always allow for accurate catchment source apportionment, even if they perform well in laboratory setting (Batista et al., 2022). The present study therefore tests if absorbance, measured on grab water samples and using a confluence-based sampling strategy, can be used to determine the relative contributions of individual spatial sediment sources. This sampling strategy considers in-stream SS from upstream tributaries as the spatial sources, and in-stream SS from the downstream channel as the target SS (e.g., Collins et al., 1996, 1997b; Klages and Hsieh, 1975). This procedure circumvents challenges in determining which soil sources are contributing to target SS by using tributary SS samples to represent the spatially-integrated fingerprints of sub-catchments. Furthermore, with the confluence-based approach, difficulties in determining which particle size fractions are transported from potential soil sources (i.e., source types rather than spatial sources)

to the stream are circumvented by only considering those fractions already delivered to the tributary catchment streams (Laceby et al., 2017). This facet is important since sediment fingerprints often vary with particle size (Collins et al., 2017; Laceby et al., 2017) : particle size directly influences absorbance values (Lake et al., 2022a; Sehgal et al., 2022).

Building on the work of Lake et al. (2022a) and taking into account the aforementioned limitations regarding the resource needs in sediment fingerprinting, this study aims to obtain rapid absorbance measurements at the 200-730 nm wavelength range (i.e., sediment fingerprints) directly measured on grab water samples using a submersible UV-VIS spectrophotometer probe. These absorbance output readings will then be used directly to estimate spatial suspended sediment sources at catchment scale. To this end, we first evaluated the potential of the selected catchment to discriminate between spatial SS sources by investigating (i) differences in absorbance between source streams, and (ii) how absorbance patterns in same sampling sites compared during different campaigns, to investigate temporal (in)consistency in spatial SS source fingerprints. Secondly, modelled spatial source contributions, using the MixSIAR Bayesian mixing model (Stock et al., 2018; Stock and Semmens, 2016), were then compared with the calculated sediment budget, based on SS concentration and discharge measurements, to evaluate model performance.

3.2 Materials and Methods

Manual grab water samples were collected during storm runoff events at a series of confluences, following a confluence-based sampling strategy. The samples were analysed using a UV-VIS spectrophotometer installed in a custom-made laboratory test chamber. The absorbance spectra of the SS spatial source samples and downstream target SS sample were then used to estimate the relative contributions of each source using a Bayesian mixing model.

3.2.1 Sampling Sites

Sampling was performed in the Roudbach catchment (44 km^2 at Platen), located in the western part of Luxembourg (Figure 3.1). Land use in the catchment consists of forest, grassland and cultivated land. Lithology is characterised by schist, slates and phyllites bedrock in the northern part, and by red sandstone (“Buntsandstein”) and marls in the middle and southern parts. Altitudes range between 553 m and 260 m above sea level. Land use, lithology and elevation data is made available by the ‘Administration du Cadastre et de la Topographie’ (ACT). The climate is semi-oceanic, with monthly maximum mean temperatures varying between 0 °C in January and 18 °C in July, and a long term average annual precipitation of 845 mm (1954-1996; Pfister et al., 2005).

At each confluence (n=11), manual grab water samples were collected at three sites: at the two upstream SS source sites (between 20 and 10 m upstream of the confluence), and at the downstream target SS site (between 10 and 20 m downstream of the confluence) (Figure 3.2). At each sampling site (n=33), a 2-L grab sample was collected during three storm runoff events: campaign 1 was carried out on 03/11/2021, campaign 2 on 04/01/2022 and campaign 3 on 16/02/2022. Samples were stored in a dark, cold room (4-5 °C) and analysed in the following 2-5 days. Precipitation records from the weather station at Reichlange (see Figure 3.1b,c) were made available by the 'Administration de la Gestion de l'Eau' (AGE).

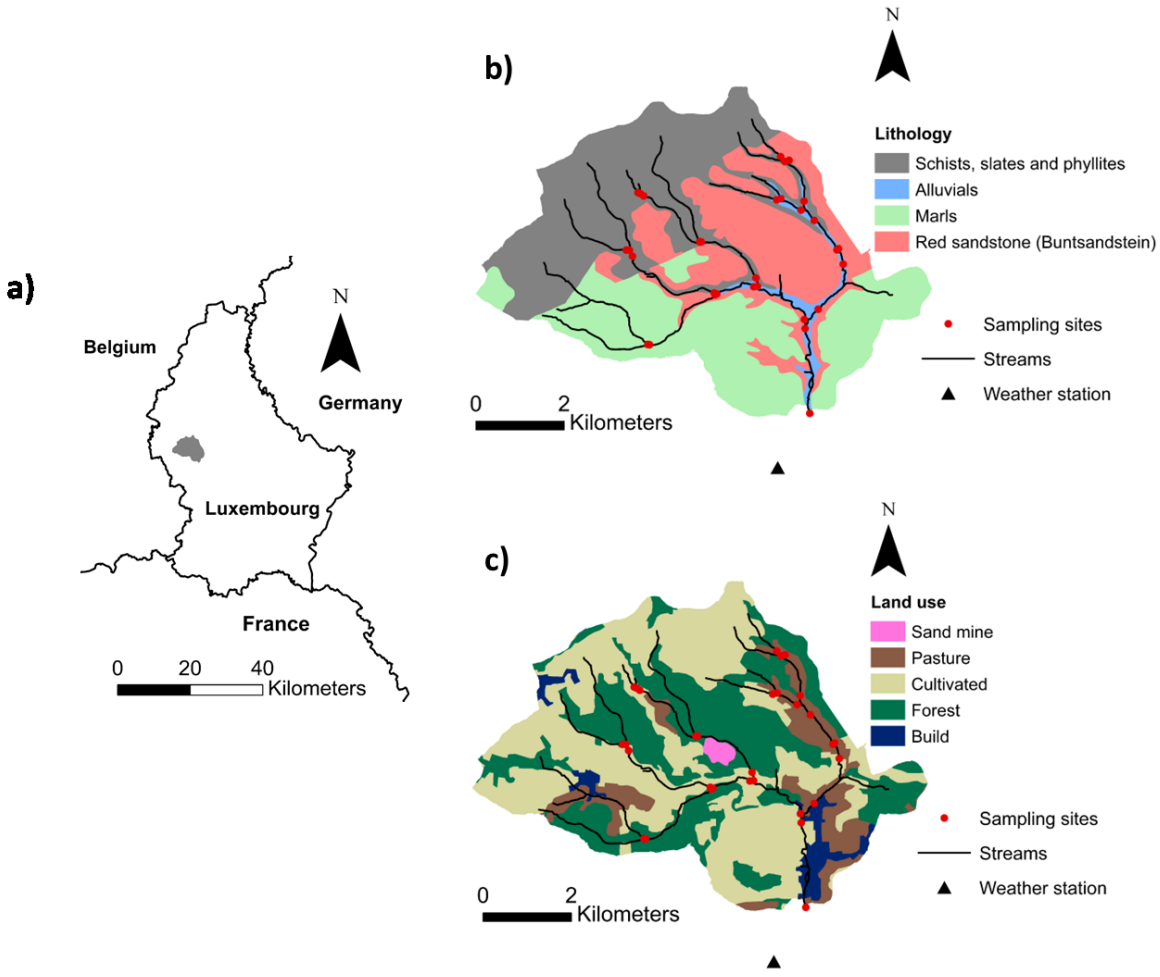

Figure 3.1 Location of the Roudbach catchment in Luxembourg (a), catchment lithology (b) and land use (c).

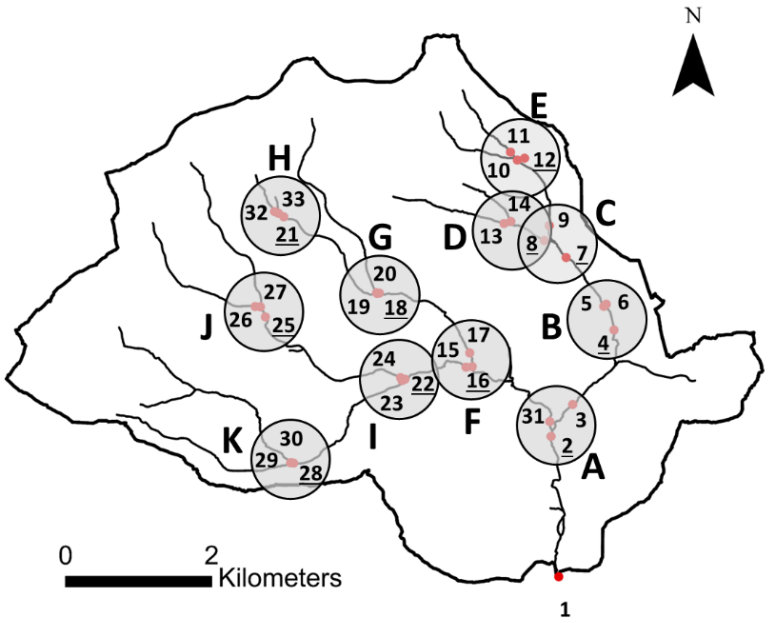

Figure 3.2 Sampling sites (numbers 1-33) within the Roudbach catchment. Each circle represents a confluence (letters A-K) enclosing the two upstream spatial source sampling sites and the downstream target suspended sediment sampling site (underlined number). Sampling site 8 is both a spatial source (confluence C) and target (confluence D) SS sampling site. The catchment outlet is located at sampling site 1.

3.2.2 Laboratory Analyses

A sub-sample of each grab water sample was filtered to determine its suspended sediment concentration (SSC) by filtering a known volume through pre-weighed 1.2 µm pore size Whatman GF/C glass fibre filters. Filters were dried at 105°C and weighed, and after filtration, again dried at 105°C and weighed. The filtrate water for each sample was collected and stored for 1-3 days. Measured SSCs for all sampling sites, for the three campaigns, are shown in Table 3.1.

Grab samples were analysed using a S::can spectro::lyser™ submersible spectrophotometer probe (Scan Messtechnik GmbH, Vienna, Austria), installed in a custom-made laboratory test chamber (Figure 3.3a). The spectrophotometer records on the absorbance over the UV-VIS wavelength range (200-730 nm) at 2.5 nm intervals by measuring the transmittance of a light beam (i.e., xenon-flash light) through the water sample. The spectrophotometer, with a 15 mm optical path length, was installed horizontally in the test chamber (inner dimensions 14x10x10 cm) to avoid potential settling of SS particles on the measurement window. A magnetic stirrer was used to make sure all particles were kept in suspension (visually checked for all samples tested). Grab water samples were shaken well by hand, and an aliquot of ca. 1.2 L was poured into the test chamber. After allowing homogenisation within the test chamber for 2 minutes, the spectrophotometer measured for 6

minutes at 2 minute intervals (n=4). After each grab sample, the test chamber was rinsed with milli-Q water and dried. Absorbance at each measured wavelength was divided by measured SSCs to eliminate the effect of SSC on absorbance (see Lake et al., 2022a).

The absorbance of the grab water samples after filtration was measured using the multifunctional slide provided by the manufacturer (Scan Messtechnik GmbH, Vienna, Austria; Figure 3.3b). Measurements were made over a 6 minute timeframe, at 2 minute intervals (n=4). After each sample, the slide was rinsed with milli-Q water and dried. Grab sample absorbance measurements were then compensated by subtracting the filtered water absorbance spectrum of the corresponding grab sample to eliminate the influence of the dissolved, non-SS components on absorbance spectra. Similarly, Lake et al. (2022a) compensated their absorbance measurements by subtracting the absorbance of the deionized water used during the experiments.

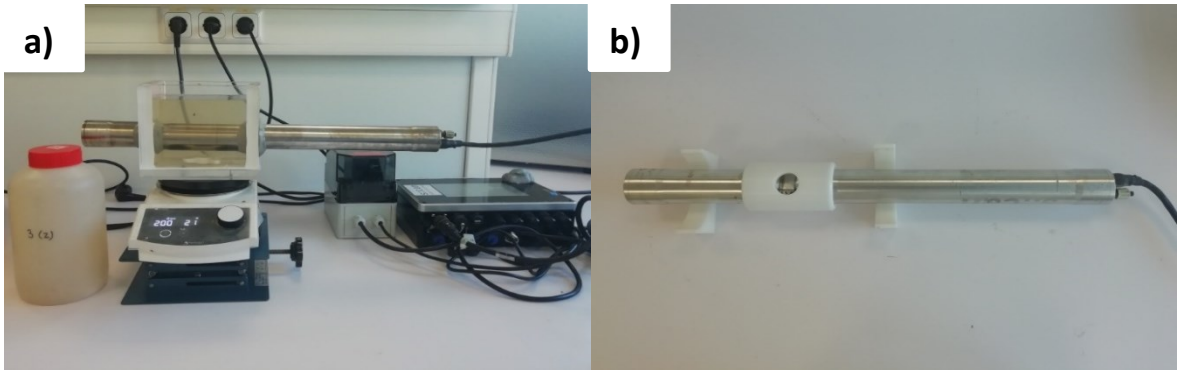

Figure 3.3 Photograph of the self-made test chamber with the spectrophotometer probe and the magnetic stirrer during the measurements of the grab samples (a). Photograph of the spectrophotometer probe with the multifunctional slide during the measurements of the filtered water samples (b).

3.2.3 Discharge Measurements

At five sampling sites (sites 1, 3, 17, 23, 31; Figure 3.2), the water level was measured continuously at 15 minute intervals during the period 22/10/2021 – 22/03/2022 using ISCO 4120 pressure probes. Discharge time series were created by means of a rating curve between water level and discharge. Water levels and discharges were measured in parallel during the days of the sampling campaigns (n = 3), at different times during the day (n = 4) to cover relatively higher and lower discharges.

Specific discharge was calculated for each site with available discharge measurements The surface catchment area (Table B.1) contributing to discharge at each site was calculated using ArcMap 10.5 (ESRI, Redlands, CA). Specific discharge data and computed catchment areas were then used to estimate discharge at the ungauged sampling sites using the drainage area method (e.g., Emerson

et al., 2005). Estimated discharges for all sampling sites, for the three campaigns, are shown in Table 3.1.

3.2.4 Evaluating the Use of Absorbance Spectra for Sediment Source Fingerprinting

The following analyses were carried out to evaluate the potential use of absorbance to fingerprint spatial SS sources under field conditions: analysis of the differences between spatial source absorbance values and patterns therein (section 3.2.4.1); evaluation of modelled spatial source contributions against the estimated sediment budgets (section 3.2.4.2), and; comparison of model results when using different wavelength selection procedures, to evaluate the possibility of omitting the need for absorbance compensation and to eventually reduce un-mixing calculation times (section 3.2.4.3).

3.2.4.1 Absorbance Patterns

Absorbance patterns were analysed in two different ways. First, average absorbance over the full range of wavelengths (200-730 nm) was calculated for each sampling site and compared. Second, for each confluence, mean absorbance differences between the two sources were calculated. These approaches permit the investigation of (i) differences in mean spatial source absorbances for the same sites during the different sampling campaigns, (ii) differences in mean source absorbances between the spatial sources merging at the confluences, and (iii) whether these differences influenced deviations between the modelled spatial source contributions and the sediment budget estimations (section 3.2.4.2).

3.2.4.2 Sediment and water budgets

Measured SSCs (section 3.2.2) and discharge data (at gauged and ungauged sites; section 3.2.3) were used to calculate the relative contribution of SS and water from the upstream tributaries to the downstream sampling sites (Table 3.1). The sediment budget was then used to evaluate the un-mixing modelling predictions of spatial source contributions using the absorbance data as a fingerprint (section 3.2.4.3).

3.2.4.3 Un-mixing modelling

The MixSIAR model (Stock et al., 2018; Stock and Semmens, 2016) was used to un-mix the downstream target SS into the spatial source contributions using absorbance data. Model runs were executed for all sampled confluences, including when absorbance values from the target SS were outside the range of absorbance values of the spatial source streams. For all model runs, the Markov Chain Monte Carlo parameters were set as long (chain length = 300.000, burn = 200.000,

thin = 100, chains = 3). Model convergence was evaluated using the Gelman-Rubin diagnostic (variables <1.1). For each model run, MixSIAR output predicts a relative average contribution of each source with its corresponding standard deviations. All models were run using the High Performance Computing facility at the Luxembourg Institute of Science and Technology.

The modelling approach applied herein used the wavelengths (with 2.5 nm intervals) in the 200-730 nm range (Lake et al., 2022a) as fingerprints (n=213). Absorbance data for all grab samples were compensated for: (i) the absorbance of the filtered water to account only for the absorbance influenced by the SS (section 3.2.2; Lake et al., 2022a), and; (ii) the measured SSC to eliminate the effect of concentration (Lake et al., 2022a). Modelled spatial source contributions were compared with the sediment budgets.

Two other modelling approaches were tested and reported in this study. These approaches focus on the use of the 390-730 nm wavelength range. This part of the absorbance spectrum, the visible light spectrum, is highly related to turbidity (e.g., Rieger et al., 2004) and is therefore mainly influenced by SS particles. Using only this part of the wavelength range, removes, in principle, the effect of dissolved components that primarily influence wavelengths in the 200-390 nm range (e.g., Byrne et al., 2011; Figure B.2). A modelling approach using only the 390-730 nm wavelengths range should not therefore require compensation for the filtered water to eliminate the influence of dissolved components on the spectra. This approach also reduces computation time due to the lower number of wavelengths (n=137). Subsequently, so as to further reduce computation times, a second modelling approach was tested using the absorbance measurements in the 390-730 nm range with a lower resolution (absorbance readings at 10 nm intervals; n=35). This approach maintained the broad patterns of the absorbance data, while reducing the number of input wavelengths considered.

3.3 Results

3.3.1 Water and sediment budget

Total precipitation (in Reichlange) for the sampled storm runoff events was 10.9 mm for campaign 1, 47.2 mm for campaign 2, and 18.1 mm for campaign 3. An overview of the precipitation records and measured discharge at the catchment outlet in Platen is provided in Figure 3.4. Campaign 1 was conducted during one of the first storm runoff events of the hydrological year, during wetting-up. Campaign 2 took place during a large storm runoff event with much higher discharges than campaigns 1 and 3. Campaign 3 was performed during a storm runoff event of similar magnitude to campaign 1, though with the catchment being in a wetted-up state before the start of the event.

Table 3.1 presents estimated discharges, measured SSCs and estimated SS fluxes plus the relative source contributions of discharge and SS at the time of sampling. The relative contribution of discharge delivered by each source was mostly stable during the three sampling campaigns at most confluences, with absolute deviations < 2%. There was, however, a clear exception observed in the case of confluence C, wherein campaign 2 the relative discharge deviated by 38% and 39% compared with campaigns 1 and 3, respectively. This deviation was also apparent in the relative contribution of SS loads. Site 8 was the dominant contributing SS source in confluence C (Figure 3.2) during campaign 1 and 3 (90 and 83%, respectively), while its contribution was much smaller (5%) during campaign 2. The relative contribution of SS loads to downstream sites showed overall higher variability than discharge, for all three campaigns. Sources that dominated in terms of discharge also dominated in terms of the SS load. However, SS load relative contributions showed higher variability, with for instance confluence K showing a constant contribution from site 30 in terms of discharge (ca. 71%) for all three campaigns, while the corresponding SS load contributions were 64, 91 and 57% for campaigns 1, 2 and 3, respectively.

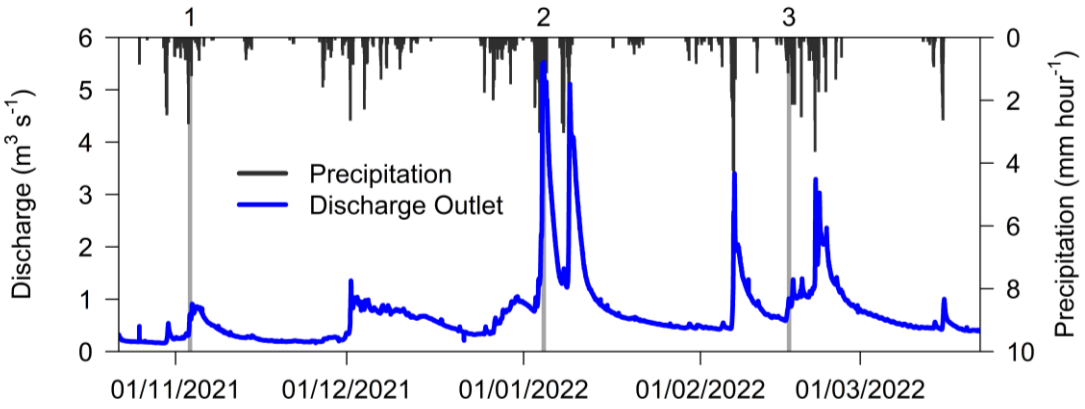

Figure 3.4 Precipitation records from the weather station in Reichlange, and measured discharge at the Roudbach catchment outlet in Platen (Figure 3.2). The sampling campaigns are highlighted in grey, and indicated by the campaign number (1-3) above the graph.

In Figure 3.5, a spatial overview of the SS fluxes within the catchment is shown for the three campaigns. At the downstream confluence (confluence A; Figure 3.2), most SS originated from the western tributary (contributing to sampling site 31). Here, during all three campaigns, the highest SS fluxes were measured in the southwestern streams (corresponding to sampling sites 15, 23 and 24; Figure 3.2). In the eastern tributary (contributing to sampling site 3), most of the SS came from the southern areas, with the northern streams showing relatively lower sediment fluxes. As observed in the eastern branch of the catchment, most northern streams in the western branch showed as well relatively low SS fluxes for all three sampling campaigns.

Table 3.1 Summary of the hydro-sedimentological data at all sampled spatial source sites for the three sampling campaigns. Data shown are the measured suspended sediment concentrations (SSCs), estimated discharge values, relative source discharge contributions to the downstream target SS site (in %; computed using a mass-balance approach), the estimated sediment flux, and the relative spatial source sediment load contribution at the time of sampling.

Confluence	Campaign	Source sampling site	SSC (mg L^{-1})	Discharge ($m^3 s^{-1}$)	Discharge (%)	Sediment flux (g s^{-1})	Sediment load (%)
A	1	31	35.1	0.44	68	15.5	60
		3	49.8	0.21	32	10.3	40
	2	31	683.6	3.32	70	2271	85
		3	281.8	1.43	30	403	15
	3	31	42.2	0.63	70	27	74
		3	35.2	0.27	30	9.7	26
B	1	5	28.0	0.14	98	3.9	99
		6	11.4	0.004	2	0.04	1
	2	5	160.0	0.98	98	156	99
		6	60.7	0.02	2	1.5	1
	3	5	19.9	0.19	98	3.8	99
		6	6.8	0.005	2	0.03	1
C	1	8	66.2	0.07	53	4.5	90
		9	8.3	0.06	47	0.5	10
	2	8	83.0	0.07	15	5.7	5
		9	279.6	0.39	85	108	95
	3	8	22.3	0.09	54	1.9	83
		9	5.9	0.07	46	0.4	17
D	1	13	75.3	0.03	49	2.1	70
		14	30.6	0.03	51	0.9	30
	2	13	78.2	0.19	50	15.2	56
		14	60.4	0.20	50	11.9	44
	3	13	28.4	0.04	49	1.1	55
		14	23.5	0.04	51	0.9	45
E	1	10	-	-	-	-	-
		11	-	-	-	-	-
	2	10	459.8	0.10	47	47.2	67
		11	200.7	0.11	53	22.9	33
	3	10	15.5	0.02	47	0.3	68
		11	6.4	0.02	53	0.14	32
F	1	15	35.1	0.29	71	10.1	78
		17	24.8	0.12	29	2.9	22
	2	15	484.9	2.02	72	978	79
		17	328.4	0.79	28	259	21
	3	15	38.1	0.39	72	15	91
		17	9.0	0.15	28	1.4	9

Confluence	Campaign	Sampling site	SSC (mg L^{-1})	Discharge ($m^3 s^{-1}$)	Discharge (%)	Sediment flux (g s^{-1})	Sediment load (%)
G	1	19	8.9	0.05	55	0.4	40
		20	16.6	0.04	45	0.6	60
	2	19	320.2	0.35	55	114	67
		20	196.8	0.29	45	57	33
	3	19	10.9	0.07	55	0.75	66
		20	6.6	0.06	45	0.39	34
H	1	32	-	-	-	-	-
		33	-	-	-	-	-
	2	32	149.7	0.14	70	20.5	75
		33	132.2	0.06	30	7.0	25
	3	32	12.3	0.03	70	0.3	94
		33	2.0	0.01	60	0.02	6
I	1	23	49.5	0.16	57	7.7	76
		24	18.1	0.12	43	2.4	24
	2	23	492.7	1.06	56	520	58
		24	453.8	0.83	44	375	42
	3	23	47.3	0.20	56	9.6	68
		24	28.9	0.16	44	4.6	32
J	1	26	33.3	0.04	51	1.5	60
		27	23.6	0.04	49	1.0	40
	2	26	369.2	0.28	51	104	60
		27	256.7	0.27	49	68	40
	3	26	11.2	0.06	51	0.6	50
		27	11.3	0.05	49	0.6	50
K	1	29	43.3	0.04	29	1.7	36
		30	31.2	0.10	71	3.0	64
	2	29	133.3	0.24	29	33	9
		30	567.5	0.61	71	344	91
	3	29	41.7	0.05	29	2.0	43
		30	22.5	0.12	71	2.7	57

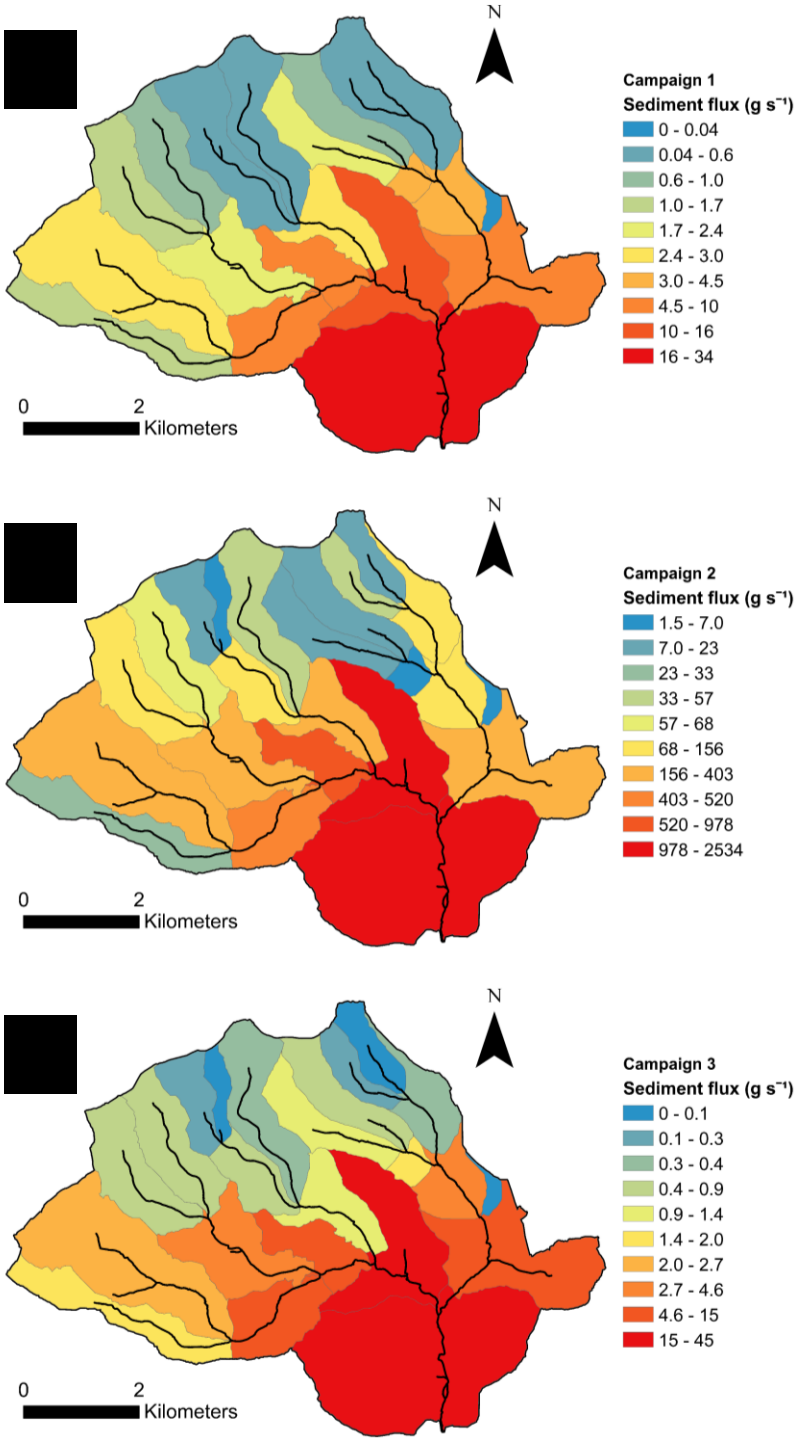

Figure 3.5 Spatial overview of suspended sediment (SS) fluxes for the three sampling campaigns in the Roudbach catchment; campaign 1 (a), campaign 2 (b), campaign 3 (c). Areas depicted are the sub-catchments belonging to the different SS spatial source sites (n=22) for each of the confluences. Colour values represent the different ranges of SS loads, using the Jenks natural breaks classification method applied to 10 intervals (Jenks, 1967).

3.3.2 Absorbance patterns

Average absorbance (per unit SS) for the same sites (Figure 3.6), measured during the three sampling campaigns, showed pronounced variability. The sites sampled during campaign 3 generally had the highest average absorbance (except for sites 6 and 14 where highest average absorbance was measured during campaign 2). Average absorbance was lower during campaign 2 than during campaigns 1 and 3 for most of the sites located on the western side of the catchment (sites 15-33). Exceptions in this regard were sites 18 and 20, where the average absorbance was highest for campaign 2 (by 18 and 33% respectively). For the sampling sites on the eastern side of the catchment (sites 1-14), the lowest absorbances were measured for either campaign 1 or 2, with the lowest average absorbances measured during campaign 1 at sampling sites 6, 9, 11 and 12. Site 13 showed the lowest variability in average absorbance between the three campaigns (maximum difference of 15%). Average absorbance values per campaign, combining all sites, were significantly different (Mann-Whitney test; $p < 0.05$ for campaigns 1 and 2; $p < 0.01$ for campaigns 1 and 3, and 2 and 3).

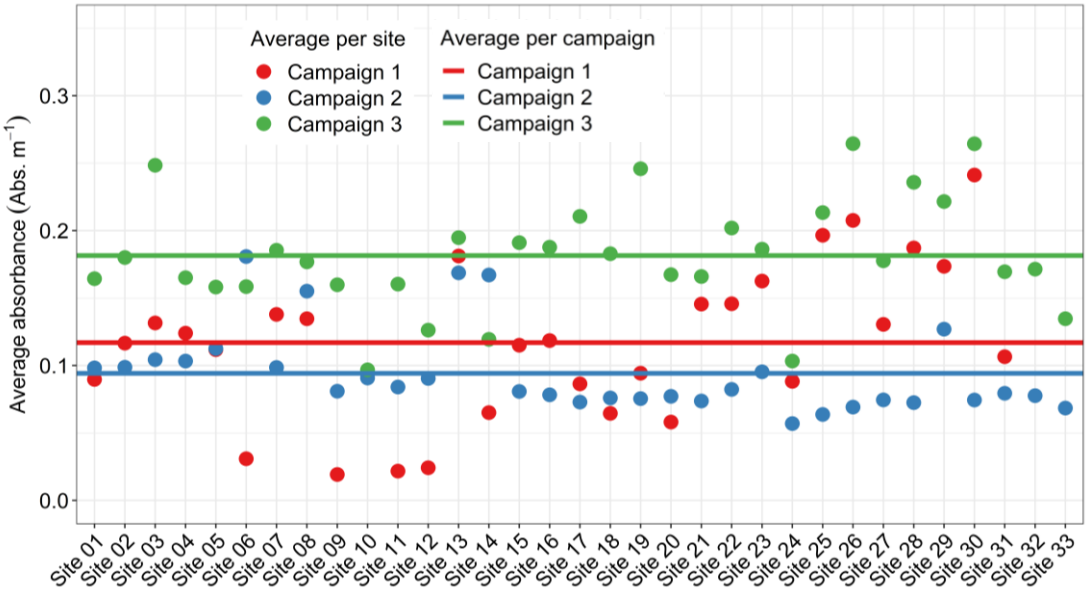

Figure 3.6 Average absorbance (represented by circular symbols) for each of the sampling sites, per campaign. The horizontal lines represent the average absorbance of all sampling sites for each campaign.

Figure 3.7 shows the difference in average absorbance between the two spatial sources contributing to each confluence, per campaign. For confluences in the northern and central parts of the catchment (Confluences B, C, D, F and K; Figure 3.2), samples collected during campaign 1 had the largest difference in average source absorbance (0.082 Abs m^{-1} vs. 0.053 Abs m^{-1} for the other confluences). In contrast, for confluences A and I in the southern part of the catchment,

samples collected during campaign 3 showed the highest differences in average source absorbance. For confluences in the northern part of the catchment (Confluences G, J; Figure 3.2), samples collected during campaign 3 showed highest differences in average absorbances (0.083 vs 0.045 Abs m^{-1}) compared with other confluences (confluences E and H are discarded as no data were available for campaign 1). For campaign 2, differences in source absorbance values were generally lower than during the other campaigns, and none of the confluences in campaign 2 showed differences in source absorbance values being higher than those of campaign 1 or campaign 3. However, for several confluences located in the southern part of the catchment (confluences A, B, C, I and K; Figure 3.2) the average source difference (0.052 Abs m^{-1}) during campaign 2 was much higher than in the northern part (confluences E, G, H and J) of the catchment (0.0064 Abs m^{-1}).

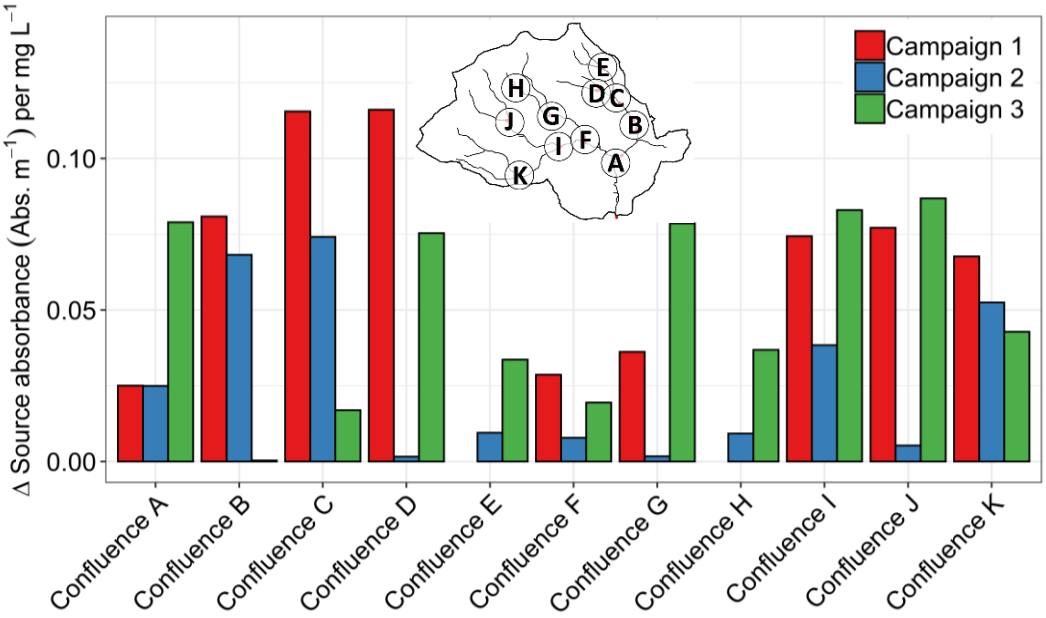

Figure 3.7 Mean absorbance differences between the two sources (**Δ** source absorbance) at each confluence, per campaign. The catchment map locating each confluence (letters A-K) is shown for reference.

Average source absorbance differences were significantly different for all confluences and campaigns (Mann-Whitney test, $p < 0.01$), except for campaign 1 at confluence F (p value=0.31), campaign 2 at confluence D (p value=0.31) and campaign 3 at confluence B (p value=1.00) where differences between the confluence sources were not statistically different.

3.3.3 Spatial Sediment Source Fingerprinting: Outcomes and Evaluation

The average difference ± standard deviation between the source fingerprinting modelling outcomes (Figure 3.8; Table B.2) and the SS budget estimates (Table 3.1) for all confluences during the three campaigns was 18 ± 15%. For individual campaigns, the corresponding average differences were 12 ± 15%, 20 ± 16% and 20 ± 12% for campaign 1, 2 and 3, respectively. The largest

differences during campaign 1 were found at confluence K (50%), during campaign 2 at confluences A, G and J (52, 32 and 38%, respectively), and during campaign 3 at confluences G and I (48 and 32%, respectively) (Figure 3.8). Deviations between source fingerprinting modelling and the SS budget did not show statistically significant relationships with discharge, SSC or difference in average source absorbance when using the entire dataset (Figure B.1; Appendix B).

From the sediment budget calculations, it was shown that relative contributions of spatial sources at specific confluences varied over the three campaigns; however, at most confluences one of the spatial SS source sites clearly contributes dominant discharge and SS loads. Exceptions in this regard were observed for confluence C and G, which showed a change in the dominant spatial source between campaigns. This change in dominant source was correctly identified by the model for confluence C, but was misclassified by the model for confluence G (Figure 3.8). The sediment budgets of confluences A, H, I and K showed relative high variability in relative contributions (≥ 20%) from same sources over the three campaigns (Table 3.1). Differences in these source contributions were correctly modelled for confluence H, with absolute deviations between modelling and the SS budget of 1% (campaign 2) and 4% (campaign 3). The dominant spatial source at confluence J (campaign 2) and confluence I (campaign 3) was correctly identified by the modelling, but overestimated when compared with the sediment budget (by 38 and 32% respectively). The sediment budget for confluences A and K showed the same dominant source for the three campaigns. This was not correctly identified by the fingerprinting model for confluence A, campaign 2, as the model identified the incorrect dominant source. For confluence K, the sediment budget indicated that source 30 dominated during the three campaigns whereas the model predicted source 29 contributed more during campaigns 1 and 3 (Figure 3.8).

3.3.4 Spatial Sediment Source Fingerprinting: Different Modelling Approaches

Figure 3.9 shows the modelling results for each confluence (A-K) and sampling campaign when using three different methods to select which wavelengths are used as fingerprints (the three methods are described in section 3.2.4.3). The three different methods generated similar results. For campaign 1, only confluence A and confluence B showed differences in the dominant contributing SS source. Higher differences in source apportionment (deviation > 20%) between the different methods were observed for confluence A (campaign 2), confluence C (campaign 1 and 3), confluence D (campaign 2) and confluence G (campaign 2). Differences between the methods using all wavelengths in the 200-730 nm range and using all wavelengths in the 390-730 nm range were on average 12.5% (5.4% when omitting the above mentioned cases with differences >20%). Differences between the methods using all wavelengths in the 390-730 nm range and using wavelengths in the 390-730 nm range at intervals of 10 nm were only 1.6%.

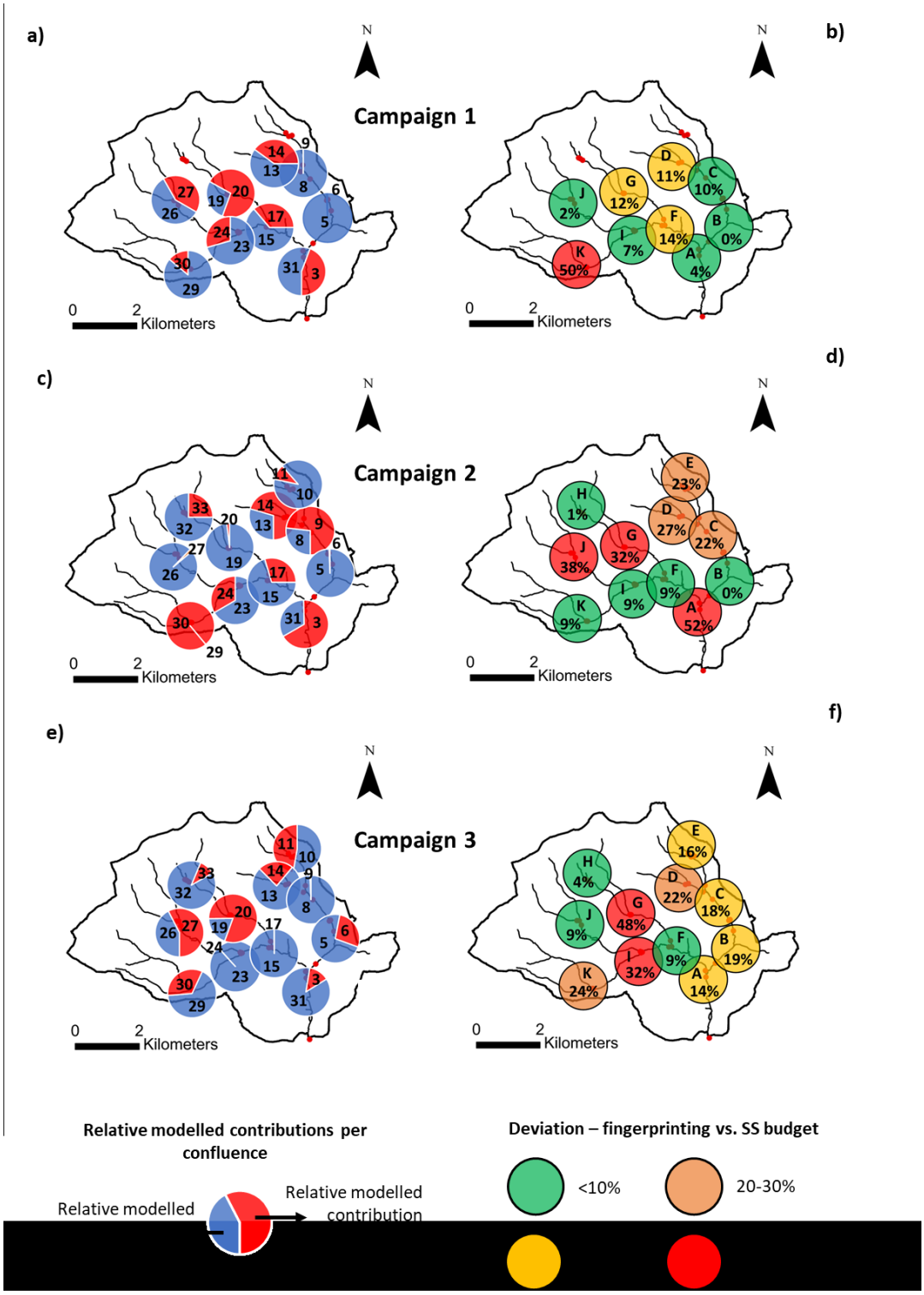

Figure 3.8 Relative modelled spatial source contributions for each of the confluences, for sampling campaigns 1 (a), 2 (c) and 3 I. Modelled source contributions are depicted in the pie-charts. Numbers within the pie-charts indicate the two upstream source sampling sites for each confluence. Percentage of deviation refers to the differences between the fingerprinting and sediment budget, based on relative estimates of source contributions, for sampling campaign 1 (b), 2 (d) and 3 (f). The colour of the confluence circles indicates the extent of deviation between the two approaches.

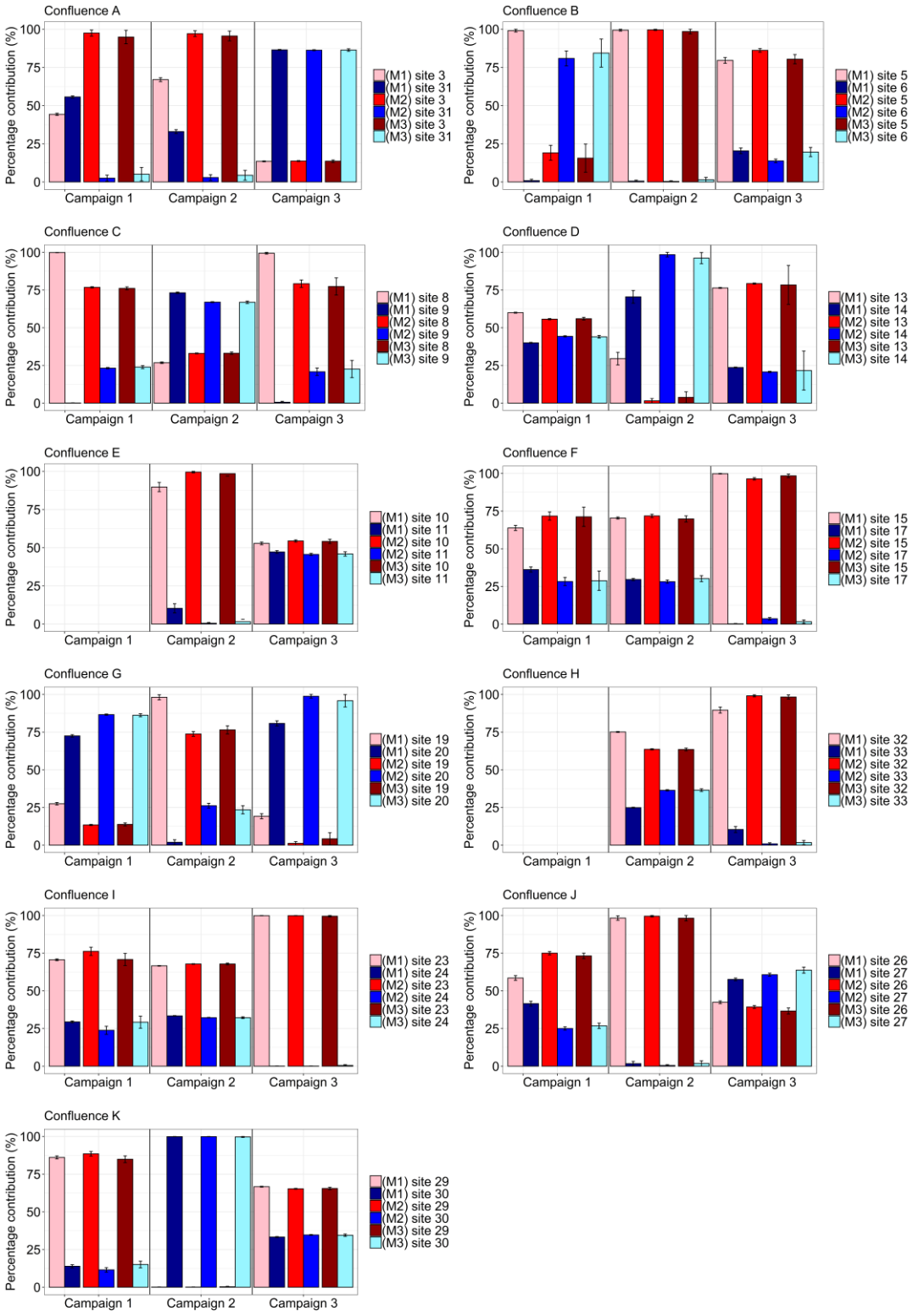

Figure 3.9 Modelling results for the sources at all confluences (A-K) for the three measurement campaigns. The results refer to the three different modelling procedures testing three different methods of fingerprint selection using different wavelengths: (M1) using 200-730 nm at 2.5 nm intervals, (M2) using 390-730 nm at 2.5 nm intervals, and (M3) using 390-730 nm at 10 nm intervals. During campaign 1, there was no data for confluences E and H.

3.4 Discussion

3.4.1 Absorbance Patterns

Absorbance values differed at the same sampling sites for the different campaigns. The results also indicated that differences between the sampling sites were generally less pronounced for campaign 2, which took place during the event of highest precipitation (Figure 3.7). The lower differences could be linked to more constant contributions of certain SS sources during longer duration rainfall events over the catchment (e.g., Walling et al., 2000), thereby indicating the activation of different sources within the spatially defined SS sources areas during the different sampling campaigns (as observed in e.g., Cooper et al., 2014b, 2015; Vercruysse et al., 2017; Vercruysse and Grabowski, 2019). Therefore, the findings of the present study highlight that a single measurement cannot represent the catchment dynamics over time, and thus that methods allowing higher temporal frequency observations are certainly valuable (e.g., Cooper et al., 2015; Pulley and Collins, 2021).

Source absorbance data should be sufficiently different to provide a robust basis for source discrimination and apportionment (Lake et al., 2022a). Herein, absorbance readings for the contributing sources of three confluences did not show significant differences (confluence F in campaign 1, confluence D in campaign 2, and confluence B in campaign 3; Figure 3.7). However, these situations did not result in higher deviations in modelled source contributions (Figure 3.8) compared with the average deviations for all confluences and campaigns (18% ± 15). In contrast, confluence K (campaign 1) and confluence G and I (campaign 3) showed very high modelled deviations (respectively 50, 48 and 32%), even though differences in absorbance for the contributing sources of these confluences were relatively high. This indicates no clear relationship between modelling performance and differences between the absorbance spectra of individual source (Figure B.1).

From the results, it was evident that there is a spatial pattern in absorbance differences between sources merging at different confluences. The main spatial pattern can be found when comparing the average absorbance for the confluences in the northern part of the catchment to those in the southern part. In the northern confluences, there is a relative low difference between sources (e.g., confluence E and H). This could potentially be explained by the more similar land uses and lithologies in the contributing areas (Figure 3.1; Tables B.1 and B.2). Source streams are thus more likely to transport sediment yielding similar absorbance spectra. With SS source properties influencing absorbance readings (Lake et al., 2022a; Martínez-Carreras et al., 2016; Sehgal et al., 2022), similarity between sources thus provides a limited basis for source discrimination.

Nevertheless, similarities in land use and geology do not always seem to explain the small differences in source absorbances for all confluences. Sources at confluence J (Table B.3 and B.4) are for example largely influenced by the same land use (i.e., forest and cultivated lands) and lithology (i.e., schists, slates and phyllites), but resulted in clearly different absorbance patterns for campaigns 1 and 3 (Figure 3.7). These differences could be related to differences in source activations, or a better connectivity of specific sources to the streams under certain conditions (e.g., Fryirs, 2012). The different activation of sources can also be related to one stream (at sampling site 26) starting immediately downstream of a small village, which, upon activation might deliver SS originating from damaged road verges (Collins et al., 2010) and urban sources (Charlesworth and Lees, 2001), thereby affecting the absorbance signal.

3.4.2 Modelling Relative Spatial Source Contributions

This work revealed reasonably small deviations between the spatial source estimates based on sediment fingerprinting and the alternative sediment budgeting approach, with an average deviation for all confluences and campaigns of 18 ± 15%. The magnitude of deviation was similar to results found by Lake et al. (2022a). Therein, the use of absorbance was evaluated by means of artificial mixtures in a laboratory set-up, reporting errors of 14.5 ± 13% compared with the known source contributions to artificial mixtures.

There were several instances in which downstream absorbance values did not fall in between the absorbance values from the sources (for all wavelengths). It is common practise in many fingerprinting studies to discard these out of range fingerprints (e.g., Collins et al., 2020; Evrard et al., 2022), due to issues concerning non-conservative behaviour of SS properties. However, this was not deemed necessary in the work reported herein. The distance between the source SS sampling sites and the downstream target SS sampling site was small (20–40 m for confluences E-K, slightly larger for confluences A-D due to field situation/site accessibility). Therefore, logically, it seems unlikely that substantial alterations to SS properties had occurred when SS was transported over such short distances. Furthermore, no clear excessive erosion input was observed at the different confluences in question between the source and target sampling sites. Potential intermediate SS inputs that could have influenced the absorbance measurements were therefore not considered as being of concern.

A more likely explanation for the out of range situations is related to one of the sources being highly dominant. It is expected that the absorbance values of the target SS would then be close to the absorbance values of this dominant source. However, absorbance values of the source and target SS samples are subject to sampling and laboratory measurement uncertainties. Sampling

uncertainties include the fact that the grab samples do not fully represent the stream cross-section (e.g., Bainbridge et al., 2012). Herein, we aimed to take samples from the middle of the cross-section, which was especially challenging in the wider streams. After collection, samples were stored and flocculation might have occurred (Phillips and Walling, 1995), potentially influencing the SS particle size distribution. This, in turn, might have influenced the absorbance readings (Lake et al., 2022a) measured in the laboratory set-up, despite efforts to break-up flocs by shaking the samples and using a magnetic stirrer for sample resuspension and disaggregation. Furthermore, as absorbance data were compensated for SSC, uncertainty associated with the laboratory methods used to quantify SSC gravimetrically might help explain these out of range situations. Confluences failing the range test do show rather small differences in target SS absorbance compared with the dominant source (with percentage deviations ranging between 3% and 11%). These deviations were found to be within reasonable uncertainty ranges for determining SSC (Siu et al., 2008). Therefore, we argue that out of range absorbance situations could still provide valuable information for determining highly dominant source contributions. The latter logic is supported by, for example, Evrard et al. (2022), García-Comendador et al. (2021), Pulley and Collins (2022) who all argue that the identification of dominant SS sources can still be very informative. Similar out of range observations were made by Lake et al. (2022a), resulting in a contribution of ca. 100% for the dominant source.

The MixSIAR model (Stock et al., 2018; Stock and Semmens, 2016) was used to apportion the target SS collected downstream at each confluence. Alternatively, a deconvolutional MixSIAR (Blake et al., 2018) model can be applied, which allows accounting for structural hierarchy inside the catchment by progressively applying MixSIAR to downstream confluences. In this case, target SS samples can serve as sources for confluences downstream, thereby reducing the number of samples that need to be collected. In our case, however, the need to apply a deconvolutional MixSIAR approach was negated by the design of our proof-of-concept study.

3.4.3 Comparison of Modelling Approaches

In this study, we opted to use all wavelengths (200-730 nm, at 2.5 nm intervals) in the Bayesian modelling framework (MixSIAR) instead of selecting an optimal set of fingerprints through the application of statistical tests (e.g., using a Kruskal-Wallis test combined with a discriminant function analysis) as used in many sediment fingerprinting studies (e.g., Batista et al., 2022; Gaspar et al., 2022; Nosrati et al., 2022). Lake et al. (2022a) obtained accurate results using the same method. This is supported by other studies (e.g., Sherriff et al., 2015), in which it has been suggested that the inclusion of a higher number of fingerprints can improve model performance and decrease the uncertainty associated with the results. Here, the use of all wavelengths over a selected sub-

set is also beneficial because it facilitates the implementation of a standardized approach allowing for comparisons between studies (Evrard et al., 2022).

Despite the aforementioned advantages regarding the use of all wavelengths, there are some disadvantages. Using all wavelengths contributes to long model computation times, with collinearity between fingerprints. To account for these issues, two other modelling approaches were tested. The different modelling approaches tested compared well with each other, with similar modelling outcomes when comparing the 390-730 nm range with the whole range of 200-730 nm (as proposed by Lake et al., 2022a). Limiting the range of wavelengths used has another advantage by removing the need for compensation for the absorbance of background water (i.e., filtered water); dissolved components mainly influence the 200-390 nm range (see Figure B.2, and e.g., Rieger et al., 2004). However, minimal effects of dissolved components were observed for measurements in the 390-730 nm range (Figure B.2). The use of the 390-730 nm range can thus contribute to reducing issues associated with laboratory workload by eliminating the need for filtering and measuring absorbance on filtered water samples.

3.4.4 Outlook for High Spatial and Temporal Resolution Sediment Source Fingerprinting

Applying the confluence-based approach directly addresses some known challenges associated with sediment fingerprinting, including issues concerning which particle size fraction is being transported from the sources to the channel system. Furthermore, the confluence based approach can provide a better spatial overview of SS origins (Figure 3.5), in contrast to most other (i.e., classical) sediment fingerprinting studies which have aimed to apportion SS contributions based on different land uses (i.e., individual source types). Applying this more classical approach would require the separation of the relevant particle size fractions to create proxy SS soil source samples (e.g., for distinguishing land uses) that can be measured with a submersible spectrophotometer. Exploration of this could be a potential future research topic. Such an approach has the advantage that only one spectrophotometer would be needed at the catchment outlet instead of three spectrophotometers, when measuring *in situ*, using a confluence-based approach. This would then reduce the initial purchasing costs of the spectrophotometer (ca. US$20.000 each).

The results obtained using absorbance for tracing SS spatial sources were validated using a sediment budget approach (e.g., Lake et al., 2022b; Tiecher et al., 2022). The need for such independent evaluation when using sediment fingerprinting has been long emphasized (e.g., Collins and Walling, 2004). Estimation of the suspended sediment budget was possible because discharge data were available for some of the sites, permitting calculations of actual SS loads. For the sites where discharge data were not available, the drainage area method was used to estimate discharge

(e.g., Emerson et al., 2005). This simple method assumes that discharge is solely a function of catchment area, and will likely introduce uncertainties into the calculations. This is most likely for the sites located higher upstream in the catchment (northern sites), where discharges were low compared with the downstream sites. Despite such uncertainties, the discharge data combined with SSC measurements allowed for an independent evaluation of the contribution of the different SS sources estimated using source fingerprinting, whereas many SS fingerprinting studies do not evaluate predicted source proportions using independent evidence. Instead, an increasing number of recent publications rely on the results of either virtual or artificial mixture tests (e.g., Batista et al., 2022). Although this is an important step in state-of-the-art decision trees for applying sediment source fingerprinting, they have inherent uncertainties and limitations (Collins et al., 2017). Mixtures represent ideal situations (i.e., sources are known, negligible particle size selectivity effects and no out of range fingerprints), meaning that even 'acceptable' modelling results (i.e., modelled results are in agreement with the known proportions in the mixtures) do not always translate into accurate catchment source apportionments (Batista et al., 2022). Clearly, other means to evaluation the un-mixing results using the absorbance data could involve applying more classical sediment fingerprinting approaches and their conventional fingerprint properties.

The approach tested in the present study can facilitate an increase in the temporal resolution of observations for elucidating potential changes in SS source contributions, due to the relatively easy analysis of the water samples. Such information can facilitate the reliable targeting of management solutions to prevent excessive SS transport (e.g., Vercruysse et al., 2017; Vercruysse and Grabowski, 2019). To facilitate an increase in high frequency observations of SS source contributions even further, it is key to reduce sampling and laboratory analyses to a minimum. Here, the use of the absorbance in the 390-730 nm range eliminates the need for compensation for the absorbance of background (filtered) water (i.e., absorbance influenced by dissolved components). This could then allow the direct use of absorbance data collected *in situ* with a submerged spectrophotometer at high frequency (i.e., minutes) to fingerprint SS sources, further reducing sampling needs and laboratory workloads. Here, the use of *in situ* absorbance measurements would additionally reduce issues associated with potential alteration of SS properties during transport and storage (Smith and Owens, 2014). Clearly, however, regular sampling to confirm the reliability of the absorbance data would still be needed (Gamerith et al., 2011).

There remains the need to compensate absorbance spectra for SSCs. When using a submerged spectrometer to trace SS sources at high frequency, compensation can be done by establishing a rating curve between SSC and turbidity (the latter also being measured by the spectrophotometer). To this end, a number of grab samples need to be collected and their SSCs need to be measured in the laboratory. Another consideration is the maintenance of the spectrophotometer while installed

in situ. The spectrophotometer used in this study can be equipped with an automatic cleaning brush (s::can GmbH, Vienna, Austria) that cleans the sensor lens before every measurement, to mechanically remove fouling (e.g., Sehgal et al., 2022). Additionally, regular manual cleaning is also advised, e.g., bi-weekly (Martínez-Carreras et al., 2016).

3.5 Conclusions

In this research, the use of absorbance at a range of wavelengths (i.e., fingerprints) to apportion SS spatial source contributions using a confluence-based sampling strategy was tested. This new research builds upon the work presented by Lake et al. (2022a), who tested and evaluated the absorbance approach in a laboratory setting using artificially created source samples and mixtures. The results presented herein suggested that confluences in the northern part of the study catchment exhibited lower differences between source absorbance compared with confluences in the southern part, indicating the potential influence of different spatial sources. Absorbance measured at the same sampling sites varied over time, indicating the need for repeat sampling if catchment SS dynamics are to be well understood. Modelled SS spatial source contributions showed deviations of 18 ± 15% from the corresponding source contributions estimated using sediment budgets. While dominant spatial sources were mostly well identified using the absorbance fingerprinting approach, some clear deviations from the budget approach were observed. Care is thus needed when using absorbance for fingerprinting and independent evaluation of the results should be undertaken on a regular basis.

There were no clear indications of improved model performances with higher source absorbance differences, increasing discharges or higher SSCs. Furthermore, it was shown that different modelling procedures gave comparable spatial source estimates. Hence, computation times could be reduced by using a lower number of wavelengths as fingerprints. Overall, this research has shown that, despite some uncertainties in the modelling results, absorbance could potentially be used as a sediment fingerprint in natural environments, reducing the need for conventional resource intensive sampling and laboratory analyses. The method reported herein, using a submerged spectrophotometer, could thus contribute to easier ways of estimating SS source contributions and such information is urgently needed to improve the targeting of sediment control strategies in many river catchments.

Chapter 4 Using Particle Size Distributions to Fingerprint Suspended Sediment Sources – Evaluation at Laboratory and Catchment Scales

Abstract

Applications of sediment source fingerprinting studies are growing globally despite the high costs and workloads associated with the analyses of conventional fingerprint properties on target sediment samples collected using traditional methods. To this end, there is a need to test new fingerprint properties that can overcome these challenges. Sediment particle size could potentially contribute here since it is relatively easy to measure but, until now, has rarely been deployed as a fingerprint itself. Instead, particle size has been used to ensure that source and target sediment samples are more directly comparable on the basis of the fingerprints used. Accordingly, this work examined whether particle size distributions (PSDs) could be used as a reliable fingerprint for apportioning sediment sources, in combination with a grain size un-mixing model. Application of PSDs as a fingerprint was tested at two scales: (i) in a laboratory setting where soil samples with known PSDs were used to generate artificial mixtures to evaluate un-mixing model results, and (ii) a catchment setting comparing PSDs in a confluence-based approach to test if downstream target sediment PSDs could be un-mixed into the contributions of sediment coming from an upstream and a tributary sampling site. Laboratory results showed that the known proportions of the two, three and four soil samples in the artificial mixtures were predicted accurately using the AnalySize grain size un-mixing model, giving average absolute errors of 9%, 8% and 6%, respectively. Catchment results showed variable performances when comparing un-mixing results with sediment budget estimations, with the best results obtained at higher discharge values during storm runoff events. Overall, our results suggest the potential of using PSDs for estimating contributions of sediment sources delivering SS with distinct PSDs when sources are located at short distance to the downstream sampling site.

4.1 Introduction

Information on sediment origin can help target remedial actions to mitigate erosion in river catchments (Belmont et al., 2011). The sediment fingerprinting approach is a widely-adopted method to assemble this information, allowing the quantification of the relative contributions of different sources to target suspended sediment (SS) collected downstream (see reviews by e.g.,

Collins et al., 2017, 2020; Haddadchi et al., 2013; Owens et al., 2016). To apply the method, both source and SS samples need to be collected. Potential sources are normally sampled manually, while SS is often collected using time-integrated sediment traps (e.g., García-Comendador et al., 2021; Pulley and Collins, 2021), or automatic water samplers (e.g., Legout et al., 2021; Vale et al., 2020). Selected properties or 'fingerprints' are then measured on the SS and compared with the corresponding fingerprint values measured on the potential source samples. This comparison allows for estimations of the relative contribution of each source to the target SS using un-mixing models.

A wide range of soil and sediment properties has been used for source fingerprinting, e.g., geochemistry, fallout radionuclides, colour properties, stable isotopes, compound specific stable isotopes, and mineral magnetic properties (Blake et al., 2012; Collins et al., 1997c; Martínez-Carreras et al., 2010a; Oldfield et al., 1985; Revel-Rolland et al., 2005; Upadhayay et al., 2022; Wallbrink et al., 1998). A common issue is selecting the particle size fraction to analyse (e.g., Collins et al., 2017; Koiter et al., 2013, 2018; Laceby et al., 2017; Smith and Blake, 2014). This relates to the essence of an effective fingerprinting property, where fingerprints must both differentiate between sources while behaving conservatively (Walling et al., 1993). However, fingerprint values often vary with particle size in a non-linear manner that is difficult to generalize (Horowitz and Elrick, 1987; Russell et al., 2001). For instance, total organic carbon (Wynn et al., 2005) and radionuclides (Horowitz and Elrick, 1987) are generally enriched in the finer particle size fractions, while different mineral magnetic properties (e.g., Hatfield and Maher, 2009) and colour parameters (e.g., Pulley and Rowntree, 2016) are linked to different particle size fractions.

Various approaches have been adopted to account for particle size in sediment fingerprinting studies to facilitate direct comparison between the properties of target SS and possible sources. The most commonly-applied approach is to fractionate SS and source samples by sieving (Laceby et al., 2017). Here, source materials and target SS samples are commonly sieved to <63 µm (Walling et al., 1993), since this fraction is considered to account for most of the SS load transported by rivers (e.g., Legout et al., 2013; Walling et al., 2000). In other studies, samples are sieved to different fractions and separate fingerprint analyses performed for isolated fractions (e.g., Gaspar et al., 2019, 2022; Motha et al., 2002). Another approach is to sieve and then apply correction factors (e.g., Collins et al., 1997a; He and Walling, 1996). However, the underlying assumptions used for these correction factors were challenged by Smith and Blake (2014) due to the fact that positive linear relationships between particle size and fingerprint concentrations do not apply to all fingerprint properties (Horowitz, 1991; Russell et al., 2001). Given these uncertainties, recent reviews have stressed the need to consider both the most representative particle size fraction for

the target sediment in question and to examine dependency of fingerprint properties on particle size, especially where a broad size fraction is used (Collins et al., 2017).

Alternatively, the confluence-based sediment fingerprinting approach has been proposed to facilitate direct comparison between the properties of downstream target SS samples and possible sources (i.e., different tributaries used to represent upstream catchment sources) (Collins et al., 1996, 1997b; Nosrati et al., 2018, 2019; Patault et al., 2019; Vale et al., 2016). Here, uncertainties regarding which particle size fractions are delivered from hillslope sources to streams are minimised, reducing potential uncertainties associated with particle size enrichment or depletion and the concomitant effects on fingerprint properties (Laceby et al., 2017). However, in-stream hydrodynamic processes result in mobilization of different SS size fractions and affect SS flocculation, that might still cause uncertainty as to which particle sizes are present at different sections of the stream (e.g., Droppo, 2004; Grangeon et al., 2014), challenging fingerprint conservation.

While the consideration of particle size in sediment fingerprinting is mainly limited to investigating its controls on fingerprint values, there is evidence that particle size can be used directly as a fingerprint property or tracer (Kranck and Milligan, 1985; Laceby et al., 2017). For example, Vale et al. (2016) applied a confluence-based approach to the Manawatu River catchment (New Zealand), collecting fine sediments from the riverbed using a trowel. The authors showed that varying rock types, situated in different sub-catchments and drained by different tributaries, were linked to differences in SS D_{50} values. In the same catchment, Vale et al. (2020) linked patterns in SS dynamics during storm events to differences in particle sizes. They argued that the finer particle size of mudstone (D_{50} of 16 μm) likely allowed prolonged entrainment in the water during storm events, whereas the transport of coarser mountain range and unconsolidated sediment (D_{50} of 44 μm) ceased as the storm events progressed. The results of such studies therefore suggest that temporal changes in sediment source contributions can be fingerprinted using observed changes in particle sizes or particle size distributions (PSDs). Existing work that included particle size for the sole purpose of tracing (Li et al., 2020), reported the use of particle size statistics (e.g., D_{60}, D_{70} and well as clay and silt percentages) for fingerprints to identify sediment sources of core sediment. Another study (Tang et al., 2018) looked at the spatial and temporal variability of SS source particle size input and the effects of sediment size sorting in reservoir dam deposits. Droppo et al. (2005) suggested rather than using particle size, particle shape and fractal dimension could be used to trace SS sources. Furthermore, the idea of using PSDs for sediment source fingerprinting purposes was raised in an abstract by Liu et al. (2014), where the possibility to measure PSDs from potential soil sources and compare those with the target SS collected by sediment traps was proposed. A

corresponding publication on this proposal has not been found at the time of publication of the present study.

Many recent sediment fingerprinting studies underscore increasing opportunities to measure sediment PSDs. This can be achieved using laboratory equipment such as the Beckman Coulter LS 13320 (Beckman Coulter, Inc., Fullerton, CA) and Mastersizer 3000 (Malvern Instruments Ltd, Worcestershire, UK) laser diffraction particle size analysers (as used by e.g., García-Comendador et al., 2021; Patault et al., 2019), and in-field equipment such as the LISST sensor (Sequoia Scientific, Bellevue, WA, USA), also based on laser diffraction (as used by e.g., Czuba et al., 2015; Upadhayay et al., 2021). Differences in sediment PSDs are regularly used in sedimentology to infer past sediment provenance and to reconstruct past changes in, for example, climatic conditions or tectonic processes (Beuscher et al., 2017; Dietze et al., 2012). To this end, Weltje (1997) first used PSD data together with an end-member mixing model (EMMA) to estimate the proportions of different sediment sources. Subsequent research led to the development of other end-member grain size un-mixing models such as DRS-unmixer (Heslop et al., 2007), EMMAgeo (Dietze et al., 2012), AnalySize (Paterson and Heslop, 2015), BEMMA (Yu et al., 2016) and BasEMMA (Zhang et al., 2020). These grain-size un-mixing models use the whole PSD data as input, whereas within the sediment fingerprinting community linear multivariate un-mixing models are used most widely (e.g., FingerPro and MixSIAR: Lizaga et al., 2020c; Stock et al., 2018; Stock and Semmens, 2016).

We propose the use of tracing contemporary SS sources with PSDs as a fingerprint in combination with an end-member grain size un-mixing model (AnalySize). To this end, we: (i) evaluate un-mixing model performances using artificial laboratory mixtures, with known proportions of soil samples sieved to different size fractions, and; (ii) un-mix target SS samples from a catchment scale confluence-based approach based on differences in upstream source SS PSDs, while relating the un-mixing model performances to differences in upstream source D_{50} values and observed water discharges.

4.2 Materials and Methods

This study describes two approaches using complementary methods to measure PSD. First, a LISST sensor (Sequoia Scientific, Bellevue, WA, USA) was used in controlled laboratory experiments, where PSDs were measured inside a tank set-up to evaluate the un-mixing model (section 4.2.1). Second, a Mastersizer instrument (Malvern Instruments Ltd, Worcestershire, UK) was used to measure PSDs in discrete samples collected in a catchment scale field experiment, with the un-mixing model then applied to estimate confluence sediment source contributions (section 4.2.2). The two approaches were deployed in parallel, not compared directly, with the approaches used

according to their different objectives comprising: (1) laboratory experiments aiming to measure in-tank PSDs in specified mixtures of source soils (section 4.2.1), and; (2) field experiments aiming to measure PSDs after applying ultrasound by taking sub-samples from a well-mixed environment (section 4.2.2).

4.2.1 Laboratory Experiments

Laboratory experiments were performed to evaluate the grain-size un-mixing model AnalySize under controlled conditions. Both soil samples and artificial mixtures, composed of these different soil samples, were suspended inside a tank set-up and PSD was measured using a LISST sensor. The PSDs of both the soil samples and mixtures were then used to evaluate the grain-size un-mixing model, according to the known soil sample contributions present in the mixtures. The tank set-up, as well as the soil samples and mixtures, were used previously in Lake et al. (2022a) to investigate the feasibility of using absorbance measurements obtained with a submerged spectrophotometer for un-mixing source soil sample contributions.

4.2.1.1 Soil Samples and Artificial Mixtures

Soil sampling was carried out at six different sites in Luxembourg (see Table C.1; Appendix C, for details on sampling site coordinates). Sites were selected based on differences in geochemistry and mineralogy (Lake et al., 2022a). Soil samples were collected using a trowel, after removal of the top layer of soil (0-5 cm). Care was taken to collect only material that appeared homogeneous in colour. The samples were then dried at room temperature, disaggregated with a pestle and mortar, and sieved into three different size fractions: <32 µm, 32-63 µm and 63-125 µm. This resulted in 17 soil samples (the 63-125 µm fraction for soil 6 was omitted due to the low quantities present). Soil samples are hereafter indicated by #soil.fraction, with ‘soil’ representing the soils (n=6), and ‘fraction’ the sieved particle size fraction (.1 for <32 µm; .2 for 32-63 µm; .3 for 63-125 µm). Soil samples were used to create 25 artificial mixtures. The mixtures consisted of two, three or four soil samples, with contributions chosen in order to have a majority of mixtures with a dominant soil sample (Table 4.1). Mixtures 1-9 were composed of soil samples sieved to different size fractions. Mixtures 10-25 were composed of soil samples sieved to the same particle size fraction. These two approaches were tested to see if both distinct differences in source PSDs (soil sources sieved to different fractions) and small differences in source PSDs (soil sources sieved to same size fraction) could be used for un-mixing.

Table 4.1 Soil sample input contributions (%) for the mixtures 1-9, based on theoretical input contributions, and adapted input contributions (bold), based on measured concentrations in the tank set-up.

	Mixture No.	Soil sample (%)	Soil sample (%)	Soil sample (%)	Soil sample (%)
Mixtures of samples sieved to different size fractions:					
2 soil samples	1	#3.1 (80) **(81.6)**	#4.2 (20) **(18.4)**	-	-
	2	#1.2 (80) **(83.4)**	#2.3 (20) **(16.6)**	-	-
	3	#1.1 (30) **(56.9)**	#5.3 (70) **(43.1)**	-	-
3 soil samples	4	#4.2 (10) **(20.0)**	#5.3 (80) **(57.3)**	#6.1 (10) **(22.7)**	-
	5	#1.2 (20) **(19.3)**	#3.1 (70) **(74.2)**	#4.3 (10) **(6.6)**	-
	6	#1.1 (30) **(41.5)**	#3.3 (50) **(49.5)**	#5.3 (20) **(9.0)**	-
	7	#2.3 (80) **(74.4)**	#3.1 (10) **(12.9)**	#6.2 (10) **(12.7)**	-
4 soil samples	8	#1.1 (10) **(12.4)**	#2.3 (70) **(62.9)**	#3.1 (10) **(12.5)**	#6.2 (10) **(12.3)**
	9	#1.1 (10) **(10.3)**	#2.3 (10) **(7.4)**	#3.1 (70) **(72.2)**	#6.2 (10) **(10.2)**

4.2.1.2 Laboratory Set-Up

A LISST 200X sensor (Sequoia Scientific, Bellevue, WA, United States) was used in the laboratory set-up (Figure 4.1) to measure PSDs. This sensor uses laser diffraction technology, whereby particles of different sizes diffract the laser beam at different angles (Agrawal and Pottsmith, 2000). The diffracted light is assigned to one of the 36 particle size classes, providing PSDs on the soil samples and mixtures tested (in the–1 - 500 µm range). The output value in each size class is given in µL L^{-1}. Output values were converted into percentage of volume concentration to allow comparison between different measurements, with percentage of volume concentration being independent from mass concentration.

The LISST sensor was instal–ed in a water tank (75.4 L capacity) filled with 40 L of demineralised water (Figure 4.1). The sensor was installed in a horizontal orientation to prevent the settling of particles on the sensor lens. The LISST sensor was equipped with the path reduction module to cope with all measured concentrations (Sequoia Scientific, 2018). Both individual soil samples and mixtures were tested for 10 different theoretical concentrations to investigate the influence of different concentrations on the un-mixing results (100 mg L^{-1} – 1000 mg L^{-1}, at 100 mg L^{-1} increments). A background signal (using demineralised water), measured before the start of every experiment, was saved onto the instrument and automatically compensated for during the experiments (to eliminate influence on the measurements of e.g., small scratches on the measurement window). For each theoretical concentration, the LISST sensor measured over a 10 minute period at 1.5 second interval, using a random shape algorithm (Sequoia Scientific, 2018).

After each theoretical concentration was measured, three samples were collected using a pipette. Samples were transferred into pre-weighed aluminium buckets and dried to quantify the concentrations inside the tank (i.e., 'measured concentrations').

A Vibromixer (DrM, Dr. Mueller AG, Switzerland) mixing device was used to keep the soil samples and mixtures in suspension (see Lake et al., 2022a for details on the settings and initial tests on mixing performances). From the results in Lake et al. (2022a), it appeared that measured concentrations were lower than the theoretical concentrations, with differences increasing with an increase in particle size. Soil samples sieved to the same size fractions presented similar differences between measured and theoretical concentrations. Since mixtures 1-9 used soil samples sieved to different size fractions, the actual in-tank contributions differed from the theoretical input contributions. Therefore, input contributions for these mixtures were compensated according to the measured soil sample concentrations. Table C.3 shows the measured concentrations and Table 4.1 the associated compensated soil sample input contributions for the mixtures.

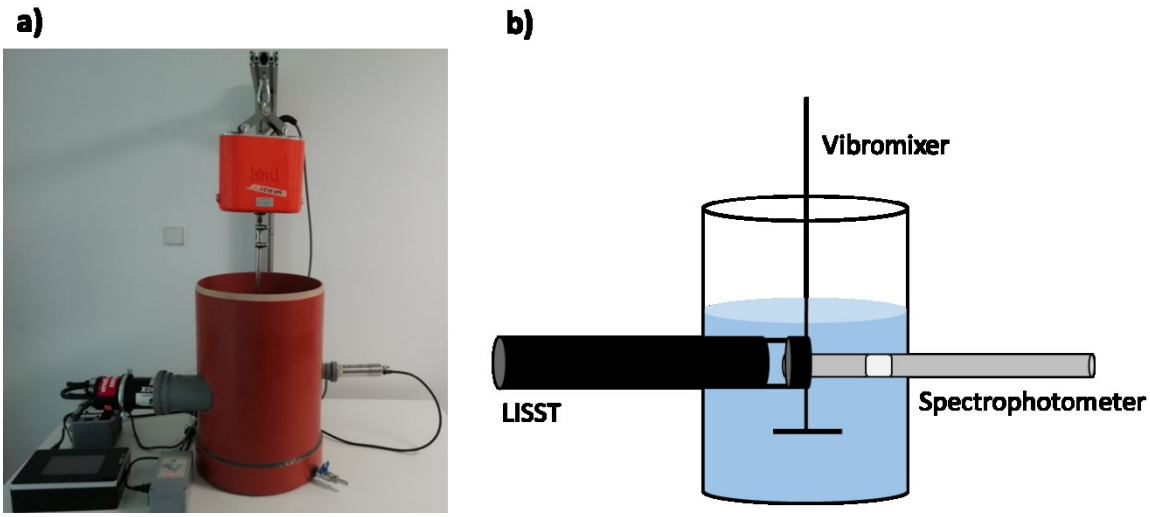

Figure 4.1 Photograph (a), and schematic representation (b) of the laboratory tank set-up. The data obtained from the spectrophotometer are discussed in Lake et al. (2022a).

4.2.2 Field Experiments

The field experiment was carried out at the confluence of a tributary draining a sub-catchment with different underlying geology, which was hypothesized to yield SS with distinct PSDs (as discussed in Walling et al., 2000) compared to the rest of the catchment. Field samples were collected using automatic water samplers (i.e., discrete samples) at pre-set times at the two upstream and downstream sites. PSDs, measured on the samples were introduced into the grain-size un-mixing model to identify the origin of the downstream target SS. A sediment budget, through a simple mass-balance, was used to evaluate the model results.

4.2.2.1 Study Area

The study area is located in the Attert River basin (247 km^2 at Useldange), in the western part of Luxembourg (Figure 4.2a). Land use is represented by forests (dominant in the higher sloping schist and sandstone areas), grasslands and croplands (Figure 4.2b). The catchment is underlain by schists, slate and phyllites bedrock in the north-west, and by red sandstone ('Buntsandstein'), marls and Luxembourg sandstone in the central and southern parts (Figure 4.2c). Altitudes range from 553 m to 238 m above sea level. The climate is semi-oceanic, with maximum mean monthly temperatures ranging between 0 to 18 °C and an average annual rainfall of ca. 845 mm (1954-1996; Pfister et al., 2005). Precipitation during the field experiments was measured at the weather station in Useldange (Figure 4.2b, 4.2c) by the 'Administration des Services Techniques d' l'Agriculture' (ASTA).

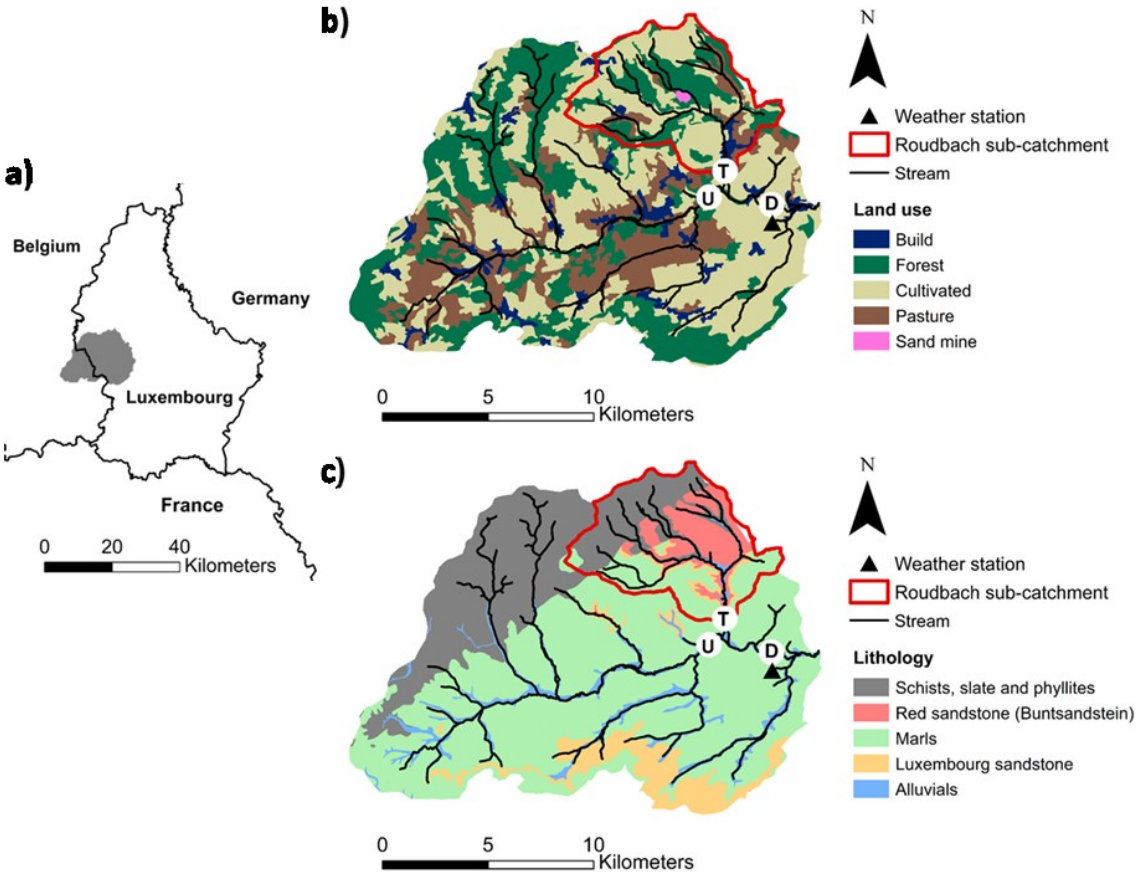

Figure 4.2 Location of the Attert River Basin in Luxembourg (a), land use and river network at Useldange (b), and lithology and river network at Useldange (c). Sampling sites (b & c) are indicated by the letters U (Upstream), T (Tributary), and D (Downstream).

Three sites were instrumented for stream water sampling (Figure 4.2b, 4.2c). Two sampling sites were located along the Attert River, upstream and downstream of the Roudbach tributary junction. The third sampling site was located at the outlet of the Roudbach tributary. The Roudbach sub-catchment drains an area of 44 km^2 and is mainly underlain by red sandstone ('Buntsandstein'), as

well as by schists, slate and phyllites bedrock in the northern part. Discrete water samples were collected during storm runoff events and low flow periods using automatic water samplers (ISCO 6712 FS; Teledyne ISCO, Lincoln, Nebraska, U.S.A). Sampling at the three sites was undertaken at the same time. Until analyses, samples were stored in a cold room (4-5 °C). At each of the three sites, turbidity was measured at 5 minute intervals using a S::can spectro::lyser^{TM} probe (Scan Messtechnik GmbH, Vienna, Austria).

4.2.2.2 Particle Size Distribution Measurements

Particle size distributions of the SS contained within the discrete water samples were measured in the laboratory using a Mastersizer 3000 (Malvern Instruments, Malvern, UK). Discrete samples were shaken for homogenization and a sub-sample was introduced into the Mastersizer hydro LV unit (3000 rpm mixer rotation speed), collecting a total of 5 measurements per sample. Samples were introduced to the Mastersizer until a certain obscuration range was achieved (usually between 3-5%) to allow for consistency between measurements. For samples with low concentrations, this obscuration range was not always achieved. The PSD of each sample was measured after applying ultrasound for 60 seconds to disaggregate potential flocs and to measure the absolute particle size (representing the primary particles; Biggs and Lant, 2000).

Organic matter (OM) was removed from a selection of samples to investigate (i) the influence of OM on the PSD shape, and (ii) to investigate whether PSDs measured from SS with OM removed improved un-mixing accuracy. To this end, a selection (n=12, 4 samples for each site) of discrete samples from period F (Figure 4.4; Table 4.2) were oven dried at 35°C. Subsequently, these samples were removed using Milli-Q water and transferred into a glass beaker. Hydrogen peroxide (H_2O_2) was added to these beakers, which were then placed on a hot plate (30-35°C). Samples were stirred and H_2O_2 was added until all OM was removed. Samples were then disaggregated in an ultrasonic bath and subsequently introduced into the Mastersizer.

4.2.2.3 Suspended Sediment Budget

A suspended sediment budget (mass-balance) was established to evaluate the un-mixing model performance. To this end, suspended sediment concentration (SSC) was measured from the discrete water samples by filtering a known volume through 1.2 µm Whatman GF/C glass fibre filters. These concentrations were used, together with the in-stream turbidity measurements, to establish a sediment calibration curve for each sampling site (Figure C.1; r^2 = 0.84, 0.86 and 0.88 and n= 126, 121 and 129 for the Upstream, Tributary and Downstream sites, respectively). Predicted SSCs and discharge data were used to calculate SS loads at 5 minute time steps. Total Downstream SS loads, based on the sum of Upstream and Tributary SS loads, were then divided

into the relative contributions of both the Upstream and Tributary sites (hereafter referred to as 'sediment budget'). At the Tributary site, turbidity values were not recorded during a 3-hour period due to very high sediment concentrations (04/06/2021 18:00 – 04/06/2021 21:00). Therefore, SSC predictions during that period were based on a linear interpolation between the available measured SSCs. Downstream discharge was calculated based on the sum of discharges from both the Upstream and Tributary sites (with half an hour delay applied as an estimate of river water travel time).

4.2.3 AnalySize Modelling

The AnalySize software (version 1.2.1; Paterson and Heslop, 2015) was used to perform the un-mixing of: (i) the artificial laboratory mixtures into the soil samples contributions, and; (ii) the field Downstream samples into the contributions of the Upstream and Tributary sources. The AnalySize model was selected based on Van Hateren et al. (2018), wherein the authors compared the performances of different end-member mixing models with decomposed grain-size distribution data using an artificial data set with known source proportions. The authors concluded that the AnalySize algorithm provided the most accurate results. Furthermore, the algorithm allows accounting for the known end-member PSD data (i.e., the Tributary and Upstream sources in this case). AnalySize is a MATLAB based software tool, which is freely available for download (Paterson and Heslop, 2020a), together with a detailed manual (Paterson and Heslop, 2020b).

The AnalySize algorithm is inspired by hyperspectral image analysis (Paterson and Heslop, 2015). Its un-mixing principle is similar to that of mass-balance un-mixing models widely used by the sediment fingerprinting community (e.g., Collins et al., 1997a; Lizaga et al., 2020c; Pulley and Collins, 2018; Stock et al., 2018), where data that are to be un-mixed can be described as a linear mixture of the contributing end-members. End-member abundance must be >0 and sum to 1 (100%). In the AnalySize algorithm, the PSD data are expressed as relative abundances of each size class and must sum to one. The un-mixing principle (Equation 4.1) can be expressed in matrix notation (Paterson and Heslop, 2015):

$$\mathrm{X} = \mathrm{AS} + \mathrm{E} \qquad \text{[Equation 4.1]}$$

where *X* is the observed data (PSD of a target SS sample; one specimen per row), *A* the abundance matrix of the constituent end-members (i.e., relative contribution of each tributary) whose signatures are given by *S* (PSD of the tributaries; one end-member per row), and sampling and measurement errors are represented by *E*. As described by Paterson and Heslop (2015), due to the imposed constraints, there is no closed form solution to Equation 4.1, which thereby has to be solved numerically.

Within AnalySize, the target SS PSD data were loaded using the 'Load Data' button. End-member PSDs were entered using the 'Defined' end-member option, as source PSD was measured and could be directly used to determine its abundance. Based on the PSDs of the tributary sources and target SS, AnalySize displays several performance indicators, including EM-r^2 (indicating the maximum squared linear correlation between the end member [EM] PSDs, being a measure of linear independence between the potential sources).

4.2.3.1 Un-Mixing of Artificial Laboratory Mixtures

The PSDs of the soil samples measured in the tank set-up were used as source data to un-mix the PSDs measured on the artificial mixtures. Source data were created by averaging all recorded PSDs over all concentrations. Mixture PSD data were introduced for each single measurement separately, with AnalySize predicting, for each measurement, the relative abundance of the soil samples mixed in the tank set-up. In the present study, size classes ranging from 1 to 500 µm were included for analysis. Modelled results were compared with the known relative soil sample contributions (section 4.2.1.2).

4.2.3.2 Un-Mixing of Suspended Sediment Field Samples

For consistency with the laboratory results, the upper size limit for the Mastersizer measurements on the field samples was set to 500 µm. This approach allowed the inclusion of the main PSD peak, while eliminating (smaller) peaks at larger particle size ranges (>500 µm) that were associated with small leaves or coarser particles (Figure C.2, Figure C.5). The five PSD measurements per sample were averaged for the source samples; all five individual measurements of the Downstream samples were used in AnalySize.

4.3 Results

4.3.1 Laboratory Experiments: Model Evaluation using Artificial Mixtures

Modelled contributions for the respective soil samples, for mixtures consisting of soil samples sieved to different size fractions, are shown in Figure 4.3a. Overall, modelled contributions predicted the same dominant soil samples compared with the known input contributions. Differences between averaged modelled contributions and known input contributions to the mixtures were small (Table A.5), with deviations >10% only observed for soil samples in mixtures 3 (14%, for soil samples #1.1 and #5.3), 4 (13%, for soil sample #5.3), 7 (11%, #2.3), 8 (10%, #1.1) and 9 (10%, #1.1).

Mixture 2 differed from the other mixtures in terms of the high standard deviations associated with the modelled contributions (34%), which were <15% for all other soil samples (Table C.4). For Mixture 2, mixture D_{50} values (Figure C.4) unexpectedly increased with increasing concentrations (up to theoretical concentrations of 600 mg L^{-1}). D_{50} values then returned to their starting values (observed at 100 mg L^{-1}) and remained constant at the higher theoretical concentrations tested (600 mg L^{-1} - 1000 mg L^{-1}). Following the patterns observed in the D_{50} values, modelled contributions (Figure C.4) for soil sample #1.2 (83% input contribution) started between 80%-100%, decreasing in a stepwise manner to ranges of 30-50%, 10-30% and 5-15%. Thereafter, for concentrations exceeding 600 mg L^{-1}, modelled contributions for the soil sample returned to very high values of 90-100%. Similar stepwise increases of D_{50} values were observed for several other mixtures and/or soil samples (e.g., soil sample #1.2, #3.1, #4.2 and #6.2). These patterns mostly occurred at lower theoretical concentrations (100-500 mg L^{-1}), which caused a spread in the modelled soil sample contributions at these lower concentrations, although to a much smaller extent than observed for mixture 2.

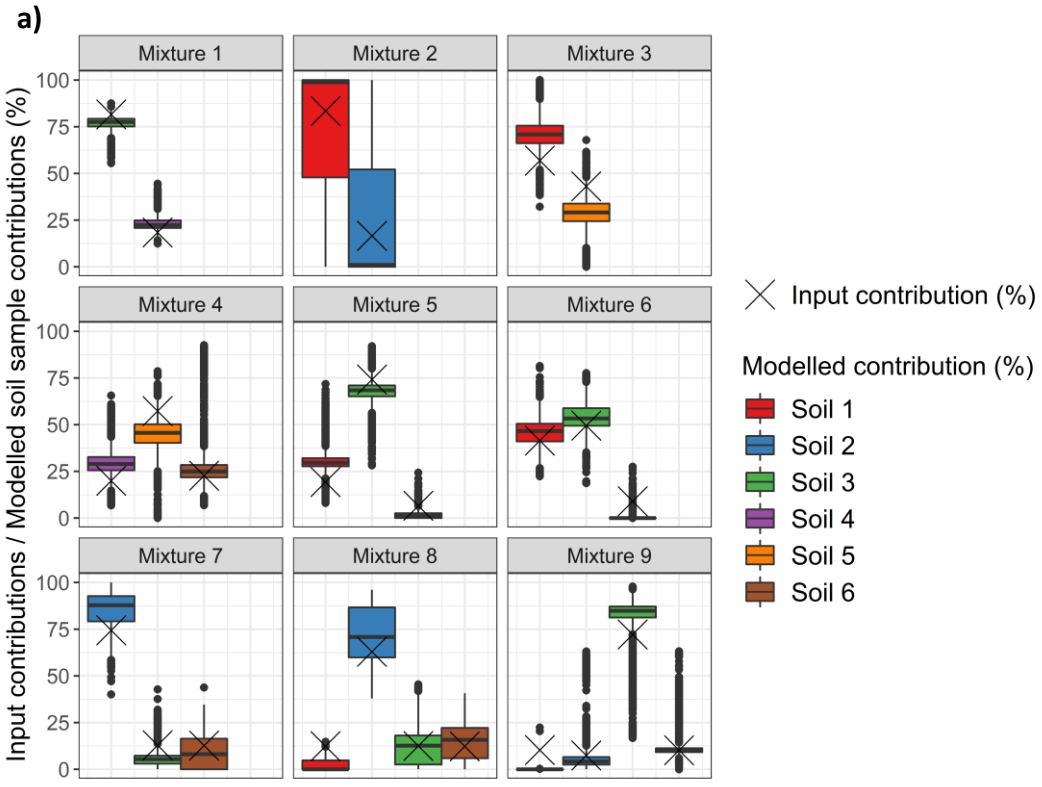

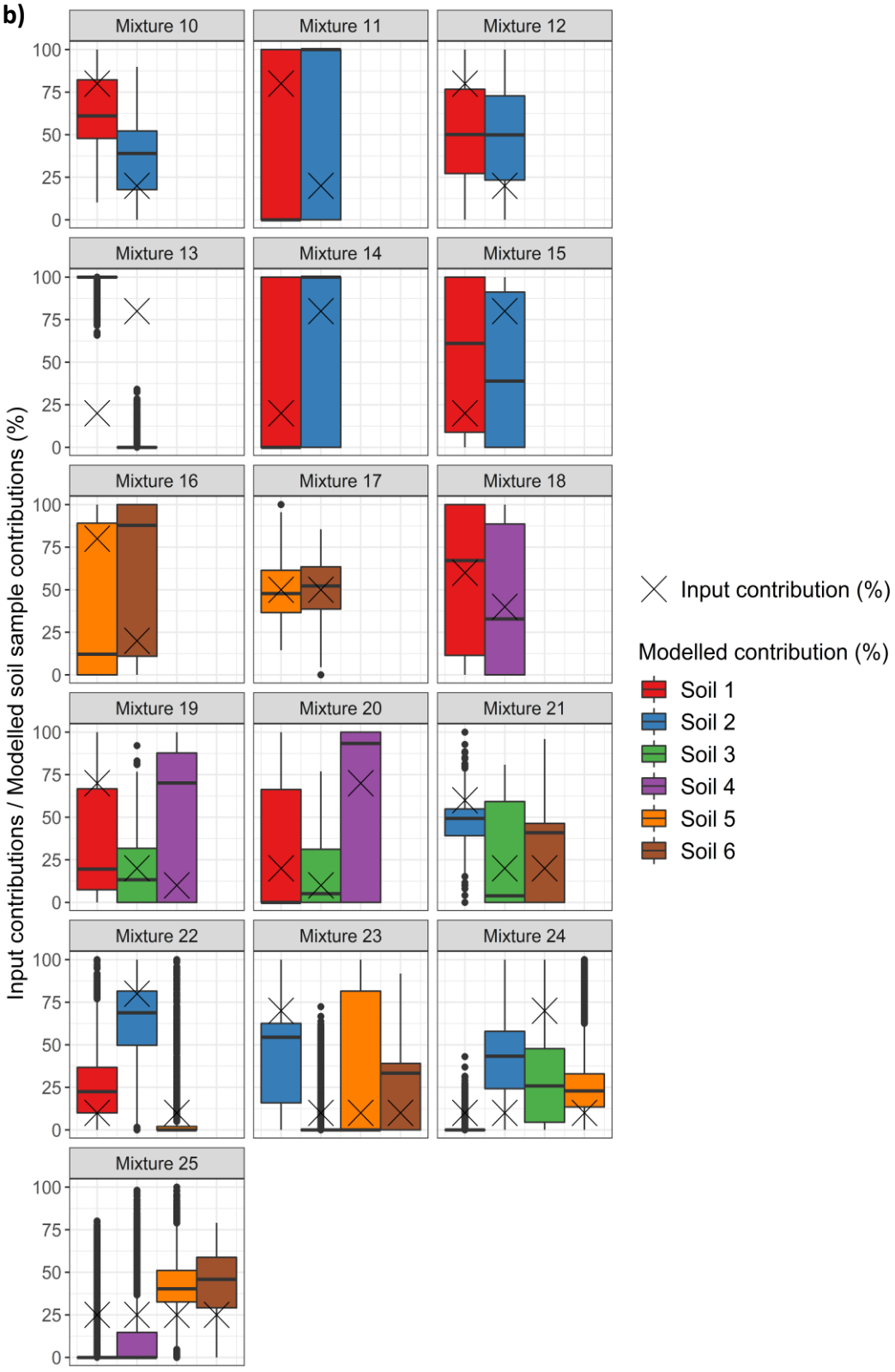

Figure 4.3 Modelled contributions (boxplots, with median shown by central line, interquartile range by box, and range by whiskers) for the laboratory experiments using artificial mixtures consisting of soil samples sieved to different size fractions. These modelled contributions are compared with the known input contributions of soil samples in each of the mixtures (black crosses). Mixtures 1-9 consist of soil samples sieved to different fractions (a). Mixtures 10-25 consist of mixtures sieved to same fractions (b).

Modelled predictions for the mixtures with soil samples sieved to the same size fractions exhibited larger deviations from the known input contributions (Figure 4.3b). For those mixtures using four soil samples, several modelled soil sample contributions were estimated at 0%. Only a few modelled soil sample contributions were close to the known input contributions. This observation was, for example, notable for the soil samples in mixture 17. Particle sizes of the soil samples in mixture 17 were, although sieved to same fractions, significantly different (t-test; p-value of < 0.001) showing a larger difference than the other soil samples sieved to the same size fractions (Figure C.3).

4.3.2 Field Experiments: Model Evaluation using Sediment Budget Estimates

An overview of discharge and precipitation data is shown in Figure 4.4, with selected periods in which field sampling was performed highlighted. Discharge and precipitation, as well as maximum measured SS concentrations (SSC) during the periods are shown in Table 4.2. Periods A, C, F and G were high discharge periods, associated with relatively high SSCs. Period B was a discharge recession. Periods D and E were small storm runoff events with measured SSC concentrations lower than during the high discharge periods. During period F, more than 20 mm of rainfall was measured within 2 hours, resulting in a relatively high discharge peak and elevated SSCs (with a maximum of 2368 mg L^{-1}) at the Tributary sampling site (Table 4.2). Period G was measured during the 2021 extreme flood event in central Europe (14/07/2021 – 15/07/2021), with a return period of >20 years for the Attert River. During the storm runoff events, D_{50} values measured on the discrete samples showed an initial increase during the rising limb of the hydrograph and then a decrease before the discharge peak.

Figure 4.5 presents the modelled predictions using the PSDs measured on the discrete samples to estimate the relative contributions of the Upstream and Tributary sites to the Downstream site. Samples collected at low and mid-flows showed a large variability in modelled contributions (periods A-F); for several cases, contributions reached 100% (and 0%) for both the Upstream and Tributary sites (e.g., periods B, E and F). During storm runoff events (periods A, C and F) the dominant modelled contributions were assigned to the Upstream site directly after the peak discharge. This aligned with the estimated sediment budget contributions, wherein the Upstream site is, in general, the dominant contributor (generally exceeding 60%) to the Downstream target SS. For the large flood event (period G), averaged modelled contributions and estimated contributions from the sediment budget demonstrated relatively small deviations over the whole measurement period (average deviation of 16%, n = 25).

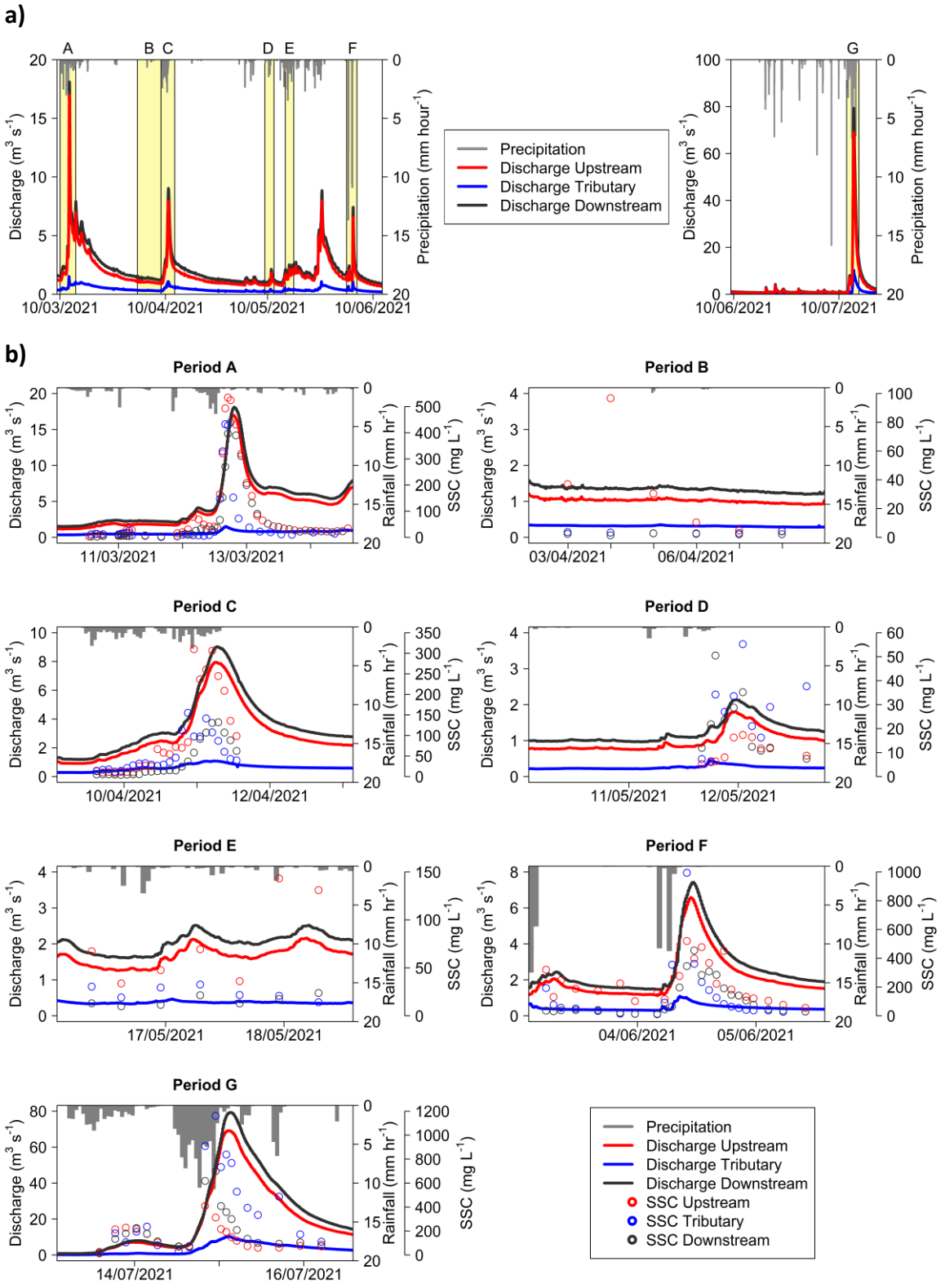

Figure 4.4 Precipitation records from the weather station in Useldange, and discharge records at the three measurement sites. Periods in which field observations were made (A-G) are highlighted in yellow (a). Detail of discharge and precipitation records for the selected periods (A-G), in combination with the measured suspended sediment concentration of the collected samples (b). For period F, the highest value (Tributary) is omitted for visual purpose (2367 mg L^{-1}, 04/06/2021 19:30. This value precedes the shown 994 mg L^{-1} value; 04/06/2021 21:00).

Table 4.2 Summary hydro-sedimentological data for the measurement periods.

Period	Start - End dates and times	Total precipitation (mm)	Sampling site	Maximum measured SSC (mg L^{-1})	Maximum discharge (m^3 s^{-1})	Total sediment load (t)	Total discharge (mm)
A	10/03/2021 21:00 - 15/03/2021 11:55	30.4	Upstream	535	17.0	250.2	10.6
			Tributary	424	1.5	13.2	6.0
			Downstream	440	18.1	212.4	9.1
B	02/04/2021 14:15 - 09/04/2021 12:00	1.6	Upstream	97	1.2	4.8	3.7
			Tributary	4	0.4	1.1	4.3
			Downstream	3	1.6	11.7	3.7
C	09/04/2021 12:00 - 13/04/2021 13:20	35.1	Upstream	310	7.9	59.6	6.5
			Tributary	155	1.1	8.8	5.0
			Downstream	132	9.0	55.7	5.9
D	10/05/2021 00:00 - 12/05/2021 17:00	4.7	Upstream	17	1.8	1.4	1.4
			Tributary	55	0.4	0.46	1.4
			Downstream	51	2.1	4.48	1.3
E	16/05/2021 00:00 - 18/05/2021 12:00	17.6	Upstream	143	2.2	3.8	2.2
			Tributary	33	0.47	0.94	1.8
			Downstream	24	2.5	4.1	2.0
F	03/06/2021 13:00 - 06/06/2021 01:00	44.2	Upstream	520	6.6	98.7	2.9
			Tributary	2368	1.1	31.4	2.2
			Downstream	455	7.4	102.2	2.6
G	13/07/2021 00:00 - 16/07/2021 12:00	101.5	Upstream	410	69.1	1039.0	35.7
			Tributary	1162	10.1	382.4	22.9
			Downstream	700	79.3	1323.0	31.3

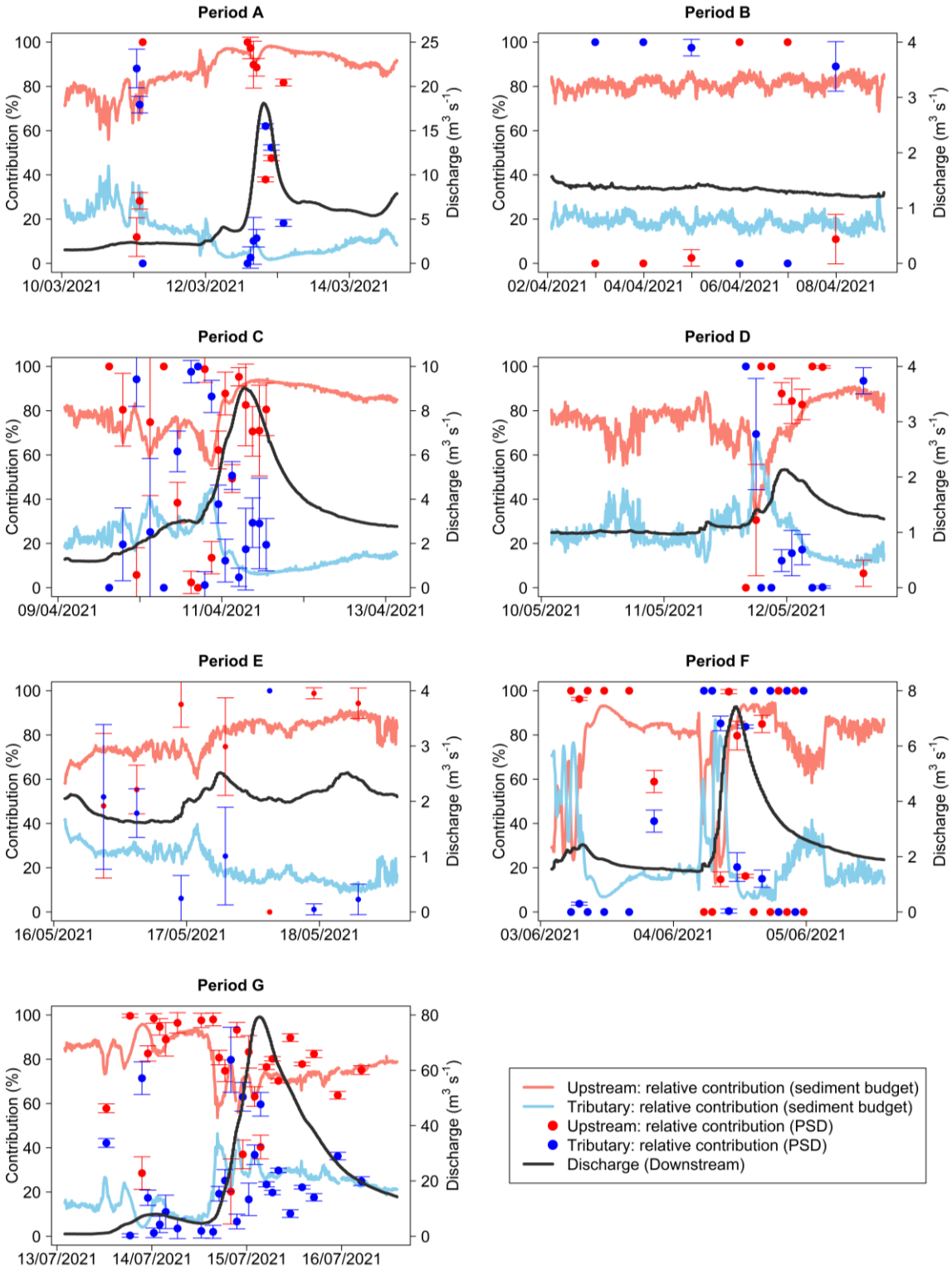

Figure 4.5 Modelled relative contributions of the Upstream and Tributary sites to the Downstream site calculated using PSDs measured on the discrete samples (periods A-G). Modelled contributions are compared with the relative sediment loads (calculated sediment budget) of the Upstream and Tributary sites (red and blue lines) to the Downstream site. Coincidence of dots and lines of similar colour indicates good agreement between the two sets of data. Error bars showing modelled standard deviations.

There were several observations where increasing contributions from the Tributary, based on sediment budget estimates, coincided with either increasing modelled Tributary contributions or increasing modelling uncertainties. For period C, contributions according to the sediment budget were ca. 50% for both the Upstream and Tributary sources during the steeper rise of the hydrograph (at a discharge of ca. 4 $m^3 s^{-1}$). Modelled contributions exhibited large variations around that time, with subsequent contributions for the Tributary source of 1.2%, 86% and 38%. Period F exhibited high variability in modelled source predictions. During the initial stages of the rising limb, this period experienced high sediment loads from the Tributary site (Figure 4.4 and Table 4.2). Modelled contributions around that time predicted dominant contributions for the Tributary (with two values predicting a contribution of 100%). During period G, overall discharges were very high and modelled results closely coincided with the source contribution estimates from the sediment budget. At the peak of the hydrograph and during the falling limb, differences between the sediment budget and modelled contributions were, however, more pronounced (within a 20% range). During the rising limb of the hydrograph in period G, there were three times at which the modelled contributions predicted the Tributary as the dominant source. These results correspond to the variabilities observed in the sediment budget contributions, where the Tributary contributions increased and decreased three times to reach maximum values of 40-45%, and minimum values of ca. 25%, before showing a more stable relative contribution after the peak discharge. Similar patterns were found for period D, where a dominant contribution from the Tributary site was predicted by the model, in agreement with the sediment budget estimates.

4.3.3 Field Experiments: Relationships between Model Performance, Discharge, Source Particle Size and Organic Matter Content

Model performance improved with increasing discharge (Figure 4.6a). For discharges <4 $m^3 s^{-1}$, a wide range of model performances was observed. Above this discharge value, 40 samples out of 46 returned a deviation between modelled and sediment budget-based estimates of <40%, 38 samples <30% and 33 samples <20%. Results (Figure 4.6a) indicate that model performance improved when discharge values exceeded 4 $m^3 s^{-1}$. Model performance did not improve when there were larger differences in source D_{50} values (Figure 4.6b) or when OM was removed before PSD measurements (Figure C.5; Table C.6).

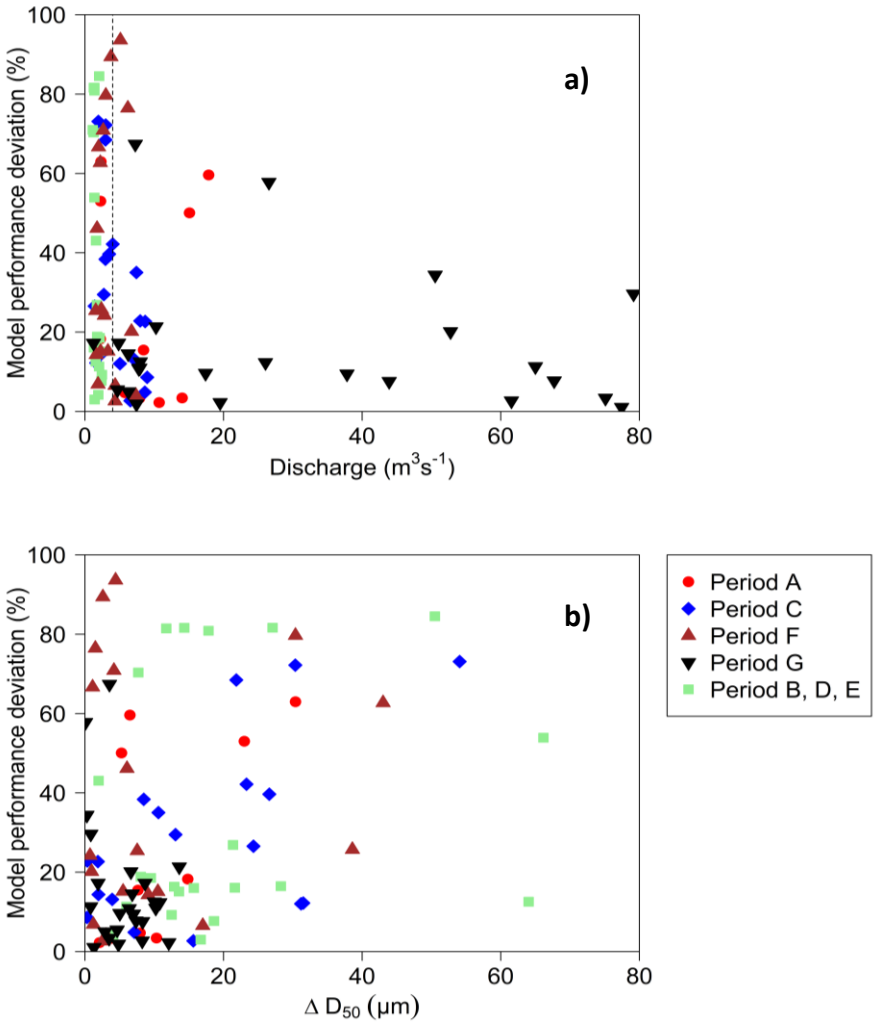

Figure 4.6 Model performance deviation (i.e., absolute difference between the modelling results and the calculated sediment budget) as (a) a function of discharge, and (b) ΔD_{50} (i.e., median particle size differences between both sources). A model performance deviation of 0% indicates no difference between the two sets of data. The discharge threshold values as discussed in the text are shown by a vertical dotted line (discharge: 4 m^3 s^{-1}, (a)). Results for the largest events (periods A, C, F and G) are shown individually; smaller events and low flow (periods B, D and E) are shown together.

4.4 Discussion

4.4.1 Evaluating Model Performance using Artificial Mixtures

Low absolute errors of 7 ± 4% were observed between the known and modelled contributions for the soil samples sieved to different size fractions (Figure 4.3a). Lake et al. (2022a) reported higher mean absolute errors of 14.5 ± 13.0% when using absorbance as a fingerprint property to model the relative source contributions of the same 9 mixtures. Here, our absolute errors between known

inputs and modelled outputs are comparable to other studies using artificial mixtures to evaluate un-mixing models, with absolute errors ranging between 10% (Gaspar et al., 2019), 9% to 11.8% (Haddadchi et al., 2014b) and 11.2% (Pulley et al., 2017). Our results herein thus indicate good accuracy and thus the suitability of the presented modelling approach to estimate the source contributions to the mixtures. On the other hand, our larger mean absolute errors of 22 ± 19% when un-mixing the laboratory mixtures consisting of soil samples sieved to the same size fractions (n= 16; Figure 4.3), indicate that smaller differences in PSD and D_{50} between source samples understandably had a negative influence on the accuracy of modelling. This inaccuracy can also be observed in the modelled contributions of either 0% or 100%. This most likely indicates the inability of the model to distinguish between sources that are similar. This limitation has been observed in previous sediment fingerprinting studies (e.g., Cooper et al., 2014a) and suggests limitations of the un-mixing model principles.

Particular consideration must be given to the fact that AnalySize predictions were mainly influenced by the measured variability in the PSDs of the mixtures. The soil samples (end-members) PSDs were averaged over all tested concentrations (100-1000 mg L^{-1} range), under the assumption that PSD remained constant during the experiment. However, with the observed variations in soil sample D_{50} values, modelling of each concentration separately would have eventually resulted in larger model inaccuracies. This is pertinent when considering the lower concentrations tested, as the higher variations in D_{50} values were observed in the 100-500 mg L^{-1} range (Figure C.4). Consequently, results for the higher concentrations would in that scenario be more constant and more accurate. Similar observations (i.e., higher inaccuracy at lower concentrations) were reported in Lake et al. (2022a).

In contrast to other studies using shear cells to investigate flocculation effects (e.g., Biggs and Lant, 2000, who used activated sludge to analyse floc size in relation to shear), the experiments here did not show signs of floc formation or aggradation inside the tank set-up. This was supported by the continuous LISST measurements (Figure C.4), which showed that D_{50} values varied little (representing the absolute PSD obtained after disaggregation and sieving). Furthermore, SSCs also varied little during the course of the experiments; a constant percentage of added soil sample or mixture material being observed in suspension (see Lake et al., 2022a, Figure C.6).

4.4.2 Un-mixing Field SS samples: Influence of Discharge, Source Particle Size, and Organic Matter Content on Model Performance

The catchment scale field experiments suggested that discharge exerts a strong control on the model performance. Walling et al. (2000) argued that, during the initial phase of storm hydrographs

(i.e., rising limb), sediment is transported from a range of different sources, and subsequent changes in particle size could be linked to changes in contributions from those different sources. After these initial sources (e.g., sediment stored on the riverbed) are depleted, however, alternative sources within the catchment can become dominant. This can result in more constant source contributions and thus a more constant texture for sediment in the stream. The latter scenario provides better conditions for making reliable source contribution estimations using PSDs as a fingerprint property. The improved accuracy of sediment fingerprinting estimates during high discharges (>4 $m^3 s^{-1}$) could also be linked to the limited settling, and thereby, improved mixing of sediment being routed through the channel system (Agrawal and Pottsmith, 2000). Discharges exceeding this threshold were observed for 12% of the time (Downstream site) during the study period (Figure 4.4; 10/03/2021 – 21/07/2021), with a mean measured discharge during that period of 2.5 m^3 s^{-1}. During this 12% of the time, 82% of the total SS load (Downstream site) was transported.

Besides the potential changes in SS source PSDs, different flocculation processes could affect the observed in-stream PSDs (e.g., Droppo, 2004; Grangeon et al., 2014). Suspended sediment floc sizes, in combination with their shape and density, determine the potential of particles to be transported due to their relationship with settling velocity (Williams et al., 2008). This corroborates with our observations that under high flow conditions, measured PSDs appeared to be more reliable for the use of un-mixing when compared with low flow conditions. Droppo (2004) argued that the aggregated sizes of SS particles are mostly being controlled by particle concentration and flow shear stress. However, the effect of these dominant in-channel flocculation processes on the measured PSDs (e.g., Grangeon et al., 2012) was assumed to be rather limited, as settling was assumed to be mostly absent (especially under high flow conditions). This suggests that most SS material observed at the source sites was transported to the downstream target SS site regardless of any flocculation occurring in between. To account for any of these in-stream flocculation processes between the sites, we hypothesized during this proof-of-concept study that these effects were minimized by measuring and comparing only the sources and downstream absolute PSDs (i.e., primary particles). Thereby, due to the absence of clear erosion or deposition between the source sites and the target SS sampling site (confirmed by visual observations), it was assumed here that the SS transported downstream was a simple sum of the SS from the upstream sources.

An increase in the D_{50} values was observed at the start of the monitored storm events, which could suggest the remobilisation of sediment stored on the riverbed (e.g., Lawler et al., 2006; Walling et al., 2000). Thereafter, D_{50} values decreased, most probably due to the depletion of these sources. Temporal variability in PSDs during events, related to the activation of different sources during the storm hydrograph, has also been observed in other studies (e.g., Grangeon et al., 2012; Slattery and

Burt, 1997; Upadhayay et al., 2021; Vale et al., 2020). It is therefore important to have a good estimation of transport times between sampling sites when using PSDs for sediment source fingerprinting. This is to avoid time-related issues in the direct comparison of the PSDs of SS samples collected at different sites. Travel times between measurements points could be subject to change depending on flow conditions. In the present study, samples from the three sites collected at the same time were compared directly (i.e., no adjustment was used for travel times). This is because of the relatively short distances (ca. 3 km), and thus short travel times, from both sources (i.e., Upstream and Tributary sites) to the Downstream sampling site. These decisions might, however, have introduced some uncertainty in the estimated source contributions using the established mass-balance sediment budget.

Previous work has shown that oxidation of organic matter can improve modelling results when fingerprinting SS sources (Pulley and Collins, 2022; Pulley and Rowntree, 2016). In the present study, the organic matter of some samples collected during period F was oxidised to investigate its effect on the PSDs (as discussed by Gray et al., 2010) and subsequent un-mixing results. Removal of the organic matter did not improve un-mixing model accuracies for those samples tested (Figure C.5; Table C.6). However, these results can be important to understand what size fractions in the PSDs were influenced by the OM. This information can then help to eliminate OM effects on the PSD, (>500 µm) to only investigate the primary particles that were hypothesized to better represents the sources.

4.4.3 Critical Considerations for Using Particle Size Data for Sediment Source Fingerprinting

Application of the approach presented herein uses differences in PSDs to discriminate between the sources. A first indication of potential differences in PSDs can be gained by looking at potential contrasts based on geology and soils (Walling et al., 2000), as was undertaken for the field experiment part of this study. This preliminary screening can help to avoid situations in which D_{50} values for different tributaries or soil sources are not sufficiently differentiated (as observed in a recent confluence-based fingerprinting study by Patault et al., 2019). Results presented herein, nonetheless, indicated that to achieve accurate un-mixing results, differences in D_{50} values can be relatively small (Figure 4.6b). This is also true for period G, with a deviation between the un-mixing results and sediment budget of 16%; i.e., the sampling period with the best performing performance. Here differences in source D_{50} values were, on average, only 6 µm.

Similarly, attention should be directed to collecting representative samples. Samples collected at different depths (Bainbridge et al., 2012) or at different distances from the channel bank (Walling

et al., 2000) can manifest distinctive SS particle sizes. This latter point relates to our suggestion that for period G, a higher level of turbulence could have resulted in better mixing of the SS in the water column, leading to more representative sampling and more representative PSD data. This situation appeared to improve the un-mixing results, even with the relatively small differences between source D_{50} values. Sampling is also affected by the field equipment used. Field samples were collected using automatic water samplers, for which installation was subject to sampling site limitations. The pumping might, as reported by Grangeon et al. (2012), create a vortex at the inlet opening of the tube that could affect the amount of SS collected and its corresponding particles sizes. This issue highlights the potential uncertainties associated with the automatic samplers deployed.

To analyse particle size, different instruments are available (herein we presented the use of two instruments: the LISST and Mastersizer). As results may differ depending on the type of equipment used (Bieganowski et al., 2018), we recommend that due care and attention are exercised when PSDs or D_{50} values are compared both within and between studies. Furthermore, many different measurement protocols were found in existing literature that can affect measurements, including different machine settings (e.g, rotating stirrer speed), sample preparations (treatment with dispersive agent, duration of ultrasound) and sampling collections (number of measurements) (Cooper et al., 2014b; Dietze et al., 2012; García-Comendador et al., 2021; Grangeon et al., 2012; Patault et al., 2019; Pulley et al., 2017, 2018). Therefore, in the absence of a standard protocol to measure PSDs, it is a good practise to use the same equipment and apply similar measurement protocols when aiming to compare PSD data directly (Bieganowski et al., 2018).

Sediment source fingerprinting results using PSD data could also be compared with un-mixing results using conventional fingerprinting properties and one of the current un-mixing models used by the international scientific community. This would allow some degree of independent validation of PSDs as a fingerprint. The independent validation of sediment source fingerprinting estimates has been rarely undertaken (e.g., Batista et al., 2022; Gaspar et al., 2019). To validate estimated source proportions using PSDs as a fingerprint herein, we used sediment budget estimates generated using conventional water sampling; this has, to date, been used in few sediment fingerprinting studies (e.g., Collins et al., 1998; Dabrin et al., 2021; Tiecher et al., 2022), mainly due to the extra costs associated with the installation of equipment and sampling (Collins et al., 2017, 2020; Collins and Walling, 2004).

4.5 Conclusions

In this research, the use of PSDs to fingerprint suspended sediment sources was tested at laboratory and catchment scales. To this end, we used an end-member grain size un-mixing modelling algorithm (AnalySize). The laboratory tests, using mixtures with soil samples sieved to different size fractions, resulted in accurate un-mixing results for the two, three and four soil samples mixtures tested. Observed absolute errors (7 ± 4%) were found to be in the same range or even smaller compared with other research using artificial mixtures to evaluate un-mixing model accuracy. Field data were collected using a confluence-based approach, with relatively short distances (ca. 3 km) between the source sampling sites and the target SS sampling site. The corresponding un-mixing results were more accurate at higher discharges (with an average deviation of 19% from the estimated sediment budget, for discharges >4 $m^3 s^{-1}$). The approach described herein, using PSDs in combination with a grain-size un-mixing model, could support the growing sediment fingerprinting community with an additional fingerprint that is relatively easy to obtain. This is especially of merit since PSD measurements are already routinely made in many sediment source fingerprinting studies.

Chapter 5 Synthesis, Conclusions and Outlook

This chapter brings together the key outcomes of the core chapters of this thesis. A synthesis of the novel research, in relation to the research questions of this thesis (section 1.6), is presented. This is accompanied by conclusions for each research question and for the overall thesis aim. Finally, possible directions for future research are presented.

5.1 Research Synthesis and Conclusions

Instruments able to measure SS properties *in situ* and at high temporal resolution were first tested in the early 2010s. Submersible spectrophotometers were used, measuring absorbance in the UV-VIS wavelength range (200 to 730 nm), to determine values of SS-associated properties (e.g., Bass et al., 2011; Martínez-Carreras et al., 2016; Sehgal et al., 2022). To determine the potential to use such submersible spectrophotometers for sediment source fingerprinting purposes, investigating whether absorbance values at different wavelengths can be used as sediment fingerprints, research question (RQ) 1 was proposed:

> *How can absorbance readings of a submerged spectrophotometer be used as sediment fingerprints to estimate source contributions from artificially created sediment mixtures in a proof-of-concept laboratory experiment?*

Data obtained from the proof-of-concept laboratory experiments (Chapter 2; Lake et al., 2022a) were used to: (i) investigate the influence of concentration and particle size on the absorbance spectra (i.e., 200-730 nm at 2.5 nm intervals) to identify compensation/normalisation needs; (ii) test the linear additivity of the absorbance spectra, this being a pre-requisite for sediment fingerprinting (e.g., Lees, 1997; Walling et al., 1993); and; (iii) evaluate the un-mixing model predictions, using known soil sample contributions to the artificial mixtures.

It is known that spectrophotometer absorbance data are influenced by SS concentration (SSC) (Thomas et al., 2017) and SS particle size (Berho et al., 2004; Bhargava and Mariam, 1994). Hence, concentration compensation is needed to remove the effect of SSC, to retain only the influence of SS properties on the absorbance spectrum. The experiments showed that absorbance over all wavelengths across the 200-730 nm spectrum increases linearly with increasing concentrations (Figure 2.4; related to the Beer-Lambert law, section 1.5.4), allowing compensation over all wavelengths through simply dividing the absorbance values by the SSC. Concentrations in the tank set-up were measured for all soil samples and mixtures (i.e., measured concentrations). When soil samples were measured independently in the tank set-up, measured concentrations were shown

to be a relative stable percentage of the theoretical input concentration (Figure 2.3). Based on these observations, similar percentages of the theoretical input concentration from the respective soil samples should remain in suspension when used in the artificial mixtures. Thus, as only soil sources and mixtures with the same theoretical concentrations were compared, compensation for (measured) concentrations was not needed (section 2.2.5).

Particle size effects relate to the higher absorbance values associated with smaller particles. Smaller particles result in higher levels of turbidity/absorbance than larger particles at same SSC (Berho et al., 2004; Bhargava and Mariam, 1994). Besides, sediment properties vary with particle size (Horowitz and Elrick, 1987; Russell et al., 2001) and can thereby influence absorbance patterns. For instance, certain SS properties (e.g., particulate organic carbon, SS loss-on-ignition, and SS carbon content and particle size) might be linked to specific wavelengths or wavelength ranges (e.g., Bass et al., 2011; Martínez-Carreras et al., 2016; Sehgal et al., 2022). Compensation for particle size effects were not deemed necessary during these proof-of-concepts experiments (Chapter 2) because measurements showed that particle size is an intrinsic property of SS that remained unchanged during the experiments (i.e., negligible breakdown/dissolution of particles, as observed from the LISST sensor measurements; Figure C.4). Absence of particle size compensation needs are then related to the relatively stable proportions of the measured concentrations compared with the theoretical input concentrations.

Furthermore, the laboratory tests showed that the blank water (i.e., demineralised water) in the tank set-up influenced the absorbance spectra due to its dissolved components (e.g., D'Acunha and Johnson, 2019; González-Morales et al., 2020; Prairie et al., 2020). To eliminate these effects on the absorbance readings (i.e., to only retain that part of the absorbance spectra influenced by the SS properties), this 'background' absorbance was subtracted from subsequent absorbance measurements. While this is an easy step to take in the laboratory experiments, compensating for the influence of dissolved components in natural waters is more challenging. This most likely requires additional measurements and thus adding extra laboratory analysis needs (e.g., measurements on filtered water as presented in Chapter 3; Lake et al., 2023), or by finding methods to eliminate those wavelengths that are mainly affected by dissolved, non-SS components present in natural waters (e.g., Rieger et al., 2004), as suggested in this study (Chapter 2).

It was observed in the experiments that absorbance measurements on the soil source samples and mixtures showed a linear additive behaviour (i.e., relative contributions of soil source absorbance add up to absorbance values measured on the mixture), suggesting its potential use for sediment source fingerprinting purposes. However, some out-of-range situations (i.e., failing the conventional range test) were observed: in instances absorbance data measured on the artificial

mixtures were higher or lower than the absorbance of all contributing soil source samples. As differences were rather small, instances of out-of-range absorbance data were nonetheless included in analyses and interpretation: importantly, dominant source contributions to the mixtures were correctly identified in these cases. Out-of-range situations were likely induced by small concentration differences between the soil source samples and mixtures (i.e., a higher or lower percentage of soil sample settling).

Finally, the un-mixing model results showed relatively accurate predictions when evaluated against the known soil source contributions. Model evaluation is used in sediment fingerprinting to assess model accuracy (e.g., Gaspar et al., 2019; Haddadchi et al., 2014b; Pulley et al., 2017) and can help in assessing the potential of novel fingerprints (Batista et al., 2022), as presented in Chapter 2. Absolute errors were on average 15%, for all soil samples in all mixtures when compared with the known soil source sample input contributions. Dominant contributions were always well-indicated by the modelling process. Analysis of mixtures consisting of two and three soil samples performed well (mean absolute errors of 15% and 13%, respectively), whereas analysis of mixtures consisting of four soil samples performed less well (with a mean absolute error of 17%). This outcome could relate to the decrease in discrimination potential upon increasing the number of sources (e.g., Lees, 1997; Vale et al., 2022). Absolute errors were found to be in the same order of magnitude when compared with other studies aiming to evaluate mixing model accuracy using artificial mixtures: Gaspar et al. (2019) reported a maximum absolute error of 10%, Haddadchi et al. (2014b) reported and absolute error between 11-29% depending on the choice of the model and fingerprints used, and Pulley et al. (2017) reported and absolute error of 11.2%.

Although this proof-of-concept laboratory experiment indicates the potential for using submersible spectrophotometers for sediment source fingerprinting purposes, issues remained to be addressed before the approach could be applied to a natural scale setting (i.e., Chapter 3). A first point of consideration was the choice of soil source samples used in the laboratory experiments. Soil samples were selected based on clear differences in both colour and geochemistry (Table A.1; soil sample minerology). These perhaps marked differences were hypothesized to influence the absorbance spectra, allowing discrimination between soil source samples. In real-world catchment systems, however, it is likely that differences between SS sources are more subtle. In Chapter 2, suggestions were made for selecting sources that could potentially give robust discrimination (i.e., based on differences in lithology). However, source selection could be further improved with a better understanding of what specific SS properties influence specific wavelengths. A more fully-informed decision could then be made on whether wavelengths, influenced by those properties that allow discrimination between potential sources in a specific catchment, could then be robustly used as sediment fingerprints. Artificial mixtures (or virtual mixtures) could thereby be used to

evaluate further the potential of using absorbance spectra for sediment source fingerprinting in specific catchments (as proposed by Batista et al., 2022).

Another important consideration is how to measure absorbance on SS source samples. Potential source samples (soil or channel banks) could be collected and tested in a laboratory set-up (as in Figure 2.2; Figure 4.1, or Figure 3.3a). However, particle size is of major concern due to its influence on absorbance through: (i) turbidity (Berho et al., 2004; Bhargava and Mariam, 1994), and; (ii) affecting potential SS fingerprint property concentrations (Horowitz and Elrick, 1987; Russell et al., 2001). Source and target SS should, therefore, comprise comparable particle size fractions (i.e., as in the laboratory experiments). It is, however, difficult to know exactly which fractions are mobilised from these sources and transported towards the target SS (Stone and Walling, 1997), which is further complicated by SS size fractions changing temporally (e.g., Lawler et al., 2006; Walling et al., 2000), depending on e.g., prevailing flow conditions. Thereby, use of the spectrophotometer has shown that in laboratory conditions, using four distinctly different soil samples already resulted in less precise and less accurate un-mixing model results than with two and three soil samples in the artificial mixtures. The number of natural soil sources that can be accurately discriminated between is therefore also likely to be rather limited, especially considering the likelihood that there will be less marked differences between natural sources than in the laboratory samples tested.

The observed out-of-range situations in the laboratory experiments (Figure 2.6) are likely a result of small deviations in measured concentrations (e.g., differences in settling) (Figure 2.3). Including these data in analysis and interpretation, obviously resulted in a clearly dominant contribution for the source presenting absorbance values similar to the out-of-range mixture absorbance. In the laboratory experiment, this mainly occurred for two sample mixtures with a clearly dominant soil sample contribution (i.e., 80%). Going forward, out-of-range situations observed in natural samples can be caused by similar problems related to concentration (compensation) issues. In the laboratory experiments, it is certain that there are no missing sources. Although, it would be challenging to argue that under catchment scale conditions dominant sources can still be identified using out-of-range data, as it can not be guaranteed that there is an additional contributing soil source that has simply not been sampled. Additionally, the range test might even be falsely satisfied when unidentified, and thus unsampled sources, contribute to the target SS sampled.

To circumvent these aforementioned issues, it was proposed in Chapter 2 to use a confluence-based sampling strategy (e.g., Collins et al., 1996, 1997b; Klages and Hsieh, 1975; Nosrati et al., 2018, 2019; Patault et al., 2019; Vale et al., 2016). This strategy only considers in-stream SS, regarding SS from upstream tributaries as spatial sources and SS of the downstream channel as the

target SS. This approach thereby eliminates concerns regarding missing soil sources and issues related to which particle sizes are being transported from soil sources to the channel systems, avoiding potential related errors for corresponding source apportionment results.

From the proof-of-concept laboratory experiments, it was concluded that submersible spectrophotometer absorbance readings, measured on artificial mixtures, can be used to provide robust apportionments of known soil source sample contributions. This proof-of-concept study only used controlled laboratory experiments, with clearly different soil samples. Therefore, the approach remained to be tested in natural, catchment scale conditions, keeping in mind source and target SS sampling strategies, together with issues related to particle size and concentration effects that impact the absorbance spectra and subsequent sediment fingerprinting results.

Considering the outcomes and recommendations as outlined in Chapter 2, Chapter 3 scaled up the presented spectrophotometer approach to answer the following research question (RQ 2):

> *Can absorbance differences from source streams in confluences be used to apportion spatial SS sources at the catchment scale?*

The study presented in Chapter 3 builds upon the proof-of-concept laboratory study presented in Chapter 2. Similarly, absorbance at the full range of UV-VIS wavelengths (i.e., 200-730 nm at 2.5 nm intervals) was used to discriminate between sources and to quantify tributary spatial source contributions in a confluence-based sampling. Grab water samples were collected at a series of confluences (n = 11) within a small (44 km^2) catchment (Roudbach catchment, Luxembourg), during several storm runoff events. Absorbance spectra were measured in a small custom-made laboratory set-up (Figure 3.3a). Subsequently, spatial SS contributions were apportioned (Figure 3.8) by un-mixing the downstream target SS absorbance into the tributary source contributions using their absorbance signals.

As for investigations presented in Chapter 2, some out of-range situations were observed in the catchment scale experiments. Such situations could be due to the manual sampling, with samples perhaps not fully representing the stream cross-section variability (e.g., Haimann et al., 2014; Horowitz et al., 1990; Rovira et al., 2012). In-stream particle sizes can be influenced by different flocculation processes (e.g., Droppo, 2004; Grangeon et al., 2014). These influences on potential particle size differences between source and target SS sampling sites were assumed to be of low importance because of the small distances (20-40 m) between the source and target SS sampling sites. The same argument holds for the assumption that new SS inputs (i.e., 'new' sources) through overland flow or channel bank erosion were negligible over this small distance, which was also supported by visual observations. On the other hand, SSCs, shown to have a large influence on the

absorbance data (Chapter 2), most likely explained the out-of-range situations. Besides potential settling in the small custom-made laboratory set-up, uncertainties could have arisen from gravimetrically determining SSCs (with found percentage deviations to be within reasonable uncertainty ranges: see Siu et al., 2008). In the out-of-range situations, the target SS sample absorbance was shown to be always relatively close to the absorbance values measured on one of the tributary source samples. So, instead of strictly applying a range test and thus eliminating these confluences, retaining them provided information on dominant sources (similar as to Chapter 2). Information that can still be highly useful in sediment source fingerprinting studies (as argued by e.g., Evrard et al., 2022; García-Comendador et al., 2021; Pulley and Collins, 2022).

The un-mixing modelling generated mean absolute errors of 18%, for all confluences (n=11) and events (n=3). This mean absolute error is in the same order of magnitude compared with those presented in Chapter 2 (15%). However, the catchment scale results in Chapter 3 wrongly identified several tributaries as being the dominant SS source. Consequently, this resulted in high modelled deviations (up to 52%; Figure 3.8) for several tributaries when comparing modelling outcomes with the sediment budget estimates. This highlights the need for an independent evaluation of modelling results when using absorbance for sediment source fingerprinting. An evaluation as presented in Chapter 3 might not, however, be feasible in many cases due to resource needs to measure discharge and SSCs at several sites within a catchment (i.e., to calculate a sediment budget). An alternative might be to use classical fingerprinting approaches and their conventional properties. Also, artificial and/or virtual mixtures could be used to evaluate the potential use of absorbance measurements for sediment fingerprinting purposes, based on catchment specific differences between sources.

The study presented in Chapter 3, contrary to commonly applied sediment fingerprinting studies that rely on sources based on land use, lithology or soil type (Bravo-Linares et al., 2018; Haddadchi et al., 2014a; Martínez-Carreras et al., 2010a; Russell et al., 2001), can help to identify tributary SS contributions. These results can be more informative on the spatial origin(s) of SS, indicating which areas within the catchment contribute most to the target SS. This requires the sampling of several confluences (here, n=11, resulting in 33 samples for a single campaign), which, using conventional sediment fingerprints, could result in high costs of analysis. Analysing a range of geochemical properties for each soil sample and SS sample could cost ca. US$10-$50) (Owens, 2022). Here, despite the initial purchase costs of a spectrophotometer (ca. US$20.000), many samples can then be easily and rapidly measured.

The presented method aims to facilitate fingerprint analysis by directly measuring absorbance on water samples. However, additional measurements are required on the filtered water to enable

compensation for the absorbance readings related directly to SS. Measurements on these filtered samples, supported by the literature (e.g., Rieger et al., 2004), indicated which wavelengths (i.e., 200-390 nm) were particularly influenced by dissolved components (Figure B.2). Accordingly, the 390-730 nm wavelength range (i.e., excluding that part of the spectrum most influenced by the dissolved components) was then used to apportion the tributary spatial source contributions, without filtered water compensation. Results showed broadly similar un-mixing results (i.e., overall deviations of 12.5%), compared with the un-mixing modelling using the full measured range 200-730 nm and compensation for filtered water. This indicates that limitations related to sampling, preparation (i.e., filtering) and laboratory analyses (i.e., measurements on filtered water) could be eliminated by obtaining absorbance data directly from *in situ* installed spectrophotometer sensor probes as long as only absorbance in the 390-730 nm range is considered.

Overall, Chapter 3 shows that absorbance could potentially be used for sediment source fingerprinting purposes in natural environments, and which reduces the needs for laboratory preparation and analysis that are incurred when using more conventional sediment fingerprints. The spectrophotometer method could therefore improve knowledge on catchment hydro-sedimentary processes by contributing to easier ways of estimating SS spatial source contributions and allowing high frequency apportionments of source contributions.

Particle size is an often considered challenge within sediment fingerprinting studies, given its controls on sediment fingerprint values (Horowitz and Elrick, 1987; Russell et al., 2001). Results presented in Chapter 2 furthermore demonstrated that particle size itself had an important influence on the absorbance readings (see also e.g., Berho et al., 2004; Bhargava and Mariam, 1994). While the consideration of particle size in sediment fingerprinting studies is often limited to its role on fingerprint values, there are indications that particle size itself could be directly used as a SS fingerprint (Kranck and Milligan, 1985; Laceby et al., 2017). To this end, Chapter 4; Lake et al. (2022b) investigated the following research question (RQ 3):

> *Can SS source particle size distributions be used as a sediment fingerprint, in combination with an end-member grain size un-mixing model?*

This research question was addressed using: (i) a proof-of-concept laboratory scale experiment, and; (ii) a catchment scale experiment.

The proof-of-concept laboratory experiment (Figure 4.1, similar to the set-up as used in Chapter 2; Figure 2.2), evaluates the un-mixing model outcomes by means of known soil sample contributions in artificial mixtures. Herein, a compensation of the soil sample contributions, according to the measured concentrations, was needed. This because particle size was defined as the relative

proportions of different size classes, with the sum of proportions over all classes adding up to 100%. Particle size distribution measurements of the individual soil source samples are thus independent of the actual measured concentration (i.e., same PSDs are observed over the different theoretical concentrations). When measuring the PSDs on the artificial mixtures, the sum of the relative contributions of all size classes also sums to 100%. The relative contribution of each source sample in the mixture influences the PSD of the mixture, and a compensation according to the measured concentration is thus needed to allow robust evaluation of the un-mixing model results.

The absolute errors of the modelling results when compared with the known (concentration-compensated) soil source contributions were 7 ± 4% (mean absolute error ± mean standard deviation). Modelling results were more accurate and precise than the results obtained using the same samples and absorbance in Chapter 2 (15 ± 13%), showing the potential to un-mix target SS PSDs into the correct source (end-member) contributions. However, as discussed in Chapter 2, the source samples used to create the artificial mixtures were very different, with sources sieved to distinctly different size fractions (i.e., <32 µm, 32-63 µm and 63-125 µm). Therefore, at the laboratory stage of this work, it remained unknown if equally good results could be obtained in a real-world catchment scale setting with eventually more similar source PSDs. Catchments where the method is most likely to be suitable are those with distinct differences in parent material (as suggested by Laceby et al., 2017; and selected in catchment scale experiments in Chapter 4). This is further supported by (Vale et al., 2016), who performed a confluence-based sediment fingerprinting study in a New-Zealand catchment where different tributaries drained areas with distinct differences in underlying geology. Results therein showed clear differences in D_{50} values (median particle size) between some tributaries.

Effects of flocculation and aggradation were assumed to be mostly absent in the laboratory experiments, supported by the LISST PSD measurements and D_{50} values (i.e., corresponding to expected sizes after sieving; Figure C.3). In the catchment scale experiments, flocculation processes could have affected particle sizes and composition between source and target SS sampling sites as sediment is generally transported as flocs, being under constant change due to physical, chemical and biological factors (Droppo, 2001). Modifications to these flocs can thereby affect SS transport/settling behaviour (Droppo, 2001, 2004). It was assumed that settling was rather limited, especially under high flow conditions, regardless of any flocculation processes (section 4.4.2). This, and the absence of (visual) clear erosion or SS inputs between the source and target SS sites (i.e., new contributing sources), suggested that the downstream target SS could be assumed as the simple combination of the upstream sources. Possible flocculation effects on the PSDs were then minimized for by only comparing absolute PSDs (i.e., representing the primary particles; Biggs and Lant, 2000) of the upstream and downstream sampling sites.

Observations presented in Chapter 4 highlight the importance in the timing of sample collection. Particle size distribution patterns are temporally variable, with D_{50} values generally higher at the start of storm run-off events, most likely due to the remobilisation of sediment stored on the river bed (e.g., Lawler et al., 2006; Walling et al., 2000). At later stages, D_{50} values then tend to decrease upon depletion of these sediments. Temporal variability in PSDs during storm runoff events, associated with the activation and deactivation of sources, has been observed in several studies (e.g., Grangeon et al., 2012; Slattery and Burt, 1997; Upadhayay et al., 2021; Vale et al., 2020). An accurate estimation of travel times between sources and target SS sampling sites is therefore recommended to avoid related issues when comparing PSDs. In Chapter 4, samples from the source and target SS sampling sites were, however, taken at the same time, which might have introduced some uncertainty to the un-mixing results.

Besides rapid measurements directly on water samples, another advantage of the approach tested in Chapter 4 is that PSD measurements are already routinely made in sediment fingerprinting studies (see Collins et al., 2020). This indicates that the necessary data may already be available in some instances. Besides using PSDs as an independent fingerprint, it can also be used in parallel to other fingerprints. The un-mixing results of the PSDs can then serve as validation to the un-mixing results obtained using the other fingerprints, or used with other properties in a composite fingerprint to potentially improve source discrimination (e.g., Collins et al., 2020; Walling, 2013).

The work presented in Chapter 4 shows that there is potential to use PSDs as a sediment fingerprint, especially during periods of higher discharge when source contributions are likely to be more stable and produce more constant SS PSDs (Walling et al., 2000). In combination with an end-member grain size un-mixing model, subsequent estimates of SS source contributions can be apportioned to the target SS. It is proposed that this approach works best in a confluence-based sampling strategy, as presented. Particle size distribution can thereby contribute to improving temporal insights into SS source contributions, through relatively easy and rapid measurements conducted directly on the water samples without pre-processing.

The findings of the three research questions allow discussion of the main, over-arching aim of this thesis:

> *Can the selected instruments (i.e., UV-VIS spectrophotometer and particle size analyser) allow for in situ and high temporal resolution SS source apportionment, to ultimately provide a better understanding of catchment hydro-sedimentary dynamics and to facilitate the implementation of targeted management solutions?*

Collectively, the research presented in this thesis demonstrates the ability of spectrophotometers and particle size analysers to measure sediment fingerprints (i.e., absorbance at the UV-VIS wavelength range and PSD, respectively). Chapters 3 and 4 showed that the sediment fingerprints could be obtained directly from laboratory measurements on water samples (i.e., in the custom-made laboratory test chamber for the spectrophotometer, or directly introduced into the Mastersizer), without any preparation needs (e.g., sieving, drying). The reduced resource needs related to laboratory preparation and analysis could thereby facilitate an increase in temporal observations of SS source contributions and changes therein. Collection of source and target SS samples, and subsequent laboratory measurements remained necessary. These remaining needs challenge SS source apportionments at even higher temporal resolutions, and over prolonged periods of time. Next steps therefore require an additional reduction or even elimination of sampling and remaining laboratory analysis needs, which could be achieved through the use of submersible sensor probes as suggested by Collins et al. (2020) and presented in the core chapters (2-4) of this thesis.

Chapter 3 showed a clear potential to directly use *in situ* absorbance measurements for SS source fingerprinting. The absorbance measurements on the filtered water samples (Figure B.2), and data from existing literature (e.g., Rieger et al., 2004) showed that the 390-730 nm wavelength range is largely influenced by the SS, and dissolved components (e.g., nitrate, nitrite, DOC) mainly influence the 200-390 nm wavelength range. Modelling results were highly similar (12.5% overall mean absolute difference) when comparing: (i) absorbance over all wavelengths (i.e., 200-730 nm) and compensated for dissolved components by the filtered water, and; (ii) absorbance in the 390-730 nm wavelength range, not compensated for the filtered water. Therefore, the use of this limited range of wavelengths (i.e., 390-730 nm) could drastically reduce sampling (i.e., *in situ* measurements) and laboratory analysis needs (i.e., direct use of absorbance, with no compensation needed). Together with the ability of the spectrophotometer to measure at high temporal resolution (i.e., minutes), this could then facilitate high temporal resolution source fingerprinting when measuring absorbance *in situ*. The spectrophotometer probe can furthermore allow for measurements of long duration, giving high temporal resolution insights of changing SS sources over e.g., different events or even different seasons. Information would thus be obtained that can subsequently be used to improve existing understanding of catchment hydro-sedimentary dynamics, supporting the implementation of targeted management solutions to prevent excessive sediment delivery and excessive SS loads in surface waters.

For the particle size analyser, it is more challenging to use *in situ* observations for sediment source fingerprinting purposes. In Chapter 4, issues concerning changes to in-stream SS particle sizes (i.e., flocculation processes) are discussed. To that end, it was opted to apply ultrasound, to disaggregate

potential flocs before the measurements, to obtain absolute particle sizes (i.e., primary particles; Biggs and Lant, 2000). This is because *in situ* PSDs measurements are largely influenced by the presence of flocs and their respective size distribution (Droppo, 2001), resulting in generally larger D_{50} values (Figure 5.1) when compared with the D_{50} values of samples collected at the same site and time, and measured by the Mastersizer (after applying ultrasounds). However, patterns of D_{50} values (Figure 5.1), measured *in situ* using the submersible LISST sensor probe (with a potential to measure at intervals as short as minutes or even seconds) follow rather similar patterns during the storm runoff events compared with the D_{50} values measured by the Mastersizer. It remains to be assessed how well these *in situ* measurements can actually be used to discriminate robustly between sources and thus allow for *in situ* and high frequency sediment fingerprinting, i.e., how well flocs/effective particle sizes represent different SS sources.

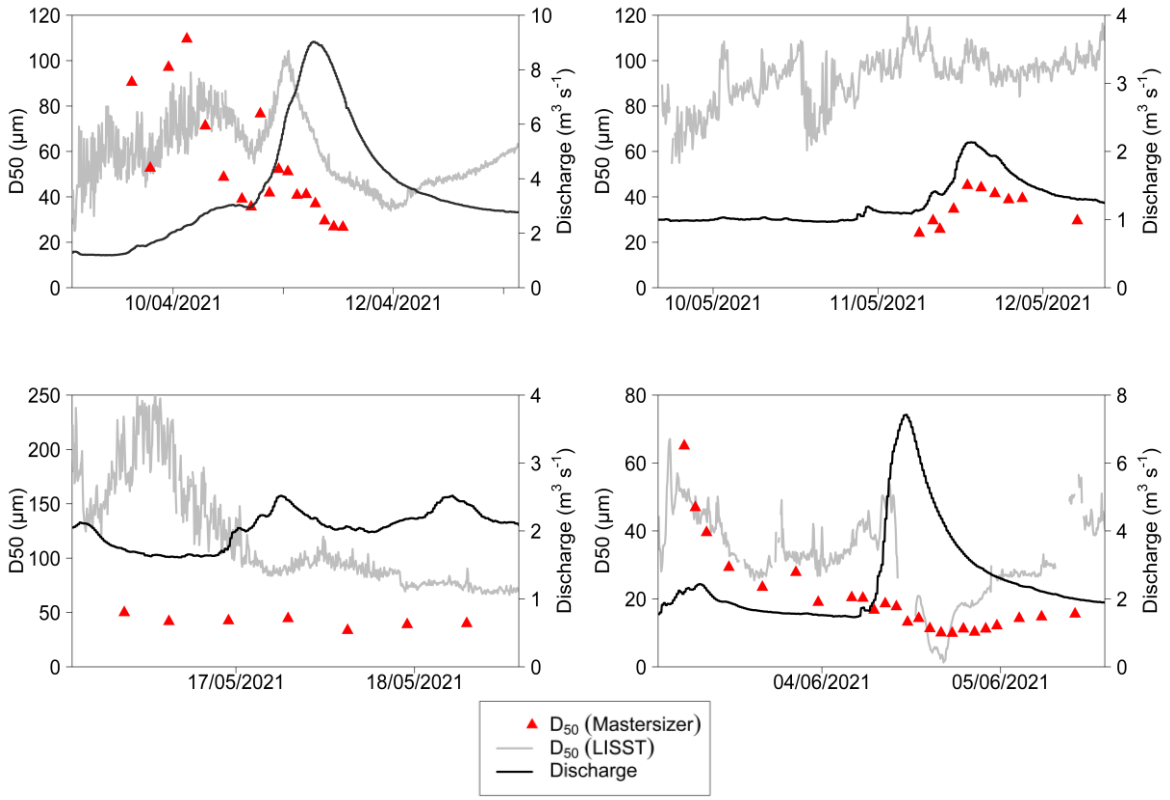

Figure 5.1 Comparison of *in situ* measured median particle size values (D_{50} values measured with a LISST 200X) and laboratory measured median particle size values (D_{50} values measured with a Mastersizer) obtained from samples collected from the Attert River at Everlange. Values are plotted together with the measured discharge.

With the use of a confluence-based sampling strategy (both when using absorbance and PSD), accurate estimations of SS travel times between sources and target SS sampling sites may be needed. In Chapter 3, due to the short distances between sampling sites (ca. 40 m), samples could be quickly collected after each other, with, in principle, limited effects of travel times. In Chapter 4,

despite distances between sampling sites being larger (ca. 3 km), travel times were not considered. It was discussed that this could have led to uncertainties in the SS source un-mixing results. An average travel time between the sites, valid for all conditions, could have been calculated and applied. An alternative approach would be to define condition specific travel times (e.g., depending on flow velocity), which might require additional measurements.

Though both approaches presented herein show the potential to increase the temporal resolution of observations, there are some attendant disadvantages. Initial purchasing costs of the instruments are an important potential constraint, with the submersible spectrophotometer sensor used in this thesis costing ca. US$20,000, and the submersible particle size analyser (LISST) ca. US$25,000 (2022 prices). The laboratory based Mastersizer used in this study costs ca. US$50.000 in 2022. These costs are rather high, especially considering that at least three submersible sensor probes are needed for measurements in a confluence-based approach (i.e., when aiming for *in situ*, high frequency measurements), which add up to initial investment costs. Conventional fingerprint costs can, however, over time, surpass the initial purchasing costs of these instruments when the costs per measurement are considered.

The use of *in situ* measurements will not likely lead to full redundancy of sampling and laboratory measurements. First, specific sampling and/or laboratory analyses remain necessary to allow for an independent evaluation of the un-mixing model outcomes. This could be done by using SSC and discharge monitoring (e.g., Collins et al., 1998; Dabrin et al., 2021; Evrard et al., 2011; Tiecher et al., 2022), which was also used in this thesis (i.e., calculated sediment budgets were used to evaluate the un-mixing model results; Chapters 3 and 4). As calculating sediment budgets require discharge and SSC data, additional measurement campaigns and/or installations are needed, which might not always be feasible (e.g., Collins et al., 2017, 2020; Collins and Walling, 2004). Other means of evaluation could be achieved through e.g., the use of more conventional fingerprints, whereby measurements of fingerprints on collected samples can then be used for evaluation at a number of times/samples. Secondly, additional resource needs remain, related to the maintenance of equipment. The sensor lenses need cleaning, for which the manufacturers of both sensor probes used in this thesis offer accessories to clean the lens mechanically to remove fouling before every measurement (e.g., Sehgal et al., 2022). Sensors can also be cleaned manually (e.g., bi-weekly; Martínez-Carreras et al., 2016) to remove attached debris. Thirdly, there remains a need to compensate the spectrophotometer absorbance data for SSC. Hence, the establishment of a calibration curve to estimate SSCs from turbidity is necessary. This generally requires the collection of samples over a range of different discharge values to account for differences in SS properties (e.g., size, shape) (Lacour et al., 2009; Lewis and Eads, 2008). Calibration curves of this ilk need confirmation on a regular basis (e.g., Collins and Walling, 2004; Navratil et al., 2011). As turbidity is

measured by the spectrophotometer itself, this offers the advantage that no additional sensor probe is needed.

Sediment property conservation is an important requirement in sediment fingerprinting (see reviews by e.g., Collins et al., 2020; Koiter et al., 2013; Walling, 2013). The composition of sediment is thus assumed not to change (i.e., remain conservative) when sediment is transported from sources to sinks, and processes that link sediment sources to the target SS are often ignored and represented by a black-box conceptual model (e.g., Koiter et al., 2013). However, properties are often not conservative (e.g., Davis and Fox, 2009; Koiter et al., 2013; Motha et al., 2002), with various physical, chemical and biological processes altering the sediment properties when transported though the landscape (e.g., Dearing et al., 1996; Owens et al., 2012; Wilkinson et al., 2009). These processes can have significant implications for sediment source fingerprinting because fingerprints measured on the SS samples may no longer be associated with the fingerprint values of the sources. A similar black-box representation was present between the source and target SS sites when using a confluence-based sampling strategy. Uncertainties were likely to be low as sediments were transported over small distances and only in-stream SS was considered: there is thus a higher likelihood that sediment properties remained stable during transport.

Overall, both instrument types (i.e., submersible spectrophotometer and particle size analysers) aim to facilitate rapid and easy measurements of sediment fingerprint values (i.e., absorbance and PSD), whilst significantly reducing resource needs related to laboratory preparation and analysis. This could permit the analysis of a larger number of samples, and an increase in the temporal resolution of SS source ascription. Besides, this thesis aimed to deliver a preliminary assessment of whether the submersible spectrophotometer and particle size analyser probes, which can measure these newly proposed fingerprints, could permit *in situ* measurements and thereby further reduce resource needs related to SS sampling and laboratory workloads. In principle, this should allow for SS source apportionments to be determined at even higher temporal frequency observations (i.e., up to minutes) and for long periods of time, which is not feasible using conventional fingerprints.

5.2 Future Research Directions

Future research directions include the application and the investigation on the use of submerged spectrophotometers installed *in situ*, to apportion SS source contributions at high frequency and over long duration, thereby providing more detailed information on catchment hydro-sedimentary dynamics. Chapter 3 provides the basis for this: it was shown that results were broadly similar when using a reduced range of wavelengths (390-730 nm) without compensating for dissolved components, compared with using the full range of wavelengths (200-730 nm) with compensation

for dissolved components. This observation indicates the viability to directly use *in situ* measured absorbance in sediment source fingerprinting. Furthermore, there is a potential to further reduce the number of wavelengths used, with the objective of reducing mixing model calculation times (e.g., from ca. 4 days when using all wavelengths (n=213; 200-730 nm range), to ca. 1 hour when using wavelengths (n=35) in the 390-730 nm range with a reading every 10 nm). Calculation times were based on using the High Performance Computing facility at the Luxembourg Institute of Science and Technology. The choice for the latter selection of absorbance values (390-730 nm, at 10 nm intervals) relates to the hypothesis that different SS properties affect absorbance values at different wavelengths. Choosing values over the whole range ensures that patterns in absorbance, and thus potential influences of different SS properties on the absorbance spectra, are retained and compared. Especially as links between specific SS properties and absorbance values at specific wavelength (ranges) remain to be determined (need to build on the work by e.g., Bass et al., 2011; Martínez-Carreras et al., 2016; Sehgal et al., 2022). If the response of absorbance spectra to specific SS properties is investigated in more detail, only those wavelengths influenced by properties discriminating between sources can then be used for sediment fingerprinting. Thereby leading to a potential further reduction in model calculation times, as well as a reduction in uncertainty due to the exclusion of wavelengths that are not useful (i.e., wavelengths that do not specifically relate to specific SS properties) or the exclusion of multiple wavelengths relating to a single property (i.e., over-parameterization). By creating a more standardised methodology that is easy to adopt, a wider uptake, potentially beyond the academic research domain, can be achieved (Evrard et al., 2022), leading to a larger uptake by water managers and policy makers to address erosion and sediment transport processes (Owens, 2022).

In Chapter 3, the approach of using a submersible spectrophotometer has only been applied to a small catchment with relatively distinct differences in sub-catchment lithologies. It therefore remains to be tested how well the presented method works (i.e., how well absorbance obtained from SS sources discriminate) in a variety of catchments (i.e., with more or less distinct differences between sources related to e.g., lithology and/or land uses). Investigating the suitability of submersible spectrophotometers in a variety of catchments relates to the suggestion made in Chapter 2, i.e., relating SS properties to absorbance values at specific wavelengths. Understanding absorbance responses of specific SS properties (e.g., from commonly used sediment fingerprint properties, such as geochemistry and colour parameters), can thereby thus indicate the likelihood that the proposed method could be successfully applied to specific catchments.

Building upon the results presented in Chapters 2 and 3, a first investigation into the use of *in situ* absorbance measurements for sediment source fingerprinting purposes was performed. The same confluence-based sampling approach as presented in Chapter 4 was used, whereby submersible

spectrophotometers were installed in the three sampling sites. Measurements took place for a total duration of 5 months (from March 2021 to the end of July 2021), at 5 minute intervals. The first results showed that there were some problems associated with the calibration curves (Figure C.1), as SSC was estimated to compensate the absorbance spectra. Ideally, as was assumed in Chapter 4, the sum of the SS loads of the tributary sources should correspond to the SS load observed at the downstream target SS site. However, calculated sediment loads were found to be much lower (Table 4.2) at the downstream target SS site compared with the sum of the tributary sources for all main rainfall-runoff periods. This suggests that large amounts of sediment were stored between the sampled sites, but this did not correspond with visual observations. Problems with the calibration curve at one of the sites is more likely, which could be associated with an inaccurate representation of the cross-sectional variation (i.e., from where samples are collected). This situation highlights the importance of selecting water sampling/measuring locations with due care and attention (e.g., Haimann et al., 2014; Horowitz et al., 1990; Rovira et al., 2012).

Finally, an important consideration is the usability of the high frequency source fingerprinting data, and what novel information this data can provide. For instance, as seen in Chapter 4, the best results were obtained at relative high discharge values. This outcome raises the question as to whether the approaches might be reliable at relatively low flow conditions, together with the fact that most sediment is transported during the (more extreme) storm runoff events (e.g., section 4.4.2; Gonzalez-Hidalgo et al., 2010). Further investigations are warranted to assess whether only absorbance data (and PSD data), obtained during certain storm runoff events (i.e., exceeding certain discharge threshold values), could eventually be used for sediment fingerprinting purposes. Furthermore, the use of high temporal resolution sediment source fingerprinting is likely to be warranted most in highly dynamic and most likely smaller catchments, where lower temporal measurement resolutions might miss important changes in source contributions. At larger spatial scales, on the other hand, averaging processes often mean that there is relatively less change in sediment dynamics and in source contributions over time, leading to a lower interest in high temporal resolution observations.

Appendix A Supplementary Information to Chapter 2

A.1 Experimental protocol

Before every experiment, the same protocol was adopted to ensure as consistent conditions as possible.

Before starting the experiments:

1. Demounting and cleaning the LISST path length reduction module (the path length reduction module provided by the manufacturer was installed due to the concentrations of SS used in the laboratory experiments).
2. Cleaning of the inside of the tank set-up to ensure no particles from earlier experiments are remaining inside.
3. Cleaning of the optical windows from both the spectrophotometer (using a 15 mm path length insert being appropriate for the SS concentrations as set (see section 2.2.4)) and the LISST (without the path length reduction module).
4. Filling the tank with 40 L of demineralised water.
5. Installation of the LISST path length reduction module (being submerged).
6. Measuring after 5-10 minutes the background readings required for the LISST sensor, which should be measured in stagnant water.
7. Starting of the vibromixer.
8. Initiation of the spectrophotometer measurements to define the background readings (i.e., mixing demineralised water for a duration of 10 minutes; see section 2.2.4).

Start of the experiments

1. Adding soil sample material (either 1 soil sample or mixture) to the water in the tank set-up to reach an initial theoretical concentration of 100 mg L^{-1}.
2. After 10 minutes of measurements, three water samples are collected with a pipette (see Figure 2.1b for sampling locations; Chapter 2), transferred into pre-weighted alumimium cups, and oven dried at at least 75°C, to determine concentrations. These 'measured' concentrations were defined as the weight of soil material present in the cups divided by the volume of water sampled and expressed in mg L^{-1}.
3. After collection of the water samples in the aluminium cups, the concentration within the tank was progressively increased at 100 mg L^{-1} intervals, up to 1000 mg L^{-1}. After each 10 minutes of measurement, three water samples were collected (step 2).

Appendix A

After the experiments

1. Emptying water from the tank set-up after finishing the experiment.
2. Weighing the dried water samples in the aluminium cups. These cups are weighed to determine 'measured' concentrations. These 'measured' concentrations were defined as the weight of the aluminium cups plus soil sample minus the weight of the clean aluminium cup (pre-weighted). This value, representing the weight of the soil material present in the dried water sample, is divided by the volume of water sampled to obtain the concentration (expressed in mg L^{-1}).

Set-up settings and water sampling considerations

The vibromixer was installed at 10 cm above the bottom of the tank, which is slightly lower than the 13.5 cm recommended. We chose this height, however, as well as the chosen vibrating speed to obtain the best possible homogeneous mixing, based on preliminary tests. These tests also explored how the formation of air bubbles, which mainly affect the LISST sensor measurements, could be reduced together with the establishment of an optimal vibrating speed (Figure A.1 and A.2).

The three water samples were collected at 20 cm below the water surface, as preliminary sampling results at three different depths (10, 20 and 30 cm; soil sample 2, 63-125 µm fraction) showed relatively homogenous concentrations with depth and with location (Figure A.3). Therefore, only the 20 cm depth was used

Table A.1 Relative mineral content (%) of the soil samples (fraction 32-63 µm) obtained from semi-quantitative XRD-analyses using the DIFFRAC.EVA software (version 4.3), when relative content >4%: * 4-10%, **10-30%, and *** >30%. Analyses were carried out at the Institut Terre et Environnement de Strasbourg (ITES; France).

	Quartz	Goethite	K-feldspar	Muscovite	Albite	Montmorillonite	Calcite
Soil 1	***	**	*			*	*
Soil 2	***		*	*	*		
Soil 3	***		**	*	*		
Soil 4	***		**				
Soil 5	***		*		*		
Soil 6	***			**	*		

Table A.2 Overview of the laboratory experiments: Individual soil samples and artificial mixtures using two, three and four soil sample mixtures with their known relative contributions.

Individual soil sample	
Sample	Known contribution
#1.1	100%
#1.2	100%
#1.3	100%
#2.1	100%
#2.2	100%
#2.3	100%
#3.1	100%
#3.2	100%
#3.3	100%
#4.1	100%
#4.2	100%
#4.3	100%
#5.1	100%
#5.2	100%
#5.3	100%
#6.1	100%
#6.2	100%

2 soil sample mixtures				
Mixture	Sample	Known contribution	Sample	Known contribution
1	#1.1	80%	#2.1	20%
2	#1.2	80%	#2.2	20%
3	#1.3	80%	#2.3	20%
4	#1.1	20%	#2.1	80%
5	#1.2	20%	#2.2	80%
6	#1.3	20%	#2.3	80%
7	#5.2	80%	#6.2	20%
8	#5.1	50%	#6.1	50%
9	#1.3	60%	#4.3	40%
10	#3.1	80%	#4.2	20%
11	#1.2	80%	#2.3	20%
12	#1.1	30%	#5.3	70%

3 soil sample mixtures						
Mixture	Sample	Known contribution	Sample	Known contribution	Sample	Known contribution
13	#1.2	70%	#3.2	20%	#4.2	10%
14	#1.2	20%	#3.2	10%	#4.2	70%
15	#2.2	60%	#3.2	20%	#6.2	20%
16	#1.1	10%	#2.1	80%	#5.1	10%
17	#4.2	10%	#5.3	80%	#6.1	10%
18	#1.2	20%	#3.1	70%	#4.3	10%
19	#1.1	30%	#3.3	50%	#5.3	20%
20	#2.3	80%	#3.1	10%	#6.2	10%

4 soil sample mixtures								
Mixture	Sample	Known contribution	Sample	Known contribution	Sample	Known contribution	Sample	Known contribution
21	#2.2	70%	#3.2	10%	#5.2	10%	#6.2	10%
22	#1.1	10%	#2.1	10%	#3.1	70%	#5.1	10%
23	#3.1	25%	#4.1	25%	#5.1	25%	#6.1	25%
24	#1.1	10%	#2.3	10%	#3.1	70%	#6.2	10%
25	#1.1	10%	#2.3	70%	#3.1	10%	#6.2	10%

Table A.3 Mean absolute errors (AE) between MixSIAR predicted and known soil sample ('source') contributions in the artificial mixtures, with associated standard errors (SE).

	Source %	**AE (SE)**	**Source %**	**AE (SE)**
Mixture 1	80	17.0 (0.8)	20	17.0 (0.8)
Mixture 2	80	19.2 (0.3)	20	19.2 (0.3)
Mixture 3	80	14.5 (2.5)	20	14.5 (2.5)
Mixture 4	20	7.2 (2.7)	80	7.2 (2.7)
Mixture 5	20	21.7 (6.2)	80	21.7 (6.2)
Mixture 6	20	11.1 (4.1)	80	11.1 (4.1)
Mixture 7	80	10.3 (1.3)	20	10.3 (1.3)
Mixture 8	50	18.9 (0.2)	50	18.9 (0.2)
Mixture 9	60	12.0 (4.1)	40	12.0 (4.1)
Mixture 10	80	19.9 (0.0)	20	19.9 (0.0)
Mixture 11	80	26.7 (2.6)	20	26.7 (2.6)
Mixture 12	30	6.0 (0.2)	70	6.0 (0.2)

	Source %	**AE (SE)**	**Source %**	**AE (SE)**	**Source %**	**AE (SE)**
Mixture 13	70	20.3 (6.5)	20	27.7 (1.8)	10	7.5 (6.6)
Mixture 14	20	3.2 (4.7)	10	12.1 (0.8)	70	11.5 (5.3)
Mixture 15	60	8.1 (5.2)	20	8.9 (3.1)	20	3.9 (2.4)
Mixture 16	10	27.0 (3.0)	80	26.3 (5.6)	10	2.6 (3.0)
Mixture 17	10	3.9 (6.5)	80	3.3 (8.4)	10	1.8 (0.4)
Mixture 18	20	11.8 (10.2)	70	21.0 (11.5)	10	8.8 (1.3)
Mixture 19	30	15.5 (4.1)	50	41.0 (4.6)	20	25.5 (0.8)
Mixture 20	80	8.3 (10.7)	10	3.7 (10.7)	10	5.3 (0.5)

	Source %	**AE (SE)**	**Source %**	**AE (SE)**	**Source %**	**AE (SE)**	**Source %**	**AE (SE)**
Mixture 21	70	13.4 (2.4)	10	15.5 (2.6)	10	6.2 (2.4)	10	5.1 (1.6)
Mixture 22	10	32.3 (2.7)	10	14.3 (1.0)	70	48.8 (3.2)	10	3.9 (1.2)
Mixture 23	25	25.1 (2.1)	25	16.6 (2.8)	25	21.8 (0.7)	25	11.5 (0.5)
Mixture 24	10	45.5 (2.7)	10	9.1 (0.4)	70	40.7 (3.1)	10	4.3 (0.4)
Mixture 25	10	2.8 (0.5)	70	13.0 (1.3)	10	4.2 (0.8)	10	6.1 (0.7)

Table A.4 Overview of mixtures and those concentrations where the Gelman-Rubin diagnostics value exceed the threshold value of 1.1, including the number of variables exceeding this threshold.

Mixture	Gelman-Rubin
1	-
2	-
3	-
4	-
5	-
6	-
7	-
8	-
9	-
10	-
11	-
12	-
13	200, 1000 mg L^{-1}: 1>1.1 700, 800, 900 mg L^{-1}: 2>1.1 300, 600 mg L^{-1}: 3>1.1
14	-
15	-
16	300 mg L^{-1}: 3>1.1
17	100, 400–900 mg L^{-1}: 3>1.1
18	700 mg L^{-1}: 3>1.1
19	100-400, 600-1000 mg L^{-1}: 3>1.1
20	-
21	100, 600mg L^{-1}: 2>1.1 200-500, 700, 900 mg L^{-1}: 2>1.1
22	100, 300, mg L^{-1}: 4>1.1 200 mg L^{-1}: 2>1.1 400 mg L^{-1}: 3>1.1
23	100-500, 800-1000 mg L^{-1}: 4>1.1 600 mg L^{-1}: 2>1.1 700 mg L^{-1}: 3>1.1
24	200 mg L^{-1}: 3>1.1
25	200, 500, 700, 900, 1000 mg L^{-1}: 3>1.1 400 mg L^{-1}: 1>1.1 600 mg L^{-1}: 4>1.1 800 mg L^{-1}: 2>1.1

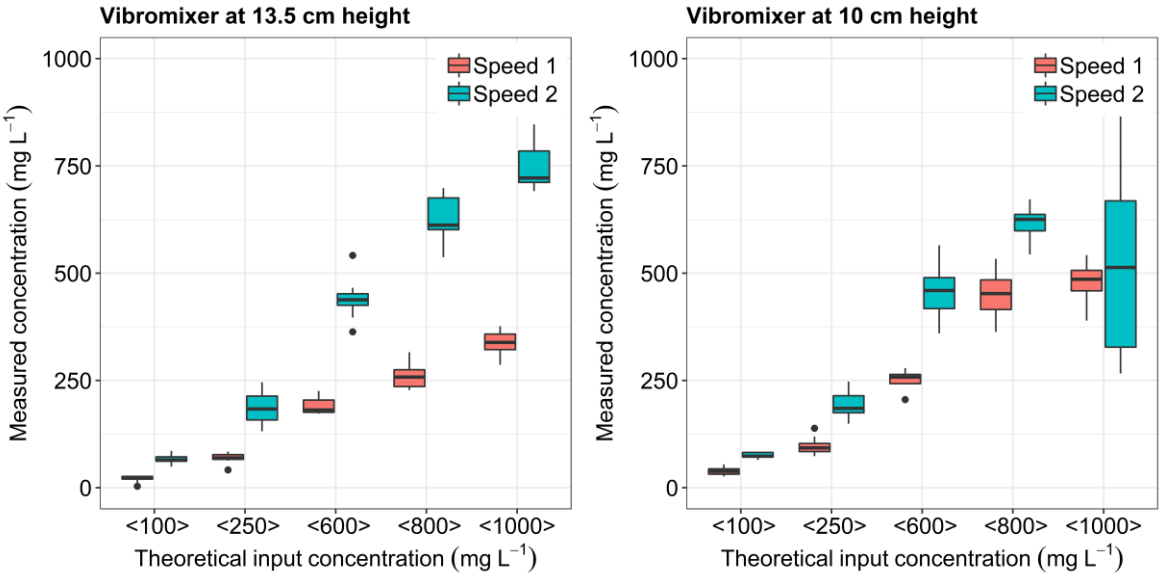

Figure A.1 Speed 1 and Speed 2 comparison (vibromixer) to decide which speed best mixes soil material introduced into the experimental tank. Lower speeds were not considered due to clear visible deposition of soil material. Tests were executed with <63 µm material (not used in the experiments described here).

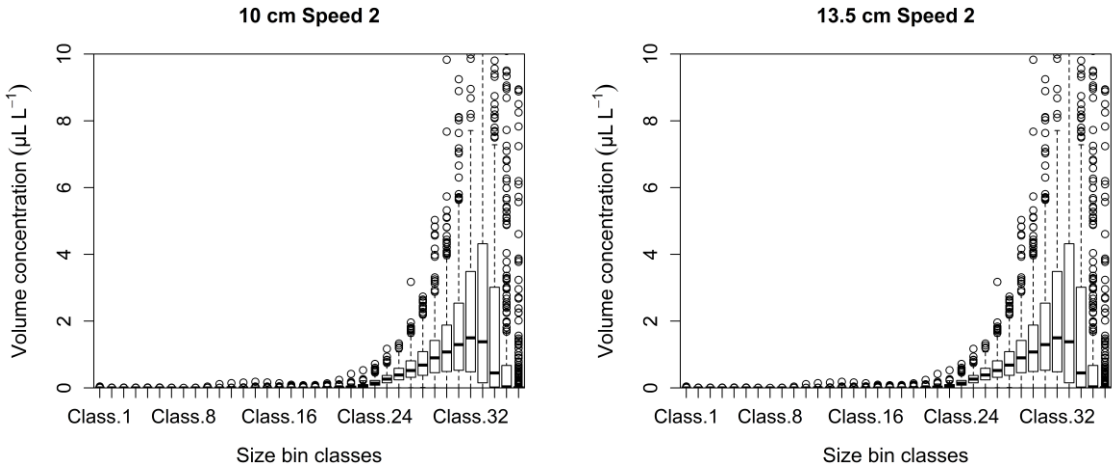

Figure A.2 Bubble influences from the vibromixer at speed 2. Based on less bubbles and therefore less influence on the LISST measurements (left), the 10 cm height for installing the virbomixer plate was selected in these experiments given the more severe bubble problem observed at the 13.5 cm height (right).

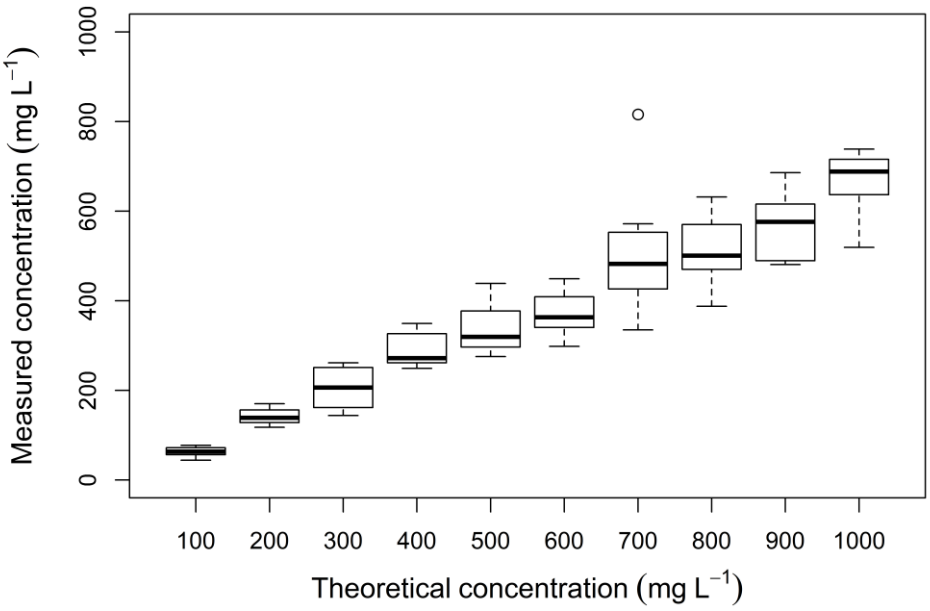

Figure A.3 Homogeneity of concentration. Results show the variability of measured concentrations at 10 different position inside the experimental tank set-up (3 heights at 3 locations, additional sample 5 cm above the bottom). Test here used soil sample #2.3 (soil 2, 63-125 µm).

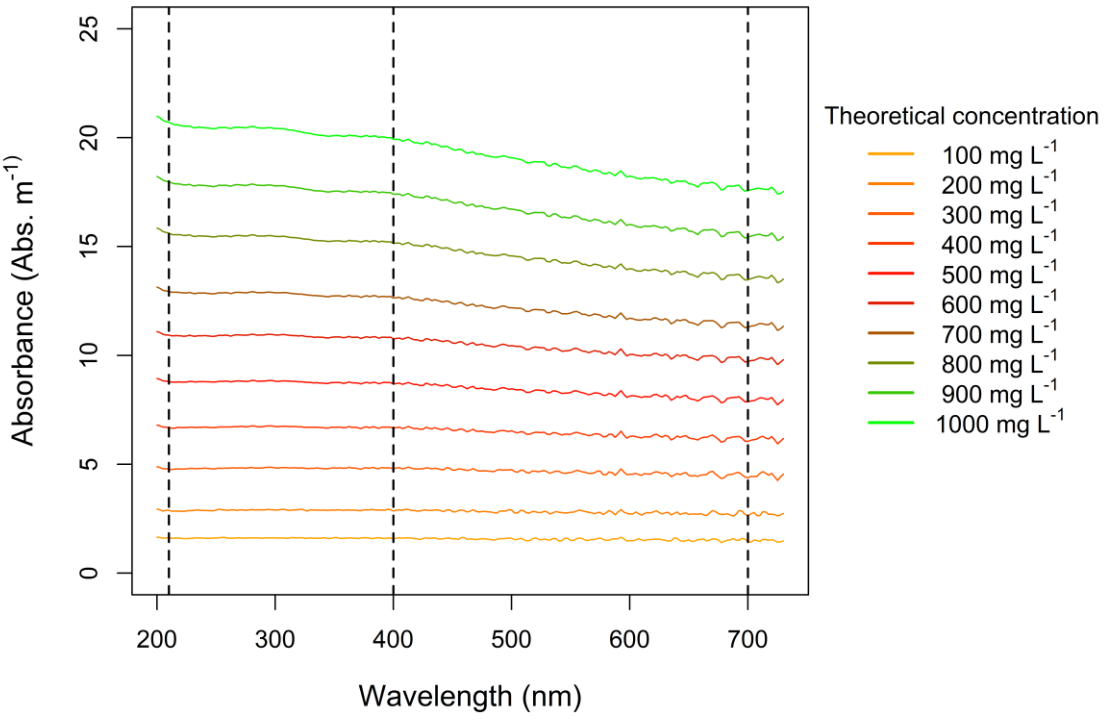

Figure A.4 Absorbance response over the whole range of measured wavelengths (200-730 nm) for soil sample #2.3 (soil 2, 63-125 µm) at the ten different (theoretical) concentrations, compensated for background absorbance (demineralised water; 0 mg L^{-1}). Dashed lines indicate those wavelengths, beside the average over all wavelengths, that are used for analysis

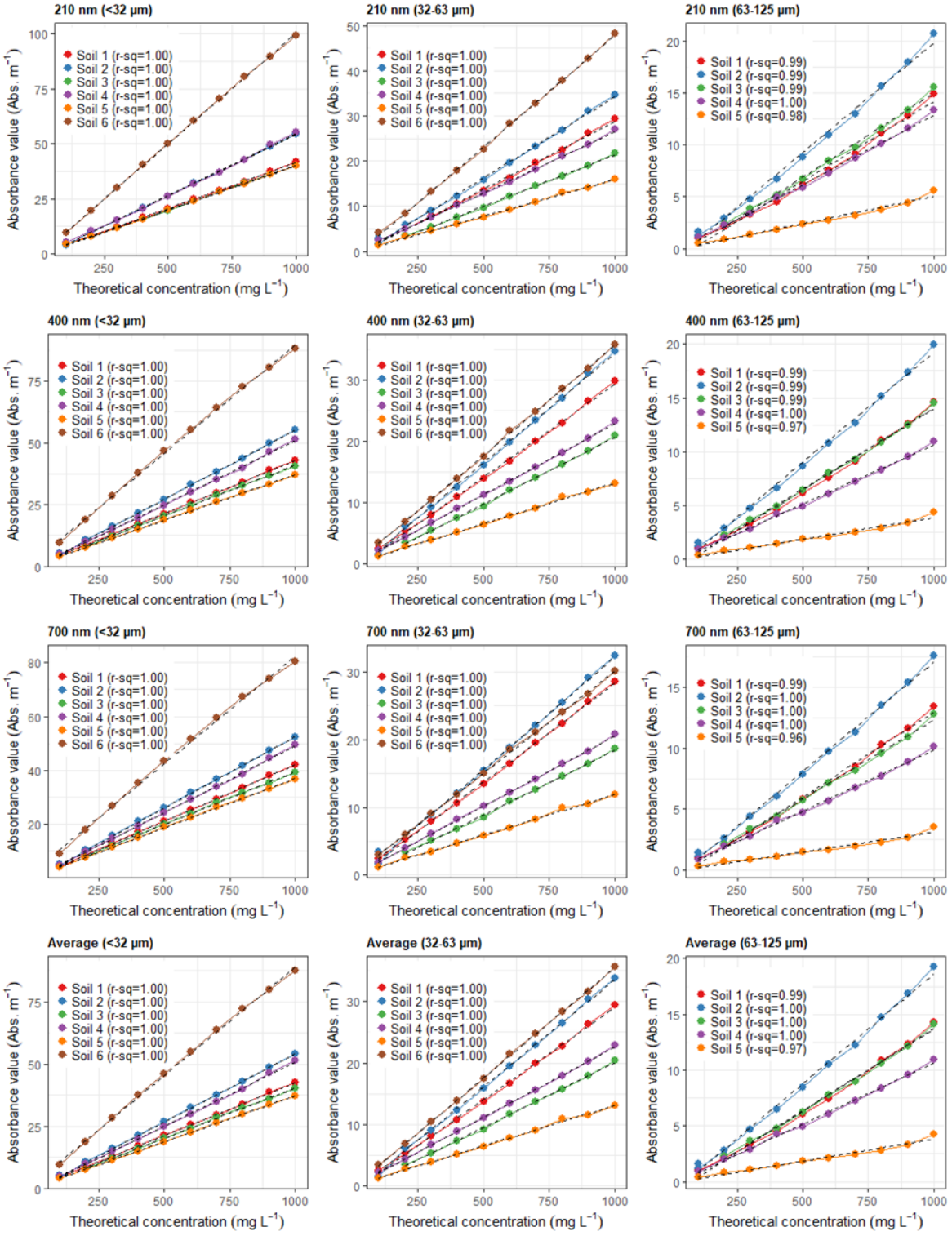

Figure A.5 Absorbance values plotted against theoretical concentrations, for particle sizes <32 µm (left), 32-63 µm (middle) and 63-125 µm (right). Dotted lines show the linear regression, with the corresponding r^2 values (r-sq) shown in the legend.

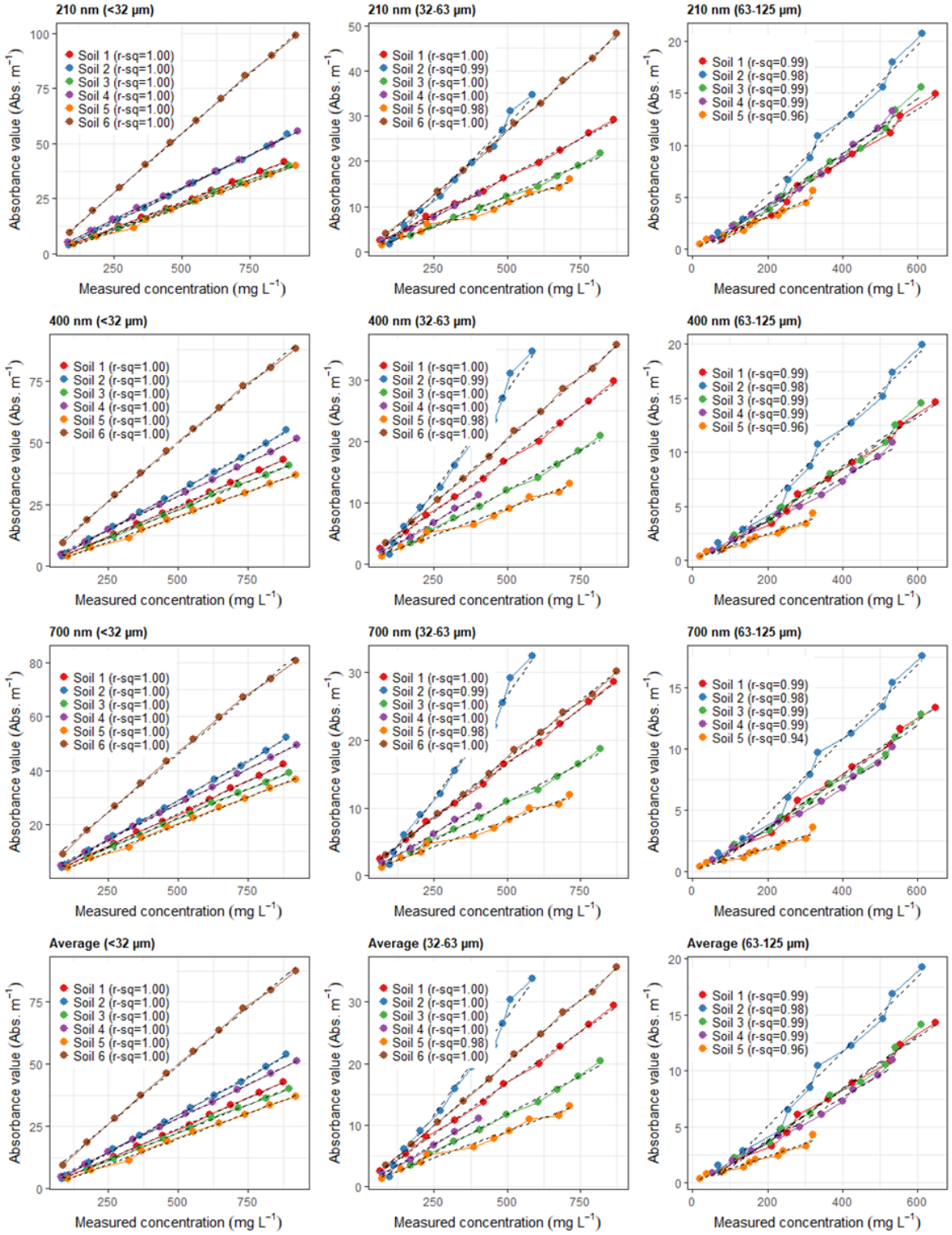

Figure A.6 Absorbance values plotted against measured concentrations, for particle sizes <32 µm (left), 32-63 µm (middle) and 63-125 µm (right). Dotted lines show the linear regression, with the corresponding r^2 values (r-sq) shown in the legend.

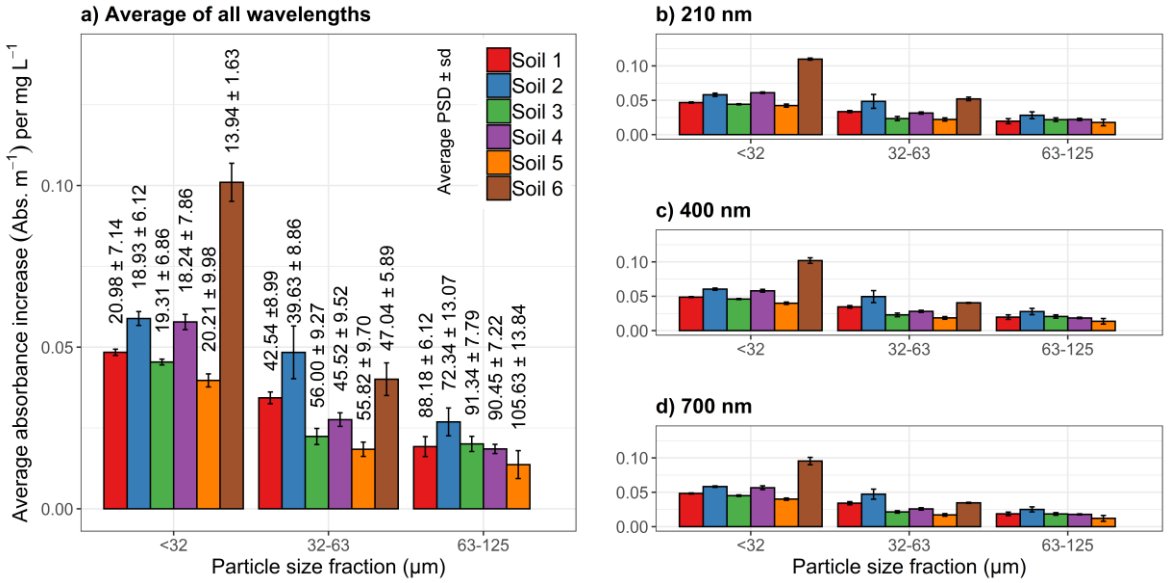

Figure A.7 Average increases in absorbance per mg L^{-1} (absorbance values divided by measured concentrations) for average absorbance over (a) all wavelengths, (b) 210 nm, (c) 400 nm, and (d) 700 nm, for all 17 soil samples (indicated by #soil.fraction, with 'soil' representing the test soils (n=6), and 'fraction' the sieved fraction size (.1 for <32 µm; .2 for 32-63 µm; .3 for 63-125 µm). Values inside the plot refer to the average (PSD) and standard deviation (SD) of measured particle size distributions per sample and dry sieved fraction measured with the LISST sensor inside the experimental tank.

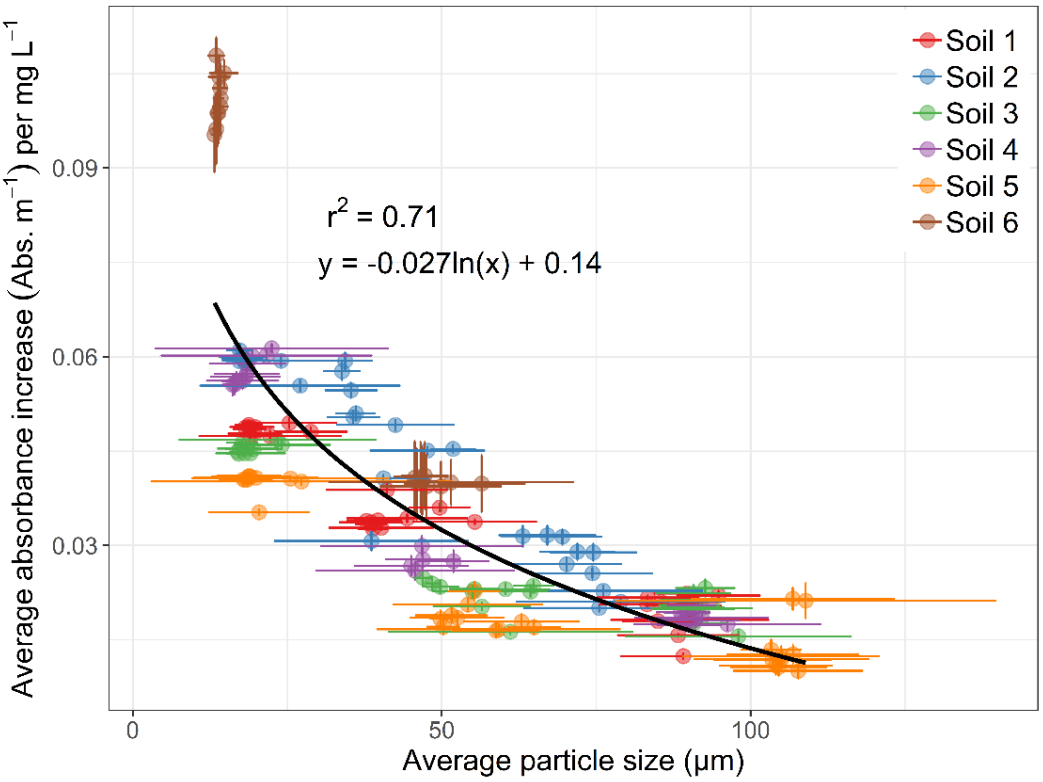

Figure A.8 Relationship between average increases in absorbance per mg L^{-1} (absorbance values divided by measured concentrations) as a function of average particle size measured with the LISST sensor inside the experimental tank. Particle size values and corresponding standard deviations were calculated for every sample and for every concentration separately.

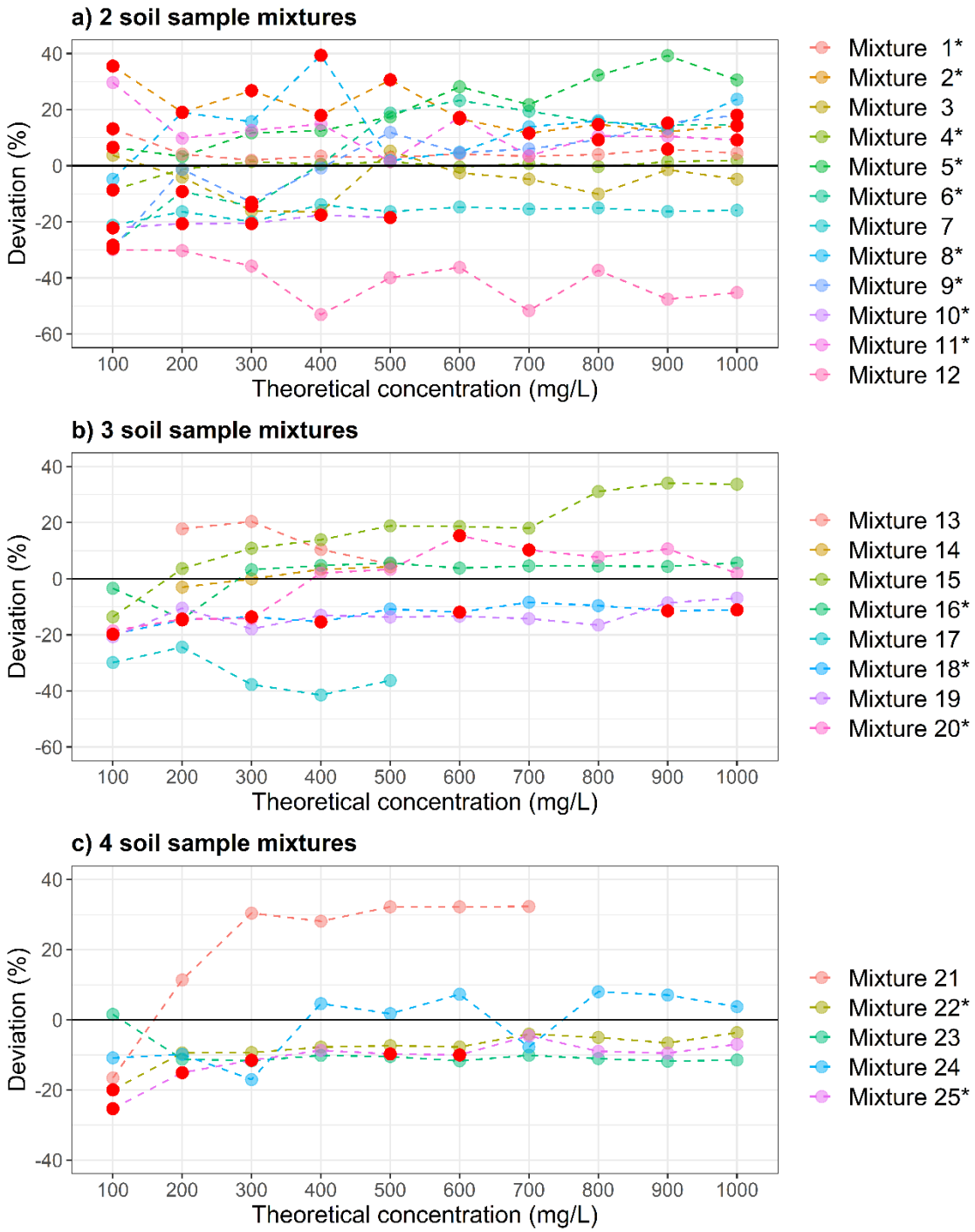

Figure A.9 Un-mixing of artificial mixtures; deviations between measured absorbance and 'expected' absorbance based on a single soil sample absorbance signal (mass-balance), shown for 2 (a), 3 (b) and 4 (c) soil sample mixtures. Red dots (a, b and c) indicate those situations in which absorbance values from the artificial mixtures are larger or smaller than the absorbance values measured for both individual soil samples comprising that mixture (concerned mixtures are indicated by * in the legend).

Appendix B Supplementary Information to Chapter 3

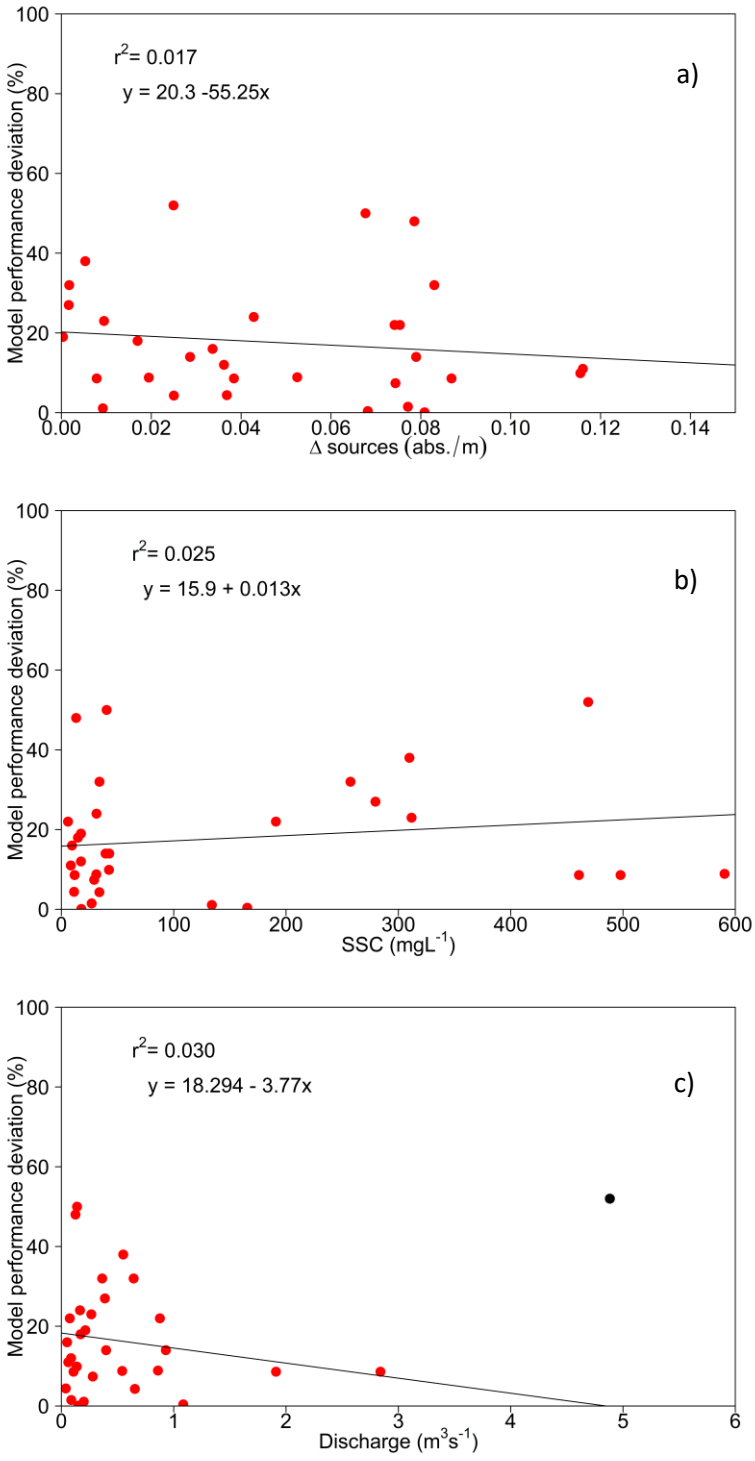

Figure B.1 Relationships between model performance deviation (being the difference between the modelling outcomes and the sediment budget) and: difference in source absorbance (a), suspended sediment concentration (SSC) (b), discharge (c) with outlier highlighted in black not used in relation.

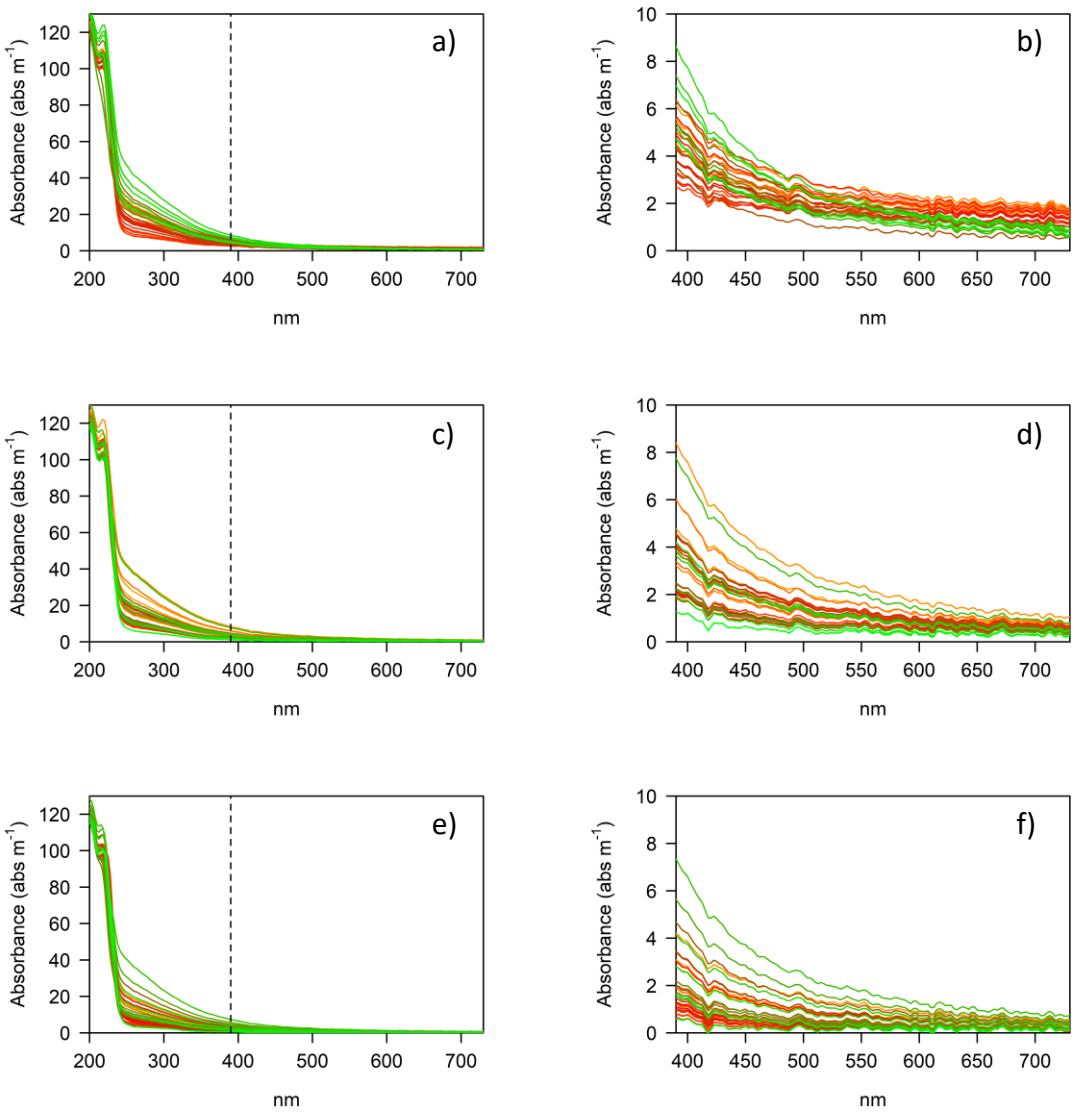

Figure B.2 Overview of absorbance spectra of the filtered water samples per campaign. Spectra are shown over the whole range of measured wavelengths (200-730 nm): campaign 1 (a), campaign 2 (c), campaign 3 (e). Details on the spectra beyond 390 nm (indicated by the dotted lines in a, c and e), are shown for campaign 1 (b), campaign 2 (d), campaign 3 (f).

Table B.1 Drainage area for each sampling site.

Sampling site	Drainage area each sampling site (km^2)
1	44.0
2	37.6
3	10.9
4	8.3
5	7.5
6	0.2
7	6.7
8	3.4
9	2.9
10	0.8
11	0.9
12	2.0
13	1.5
14	1.5
15	16.1
16	22.5
17	6.3
18	4.9
19	2.7
20	2.2
21	1.5
22	14.8
23	8.3
24	6.5
25	4.2
26	2.2
27	2.0
28	6.6
29	1.9
30	4.7
31	25.5
32	1.1
33	0.5

Table B.2 Predicted suspended sediment modelled contributions (%) for each confluence (outcomes MixSIAR model), with modelled standard deviations (%). Sediment load (%) represents the outcomes from the sediment budget calculations.

Confluence	Campaign	Source sampling site	Modelled contribution (%)	Modelled standard deviation (%)	Sediment load (%)
A	1	31	55.7	0.7	60
		3	44.3	0.7	40
	2	31	33	1.3	85
		3	67	1.3	15
	3	31	86.5	0.3	74
		3	13.5	0.3	26
B	1	5	99.1	0.9	99
		6	0.9	0.9	1
	2	5	99.4	0.6	99
		6	0.6	0.6	1
	3	5	79.6	1.9	99
		6	20.4	1.9	1
C	1	8	99.9	0.1	90
		9	0.1	0.1	10
	2	8	26.8	0.5	5
		9	73.2	0.5	95
	3	8	99.4	0.6	83
		9	0.6	0.6	17
D	1	13	60	0.3	70
		14	40	0.3	30
	2	13	29.5	4.2	56
		14	70.5	4.2	44
	3	13	76.4	0.3	55
		14	23.6	0.3	45
E	1	10	NaN	NaN	-
		11	NaN	NaN	-
	2	10	89.7	3	67
		11	10.3	3	33
	3	10	52.8	0.9	68
		11	47.2	0.9	32
F	1	15	63.8	1.7	78
		17	36.2	1.7	22
	2	15	70.4	0.7	79
		17	29.6	0.7	21
	3	15	99.8	0.2	91
		17	0.2	0.2	9

Confluence	Campaign	Source sampling site	Modelled contribution (%)	Modelled standard deviation (%)	Sediment load (%)
G	1	19	27.5	0.8	40
		20	72.5	0.8	60
	2	19	98.1	1.7	67
		20	1.9	1.7	33
	3	19	19.2	1.7	66
		20	80.8	1.7	34
H	1	32	NaN	NaN	-
		33	NaN	NaN	-
	2	32	75.1	0.3	75
		33	24.9	0.3	25
	3	32	89.6	2	94
		33	10.4	2	6
I	1	23	70.6	0.6	76
		24	29.4	0.6	24
	2	23	66.6	0.2	58
		24	33.4	0.2	42
	3	23	99.9	0.1	68
		24	0.1	0.1	32
J	1	26	58.5	1.6	60
		27	41.5	1.6	40
	2	26	98.3	1.5	60
		27	1.7	1.5	40
	3	26	42.4	0.9	50
		27	57.6	0.9	50
K	1	29	86.1	1	36
		30	13.9	1	64
	2	29	0.1	0.1	9
		30	99.9	0.1	91
	3	29	66.7	0.3	43
		30	33.3	0.3	57

Table B.3 Percentage of different land uses for each SS source stream site, shown per confluence. Data used was made available by the 'Administration du Cadastre et de la Topographie' (ACT), (Corine Land Cover 2018).

Confluence A	Site 3	Site 31
Land use	Contribution (%)	Contribution (%)
Forest	34	44
Cultivated	45	47
Pasture	20	6
Build	0	2
Sand mining	0	1
Confluence C	Site 8	Site 9
Land use	Contribution (%)	Contribution (%)
Forest	22	39
Cultivated	70	43
Pasture	8	18
Build	0	0
Sand mining	0	0
Confluence E	Site 10	Site 11
Land use	Contribution (%)	Contribution (%)
Forest	12	32
Cultivated	79	64
Pasture	9	4
Build	0	0
Sand mining	0	0
Confluence G	Site 19	Site 20
Land use	Contribution (%)	Contribution (%)
Forest	35	56
Cultivated	55	44
Pasture	10	0
Build	0	0
Sand mining	0	0
Confluence I	Site 23	Site 24
Land use	Contribution (%)	Contribution (%)
Forest	38	37
Cultivated	47	57
Pasture	12	2
Build	3	4
Sand mining	0	0
Confluence K	Site 29	Site 30
Land use	Contribution (%)	Contribution (%)
Forest	50	24
Cultivated	45	52
Pasture	5	18
Build	0	5
Sand mining	0	0

Confluence B	Site 5	Site 6
Land use	Contribution (%)	Contribution (%)
Forest	30	66
Cultivated	49	7
Pasture	21	27
Build	0	0
Sand mining	0	0
Confluence D	Site 13	Site 14
Land use	Contribution (%)	Contribution (%)
Forest	22	23
Cultivated	77	71
Pasture	1	6
Build	0	0
Sand mining	0	0
Confluence F	Site 15	Site 17
Land use	Contribution (%)	Contribution (%)
Forest	38	53
Cultivated	51	40
Pasture	7	4
Build	3	0
Sand mining	1	3
Confluence H	Site 32	Site 33
Land use	Contribution (%)	Contribution (%)
Forest	23	21
Cultivated	77	79
Pasture	0	0
Build	0	0
Sand mining	0	0
Confluence J	Site 26	Site 27
Land use	Contribution (%)	Contribution (%)
Forest	29	48
Cultivated	61	45
Pasture	0	0
Build	10	2
Sand mining	0	0

Appendix B

Table B.4 Percentage of different lithologies for each SS source stream site, shown per confluence. Data used was made available by the 'Service Géologique du Luxembourg.'

Confluence A	Site 3	Site 31
Lithology	Contribution (%)	Contribution (%)
Marls	16	26
Schists	35	49
Buntsandstein	44	23
Alluvials	5	1
Confluence C	Site 8	Site 9
Lithology	Contribution (%)	Contribution (%)
Marls	0	0
Schists	57	57
Buntsandstein	39	41
Alluvials	5	2
Confluence E	Site 10	Site 11
Lithology	Contribution (%)	Contribution (%)
Marls	0	0
Schists	76	87
Buntsandstein	24	13
Alluvials	0	0
Confluence G	Site 19	Site 20
Lithology	Contribution (%)	Contribution (%)
Marls	0	0
Schists	85	89
Buntsandstein	15	11
Alluvials	0	0
Confluence I	Site 23	Site 24
Lithology	Contribution (%)	Contribution (%)
Marls	60	63
Schists	38	0
Buntsandstein	2	37
Alluvials	0	0
Confluence K	Site 29	Site 30
Lithology	Contribution (%)	Contribution (%)
Marls	77	42
Schists	23	58
Buntsandstein	0	0
Alluvials	0	0

Confluence B	Site 5	Site 6
Lithology	Contribution (%)	Contribution (%)
Marls	0	0
Schists	50	0
Buntsandstein	45	99
Alluvials	5	1
Confluence D	Site 13	Site 14
Lithology	Contribution (%)	Contribution (%)
Marls	0	0
Schists	56	64
Buntsandstein	43	32
Alluvials	1	3
Confluence F	Site 15	Site 17
Lithology	Contribution (%)	Contribution (%)
Marls	42	0
Schists	46	73
Buntsandstein	12	27
Alluvials	1	0
Confluence H	Site 32	Site 33
Lithology	Contribution (%)	Contribution (%)
Marls	0	0
Schists	100	100
Buntsandstein	0	0
Alluvials	0	0
Confluence J	Site 26	Site 27
Lithology	Contribution (%)	Contribution (%)
Marls	0	0
Schists	96	94
Buntsandstein	4	6
Alluvials	0	0

Appendix C Supplementary Information to Chapter 4

Table C.1 Coordinates of and baseline information for soil sampling sites. Geology data retrieved from 'Service Géologique du Luxembourg.'

Soil	Latitude	Longitude	Land use	Geology
1	49.497028	6.005050	Forest	Oolitic iron stone (Minette)
2	49.483854	6.054251	Agriculture (cropland)	Marls, argillites and iron ore
3	49.456871	5.990764	Forest	Marls and limestone
4	49.746973	5.870103	Forest	Marls and sandstone
5	49.715606	5.90043	Forest	Calcereous sandstone (Luxembourg sandstone)
6	49.835121	5.799219	Forest	Schists, and siliceous sandstones

Table C.2 Mixtures with component soil samples and their known relative contributions. Soil samples are indicated by #soil.fraction, representing the (original) collected soil (n=6), and fraction representing the sieved particle size (.1 for <32 µm, .2 for 32-63 µm and .3 for 63-125 µm).

	Mixture No.	Soil sample (%)	Soil sample (%)	Soil sample (%)	Soil sample (%)
Mixtures of samples sieved to different size fractions:					
2 soil samples	1	#3.1 (80%)	#4.2 (20%)	-	-
	2	#1.2 (80%)	#2.3 (20%)	-	-
	3	#1.1 (30%)	#5.3 (70%)	-	-
3 soil samples	4	#4.2 (10%)	#5.3 (80%)	#6.1 (10%)	-
	5	#1.2 (20%)	#3.1 (70%)	#4.3 (10%)	-
	6	#1.1 (30%)	#3.3 (50%)	#5.3 (20%)	-
	7	#2.3 (80%)	#3.1 (10%)	#6.2 (10%)	-
4 soil samples	8	#1.1 (10%)	#2.3 (70%)	#3.1 (10%)	#6.2 (10%)
	9	#1.1 (10%)	#2.3 (10%)	#3.1 (70%)	#6.2 (10%)
Mixtures of samples sieved to the same size fraction:					
2 soil samples	10	#1.1 (80%)	#2.1 (20%)	-	-
	11	#1.2 (80%)	#2.2 (20%)	-	-
	12	#1.3 (80%)	#2.3 (20%)	-	-
	13	#1.1 (20%)	#2.1 (80%)	-	-
	14	#1.2 (20%)	#2.2 (80%)	-	-
	15	#1.3 (20%)	#2.3 (80%)	-	-
	16	#5.2 (80%)	#6.2 (20%)	-	-
	17	#5.1 (50%)	#6.1 (50%)	-	-
	18	#1.3 (60%)	#4.3 (40%)	-	-
3 soil samples	19	#1.2 (70%)	#3.2 (20%)	#4.2 (10%)	-
	20	#1.2 (20%)	#3.2 (10%)	#4.2 (70%)	-
	21	#2.2 (60%)	#3.2 (20%)	#6.2 (20%)	-
	22	#1.1 (10%)	#2.1 (80%)	#5.1 (10%)	-
4 soil samples	23	#2.2 (70%)	#3.2 (10%)	#5.2 (10%)	#6.2 (10%)
	24	#1.1 (10%)	#2.1 (10%)	#3.1 (70%)	#5.1 (10%)
	25	#3.1 (25%)	#4.1 (25%)	#5.1 (25%)	#6.1 (25%)

Table C.3 Upper part: concentrations measured in the tank set-up, presented as a percentage of theoretical (target) concentrations. Lower part: input concentrations, based on theoretical input concentrations, and adapted input concentrations (bold), based on measured concentrations.

Soil sample	Concentration measured in tank set-up (in %) compared with input (theoretical) concentrations		Soil sample	Concentration measured in tank set-up (in %) compared with input (theoretical) concentrations	
#1.1	88.4		#4.1	86.7	
#1.2	80.8		#4.2	80.1	
#2.3	63.9		#4.3	55.0	
#2.1	90.2		#4.1	94.9	
#2.2	64.2		#4.2	70.9	
#2.3	64.1		#4.3	28.7	
#3.1	88.9		#5.1	90.8	
#3.2	84.0		#6.2	87.6	
#3.3	63.2		#6.3	-	
	Mixture No.	Soil sample (%)	Soil sample (%)	Soil sample (%)	Soil sample (%)
Mixtures of samples sieved to different size fractions:					
2 soil samples	1	#3.1 (80) **(81.6)**	#4.2 (20) **(18.4)**	-	-
	2	#1.2 (80) **(83.4)**	#2.3 (20) **(16.6)**	-	-
	3	#1.1 (30) **(56.9)**	#5.3 (70) **(43.1)**	-	-
3 soil samples	4	#4.2 (10) **(20.0)**	#5.3 (80) **(57.3)**	#6.1 (10) **(22.7)**	-
	5	#1.2 (20) **(19.3)**	#3.1 (70) **(74.2)**	#4.3 (10) **(6.6)**	-
	6	#1.1 (30) **(41.5)**	#3.3 (50) **(49.5)**	#5.3 (20) **(9.0)**	-
	7	#2.3 (80) **(74.4)**	#3.1 (10) **(12.9)**	#6.2 (10) **(12.7)**	-
4 soil samples	8	#1.1 (10) **(12.4)**	#2.3 (70) **(62.9)**	#3.1 (10) **(12.5)**	#6.2 (10) **(12.3)**
	9	#1.1 (10) **(10.3)**	#2.3 (10) **(7.4)**	#3.1 (70) **(72.2)**	#6.2 (10) **(10.2)**

Appendix C

Table C.4 Modelled contributions and standard deviations (AnalySize), for the artificial mixtures using soil samples sieved to different fractions.

	Mixture No.	Soil sample (%)	Soil sample (%)	Soil sample (%)	Soil sample (%)
2 soil samples	1	#3.1 (76.7 ± 3.8)	#4.2 (23.3 ± 3.8)	-	-
	2	#1.2 (76.3 ± 34.3)	#2.3 (23.7 ± 34.3)	-	-
	3	#1.1 (70.7 ± 7.9)	#5.3 (29.3 ± 7.9)	-	-
3 soil samples	4	#4.2 (29.5 ± 6.4)	#5.3 (43.9 ± 11.5)	#6.1 (26.6 ± 10.5)	-
	5	#1.2 (31.2 ± 6.7)	#3.1 (67.1 ± 6.9)	#4.3 (1.8 ± 2.3)	-
	6	#1.1 (45.5 ± 7.4)	#3.3 (54.3 ± 7.4)	#5.3 (0.1 ± 1.2)	-
	7	#2.3 (85.3 ± 8.9)	#3.1 (5.5±4.0)	#6.2 (9.1 ± 8.8)	-
4 soil samples	8	#1.1 (1.9 ± 3.1)	#2.3 (72.6 ± 14.6)	#3.1 (11.2 ± 8.5)	#6.2 (14.2 ± 9.3)
	9	#1.1 (0.0 ± 0.4)	#2.3 (5.7 ± 7.1)	#3.1 (81.0 ± 11.8)	#6.2 (13.3 ± 9.9)

Table C.5 Differences between the average modelled and compensated known soil sample contributions.

	Mixture No.	Soil sample (difference)	Soil sample (difference)	Soil sample (difference)	Soil sample (difference)
2 soil samples	1	#3.1 (4.9%)	#4.2 (4.9%)	-	-
	2	#1.2 (7.1%)	#2.3 (7.1%)	-	-
	3	#1.1 (13.8%)	#5.3 (13.8%)	-	-
3 soil samples	4	#4.2 (9.5%)	#5.3 (13.4%)	#6.1 (3.9%)	-
	5	#1.2 (11.9%)	#3.1 (7.1%)	#4.3 (4.8%)	-
	6	#1.1 (4.0%)	#3.3 (4.8%)	#5.3 (8.9%)	-
	7	#2.3 (10.9%)	#3.1 (7.4%)	#6.2 (3.6%)	-
4 soil samples	8	#1.1 (10.5%)	#2.3 (9.7%)	#3.1 (1.3%)	#6.2 (1.9%)
	9	#1.1 (10.3%)	#2.3 (1.7%)	#3.1 (8.8%)	#6.2 (3.1%)

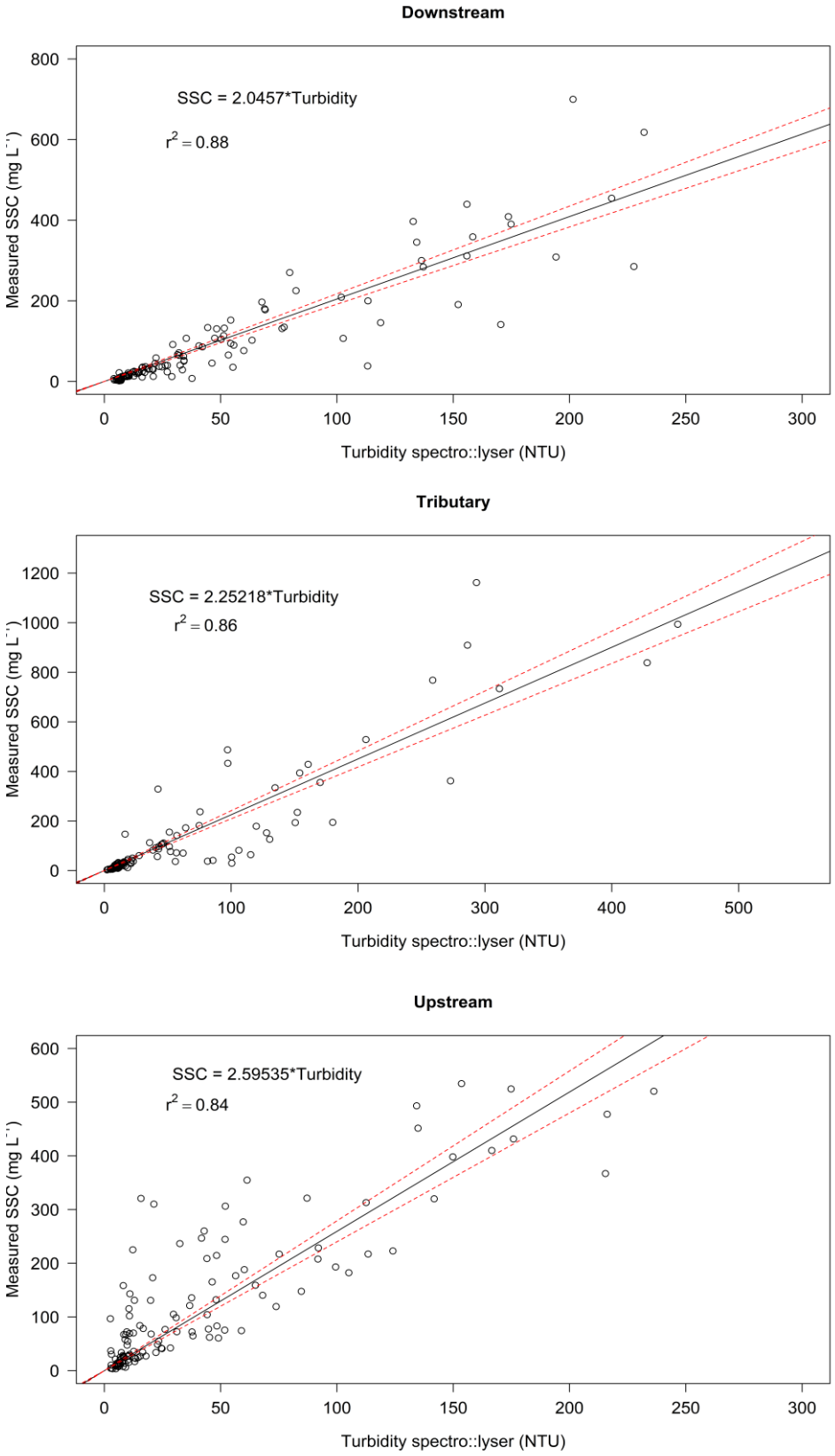

Figure C.1 Calibration relationships between turbidity (measured from spectro::lyser) and measured SSC for the Upstream, Tributary and Downstream measurement sites. Red dashed lines represent the 95% confidence intervals.

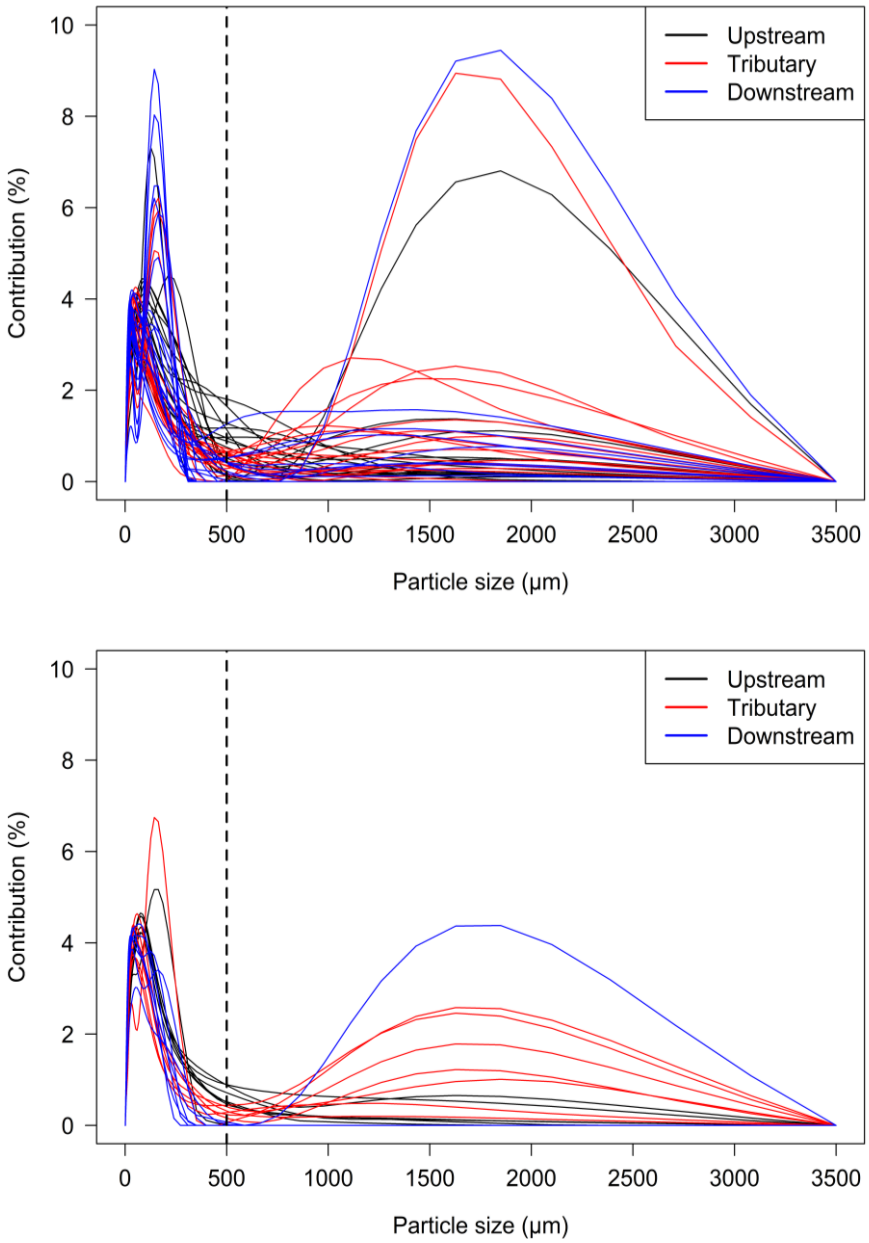

Figure C.2 Overview for decision selecting the upper particle size boundary using the Mastersizer data. Top: Period C, below: period E. Distribution shown after applying Ultrasound (US), with the vertical dotted line showing the particle size distribution patterns at 500 µm. This limit was selected as the upper size limit to exclude the influence of unknown peaks observed above this size. Second peaks observed at the higher particle sizes (>500 µm) were often only observed after applying ultrasounds.

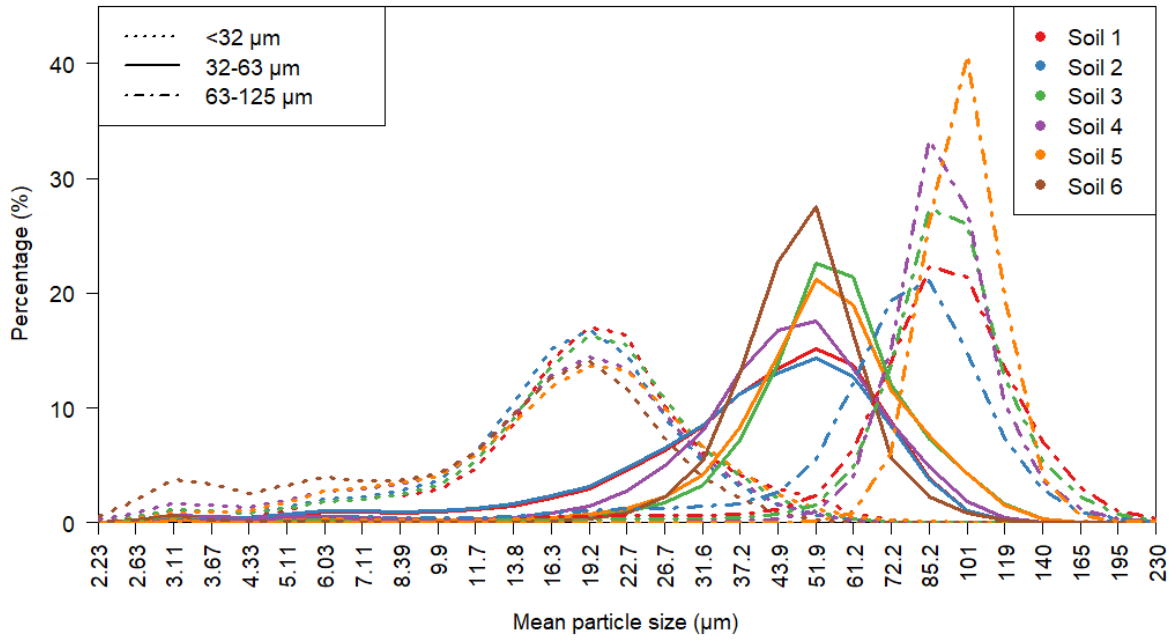

Figure C.3 Average particle size distributions of the 17 soil samples, plotted against the mean particle size (µm) for the 36 classes. Distributions of the different soil samples are shown according to test soil (indicated by colour; top right) and the fraction the soil sample was sieved to (indicated by line type; top left).

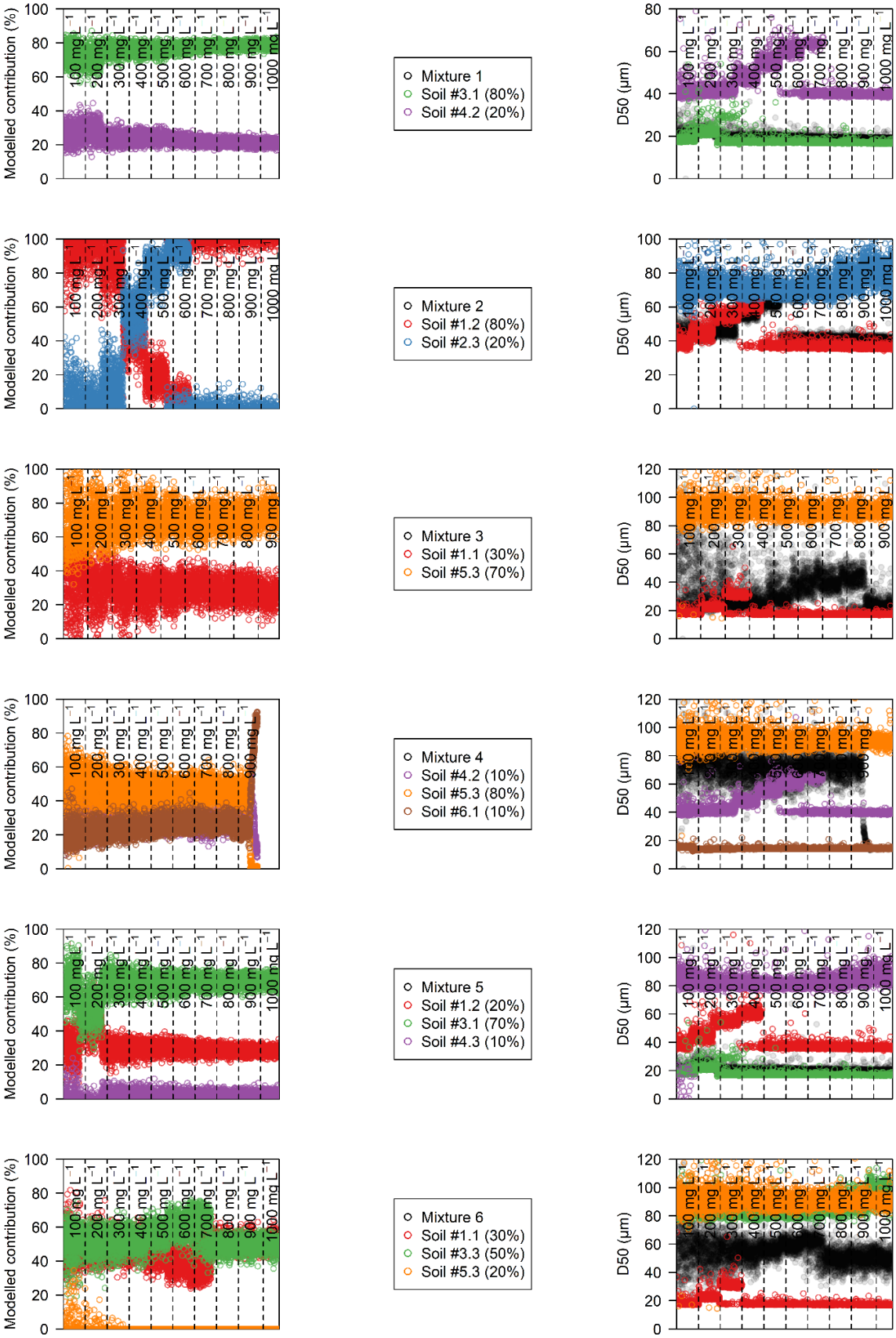
Modelled contribution (%)
D50 (µm)
100 mg L⁻¹
200 mg L⁻¹
300 mg L⁻¹
400 mg L⁻¹
500 mg L⁻¹
600 mg L⁻¹
700 mg L⁻¹
800 mg L⁻¹
900 mg L⁻¹
1000 mg L⁻¹
Mixture 1
Soil #3.1 (80%)
Soil #4.2 (20%)
Mixture 2
Soil #1.2 (80%)
Soil #2.3 (20%)
Mixture 3
Soil #1.1 (30%)
Soil #5.3 (70%)
Mixture 4
Soil #4.2 (10%)
Soil #5.3 (80%)
Soil #6.1 (10%)
Mixture 5
Soil #1.2 (20%)
Soil #3.1 (70%)
Soil #4.3 (10%)
Mixture 6
Soil #1.1 (30%)
Soil #3.3 (50%)
Soil #5.3 (20%)

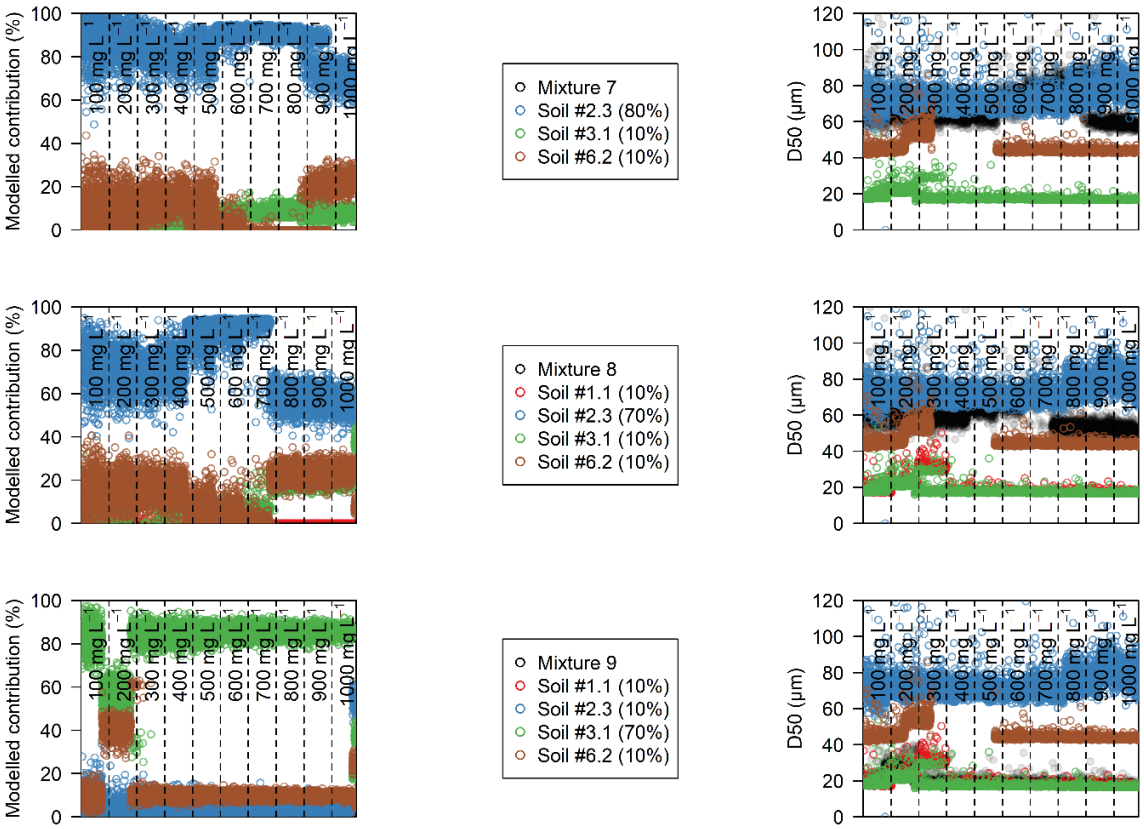

Figure C.4 Patterns of D_{50} values and modelled contribution percentages for the different theoretical input concentrations, for those mixtures consisting of soil samples sieved to different fractions (mixtures 1 to 9; top to bottom). In brackets after each soil sample is the theoretical input contribution shown.

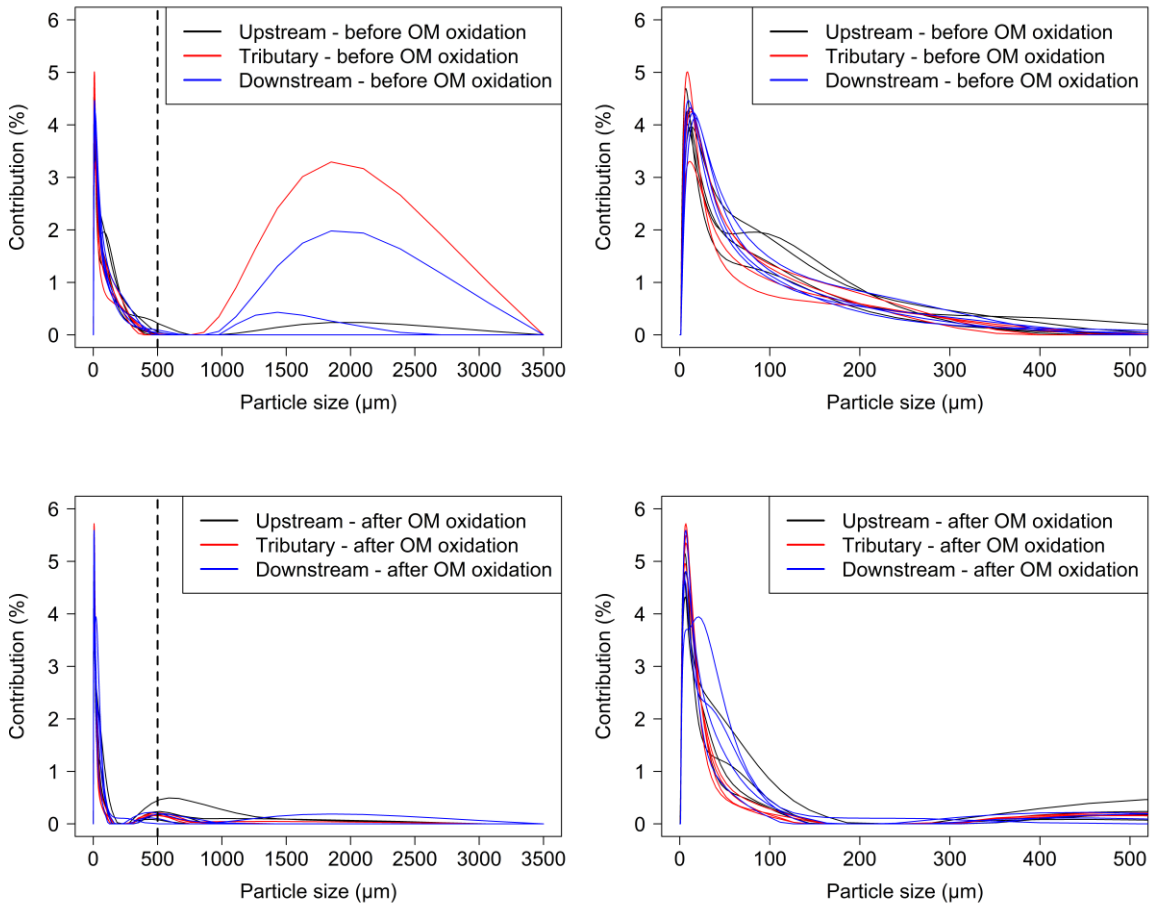

Figure C.5 Particle size distributions for a selection of samples from Period F, with and without Organic Matter (OM) oxidation. Left figures: PSD before and after OM oxidation shown for all particle size classes (0-3500 µm). Right figures: same PSD shown for maximum particle size classes of 500 µm.

Table C.6 Un-mixing results from AnalySize before and after oxidation (using H_2O_2) of organic matter. Comparisons only showed a clear difference for one out of four instances (sample collected 04/06/2021 at 22:30). Here, the average contribution for the Upstream site decreased from 80% (before oxidation) to 43% (after oxidation). Results for period F showed that the modelled contributions without Organic Matter (OM) oxidation were more consistent with the sediment budget calculations (Figure 4.5).

Timing	Upstream (% ± st.deviation) **Before oxidation**	Tributary (% ± st.deviation) **Before oxidation**		Upstream (% ± st.deviation) **After oxidation**	Tributary (% ± st.deviation) **After oxidation**
04/06/2021 21:00	99.56 ± 0.92	0.44 ± 0.92		100.00 ± 0	0.00 ± 0
04/06/2021 22:30	79.69 ± 6.47	20.31 ± 6.47		42.51 ± 0.94	57.49 ± 0.94
05/06/2021 00:00	16.25 ± 0.77	83.75 ± 0.77		0.72 ± 1.47	99.28 ± 1.47
05/06/2021 01:30	0.00 ± 0	100.00 ± 0		8.55 ± 0.93	91.45 ± 0.93

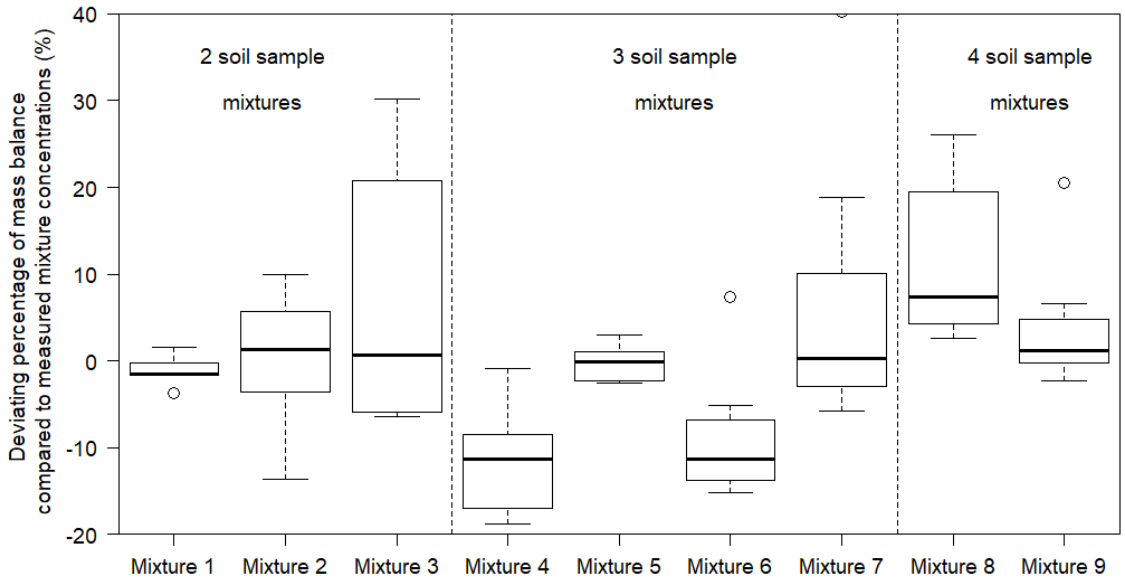

Figure C.6 Percentage deviations of mass-balance (estimation for mixture concentrations based on measured concentrations from individual soil sample tests, relative to their input contribution) against measured mixture concentrations. Positive values here indicate a higher expected mixture concentration (mass-balance) compared to the real measured mixture concentration. Data shown are median values, 25th and 75th percentiles (boxes) and 5th and 95th percentiles (whiskers).

List of References

Abedini, M., Md Said, M.A., Ahmad, F., 2012. Effectiveness of check dam to control soil erosion in a tropical catchment (The Ulu Kinta Basin). Catena 97, 63–70. https://doi.org/10.1016/j.catena.2012.05.003

Acornley, R.M., Sear, D.A., 1999. Sediment transport and siltation of brown trout (Salmo trutta L.) spawning gravels in chalk streams. Hydrological Processes 13 (3), 447–458. https://doi.org/10.1002/(SICI)1099-1085(19990228)13:3<447::AID-HYP749>3.0.CO;2-G

Affandi, F.A., Ishak, M.Y., 2019. Impacts of suspended sediment and metal pollution from mining activities on riverine fish population—a review. Environmental Science and Pollution Research 26 (17), 16939–16951. https://doi.org/10.1007/s11356-019-05137-7

Agrawal, Y.C., Pottsmith, H.C., 2000. Instruments for particle size and settling velocity observations in sediment transport. Marine Geology 168 (1–4), 89–114. https://doi.org/10.1016/S0025-3227(00)00044-X

Agrawal, Y.C., Whitmire, A., Mikkelsen, O.A., Pottsmith, H.C., 2008. Light scattering by random shaped particles and consequences on measuring suspended sediments by laser diffraction. Journal of Geophysical Research: Oceans 113 (4), 1–11. https://doi.org/10.1029/2007JC004403

Allan, R.J., 1986. The role of particulate matter in the fate of contaminants in aquatic ecosystems. Inland Waters Directorate, Environment Canada Scientific Series No. 142, Burlington, Ontario, Canada 128 pp.

Amundson, R., Berhe, A.A., Hopmans, J.W., Olson, C., Sztein, A.E., Sparks, D.L., 2015. Soil and human security in the 21st century. Science 348 (6235). https://doi.org/10.1126/science.1261071

Baartman, J.E.M., Masselink, R., Keesstra, S.D., Temme, A.J.A.M., 2013a. Linking landscape morphological complexity and sediment connectivity. Earth Surface Processes and Landforms 38 (12), 1457–1471. https://doi.org/10.1002/esp.3434

Baartman, J.E.M., Temme, A.J.A.M., Veldkamp, T., Jetten, V.G., Schoorl, J.M., 2013b. Exploring the role of rainfall variability and extreme events in long-term landscape development. Catena 109, 25–38. https://doi.org/10.1016/j.catena.2013.05.003

Baartman, J.E.M., Van Gorp, W., Temme, A.J.A.M., Schoorl, J.M., 2012. Modelling sediment

dynamics due to hillslope-river interactions: Incorporating fluvial behaviour in landscape evolution model LAPSUS. Earth Surface Processes and Landforms 37 (9), 923–935. https://doi.org/10.1002/esp.3208

Bainbridge, Z.T., Wolanski, E., Álvarez-Romero, J.G., Lewis, S.E., Brodie, J.E., 2012. Fine sediment and nutrient dynamics related to particle size and floc formation in a Burdekin River flood plume, Australia. Marine Pollution Bulletin 65 (4–9), 236–248. https://doi.org/10.1016/j.marpolbul.2012.01.043

Bass, A.M., Bird, M.I., Liddell, M.J., Nelson, P.N., 2011. Fluvial dynamics of dissolved and particulate organic carbon during periodic discharge events in a steep tropical rainforest catchment. Limnology and Oceanography 56 (6), 2282–2292. https://doi.org/10.4319/lo.2011.56.6.2282

Batista, P.V.G., Laceby, J.P., Davies, J., Carvalho, T.S., Tassinari, D., Silva, M.L.N., Curi, N., Quinton, J.N., 2021. A framework for testing large-scale distributed soil erosion and sediment delivery models: Dealing with uncertainty in models and the observational data. Environmental Modelling and Software 137. https://doi.org/10.1016/j.envsoft.2021.104961

Batista, P.V.G., Laceby, J.P., Evrard, O., 2022. How to evaluate sediment fingerprinting source apportionments. Journal of Soils and Sediments (0123456789). https://doi.org/10.1007/s11368-022-03157-4

Belmont, P., Gran, K.B., Schottler, S.P., Wilcock, P.R., Day, S.S., Jennings, C., Lauer, J.W., Viparelli, E., Willenbring, J.K., Engstrom, D.R., Parker, G., 2011. Large shift in source of fine sediment in the upper Mississippi River. Environmental Science and Technology 45 (20), 8804–8810. https://doi.org/10.1021/es2019109

Ben-David, M., Hanley, T.A., Schell, D.M., 1998. Fertilization of terrestrial vegetation by spawning pacific salmon : the role of flooding and predator activity. Canadian Journal of Fisheries and Aquatic Sciences 47–55. https://doi.org/10.2307/3546545

Berho, C., Pouet, M.F., Bayle, S., Azema, N., Thomas, O., 2004. Study of UV-vis responses of mineral suspensions in water. Colloids and Surfaces A: Physicochemical and Engineering Aspects 248 (1–3), 9–16. https://doi.org/10.1016/j.colsurfa.2004.08.046

Beuscher, S., Krüger, S., Ehrmann, W., Schmiedl, G., Milker, Y., Arz, H., Schulz, H., 2017. End-member modelling as a tool for climate reconstruction — An Eastern Mediterranean case study. PLoS ONE 12 (9), 1–22. https://doi.org/10.1371/journal.pone.0185136

Bhargava, D.S., Mariam, D.W., 1994. Effects of particle sizes on the turbidity evaluation. Journal of the Institution of Engineers(India): Environmental Engineering Division 74, 27–34.

Bieganowski, A., Ryżak, M., Sochan, A., Barna, G., Hernádi, H., Beczek, M., Polakowski, C., Makó, A., 2018. Laser Diffractometry in the Measurements of Soil and Sediment Particle Size Distribution. Advances in Agronomy 151, 215–279. https://doi.org/10.1016/bs.agron.2018.04.003

Biggs, C.A., Lant, P.A., 2000. Activated sludge flocculation: On-line determination of floc size and the effect of shear. Water Research 34 (9), 2542–2550. https://doi.org/10.1016/S0043-1354(99)00431-5

Bilby, R.E., Fransen, B.R., Bisson, P.A., 1996. Incorporation of nitrogen and carbon from spawning coho salmon into the trophic system of small streams: Evidence from stable isotopes. Canadian Journal of Fisheries and Aquatic Sciences 53, 164–173. https://doi.org/10.1139/f95-159

Bilotta, G.S., Brazier, R.E., 2008. Understanding the influence of suspended solids on water quality and aquatic biota. Water Research 42 (12), 2849–2861. https://doi.org/10.1016/J.WATRES.2008.03.018

Blake, W.H., Boeckx, P., Stock, B.C., Smith, H.G., Bodé, S., Upadhayay, H.R., Gaspar, L., Goddard, R., Lennard, A.T., Lizaga, I., Lobb, D.A., Owens, P.N., Petticrew, E.L., Kuzyk, Z.Z.A., Gari, B.D., Munishi, L., Mtei, K., Nebiyu, A., Mabit, L., Navas, A., Semmens, B.X., 2018. A deconvolutional Bayesian mixing model approach for river basin sediment source apportionment. Scientific Reports 8 (1), 1–12. https://doi.org/10.1038/s41598-018-30905-9

Blake, W.H., Ficken, K.J., Taylor, P., Russell, M.A., Walling, D.E., 2012. Tracing crop-specific sediment sources in agricultural catchments. Geomorphology 139–140, 322–329. https://doi.org/10.1016/j.geomorph.2011.10.036

Boardman, J., Poesen, J., 2006. Soil erosion in Europe. John Wiley & Sons Ltd ISBN: 978.

Borrelli, P., Panagos, P., Alewell, C., Ballabio, C., de Oliveira Fagundes, H., Haregeweyn, N., Lugato, E., Maerker, M., Poesen, J., Vanmaercke, M., Robinson, D.A., 2022. Policy implications of multiple concurrent soil erosion processes in European farmland. Nature Sustainability. https://doi.org/10.1038/s41893-022-00988-4

Borrelli, P., Robinson, D.A., Fleischer, L.R., Lugato, E., Ballabio, C., Alewell, C., Meusburger, K., Modugno, S., Schütt, B., Ferro, V., Bagarello, V., Oost, K. Van, Montanarella, L., Panagos, P.,

2017. An assessment of the global impact of 21st century land use change on soil erosion. Nature Communications 8 (1). https://doi.org/10.1038/s41467-017-02142-7

Borrelli, P., Robinson, D.A., Panagos, P., Lugato, E., Yang, J.E., Alewell, C., Wuepper, D., Montanarella, L., Ballabio, C., 2020. Land use and climate change impacts on global soil erosion by water (2015-2070). Proceedings of the National Academy of Sciences of the United States of America 117 (36), 21994–22001. https://doi.org/10.1073/pnas.2001403117

Borselli, L., Cassi, P., Torri, D., 2008. Prolegomena to sediment and flow connectivity in the landscape: A GIS and field numerical assessment. Catena 75 (3), 268–277. https://doi.org/10.1016/j.catena.2008.07.006

Bradford, J.M., Truman, C.C., Huang, C., 1992. Comparison of three measures of resistance of soil surface seals to raindrop splash. Soil Technology 5 (1), 47–56. https://doi.org/10.1016/0933-3630(92)90006-M

Bravo-Linares, C., Schuller, P., Castillo, A., Ovando-Fuentealba, L., Muñoz-Arcos, E., Alarcón, O., de los Santos-Villalobos, S., Cardoso, R., Muniz, M., Meigikos dos Anjos, R., Bustamante-Ortega, R., Dercon, G., 2018. First use of a compound-specific stable isotope (CSSI) technique to trace sediment transport in upland forest catchments of Chile. Science of the Total Environment 618, 1114–1124. https://doi.org/10.1016/j.scitotenv.2017.09.163

Brown, A.G., 1985. The potential use of pollen in the identification of suspended sediment sources. Earth Surface Processes and Landforms 10 (1), 27–32. https://doi.org/10.1002/esp.3290100106

Bryan, R.B., 2000. Soil erodibility and processes of water erosion on hillslope. Geomorphology 32 (3–4), 385–415. https://doi.org/10.1016/S0169-555X(99)00105-1

Byrne, A.J., Chow, C., Trolio, R., Lethorn, A., Lucas, J., Korshin, G. V., 2011. Development and validation of online surrogate parameters for water quality monitoring at a conventional water treatment plant using a UV absorbance spectrolyser. Proceedings of the 2011 7th International Conference on Intelligent Sensors, Sensor Networks and Information Processing, ISSNIP 2011 200–204. https://doi.org/10.1109/ISSNIP.2011.6146515

Carter, J., Walling, D.E., Owens, P.N., Leeks, G.J.L., 2006. Spatial and temporal variability in the concentration and speciation of metals in suspended sediment transported by the River Aire, Yorkshire, UK. Hydrological Processes 20, 3007–3027. https://doi.org/10.1002/hyp.6156

Cavalli, M., Trevisani, S., Comiti, F., Marchi, L., 2013. Geomorphometric assessment of spatial sediment connectivity in small Alpine catchments. Geomorphology 188, 31–41. https://doi.org/10.1016/j.geomorph.2012.05.007

Charlesworth, S.M., Lees, J.A., 2001. The application of some mineral magnetic measurements and heavy metal analysis for characterising fine sediments in an urban catchment, Coventry, UK. Journal of Applied Geophysics 48 (2), 113–125. https://doi.org/10.1016/S0926-9851(01)00084-2

Chen, D., Wei, W., Chen, L., 2017. Effects of terracing practices on water erosion control in China: A meta-analysis. Earth-Science Reviews 173, 109–121. https://doi.org/10.1016/j.earscirev.2017.08.007

Collins, A.L., 1995. The use of composite fingerprints for tracing the source of suspended sediment in river basins (Doctoral dissertation, University of Exeter).

Collins, A.L., Blackwell, M., Boeckx, P., Chivers, C.A., Emelko, M., Evrard, O., Foster, I., Gellis, A., Gholami, H., Granger, S., Harris, P., Horowitz, A.J., Laceby, J.P., Martinez-Carreras, N., Minella, J., Mol, L., Nosrati, K., Pulley, S., Silins, U., da Silva, Y.J., Stone, M., Tiecher, T., Upadhayay, H.R., Zhang, Y., 2020. Sediment source fingerprinting: benchmarking recent outputs, remaining challenges and emerging themes. Journal of Soils and Sediments 20 (12), 4160–4193. https://doi.org/10.1007/s11368-020-02755-4

Collins, A.L., Burak, E., Harris, P., Pulley, S., Cardenas, L., Tang, Q., 2019. Field scale temporal and spatial variability of δ13C, δ15N, TC and TN soil properties: Implications for sediment source tracing. Geoderma 333, 108–122. https://doi.org/10.1016/j.geoderma.2018.07.019

Collins, A.L., Pulley, S., Foster, I.D.L., Gellis, A., Porto, P., Horowitz, A.J., 2017. Sediment source fingerprinting as an aid to catchment management: A review of the current state of knowledge and a methodological decision-tree for end-users. Journal of Environmental Management 194, 86–108. https://doi.org/10.1016/j.jenvman.2016.09.075

Collins, A.L., Walling, D.., Leeks, G.J.L., 1996. Composite fingerprinting of the spatial source of fluvial suspended sediment : a case study of the Exe and Severn river basins, United Kingdom. Géomorphologie : Relief, Processus, Environnement 2 (2), 41–53. https://doi.org/10.3406/morfo.1996.877

Collins, A.L., Walling, D.E., 2002. Selecting fingerprint properties for discriminating potential suspended sediment sources in river basins. Journal of Hydrology 261 (1–4), 218–244. https://doi.org/10.1016/S0022-1694(02)00011-2

Collins, A.L., Walling, D.E., 2004. Documenting catchment suspended sediment sources: problems, approaches and prospects. Progress in Physical Geography: Earth and Environment 28 (2), 159–196. https://doi.org/10.1191/0309133304pp409ra

Collins, A.L., Walling, D.E., Leeks, G.J.L., 1997a. Source type ascription for fluvial suspended sediment based on a quantitative composite fingerprinting technique. Catena 29 (1), 1–27. https://doi.org/10.1016/S0341-8162(96)00064-1

Collins, A.L., Walling, D.E., Leeks, G.J.L., 1997b. Fingerprinting the origin of fluvial suspended sediment in larger river basins: Combining assessment of spatial provenance and source type. Geografiska Annaler, Series A: Physical Geography 79 (4), 239–254. https://doi.org/10.1111/j.0435-3676.1997.00020.x

Collins, A.L., Walling, D.E., Leeks, G.J.L., 1997c. Use of the geochemical record preserved in floodplain deposits to reconstruct recent changes in river basin sediment sources. Geomorphology 19 (1–2), 151–167. https://doi.org/10.1016/s0169-555x(96)00044-x

Collins, A.L., Walling, D.E., Leeks, G.J.L., 1998. Use of composite fingerprints to determine the provenance of the contemporary suspended sediment load transported by rivers. Earth Surface Processes and Landforms 23 (1), 31–52. https://doi.org/10.1002/(SICI)1096-9837(199801)23:1<31::AID-ESP816>3.0.CO;2-Z

Collins, A.L., Walling, D.E., Stroud, R.W., Robson, M., Peet, L.M., 2010. Assessing damaged road verges as a suspended sediment source in the Hampshire Avon catchment, southern United Kingdom. Hydrological Processes 24 (9), 1106–1122. https://doi.org/10.1002/hyp.7573

Collins, A.L., Zhang, Y.S., Hickinbotham, R., Bailey, G., Darlington, S., Grenfell, S.E., Evans, R., Blackwell, M., 2013. Contemporary fine-grained bed sediment sources across the River Wensum Demonstration Test Catchment, UK. Hydrological Processes 27 (6), 857–884. https://doi.org/10.1002/hyp.9654

Cooper, R.J., Krueger, T., 2017. An extended Bayesian sediment fingerprinting mixing model for the full Bayes treatment of geochemical uncertainties. Hydrological Processes 31 (10), 1900–1912. https://doi.org/10.1002/hyp.11154

Cooper, R.J., Krueger, T., Hiscock, K.M., Rawlins, B.G., 2014a. Sensitivity of fluvial sediment source apportionment to mixing model assumptions: A Bayesian model comparison. Water Resources Research 50 (11), 9031–9047. https://doi.org/10.1002/2014WR016194

Cooper, R.J., Krueger, T., Hiscock, K.M., Rawlins, B.G., 2015. High-temporal resolution fluvial

sediment source fingerprinting with uncertainty: A Bayesian approach. Earth Surface Processes and Landforms 40 (1), 78–92. https://doi.org/10.1002/esp.3621

Cooper, R.J., Rawlins, B.G., Lézé, B., Krueger, T., Hiscock, K.M., 2014b. Combining two filter paper-based analytical methods to monitor temporal variations in the geochemical properties of fluvial suspended particulate matter. Hydrological Processes 28 (13), 4042–4056. https://doi.org/10.1002/hyp.9945

Czuba, J.A., Straub, T.D., Curran, C.A., Landers, M.N., Domanski, M.M., 2015. Comparison of fluvial suspended-sediment concentrations and particle-size distributions measured with in-stream laser diffraction and in physical samples. Water Resources Research 51 (1), 320–340. https://doi.org/10.1002/2014wr015697

D'Acunha, B., Johnson, M.S., 2019. Water quality and greenhouse gas fluxes for stormwater detained in a constructed wetland. Journal of Environmental Management 231, 1232–1240. https://doi.org/10.1016/j.jenvman.2018.10.106

Dabrin, A., Bégorre, C., Bretier, M., Dugué, V., Masson, M., Le Bescond, C., Le Coz, J., Coquery, M., 2021. Reactivity of particulate element concentrations: apportionment assessment of suspended particulate matter sources in the Upper Rhône River, France. Journal of Soils and Sediments 21 (2), 1256–1274. https://doi.org/10.1007/s11368-020-02856-0

Davis, C.M., Fox, J.F., 2009. Sediment fingerprinting: review of the method and future improvements for allocating nonpoint source pollution. Journal of Environmental Engineering-Asce 135 (7), 490–504. https://doi.org/10.1061/(ASCE)0733-9372(2009)135:7(490)

Dean, D.J., Topping, D.J., Schmidt, J.C., Griffiths, R.E., Sabol, T.A., 2016. Sediment supply versus local hydraulic controls on sediment transport and storage in a river with large sediment loads. Journal of Geophysical Research : Earth Surface 121, 82–110. https://doi.org/10.1002/2015JF003436

Dearing, J.A., Hay, K.L., Baban, S.M.J., Huddleston, A.S., Wellington, E.M.H., Loveland, P.J., 1996. Magnetic susceptibility of soil: An evaluation of conflicting theories using a national data set. Geophysical Journal International 127 (3), 728–734. https://doi.org/10.1111/j.1365-246X.1996.tb04051.x

Devereux, O.H., Prestegaard, K.L., Needelman, B.A., Gellis, A.C., 2010. Suspended-sediment sources in an urban watershed, Northeast Branch Anacostia River, Maryland. Hydrological Processes 24 (11), 1391–1403. https://doi.org/10.1002/hyp.7604

Dey, S., 2014. Bed-load transport. In: Fluvial Hydrodynamics. Springer, Berlin, Heidelberg 261–326. https://doi.org/10.1007/978-3-642-19062-9_5

Dietze, E., Hartmann, K., Diekmann, B., IJmker, J., Lehmkuhl, F., Opitz, S., Stauch, G., Wünnemann, B., Borchers, A., 2012. An end-member algorithm for deciphering modern detrital processes from lake sediments of Lake Donggi Cona, NE Tibetan Plateau, China. Sedimentary Geology 243–244, 169–180. https://doi.org/10.1016/j.sedgeo.2011.09.014

Douglas, G., Palmer, M., Caitcheon, G., 2003. The provenance of sediments in Moreton Bay, Australia: A synthesis of major, trace element and Sr-Nd-Pb isotopic geochemistry, modelling and landscape analysis. Hydrobiologia 494, 145–152. https://doi.org/10.1023/A:1025454013160

Droppo, I.G., 2001. Rethinking what constitutes suspended sediment. Hydrological Processes 15 (9), 1551–1564. https://doi.org/10.1002/hyp.228

Droppo, I.G., 2004. Structural controls on floc strength and transport. Canadian Journal of Civil Engineering 31 (4), 569–578. https://doi.org/10.1139/L04-015

Droppo, I.G., Nackaerts, K., Walling, D.E., Williams, N., 2005. Can flocs and water stable soil aggregates be differentiated within fluvial systems? Catena 60 (1), 1–18. https://doi.org/10.1016/j.catena.2004.11.002

Droppo, I.G., Ongley, E.D., 1994. Flocculation of suspended sediment in rivers of southeastern Canada. Water Research 28 (8), 1799–1809. https://doi.org/10.1016/0043-1354(94)90253-4

Emerson, D.G., Vecchia, A. V., Dahl, A.L., 2005. Evaluation of drainage-area ratio method used to estimate streamflow for the Red river of the north basin, North Dakota and Minnesota. US Geological Survey Scientific Investigations Report.

Evrard, O., Batista, P.V.G., Company, J., Dabrin, A., Foucher, A., Frankl, A., García-Comendador, J., Huguet, A., Lake, N., Lizaga, I., Martínez-Carreras, N., Navratil, O., Pignol, C., Sellier, V., 2022. Improving the design and implementation of sediment fingerprinting studies: summary and outcomes of the TRACING 2021 Scientific School. Journal of Soils and Sediments 22 (6), 1648–1661. https://doi.org/10.1007/s11368-022-03203-1

Evrard, O., Navratil, O., Ayrault, S., Ahmadi, M., Némery, J., Legout, C., Lefèvre, I., Poirel, A., Bonté, P., Esteves, M., 2011. Combining suspended sediment monitoring and fingerprinting to determine the spatial origin of fine sediment in a mountainous river catchment. Earth Surface Processes and Landforms 36 (8), 1072–1089. https://doi.org/10.1002/esp.2133

FAO, 2015. The Status of the World's Soil Resources (Main Report). Available at: https://www.fao.org/3/i5199e/I5199E.pdf. (Accessed November 2022).

FAO, 2016. Global Soil Partnership endorses guidelines on sustainable soil management. Available at: https://www.fao.org/global-soil-partnership/resources/highlights/detail/en/c/416516/. (Accessed November 2022).

Farnsworth, K.L., Milliman, J.D., 2003. Effects of climatic and anthropogenic change on small mountainous rivers: the Salinas River example. Global and Planetary Change 39 (1–2), 53–64. https://doi.org/10.1016/S0921-8181(03)00017-1

Fettweis, M., Lee, B.J., 2017. Spatial and seasonal variation of biomineral suspended particulate matter properties in high-turbid nearshore and low-turbid offshore zones. Water 9 (9). https://doi.org/10.3390/w9090694

Fiener, P., Auerswald, K., Weigand, S., 2005. Managing erosion and water quality in agricultural watersheds by small detention ponds. Agriculture, Ecosystems and Environment 110 (3–4), 132–142. https://doi.org/10.1016/j.agee.2005.03.012

Foley, J.A., Ramankutty, N., Brauman, K.A., Cassidy, E.S., Gerber, J.S., Johnston, M., Mueller, N.D., O'Connell, C., Ray, D.K., West, P.C., Balzer, C., Bennett, E.M., Carpenter, S.R., Hill, J., Monfreda, C., Polasky, S., Rockström, J., Sheehan, J., Siebert, S., Tilman, D., Zaks, D.P.M., 2011. Solutions for a cultivated planet. Nature 478 (7369), 337–342. https://doi.org/10.1038/nature10452

Förstner, U., Muller, G., 1974. Schwermetalle in flussen und seen als ausdruck der umweltverschmutzung. Springer, Berlin 225 pp. https://doi.org/10.1007/978-3-642-49242-6

Foster, I.D.L., Lees, J.A., Owens, P.N., Walling, D.E., 1998. Mineral magnetic characterization of sediment sources from an analysis of lake and floodplain sediments in the catchments of the Old Mill Reservoir and Slapton Ley, South Devon, UK. Earth Surface Processes and Landforms 23 (8), 685–703. https://doi.org/10.1002/(SICI)1096-9837(199808)23:8<685::AID-ESP873>3.0.CO;2-8

Foster, I.D.L., Mighall, T.M., Proffitt, H., Walling, D.E., Owens, P.N., 2006. Post-depositional 137Cs mobility in the sediments of three shallow coastal lagoons, SW England. Journal of Paleolimnology 35 (4), 881–895. https://doi.org/10.1007/s10933-005-6187-6

Foster, I.D.L., Walling, D.E., 1994. Using reservoir deposits to reconstruct changing sediment yields and sources in the catchment of the old mill reservoir, south devon, uk, over the past 50

years. Hydrological Sciences Journal 39 (4), 347–368. https://doi.org/10.1080/02626669409492755

Frankl, A., Evrard, O., Cammeraat, E., Tytgat, B., Verleyen, E., Stokes, A., 2022. Tracing hotspots of soil erosion in high mountain environments: how forensic science based on plant eDNA can lead the way. An opinion. Plant and Soil 476 (1–2), 729–742. https://doi.org/10.1007/s11104-021-05261-9

Frankl, A., Prêtre, V., Nyssen, J., Salvador, P.G., 2018. The success of recent land management efforts to reduce soil erosion in northern France. Geomorphology 303, 84–93. https://doi.org/10.1016/j.geomorph.2017.11.018

Franks, S.W., Rowan, J.S., 2000. Multi-parameter fingerprinting of sediment sources: Uncertainty estimation and tracer selection. In L. R. Bentley, J. F. Sykes, C. A. Brebbia, W. G. Gray, G. F. Pinder, L. R. Bentley, J. F. Sykes, C. A. Brebbia, W. G. Gray, & G. F. Pinder (Eds.). Computational Methods in Water Resources: Volume 2 - Computational Methods, Surface Water Systems and Hydrology, 1067–1074.

Fryirs, K., 2012. (Dis) Connectivity in catchment sediment cascades: a fresh look at the sediment delivery problem. Earth Surface Processes and Landforms 38 (1), 30–46. https://doi.org/10.1002/esp.3242

Fryirs, K.A., Brierley, G.J., Preston, N.J., Kasai, M., 2007. Buffers, barriers and blankets: The (dis)connectivity of catchment-scale sediment cascades. Catena 70 (1), 49–67. https://doi.org/10.1016/j.catena.2006.07.007

Fuwa, K., Valle, B.L., 1963. The physical basis of analytical atomic absorption spectrometry. The pertinence of the beer-lambert law. Analytical Chemistry 35 (8), 942–946. https://doi.org/10.1021/ac60201a006

Gamerith, V., Steger, B., Hochedlinger, M., Gruber, G., 2011. Assessment of UV/VIS-spectrometry performance in combined sewer monitoring under wet weather conditions. 12th International Conference on Urban Drainage, Porto Alegre/Brazil 10–15.

García-Comendador, J., Martínez-Carreras, N., Fortesa, J., Company, J., Borràs, A., Estrany, J., 2021. Combining sediment fingerprinting and hydro-sedimentary monitoring to assess suspended sediment provenance in a mid-mountainous Mediterranean catchment. Journal of Environmental Management 299, 113593. https://doi.org/10.1016/j.jenvman.2021.113593

Gaspar, L., Blake, W.H., Lizaga, I., Latorre, B., Navas, A., 2022. Particle size effect on geochemical composition of experimental soil mixtures relevant for unmixing modelling. Geomorphology 403, 108178. https://doi.org/10.1016/j.geomorph.2022.108178

Gaspar, L., Blake, W.H., Smith, H.G., Lizaga, I., Navas, A., 2019. Testing the sensitivity of a multivariate mixing model using geochemical fingerprints with artificial mixtures. Geoderma 337, 498–510. https://doi.org/10.1016/j.geoderma.2018.10.005

Gaspar, L., Navas, A., 2013. Vertical and lateral distributions of 137Cs in cultivated and uncultivated soils on Mediterranean hillslopes. Geoderma 207–208 (1), 131–143. https://doi.org/10.1016/j.geoderma.2013.04.034

Golterman, H.L. (ed), 1977. Interactions between sediment and fresh water. Dr. W. Junk Publishers, The Hague.

Golterman, H.L., Sly, P.G., Thomas, R.L., 1983. Study of the relationship between water quality and sediment transport: a guide for the collection and interpretation of sediment quality data. UNESCO, Paris 231 pp.

Gonzalez-Hidalgo, J.C., Batalla, R.J., Cerdá, A., de Luis, M., 2010. Contribution of the largest events to suspended sediment transport across the USA. Land Degradation and Development 21 (2), 83–91. https://doi.org/10.1002/ldr.897

González-Morales, D., Valencia, A., Díaz-Nuñez, A., Fuentes-Estrada, M., López-Santos, O., García-Beltrán, O., 2020. Development of a low-cost UV-Vis spectrophotometer and its application for the detection of mercuric ions assisted by chemosensors. Sensors 20 (3), 906. https://doi.org/10.3390/s20030906

Grangeon, T., Droppo, I.G., Legout, C., Esteves, M., 2014. From soil aggregates to riverine flocs: A laboratory experiment assessing the respective effects of soil type and flow shear stress on particles characteristics. Hydrological Processes 28 (13), 4141–4155. https://doi.org/10.1002/hyp.9929

Grangeon, T., Legout, C., Esteves, M., Gratiot, N., Navratil, O., 2012. Variability of the particle size of suspended sediment during highly concentrated flood events in a small mountainous catchment. Journal of Soils and Sediments 12 (10), 1549–1558. https://doi.org/10.1007/s11368-012-0562-5

Gray, A.B., Pasternack, G.B., Watson, E.B., 2010. Hydrogen peroxide treatment effects on the particle size distribution of alluvial and marsh sediments. Holocene 20 (2), 293–301.

https://doi.org/10.1177/0959683609350390

Gregory, K.J., Walling, D.E., 1973. Drainage basin form and process. Edward Arnold, London 456 pp.

Grimshaw, D.L., Lewin, J., 1980. Source identification for suspended sediments. Journal of Hydrology 47 (1–2), 151–162. https://doi.org/10.1016/0022-1694(80)90053-0

Grotzinger, J., Jordan, T.H., Press, F., Siever, R., 2007. Understanding earth. W.H. Freeman and Company, 5th edition.

Guan, Z., Tang, X.Y., Yang, J.E., Ok, Y.S., Xu, Z., Nishimura, T., Reid, B.J., 2017. A review of source tracking techniques for fine sediment within a catchment. Environmental Geochemistry and Health 39 (6), 1221–1243. https://doi.org/10.1007/s10653-017-9959-9

Haddadchi, A., Nosrati, K., Ahmadi, F., 2014a. Differences between the source contribution of bed material and suspended sediments in a mountainous agricultural catchment of western Iran. Catena 116, 105–113. https://doi.org/10.1016/j.catena.2013.12.011

Haddadchi, A., Olley, J., Laceby, P., 2014b. Accuracy of mixing models in predicting sediment source contributions. Science of the Total Environment 497–498, 139–152. https://doi.org/10.1016/j.scitotenv.2014.07.105

Haddadchi, A., Olley, J., Pietsch, T., 2015. Quantifying sources of suspended sediment in three size fractions. Journal of Soils and Sediments 15 (10), 2086–2100. https://doi.org/10.1007/s11368-015-1196-1

Haddadchi, A., Ryder, D.S., Evrard, O., Olley, J., 2013. Sediment fingerprinting in fluvial systems: Review of tracers, sediment sources and mixing models. International Journal of Sediment Research 28 (4), 560–578. https://doi.org/10.1016/S1001-6279(14)60013-5

Haimann, M., Liedermann, M., Lalk, P., Habersack, H., 2014. An integrated suspended sediment transport monitoring and analysis concept. International Journal of Sediment Research 29 (2), 135–148. https://doi.org/10.1016/S1001-6279(14)60030-5

Hatfield, R.G., Maher, B.A., 2009. Fingerprinting upland sediment sources: particle size-specific magnetic linkages between soils, lake sediments and suspended sediments. Earth Surface Processes and Landforms 34 (10), 1359–1373. https://doi.org/10.1002/esp.1824

He, Q., Owens, P., 1995. Determination of suspended sediment provenance using Caesium-137, unsupported Lead-210 and Radium-226: a numerical mixing model approach. Sediment and

water quality in river catchments, 207–227.

He, Q., Walling, D.E., 1996. Interpreting particle size effects in the adsorption of 137Cs and unsupported 210Pb by mineral soils and sediments. Journal of Environmental Radioactivity 30 (2), 117–137. https://doi.org/10.1016/0265-931X(96)89275-7

Heckmann, T., Schwanghart, W., 2013. Geomorphic coupling and sediment connectivity in an alpine catchment - Exploring sediment cascades using graph theory. Geomorphology 182, 89–103. https://doi.org/10.1016/j.geomorph.2012.10.033

Heslop, D., von Dobeneck, T., Höcker, M., 2007. Using non-negative matrix factorization in the "unmixing" of diffuse reflectance spectra. Marine Geology 241 (1–4), 63–78. https://doi.org/10.1016/j.margeo.2007.03.004

Hilton, J., O'Hare, M., Bowes, M.J., Jones, J.I., 2006. How green is my river? A new paradigm of eutrophication in rivers. Science of The Total Environment 365 (1–3), 66–83. https://doi.org/10.1016/J.SCITOTENV.2006.02.055

Horowitz, A.J., 1985. A primer on sediment-trace metal chemistry. US Geological Survey Water Supply Paper 67 pp.

Horowitz, A.J., 1991. A Primer on sediment-trace element chemistry. Chelsea: Lewis Publishers 136.

Horowitz, A.J., 2013. A review of selected inorganic surface water quality-monitoring practices: Are we really measuring what we think, and if so, are we doing it right? Environmental Science and Technology 47 (6), 2471–2486. https://doi.org/10.1021/es304058q

Horowitz, A.J., Elrick, K.A., 1987. The relation of stream sediment surface area, grain size and composition to trace element chemistry. Applied Geochemistry 2 (4), 437–451. https://doi.org/10.1016/0883-2927(87)90027-8

Horowitz, A.J., Elrick, K.A., Hooper, R.C., 1989. A comparison of instrumental dewatering methods for the separation and concentration of suspended sediment for subsequent trace element analysis. Hydrological Processes 3 (2), 163–184. https://doi.org/10.1002/hyp.3360030206

Horowitz, A.J., Rinella, F.A., Edwards, T.K., Roche, R.L., Lamothe, P., Miller, T.L., Rickert, D.A., 1990. Variations in suspended sediment and associated trace element concentrations in selected riverine cross sections. Environmental Science and Technology 24 (9), 1313–1320. https://doi.org/10.1021/es00079a003

House, W.A., 2003. Geochemical cycling of phosphorus in rivers. Applied Geochemistry 18, 739–748. https://doi.org/10.1016/S0883-2927(02)00158-0

Hudson-Edwards, K.A., Macklin, M.G., Curtis, C.D., Vaughan, D.J., 1998. Chemical remobilization of contaminant metals within floodplain sediments in an incising river system: implications for dating and chemostratigraphy. Earth Surface Processes and Landforms 23 (8), 671–684. https://doi.org/10.1002/(SICI)1096-9837(199808)23:8<671::AID-ESP871>3.0.CO;2-R

Jenks, G.F., 1967. The data model concept in statistical mapping. International Yearbook of Cartography 7, 186–190.

Jones, R.J.A., Le Bissonnais, Y., Diaz, J.S., Düwel, O., Øygarden, L., Bazzoffi, P., Prasuhn, V., Yordanov, Y., Strauss, P., Rydell, B., Uveges, J.B., Loj, G., Lane, M., Vandekerckhove, L., 2003. EU Soil Thematic Strategy : Technical Working Group on Erosion Work Package 2: Nature and extent of soil erosion in Europe. Interim Report version 3.31 (October), 1–27.

Kagabo, D.M., Stroosnijder, L., Visser, S.M., Moore, D., 2013. Soil erosion, soil fertility and crop yield on slow-forming terraces in the highlands of Buberuka, Rwanda. Soil and Tillage Research 128, 23–29. https://doi.org/10.1016/j.still.2012.11.002

Keesstra, S., Nunes, J.P., Saco, P., Parsons, T., Poeppl, R., Masselink, R., Cerdà, A., 2018. The way forward: Can connectivity be useful to design better measuring and modelling schemes for water and sediment dynamics? Science of the Total Environment 644, 1557–1572. https://doi.org/10.1016/j.scitotenv.2018.06.342

Keesstra, S.D., 2007. Impact of natural reforestation on floodplain sedimentation in the Dragonja basin, SW Slovenia. Earth Surface Processes and Landforms 32, 49–65. https://doi.org/10.1002/esp

Keesstra, S.D., van Dam, O., Verstraeten, G., van Huissteden, J., 2009. Changing sediment dynamics due to natural reforestation in the Dragonja catchment, SW Slovenia. Catena 78 (1), 60–71. https://doi.org/10.1016/j.catena.2009.02.021

Kirchner, J.W., Feng, X., Neal, C., Robson, A.J., 2004. The fine structure of water-quality dynamics: The (high-frequency) wave of the future. Hydrological Processes 18 (7), 1353–1359. https://doi.org/10.1002/hyp.5537

Klages, M.G., Hsieh, Y.P., 1975. Suspended solids carried by the Gallatin River of southwestern Montana: II. Using mineralogy for inferring sources. Journal of Environmental Quality 4, 68–73. https://doi.org/10.2134/jeq1975.00472425000400010016x

Koiter, A.J., Owens, P.N., Petticrew, E.L., Lobb, D.A., 2013. The behavioural characteristics of sediment properties and their implications for sediment fingerprinting as an approach for identifying sediment sources in river basins. Earth-Science Reviews 125, 24–42. https://doi.org/10.1016/j.earscirev.2013.05.009

Koiter, A.J., Owens, P.N., Petticrew, E.L., Lobb, D.A., 2018. Assessment of particle size and organic matter correction factors in sediment source fingerprinting investigations: An example of two contrasting watersheds in Canada. Geoderma 325 (October 2017), 195–207. https://doi.org/10.1016/j.geoderma.2018.02.044

Kondolf, G.M., Schmitt, R.J.P., Carling, P., Darby, S., Arias, M., Bizzi, S., Castelletti, A., Cochrane, T.A., Gibson, S., Kummu, M., Oeurng, C., Rubin, Z., Wild, T., 2018. Changing sediment budget of the Mekong: Cumulative threats and management strategies for a large river basin. Science of the Total Environment 625, 114–134. https://doi.org/10.1016/j.scitotenv.2017.11.361

Kongas, M., 2003. Mineral slurry on-stream particle size analysis. Filtration & Separation 40 (7), 36–37. https://doi.org/10.1016/S0015-1882(03)00730-4

Kranck, K., Milligan, T.G., 1985. Origin of grain size spectra of suspension deposited sediment. Geo-marine letters 5, 61–66. https://doi.org/10.1007/BF02629800

Krishnappan, B.G., Chambers, P.A., Benoy, G., Culp, J., 2009. Sediment source identification: A review and a case study in some Canadian streams. Canadian Journal of Civil Engineering 36 (10), 1622–1633. https://doi.org/10.1139/L09-110

Kronvang, B., Laubel, A., Larsen, S.E., Friberg, N., 2003. Pesticides and heavy metals in Danish streambed sediment. Hydrobiologia 494, 93–101. https://doi.org/10.1023/A:1025441610434

Laceby, J.P., Evrard, O., Smith, H.G., Blake, W.H., Olley, J.M., Minella, J.P.G., Owens, P.N., 2017. The challenges and opportunities of addressing particle size effects in sediment source fingerprinting: A review. Earth-Science Reviews 169, 85–103. https://doi.org/10.1016/j.earscirev.2017.04.009

Laceby, J.P., McMahon, J., Evrard, O., Olley, J., 2015. A comparison of geological and statistical approaches to element selection for sediment fingerprinting. Journal of Soils and Sediments 15 (10), 2117–2131. https://doi.org/10.1007/s11368-015-1111-9

Lacour, C., Joannis, C., Chebbo, G., 2009. Assessment of annual pollutant loads in combined

sewers from continuous turbidity measurements: Sensitivity to calibration data. Water Research 43 (8), 2179–2190. https://doi.org/10.1016/j.watres.2009.02.017

Lake, N.F., Martínez-Carreras, N., Iffly, J.F., Shaw, P.J., Collins, A.L., 2023. Use of a submersible spectrophotometer probe to fingerprint spatial suspended sediment sources at catchment scale. Science of the Total Environment 873 (February). https://doi.org/10.1016/j.scitotenv.2023.162332

Lake, N.F., Martínez-Carreras, N., Shaw, P.J., Collins, A.L., 2022a. High frequency un-mixing of soil samples using a submerged spectrophotometer in a laboratory setting—implications for sediment fingerprinting. Journal of Soils and Sediments 22 (1), 348–364. https://doi.org/10.1007/s11368-021-03107-6

Lake, N.F., Martínez-Carreras, N., Shaw, P.J., Collins, A.L., 2022b. Using particle size distributions to fingerprint suspended sediment sources — Evaluation at laboratory and catchment scales. Hydrological Processes 36 (10), e14726. https://doi.org/10.1002/hyp.14726

Lal, R., 2003. Soil erosion and the global carbon budget. Environment International 29 (4), 437–450. https://doi.org/10.1016/S0160-4120(02)00192-7

Latorre, B., Lizaga, I., Gaspar, L., Navas, A., 2021. A novel method for analysing consistency and unravelling multiple solutions in sediment fingerprinting. Science of the Total Environment 789, 147804. https://doi.org/10.1016/j.scitotenv.2021.147804

Lauber, C.L., Ramirez, K.S., Aanderud, Z., Lennon, J., Fierer, N., 2013. Temporal variability in soil microbial communities across land-use types. ISME Journal 7 (8), 1641–1650. https://doi.org/10.1038/ismej.2013.50

Lawler, D.M., Petts, G.E., Foster, I.D.L., Harper, S., 2006. Turbidity dynamics during spring storm events in an urban headwater river system: The Upper Tame, West Midlands, UK. Science of the Total Environment 360 (1–3), 109–126. https://doi.org/10.1016/j.scitotenv.2005.08.032

Lees, J.A., 1997. Mineral magnetic properties of mixtures of environmental and synthetic materials: Linear additivity and interaction effects. Geophysical Journal International 131 (2), 335–346. https://doi.org/10.1111/j.1365-246X.1997.tb01226.x

Legout, C., Freche, G., Biron, R., Esteves, M., Navratil, O., Nord, G., Uber, M., Grangeon, T., Hachgenei, N., Boudevillain, B., Voiron, C., Spadini, L., 2021. A critical zone observatory dedicated to suspended sediment transport: The meso-scale Galabre catchment (southern French Alps). Hydrological Processes 35 (3), 1–6. https://doi.org/10.1002/hyp.14084

Legout, C., Poulenard, J., Nemery, J., Navratil, O., Grangeon, T., Evrard, O., Esteves, M., 2013. Quantifying suspended sediment sources during runoff events in headwater catchments using spectrocolorimetry. Journal of Soils and Sediments 13 (8), 1478–1492. https://doi.org/10.1007/s11368-013-0728-9

Leppard, G.G., 1985. Transmission electron microscopy applied to water fractionation studies - a new look at DOC. Water Quality Research Journal 20 (2), 100–110. https://doi.org/10.2166/wqrj.1985.021

Lewis, J., Eads, R., 2008. Implementation guide for turbidity threshold sampling: principles, procedures, and analysis. General Technical Report. PSW-GTR-212. Albany, CA: US Department of Agriculture, Forest Service, Pacific Southwest Research Station. 86 p.

Li, Z., Xu, X., Zhang, Y., Wang, K., 2020. Fingerprinting sediment sources in a typical karst catchment of southwest China. International Soil and Water Conservation Research 8 (3), 277–285. https://doi.org/10.1016/j.iswcr.2020.06.005

Liss, S.N., Droppo, I.G., Flannigan, D.T., Leppard, G.G., 1996. Floc architecture in wastewater and natural riverine systems. Environmental Science and Technology 30 (2), 680–686. https://doi.org/10.1021/es950426r

Liu, C., Lobb, D., Li, S., Owens, P., Kuzyk, Z., 2014. Using sediment particle size distribution to evaluate sediment sources in the Tobacco Creek Watershed. Geophysical Research Abstracts EGU General Assembly 2014 Vol. 16, E.

Lizaga, I., Gaspar, L., Latorre, B., Navas, A., 2020a. Variations in transport of suspended sediment and associated elements induced by rainfall and agricultural cycle in a Mediterranean agroforestry catchment. Journal of Environmental Management 272, 111020. https://doi.org/10.1016/j.jenvman.2020.111020

Lizaga, I., Latorre, B., Gaspar, L., Navas, A., 2020b. Consensus ranking as a method to identify non-conservative and dissenting tracers in fingerprinting studies. Science of the Total Environment 720, 137537. https://doi.org/10.1016/j.scitotenv.2020.137537

Lizaga, I., Latorre, B., Gaspar, L., Navas, A., 2020c. FingerPro: an R package for tracking the provenance of sediment. Water Resources Management 34 (12), 3879–3894. https://doi.org/10.1007/s11269-020-02650-0

Malvern Instruments Ltd. Mastersizer 3000 User Manual (issue 2.1), 2013.

Marsh, 1864. George Perkins. Man and Nature. Vol. 1., Library of Alexandria.

Martínez-Carreras, N., 2010. Suspended sediment transport, properties and sources in the Attert River basin (Luxembourg) (Doctoral dissertation, University of Barcelona, Spain), 196 p.

Martínez-Carreras, N., Krein, A., Gallart, F., Iffly, J.F., Pfister, L., Hoffmann, L., Owens, P.N., 2010a. Assessment of different colour parameters for discriminating potential suspended sediment sources and provenance: A multi-scale study in Luxembourg. Geomorphology 118 (1–2), 118–129. https://doi.org/10.1016/j.geomorph.2009.12.013

Martínez-Carreras, N., Krein, A., Udelhoven, T., Gallart, F., Iffly, J.F., Hoffmann, L., Pfister, L., Walling, D.E., 2010b. A rapid spectral-reflectance-based fingerprinting approach for documenting suspended sediment sources during storm runoff events. Journal of Soils and Sediments 10 (3), 400–413. https://doi.org/10.1007/s11368-009-0162-1

Martínez-Carreras, N., Schwab, M.P., Klaus, J., Hissler, C., 2016. In situ and high frequency monitoring of suspended sediment properties using a spectrophotometric sensor. Hydrological Processes 30 (19), 3533–3540. https://doi.org/10.1002/hyp.10858

Martínez-Carreras, N., Udelhoven, T., Krein, A., Gallart, F., Iffly, J.F., Ziebel, J., Hoffmann, L., Pfister, L., Walling, D.E., 2010c. The use of sediment colour measured by diffuse reflectance spectrometry to determine sediment sources: Application to the Attert River catchment (Luxembourg). Journal of Hydrology 382 (1–4), 49–63. https://doi.org/10.1016/j.jhydrol.2009.12.017

Mekonnen, M., Keesstra, S.D., Stroosnijder, L., Baartman, J.E.M., Maroulis, J., 2015. Soil conservation through sediment trapping: a review. Land Degradation and Development 26 (6), 544–556. https://doi.org/10.1002/ldr.2308

Misset, C., Recking, A., Legout, C., Poirel, A., Cazilhac, M., Esteves, M., Bertrand, M., 2019. An attempt to link suspended load hysteresis patterns and sediment sources configuration in alpine catchments. Journal of Hydrology 576, 72–84. https://doi.org/10.1016/j.jhydrol.2019.06.039

Montanarella, L., 2015. Agricultural policy: govern our soils. Nature 528, 32–33. https://doi.org/10.1038/528032a

Montgomery, D.R., 2007. Soil erosion and agricultural sustainability. Proceedings of the National Academy of Sciences of the United States of America 104 (33), 13268–13272. https://doi.org/10.1073/pnas.0611508104

Morgan, R.P.C., 1995. Measurement of soil erosion. Soil Erosion and Conservation, 2nd edition.

Longman, Essex, UK, 84–95.

Morris, G.L., 2020. Classification of management alternatives to combat reservoir sedimentation. Water 12 (3), 1–24. https://doi.org/10.3390/w12030861

Motha, J.A., Wallbrink, P.J., Hairsine, P.B., Grayson, R.B., 2002. Tracer properties of eroded sediment and source material. Hydrological Processes 16 (10), 1983–2000. https://doi.org/10.1002/hyp.397

Motha, J.A., Wallbrink, P.J., Hairsine, P.B., Grayson, R.B., 2003. Determining the sources of suspended sediment in a forested catchment in southeastern Australia. Water Resources Research 39 (3). https://doi.org/10.1029/2001WR000794

Mueller, N.D., Gerber, J.S., Johnston, M., Ray, D.K., Ramankutty, N., Foley, J.A., 2012. Closing yield gaps through nutrient and water management. Nature 490 (7419), 254–257. https://doi.org/10.1038/nature11420

Mukundan, R., Walling, D.E., Gellis, A.C., Slattery, M.C., Radcliffe, D.E., 2012. Sediment source fingerprinting: transforming from a research tool to a management tool. Journal of the American Water Resources 48 (6), 1241–1257. https://doi.org/10.1111/j.1752-1688.2012.00685.x

Mullan, D., Favis-Mortlock, D., Fealy, R., 2012. Addressing key limitations associated with modelling soil erosion under the impacts of future climate change. Agricultural and Forest Meteorology 156, 18–30. https://doi.org/10.1016/j.agrformet.2011.12.004

Navas, A., López-Vicente, M., Gaspar, L., Machín, J., 2013. Assessing soil redistribution in a complex karst catchment using fallout 137Cs and GIS. Geomorphology 196, 231–241. https://doi.org/10.1016/j.geomorph.2012.03.018

Navratil, O., Esteves, M., Legout, C., Gratiot, N., Nemery, J., Willmore, S., Grangeon, T., 2011. Global uncertainty analysis of suspended sediment monitoring using turbidimeter in a small mountainous river catchment. Journal of Hydrology 398 (3–4), 246–259. https://doi.org/10.1016/j.jhydrol.2010.12.025

Navratil, O., Evrard, O., Esteves, M., Legout, C., Ayrault, S., Némery, J., Mate-Marin, A., Ahmadi, M., Lefèvre, I., Poirel, A., Bonté, P., 2012. Temporal variability of suspended sediment sources in an alpine catchment combining river/rainfall monitoring and sediment fingerprinting. Earth Surface Processes and Landforms 37 (8), 828–846. https://doi.org/10.1002/esp.3201

Netzband, A., Reincke, H., Bergemann, M., 2002. The River Elbe. Journal of Soils and Sediments 2 (3), 112–116. https://doi.org/10.1007/bf02988462

Noel, S., Mikulcak, F., Stewart, N., Etter, H., 2015. The economics of land degradation initiative: reaping economic and environmental benefits from sustainable land management 1–24.

Nones, M., 2019. Dealing with sediment transport in flood risk management. Acta Geophysica 67 (2), 677–685. https://doi.org/10.1007/s11600-019-00273-7

Nosrati, K., Collins, A.L., Madankan, M., 2018. Fingerprinting sub-basin spatial sediment sources using different multivariate statistical techniques and the Modified MixSIR model. Catena 164, 32–43. https://doi.org/10.1016/j.catena.2018.01.003

Nosrati, K., Fathi, Z., Collins, A.L., 2019. Fingerprinting sub-basin spatial suspended sediment sources by combining geochemical tracers and weathering indices. Environmental Science and Pollution Research 26 (27), 28401–28414. https://doi.org/10.1007/s11356-019-06024-x

Nosrati, K., Govers, G., Semmens, B.X., Ward, E.J., 2014. A mixing model to incorporate uncertainty in sediment fingerprinting. Geoderma 217–218, 173–180. https://doi.org/10.1016/j.geoderma.2013.12.002

Nosrati, K., Moradian, H., Dolatkordestani, M., Mol, L., Collins, A.L., 2022. The efficiency of elemental geochemistry and weathering indices as tracers in aeolian sediment provenance fingerprinting. Catena 210, 105932. https://doi.org/10.1016/j.catena.2021.105932

O'Neal, M.R., Nearing, M.A., Vining, R.C., Southworth, J., Pfeifer, R.A., 2005. Climate change impacts on soil erosion in Midwest United States with changes in crop management. Catena 61, 165–184. https://doi.org/10.1016/j.catena.2005.03.003

Oakes, E.G.M., Hughes, J.C., Jewitt, G.P.W., Lorentz, S.A., Chaplot, V., 2012. Controls on a scale explicit analysis of sheet erosion. Earth Surface Processes and Landforms 37 (8), 847–854. https://doi.org/10.1002/esp.3203

Oeurng, C., Sauvage, S., Sánchez-Pérez, J.M., 2010. Dynamics of suspended sediment transport and yield in a large agricultural catchment, southwest France. Earth Surface Processes and Landforms 35 (11), 1289–1301. https://doi.org/10.1002/esp.1971

Oldfield, F., Clark, R.L., 1990. Lake sediment-based studies of soil erosion. In Soil erosion on agricultural land. Proceedings of a workshop sponsored by the British Geomorphological Research Group, Coventry, UK, January 1989, 201–228.

Oldfield, F., Maher, B.A., Donoghue, J., Pierce, J., 1985. Particle-size related, mineral magnetic source sediment linkages in the Rhode River catchment, Marylands, USA. Journal of the Geological Society 142 (6), 1035–1046. https://doi.org/10.1144/gsjgs.142.6.1035

Oldfield, F., Rummery, T.A., Thompson, R., Walling, D.E., 1979. Identification of suspended sediment sources by means of magnetic measurements: some preliminary tests. Water Resources Management 15 (2), 211–218. https://doi.org/10.1029/WR015i002p00211

Olley, J., Caitcheon, G., 2000. Major element chemistry of sediments from the Darling-Barwon River and its tributaries: Implications for sediment and phosphorus sources. Hydrological Processes 14 (7), 1159–1175. https://doi.org/10.1002/(SICI)1099-1085(200005)14:7<1159::AID-HYP6>3.0.CO;2-P

Orlewski, P.M., Wang, Y., Hosseinalipour, M.S., Kryscio, D., Iggland, M., Mazzotti, M., 2018. Characterization of a vibromixer: Experimental and modelling study of mixing in a batch reactor. Chemical Engineering Research and Design 137, 534–543. https://doi.org/10.1016/j.cherd.2018.08.003

Osman, K.T., 2014. Soil Degradation, Conservation and Remediation. Springer, Netherlands,. https://doi.org/10.1007/978-94-007-7590-9

Owens, P.N., 2020. Soil erosion and sediment dynamics in the Anthropocene: a review of human impacts during a period of rapid global environmental change. Journal of Soils and Sediments 20 (12), 4115–4143. https://doi.org/10.1007/s11368-020-02815-9

Owens, P.N., 2022. Sediment source fingerprinting: are we going in the right direction? Journal of Soils and Sediments 22 (6), 1643–1647. https://doi.org/10.1007/s11368-022-03231-x

Owens, P.N., Batalla, R.J., Collins, A.J., Gomez, B., Hicks, D.M., Horowitz, A.J., Kondolf, G.M., Marden, M., Page, M.J., Peacock, D.H., Petticrew, E.L., Salomons, W., Trustrum, N.A., 2005. Fine-grained sediment in river systems: Environmental significance and management issues. River Research and Applications 21 (7), 693–717. https://doi.org/10.1002/rra.878

Owens, P.N., Blake, W.H., Gaspar, L., Gateuille, D., Koiter, A.J., Lobb, D.A., Petticrew, E.L., Reiffarth, D.G., Smith, H.G., Woodward, J.C., 2016. Fingerprinting and tracing the sources of soils and sediments: Earth and ocean science, geoarchaeological, forensic, and human health applications. Earth-Science Reviews 162, 1–23. https://doi.org/10.1016/j.earscirev.2016.08.012

Owens, P.N., Blake, W.H., Giles, T.R., Williams, N.D., 2012. Determining the effects of wildfire on

sediment sources using 137Cs and unsupported 210Pb: The role of landscape disturbances and driving forces. Journal of Soils and Sediments 12 (6), 982–994. https://doi.org/10.1007/s11368-012-0497-x

Owens, P.N., Petticrew, E.L., van der Perk, M., 2010. Sediment response to catchment disturbances. Journal of Soils and Sediments 10 (4), 591–596. https://doi.org/10.1007/s11368-010-0235-1

Ozturk, M., Work, P.A., 2016. Comparison of acoustic backscatter to turbidity for suspended sediment estimation in the Sacramento-San Joaquin Delta in California. In River Sedimentation. CRC press, 346–351.

Palazón, L., Latorre, B., Gaspar, L., Blake, W.H., Smith, H.G., Navas, A., 2015. Comparing catchment sediment fingerprinting procedures using an auto-evaluation approach with virtual sample mixtures. Science of the Total Environment 532, 456–466. https://doi.org/10.1016/j.scitotenv.2015.05.003

Panagos, P., Borrelli, P., Poesen, J., Ballabio, C., Lugato, E., Meusburger, K., Montanarella, L., Alewell, C., 2015. The new assessment of soil loss by water erosion in Europe. Environmental Science and Policy 54, 438–447. https://doi.org/10.1016/j.envsci.2015.08.012

Panagos, P., Van Liedekerke, M., Borrelli, P., Köninger, J., Ballabio, C., Orgiazzi, A., Lugato, E., Liakos, L., Hervas, J., Jones, A., Montanarella, L., 2022. European Soil Data Centre 2.0: Soil data and knowledge in support of the EU policies. European Journal of Soil Science 73 (6), 1–18. https://doi.org/10.1111/ejss.13315

Parsons, A.J., Stone, P.M., 2006. Effects of intra-storm variations in rainfall intensity on interrill runoff and erosion. Catena 67 (1), 68–78. https://doi.org/10.1016/j.catena.2006.03.002

Patault, E., Alary, C., Franke, C., Abriak, N.E., 2019. Quantification of tributaries contributions using a confluence-based sediment fingerprinting approach in the Canche river watershed (France). Science of the Total Environment 668, 457–469. https://doi.org/10.1016/j.scitotenv.2019.02.458

Paterson, G.A., Heslop, D., 2015. New methods for unmixing sediment grain size data. Geochemistry, Geophysics, Geosystems 16, 4494–4506. https://doi.org/10.1002/2015GC006070

Paterson, G.A., Heslop, D., 2020a. AnalySize Algorithm. Version 1.2.1. Availlable at: https://github.com/greigpaterson/AnalySize. (Accessed March 2022).

Paterson, G.A., Heslop, D., 2020b. AnalySize Manual. Version 1.2.1. Available at: https://github.com/greigpaterson/AnalySize/blob/master/Documents/AnalySize_Manual_v1.2.1.pdf. (Accessed March 2022).

Peart, M.R., Walling, D.E., 1986. Fingerprinting sediment source: the example of a drainage basin in Devon, UK. In Drainage basin sediment delivery: proceedings of a symposium held in Albuquerque, NM.

Peart, M.R., Walling, D.E., 1988. Techniques for establishing suspended sediment sources in two drainage basins in Devon, UK: a comparative assessment. In: Sediment Budgets, M.P. Bordas & D.E. Walling (eds.), IAHS Publ 174, 269–279.

Pfister, L., Wagner, C., Vansuypeene, E., Drogue, G., Hoffmann, L., Ries, C., 2005. Atlas Climatique du Grand-Duché de Luxembourg. Musée National d'Histoire Naturelle, Société des Naturalistes Luxembourgeois, Centre de Recherce Public-Gabriel Lippmann, Administration des Services Techniques de l'Agriculture, Luxembourg, 80 p.

Phillips, D.L., Gregg, J.W., 2003. Source partitioning using stable isotopes: Coping with too many sources. Oecologia 136 (2), 261–269. https://doi.org/10.1007/s00442-003-1218-3

Phillips, J.M., Russell, M.A., Walling, D.E., 2000. Time-integrated sampling of fluvial suspended sediment: A simple methodology for small catchments. Hydrological Processes 14 (14), 2589–2602. https://doi.org/10.1002/1099-1085(20001015)14:14<2589::AID-HYP94>3.0.CO;2-D

Phillips, J.M., Walling, D.E., 1995. An assessment of the effects of sample collection, storage and resuspension on the representativeness of measurements of the effective particle size distribution of fluvial suspended sediment. Water Research 29 (11), 2498–2508.

Pimentel, D., Burgess, M., 2013. Soil erosion threatens food production. Agriculture 3 (3), 443–463. https://doi.org/10.3390/agriculture3030443

Pimentel, D., Harvey, C., Resosudarmo, P., Sinclair, K., Kurz, D., McNair, M., Crist, S., Shpritz, L., Fitton, L., Saffouri, R., Blair, R., 1995. Environmental and economic costs of soil erosion and conservation benefits. Science 267 (5201), 1117–1123. https://doi.org/10.1126/science.267.5201.1117

Poesen, J., 1992. Mechanisms of overland-flow generation and sediment production on loamy and sandy soils with and without rock fragments. In Parsons, A.J., Abrahams, A.D. (Eds.), Overland Flow Hydraulics and Erosion Mechanics. Routledge, London 275–305.

Poesen, J., 2018. Soil erosion in the Anthropocene: Research needs. Earth Surface Processes and Landforms 43 (1), 64–84. https://doi.org/10.1002/esp.4250

Poulenard, J., Legout, C., Némery, J., Bramorski, J., Navratil, O., Douchin, A., Fanget, B., Perrette, Y., Evrard, O., Esteves, M., 2012. Tracing sediment sources during floods using Diffuse Reflectance Infrared Fourier Transform Spectrometry (DRIFTS): A case study in a highly erosive mountainous catchment (Southern French Alps). Journal of Hydrology 414–415, 452–462. https://doi.org/10.1016/j.jhydrol.2011.11.022

Poulenard, J., Perrette, Y., Fanget, B., Quetin, P., Trevisan, D., Dorioz, J.M., 2009. Infrared spectroscopy tracing of sediment sources in a small rural watershed (French Alps). Science of the Total Environment 407 (8), 2808–2819. https://doi.org/10.1016/j.scitotenv.2008.12.049

Prairie, M.W., Frisbie, S.H., Rao, K.K., Saksri, A.H., Parbat, S., Mitchell, E.J., 2020. An accurate, precise, and affordable light emitting diode spectrophotometer for drinking water and other testing with limited resources. PloS one 15 (1), e0226761. https://doi.org/10.1371/journal.pone.0226761

Pulley, S., Collins, A.L., 2018. Tracing catchment fine sediment sources using the new SIFT (SedIment Fingerprinting Tool) open source software. Science of the Total Environment 635, 838–858. https://doi.org/10.1016/j.scitotenv.2018.04.126

Pulley, S., Collins, A.L., 2021. The potential for colour to provide a robust alternative to high-cost sediment source fingerprinting: Assessment using eight catchments in England. Science of the Total Environment 792, 148416. https://doi.org/10.1016/j.scitotenv.2021.148416

Pulley, S., Collins, A.L., 2022. A rapid and inexpensive colour-based sediment tracing method incorporating hydrogen peroxide sample treatment as an alternative to quantitative source fingerprinting for catchment management. Journal of Environmental Management 311, 114780. https://doi.org/10.1016/j.jenvman.2022.114780

Pulley, S., Foster, I., Collins, A.L., 2017. The impact of catchment source group classification on the accuracy of sediment fingerprinting outputs. Journal of Environmental Management 194, 16–26. https://doi.org/10.1016/j.jenvman.2016.04.048

Pulley, S., Rowntree, K., 2016. The use of an ordinary colour scanner to fingerprint sediment sources in the South African Karoo. Journal of Environmental Management 165, 253–262. https://doi.org/10.1016/j.jenvman.2015.09.037

Pulley, S., Van der Waal, B., Rowntree, K., Collins, A.L., 2018. Colour as reliable tracer to identify

the sources of historically deposited flood bench sediment in the Transkei, South Africa: A comparison with mineral magnetic tracers before and after hydrogen peroxide pre-treatment. Catena 160, 242–251. https://doi.org/10.1016/j.catena.2017.09.018

Ramos-Scharrón, C.E., MacDonald, L.H., 2007. Measurement and prediction of natural and anthropogenic sediment sources, St. John, U.S. Virgin Islands. Catena 71 (2), 250–266. https://doi.org/10.1016/j.catena.2007.03.009

Revel-Rolland, M., Arnaud, F., Chapron, E., Desmet, M., Givelet, N., Alibert, C., McCulloch, M., 2005. Sr and Nd isotopes as tracers of clastic sources in Lake Le Bourget sediment (NW Alps, France) during the Little Ice Age: Palaeohydrology implications. Chemical Geology 224 (4), 183–200. https://doi.org/10.1016/j.chemgeo.2005.04.014

Richet, J.B., Ouvry, J.F., Saunier, M., 2017. The role of vegetative barriers such as fascines and dense shrub hedges in catchment management to reduce runoff and erosion effects: Experimental evidence of efficiency, and conditions of use. Ecological Engineering 103, 455–469. https://doi.org/10.1016/j.ecoleng.2016.08.008

Rieger, L., Langergraber, G., Thomann, M., Fleischmann, N., Siegrist, H., 2004. Spectral in-situ analysis of NO2, NO3, COD, DOC and TSS in the effluent of a WWTP. Water Science and Technology 50 (11), 143–152. https://doi.org/10.2166/wst.2004.0682

Römkens, M.J.M., Helming, K., Prasad, S.N., 2002. Soil erosion under different rainfall intensities, surface roughness, and soil water regimes. Catena 46 (2–3), 103–123. https://doi.org/10.1016/S0341-8162(01)00161-8

Rovira, A., Alcaraz, C., Ibáñez, C., 2012. Spatial and temporal dynamics of suspended load at-a-cross-section: The lowermost Ebro River (Catalonia, Spain). Water Research 46 (11), 3671–3681. https://doi.org/10.1016/j.watres.2012.04.014

Rowan, J.S., Black, S., Franks, S.W., 2012. Sediment fingerprinting as an environmental forensics tool explaining cyanobacteria blooms in lakes. Applied Geography 32 (2), 832–843. https://doi.org/10.1016/j.apgeog.2011.07.004

Rowan, J.S., Goodwill, P., Franks, S.W., 2000. Uncertainty estimation in fingerprinting suspended sediment sources. In: Foster, I.D.L., (Ed.) Tracers in Geomorphology. Wiley, Chichester: 279–290.

Russell, M.A., Walling, D.E., Hodgkinson, R.A., 2001. Suspended sediment sources in two small lowland agricultural catchments in the UK. Journal of Hydrology 252 (1–4), 1–24.

https://doi.org/10.1016/S0022-1694(01)00388-2

Scan Messtechnik GmbH. Available at: http://www.s-can.at. (Accessed March 2019), 2018.

Schumm, S., 1977. The fluvial system. Wiley, New York 338 pp.

Sehgal, D., Martínez-Carreras, N., Hissler, C., Bense, V.F., Hoitink, A.J.F. (Ton), 2022. Inferring suspended sediment carbon content and particle size at high-frequency from the optical response of a submerged spectrometer. Water Resources Research 58 (5), e2021WR030624. https://doi.org/10.1029/2021wr030624

Sequoia Scientific, INC. LISST-200X Users Manual. Available at: https://www.sequoiasci.com/wp-content/uploads/2016/02/LISST-200X_Users_Manual_v1_3B.pdf. (accessed December 2022), 2018.

Shear, H., Watson, A.E.P. (eds), 1977. The fluvial transport of sediment-associated nutrients and contaminants. International Joint Commission, Windsor.

Sherriff, S.C., Franks, S.W., Rowan, J.S., Fenton, O., Ó'hUallacháin, D., 2015. Uncertainty-based assessment of tracer selection, tracer non-conservativeness and multiple solutions in sediment fingerprinting using synthetic and field data. Journal of Soils and Sediments 15 (10), 2101–2116. https://doi.org/10.1007/s11368-015-1123-5

Shi, Z., Chow, C.W.K., Fabris, R., Liu, J., Jin, B., 2022. Applications of online UV-Vis spectrophotometer for drinking water quality monitoring and process control: a review. Sensors 22 (8), 1–21. https://doi.org/10.3390/s22082987

Siu, C.Y.S., Pitt, R., Clark, S.E., 2008. Errors associated with sampling and measurement of solids: Application to the evaluation of stormwater treatment devices. In CD-ROM Proceedings of the 11th Int. Conf. on Urban Drainage, Edinburgh, UK. 1–10.

Slattery, M.C., Burt, T.P., 1997. Particle size characteristics of suspended sediment in hillslope runoff and stream flow. Earth Surface Processes and Landforms 22 (8), 705–719. https://doi.org/10.1002/(SICI)1096-9837(199708)22:8<705::AID-ESP739>3.0.CO;2-6

Smith, H.G., Blake, W.H., 2014. Sediment fingerprinting in agricultural catchments: A critical re-examination of source discrimination and data corrections. Geomorphology 204, 177–191. https://doi.org/10.1016/j.geomorph.2013.08.003

Smith, T.B., Owens, P.N., 2014. Flume- and field-based evaluation of a time-integrated suspended sediment sampler for the analysis of sediment properties. Earth Surface Processes and

Landforms 39 (9), 1197–1207. https://doi.org/10.1002/esp.3528

Sotiri, K., 2020. Integrated sediment yield and stock assessment for the Passaúna Reservoir, Brazil. Doctoral Dissertation, Karlsruher Institut für Technologie (KIT) 220. https://doi.org/10.5445/IR/1000127716

Sougnez, N., van Wesemael, B., Vanacker, V., 2011. Low erosion rates measured for steep, sparsely vegetated catchments in southeast Spain. Catena 84 (1–2), 1–11. https://doi.org/10.1016/j.catena.2010.08.010

Spencer, K.L., Wheatland, J.A., Carr, S.J., Manning, A.J., Bushby, A.J., Gu, C., Botto, L., Lawrence, T., 2022. Quantification of 3-dimensional structure and properties of flocculated natural suspended sediment. Water Research 222, 118835. https://doi.org/10.1016/j.watres.2022.118835

Stallard, R.F., 1998. Terrestrial sedimentation and the carbon cycle: Coupling weathering and erosion to carbon burial. Global Biogeochemical Cycles 12 (2), 231–257. https://doi.org/10.1029/98GB00741

Stock, B.C., Jackson, A.L., Ward, E.J., Parnell, A.C., Phillips, D.L., Semmens, B.X., 2018. Analyzing mixing systems using a new generation of Bayesian tracer mixing models. PeerJ 2018 (6), 1–27. https://doi.org/10.7717/peerj.5096

Stock, B.C., Semmens, B.X., 2016. MixSIAR GUI User Manual. Version 3.1. Available at: https://github.com/brianstock/MixSIAR. (Accessed November 2022).

Stone, P.M., Walling, D.E., 1997. Particle size selectivity considerations in suspended sediment budget investigations. Water, Air, & Soil Pollution 99 (1–4), 63–70. https://doi.org/10.1007/bf02406845

Syvitski, J.P.M., Vörösmarty, C.J., Kettner, A.J., Green, P., 2005. Impact of humans on the flux of terrestrial sediment to the global coastal ocean. Science 308 (5720), 376–381. https://doi.org/10.1126/science.1109454

Tang, Q., Collins, A.L., Wen, A., He, X., Bao, Y., Yan, D., Long, Y., Zhang, Y., 2018. Particle size differentiation explains flow regulation controls on sediment sorting in the water-level fluctuation zone of the Three Gorges Reservoir, China. Science of the Total Environment 633 (9), 1114–1125. https://doi.org/10.1016/j.scitotenv.2018.03.258

Tang, Q., Fu, B., Wen, A., Zhang, X., He, X., Collins, A.L., 2019. Fingerprinting the sources of water-mobilized sediment threatening agricultural and water resource sustainability: Progress,

challenges and prospects in China. Science China Earth Sciences 62 (12), 2017–2030. https://doi.org/10.1007/s11430-018-9349-0

Taylor, A., Blake, W.H., Keith-Roach, M.J., 2014. Estimating Be-7 association with soil particle size fractions for erosion and deposition modelling. Journal of Soils and Sediments 14 (11), 1886–1893. https://doi.org/10.1007/s11368-014-0955-8

Thomas, M.F., Azema, N., Thomas, O., 2017. Physical and aggregate properties. In Thomas, O., & Burgess, C. (Eds.). UV-visible spectrophotometry of water and wastewater. Elsevier, 2017.

Tiecher, T., Ramon, R., de Andrade, L.C., Camargo, F.A.O., Evrard, O., Minella, J.P.G., Laceby, J.P., Bortoluzzi, E.C., Merten, G.H., Rheinheimer, D.S., Walling, D.E., Barros, C.A.P., 2022. Tributary contributions to sediment deposited in the Jacuí Delta, Southern Brazil. Journal of Great Lakes Research 48 (3), 669–685. https://doi.org/10.1016/j.jglr.2022.02.006

Turowski, J.M., Rickenmann, D., Dadson, S.J., 2010. The partitioning of the total sediment load of a river into suspended load and bedload: A review of empirical data. Sedimentology 57 (4), 1126–1146. https://doi.org/10.1111/j.1365-3091.2009.01140.x

Tye, A.M., Rawlins, B.G., Rushton, J.C., Price, R., 2016. Understanding the controls on sediment-P interactions and dynamics along a non-tidal river system in a rural-urban catchment: The River Nene. Applied Geochemistry 66, 219–233. https://doi.org/10.1016/j.apgeochem.2015.12.014

Upadhayay, H.R., Granger, S.J., Collins, A.L., 2021. Dynamics of fluvial hydro-sedimentological, nutrient, particulate organic matter and effective particle size responses during the U.K. extreme wet winter of 2019–2020. Science of the Total Environment 774, 145722. https://doi.org/10.1016/j.scitotenv.2021.145722

Upadhayay, H.R., Lamichhane, S., Bajracharya, R.M., Cornelis, W., Collins, A.L., Boeckx, P., 2020. Sensitivity of source apportionment predicted by a Bayesian tracer mixing model to the inclusion of a sediment connectivity index as an informative prior: Illustration using the Kharka catchment (Nepal). Science of the Total Environment 713, 136703. https://doi.org/10.1016/j.scitotenv.2020.136703

Upadhayay, H.R., Zhang, Y., Granger, S.J., Micale, M., Collins, A.L., 2022. Prolonged heavy rainfall and land use drive catchment sediment source dynamics: Appraisal using multiple biotracers. Water Research 216 (March), 118348. https://doi.org/10.1016/j.watres.2022.118348

USDA/NRCS, 2010. 2007 National Resources Inventory: Soil Erosion on Cropland. Department, U.S. Service, Agriculture/National Resources Conservation.

Vale, S., Swales, A., Smith, H.G., Olsen, G., Woodward, B., 2022. Impacts of tracer type, tracer selection, and source dominance on source apportionment with sediment fingerprinting. Science of the Total Environment 831, 154832. https://doi.org/10.1016/j.scitotenv.2022.154832

Vale, S.S., Fuller, I.C., Procter, J.N., Basher, L.R., Dymond, J.R., 2020. Storm event sediment fingerprinting for temporal and spatial sediment source tracing. Hydrological Processes 34 (15), 3370–3386. https://doi.org/10.1002/hyp.13801

Vale, S.S., Fuller, I.C., Procter, J.N., Basher, L.R., Smith, I.E., 2016. Application of a confluence-based sediment-fingerprinting approach to a dynamic sedimentary catchment, New Zealand. Hydrological Processes 30 (5), 812–829. https://doi.org/10.1002/hyp.10611

Valentin, C., Poesen, J., Li, Y., 2005. Gully erosion: Impacts, factors and control. Catena 63 (2–3), 132–153. https://doi.org/10.1016/j.catena.2005.06.001

van Hateren, J.A., Prins, M.A., van Balen, R.T., 2018. On the genetically meaningful decomposition of grain-size distributions: A comparison of different end-member modelling algorithms. Sedimentary Geology 375, 49–71. https://doi.org/10.1016/j.sedgeo.2017.12.003

Van Oost, K., Quine, T.A., Govers, G., De Gryze, S., Six, J., Harden, J.W., Ritchie, J.C., McCarty, G.W., Heckrath, G., Kosmas, C., Giraldez, J. V., Marques Da Silva, J.R., Merckx, R., 2007. The impact of agricultural soil erosion on the global carbon cycle. Science 318 (5850), 626–629. https://doi.org/10.1126/science.1145724

van Rijn, L., 1984. Sediment transport, Part I: Bed load transport. Journal of Hydraulic Engineering 110 (10), 1431–1456.

Venter, O., Sanderson, E.W., Magrach, A., Allan, J.R., Beher, J., Jones, K.R., Possingham, H.P., Laurance, W.F., Wood, P., Fekete, B.M., Levy, M.A., Watson, J.E.M., 2016. Sixteen years of change in the global terrestrial human footprint and implications for biodiversity conservation. Nature Communications 7, 1–11. https://doi.org/10.1038/ncomms12558

Vercruysse, K., Grabowski, R.C., 2019. Temporal variation in suspended sediment transport: linking sediment sources and hydro-meteorological drivers. Earth Surface Processes and Landforms 44 (13), 2587–2599. https://doi.org/10.1002/esp.4682

Vercruysse, K., Grabowski, R.C., Hess, T., Lexartza-Artza, I., 2020. Linking temporal scales of

suspended sediment transport in rivers: towards improving transferability of prediction. Journal of Soils and Sediments 20 (12), 4144–4159. https://doi.org/10.1007/s11368-020-02673-5

Vercruysse, K., Grabowski, R.C., Rickson, R.J., 2017. Suspended sediment transport dynamics in rivers: Multi-scale drivers of temporal variation. Earth-Science Reviews 166, 38–52. https://doi.org/10.1016/j.earscirev.2016.12.016

Verstraeten, G., Poesen, J., 2001. Modelling the long-term sediment trap efficiency of small ponds. Hydrological Processes 15 (14), 2797–2819. https://doi.org/10.1002/hyp.269

Viana, C.M., Freire, D., Abrantes, P., Rocha, J., Pereira, P., 2022. Agricultural land systems importance for supporting food security and sustainable development goals: A systematic review. Science of the Total Environment 806. https://doi.org/10.1016/j.scitotenv.2021.150718

Vörösmarty, C.J., McIntyre, P.B., Gessner, M.O., Dudgeon, D., Prusevich, A., Green, P., Glidden, S., Bunn, S.E., Sullivan, C.A., Liermann, C.R., Davies, P.M., 2010. Global threats to human water security and river biodiversity. Nature 467 (7315), 555–561. https://doi.org/10.1038/nature09440

Wall, G.J., Wilding, L.P., 1976. Mineralogy and related parameters of fluvial suspended sediments in Northwestern Ohio. Journal of Environmental Quality 5 (2), 168–173. https://doi.org/10.2134/jeq1976.00472425000500020012x

Wallbrink, P.J., Murray, A.S., Olley, J.M., Olive, L.J., 1998. Determining sources and transit times of suspended sediment in the Murrumbidgee River, New South Wales, Australia, using fallout 137Cs and 210Pb. Water Resources Research 34 (4), 879–887. https://doi.org/10.1029/97WR03471

Walling, D.E., 1983. The sediment delivery problem. Journal of Hydrology 65, 209–237. https://doi.org/10.1016/0022-1694(83)90217-2

Walling, D.E., 2005. Tracing suspended sediment sources in catchments and river systems. Science of the Total Environment 344 (1-3 SPEC. ISS.), 159–184. https://doi.org/10.1016/j.scitotenv.2005.02.011

Walling, D.E., 2006. Human impact on land-ocean sediment transfer by the world's rivers. Geomorphology 79 (3–4), 192–216. https://doi.org/10.1016/j.geomorph.2006.06.019

Walling, D.E., 2013. The evolution of sediment source fingerprinting investigations in fluvial

systems. Journal of Soils and Sediments 13 (10), 1658–1675. https://doi.org/10.1007/s11368-013-0767-2

Walling, D.E., Collins, A.L., 2008. The catchment sediment budget as a management tool. Environmental Science & Policy 11 (2), 136–143. https://doi.org/10.1016/j.envsci.2007.10.004

Walling, D.E., Owens, P.N., Leeks, G.J.L., 1999. Fingerprinting suspended sediment sources in the catchment of the River Ouse, Yorkshire, UK. Hydrological Processes 13 (7), 955–975. https://doi.org/10.1002/(SICI)1099-1085(199905)13:7<955::AID-HYP784>3.0.CO;2-G

Walling, D.E., Owens, P.N., Waterfall, B.D., Leeks, G.J.L., Wass, P.D., 2000. The particle size characteristics of fluvial suspended sediment in the Humber and Tweed catchments, UK. Science of the Total Environment 251–252, 205–222. https://doi.org/10.1016/S0048-9697(00)00384-3

Walling, D.E., Peart, M.R., Oldfield, F., Thompson, R., 1979. Suspended sediment sources identified by magnetic measurements. Nature 281 (5727), 110–113. https://doi.org/10.1038/281110a0

Walling, D.E., Woodward, J.C., 1992. Use of radiometric fingerprints to derive information on suspended sediment sources. Erosion and sediment monitoring programmes in river basins. Proc. international symposium, Oslo, 1992| 210, 153–164.

Walling, D.E., Woodward, J.C., 1995. Tracing sources of suspended sediment in river basins: a case study of the River Culm, Devon, UK. Marine and Freshwater Research 46 (1), 327–336. https://doi.org/10.1071/MF9950327

Walling, D.E., Woodward, J.C., Nicholas, A.P., 1993. A multi-parameter approach to fingerprinting suspended-sediment sources. Tracers in hydrology. Proc. international symposium, Yokohama, 1993 329–338.

Wanyama, J., Herremans, K., Maetens, W., Isabirye, M., Kahimba, F., Kimaro, D., Poesen, J., Deckers, J., 2012. Effectiveness of tropical grass species as sediment filters in the riparian zone of Lake Victoria. Soil Use and Management 28 (3), 409–418. https://doi.org/10.1111/j.1475-2743.2012.00409.x

Wasson, R.J., Caitcheon, G., Murray, A.S., McCulloch, M., Quade, J., 2002. Sourcing sediment using multiple tracers in the catchment of Lake Argyle, Northwestern Australia. Environmental Management 29 (5), 634–646. https://doi.org/10.1007/s00267-001-0049-4

Weltje, G.J., 1997. End-member modeling of compositional data: Numerical-statistical algorithms for solving the explicit mixing problem. Mathematical Geology 29 (4), 503–549. https://doi.org/10.1007/bf02775085

WFD; 2000/60/EC, 2000. Directive 2000/60/EC of the European Parliament and the Council of 23.10.2000, A framework for community action in the field of water policy. Official Journal of the European Communities 71.

Wheater, H., Evans, E., 2009. Land use, water management and future flood risk. Land Use Policy 26 (SUPPL. 1), 251–264. https://doi.org/10.1016/j.landusepol.2009.08.019

Wilkinson, S.N., Wallbrink, P.J., Hancock, G.J., Blake, W.H., Shakesby, R.A., Doerr, S.H., 2009. Fallout radionuclide tracers identify a switch in sediment sources and transport-limited sediment yield following wildfire in a eucalypt forest. Geomorphology 110 (3–4), 140–151. https://doi.org/10.1016/j.geomorph.2009.04.001

Williams, N.D., Walling, D.E., Leeks, G.J.L., 2008. An analysis of the factors contributing to the settling potential of fine fluvial sediment. Hydrological Processes 22 (November 2008), 4153–4162. https://doi.org/10.1002/hyp.7015

Wilson, H.F., Saiers, J.E., Raymond, P.A., Sobczak, W. V, 2013. Hydrologic drivers and seasonality of dissolved organic carbon concentration, nitrogen content, bioavailability, and export in a forested New England stream. Ecosystems 16 (4), 604–616. https://doi.org/10.1007/s10021-013-9635-6

Wohl, E., Bledsoe, B.P., Jacobson, R.B., Poff, N.L., Rathburn, S.L., Walters, D.M., Wilcox, A.C., 2015. The natural sediment regime in rivers: Broadening the foundation for ecosystem management. BioScience 65 (4), 358–371. https://doi.org/10.1093/biosci/biv002

Wynants, M., Millward, G., Patrick, A., Taylor, A., Munishi, L., Mtei, K., Brendonck, L., Gilvear, D., Boeckx, P., Ndakidemi, P., Blake, W.H., 2020. Determining tributary sources of increased sedimentation in East-African Rift Lakes. Science of the Total Environment 717, 137266. https://doi.org/10.1016/j.scitotenv.2020.137266

Wynn, J.G., Bird, M.I., Wong, V.N.L., 2005. Rayleigh distillation and the depth profile of 13C/ 12C ratios of soil organic carbon from soils of disparate texture in Iron Range National Park, Far North Queensland, Australia. Geochimica et Cosmochimica Acta 69 (8), 1961–1973. https://doi.org/10.1016/j.gca.2004.09.003

Yu, L., Oldfield, F., 1989. A multivariate mixing model for identifying sediment source from

magnetic measurements. Quaternary Research 32 (2), 168–181. https://doi.org/10.1016/0033-5894(89)90073-2

Yu, L., Oldfield, F., 1993. Quantitative sediment source ascription using magnetic measurements in a reservoir system near Nijar, S.E. Spain. Earth Surface Processes and Landforms 18 (5), 441–454. https://doi.org/10.1002/esp.3290180506

Yu, S.Y., Colman, S.M., Li, L., 2016. BEMMA: A hierarchical Bayesian end-member modeling analysis of sediment grain-size distributions. Mathematical Geosciences 48 (6), 723–741. https://doi.org/10.1007/s11004-015-9611-0

Zabel, F., Delzeit, R., Schneider, J.M., Seppelt, R., Mauser, W., Václavík, T., 2019. Global impacts of future cropland expansion and intensification on agricultural markets and biodiversity. Nature Communications 10 (1), 1–10. https://doi.org/10.1038/s41467-019-10775-z

Zhang, X., Wang, H., Xu, S., Yang, Z., 2020. A basic end-member model algorithm for grain-size data of marine sediments. Estuarine, Coastal and Shelf Science 236 (August 2019), 106656. https://doi.org/10.1016/j.ecss.2020.106656

Zorn, M., Komac, B., 2013. Erosion. In: Bobrowsky, P.T. (eds) Encyclopedia of Natural Hazards. Encyclopedia of Earth Sciences Series. Springer, Dordrecht.